Synthesis and Characterization of Chiral Cu(II) and Ni(II) Complexes of Amino Acid Derived Ligands and Aniline Based Polymers with Functional Group

A Dissertation submitted to the
Indian Institute of Technology Guwahati
As Partial Fulfillment for the Degree of
Doctor of Philosophy

Submitted by
Rik Rani Koner

Department of Chemistry
Indian Institute of Technology Guwahati
Guwahati-781039

November 2008

Dedicated to my Late Grandmother

…….Rik

INDIAN INSTITUTE OF TECHNOLOGY, GUWAHATI

Department of Chemistry

STATEMENT

I do hereby declare that the matter embodied in this thesis is the result of investigations carried out by me in the Department of Chemistry, Indian Institute of Technology Guwahati, India under the guidance of Dr. Manabendra Ray, Associate Professor, Department of Chemistry, Indian Institute of Technology Guwahati, India.

In keeping with the general practice of reporting scientific observations, due acknowledgements have been made wherever the work described is based on the findings of other investigators.

November, 2008 (Rik Rani Koner)

I.I.T. Guwahati

INDIAN INSTITUTE OF TECHNOLOGY GUWAHATI

Department of Chemistry

CERTIFICATE

This is to certify that Rik Rani Koner has been working under my supervision since July, 2004 as a regular registered Ph. D. student. I am forwarding her thesis entitled "**Synthesis and Characterization of Chiral Cu(II) and Ni(II) Complexes of Amino Acid Derived Ligands and Aniline Based Polymers with Functional Group"** being submitted for the Ph. D. (Science) Degree of this Institute. I certify that she has fulfilled all the requirements according to the rules of this Institute regarding the investigations embodied in her thesis and this work has not been submitted elsewhere for a degree.

November, 2008 (Dr. Manabendra Ray)

I.I.T. Guwahati Supervisor

INDIAN INSTITUTE OF TECHNOLOGY, GUWAHATI

Department of Chemistry

CERTIFICATE OF COURSE WORK

This is to certify that Rik Rani Koner has satisfactorily completed all the courses required for the Ph.D degree program. These courses include

CH 603:	Supramolecules: Concepts and Applications
CH 627:	New Reagents for Organic Chemistry
CH 630:	Physical Methods inChemistry
CH 632:	Advanced Group Theroy and Application

Rik Rani Koner has successfully completed her Ph.D qualifying examination in May 2005.

Prof. A. T. Khan
Head, Department of Chemistry
I. I. T. Guwahati

Dr. T. Punniyamurthy
Secretary, DPPC
I. I. T. Guwahati

Acknowledgements

At the very outset I take opportunity to express my deep sense of gratitude to my Ph.D. supervisor Dr. Manabendra Ray, Department of Chemistry, IIT Guwahati for his able guidance, tireless efforts, constant encouragements and moral supports at each and every step of my research work, which enable me to complete my thesis work. I am fortunate enough to have his teaching about how to cultivate scientific thoughts.

I would like to acknowledge my sincere gratitude to all my doctoral committee members, Dr. Gopal Das, Professor Bhisma K. Patel and Dr. Aiyagari Ramesh for their insightful advices and valuable suggestions.

I am grateful to Professor Abu T. Khan, Head, Department of Chemistry, IIT Guwahati for his valuable suggestions and providing good research environment.

Dr. M. Nethaji at IISC will always be thankfully remembered for solving X-Ray structure of two of our compound.

I express my sincere appreciation to Dr. S. Chakraborty at civil department of IIT-Guwahati as our collaborator.

I am thankful to the Institute, Indian Institute of Technology Guwahati for providing me with the state of the art infrastructure and facilities for advanced research.

I also express my sincere thanks to all faculty members, Department of Chemistry, IIT Guwahati for their help and encouragement.

I am grateful to all non-teaching staffs of the Department for their technical support.

I would like to thank DST under FIST program for providing single crystal XRD instrument facility and B. Das for mounting the crystal.

My sincere thanks to Chandan Borgohain, K. Senapati and Shing of Central Instruments facility, IIT Guwahati for their help in all the characterizations (SEM, NMR , ESI-Ms, EPR) required during my research work.

I wish to show my gratitude to Prof. P. Banarjee (IACS) and Dr. P. K. Madhusudanan (CDRI, Lucknow) for celemental analysis (CHN).

I would like to thank my former and present group members Dr. A. Alam, Amrita Das, Subhas Sahoo, Mrigendra Dubey and S. S. Faizi for their timely help, support and for the wonderful time we shared during this period.

I extend my sincerest special thanks to Ballav, Sahoo, Avijeet, Anirban and Suman and I also take this opportunity to thank Bimlesh, Bedabrata, Gunin, Pranjal, Bolin, Prashanta, Sonit, Babuda, Sarala Di, Hari, Shiba,, Shaon, Sucheta, Aditi, Sananda, Nipa, Moitree, Mousumi and Anu for their constant help, motivation, enthusiastic company and all the wonderful time we spent in various events.

I am thankful to all research scholars and M.Sc students, Department of Chemistry, IIT Guwahati for their help.

The financial support from Council of Scientific and Industrial Research (CSIR), New Delhi in the form of JRF and SRF is duly acknowledged.

My heartfelt thanks to my husband, Subrata for his love, affection, support and for being so understand over these years.

I wish to express my sincere gratitude to my brothers and sisters for their constant unfailing support.

At last but not least, I want to express my sincere thanks to all of my family members, especially my parents, father in law and mother in law for their constant encouragements and moral supports during my research work. They are the main soul and inspiration for each and every step that I achieve in my life.

Rik Rani Koner

Abstract

This thesis represents our effort to rationalize the formation of octanuclear assembly of Cu(II) as well as the exploration of the coordination chemistry of amino acid derived reduced Schiff base ligands by systematically variation of amino acids, solvent, external ligand, substitution of ligand on aromatic ring, different metal /ligand ratio and metal ion.

During the courses we have been successful in the synthesis and characterization of complexes with different nuclearity.

It also represents our attempt to synthesize amine functionalized aniline based polymers and oligomers along with the description of a new metal mediated organic transformation.

The thesis has been divided into eight chapters. Chapter wise summary of the work is given below.

Chapter 1

Introduction

This chapter contains the up-to-date a brief literature review on different types of capsule or capsular complexes and the coordination chemistry of reduced Schiff base ligands derived from salicylaldehyde and amino-acids.

Chapter 2

Effects of amino acid side chain, pyridine, and imidazole on the octanuclear Cu(II) assembly

In the beginning of the work we followed the synthetic route used earlier for octanuclear Cu(II) capsule by changing the L-histidine to L-methionine and L-tyrosine. We could not synthesize any new capsular complex ended up always with either mononuclear or binuclear complex. At that point it became apparent that we need to understand the chemistry of this reaction in order to succeed. In this chapter we have reported the syntheses and characterization of a series of Cu(II) complexes by systematically varying the amino acid, solvent and external ligands. Analysis of the results revealed the influence of amino acid side chain and solvent on the nuclearity of the resulting complexes (Scheme I).

Role of amino acid. In absence of a strong ligand in the form of solvent and amino acid side arm, the formation of a phenoxo-bridged binuclear complex is favored irrespective of

amino acid used. The ligands being nonplanar ligands, phenoxo-bridged binuclear complex formation satisfies the coordination requirements on the Cu(II).

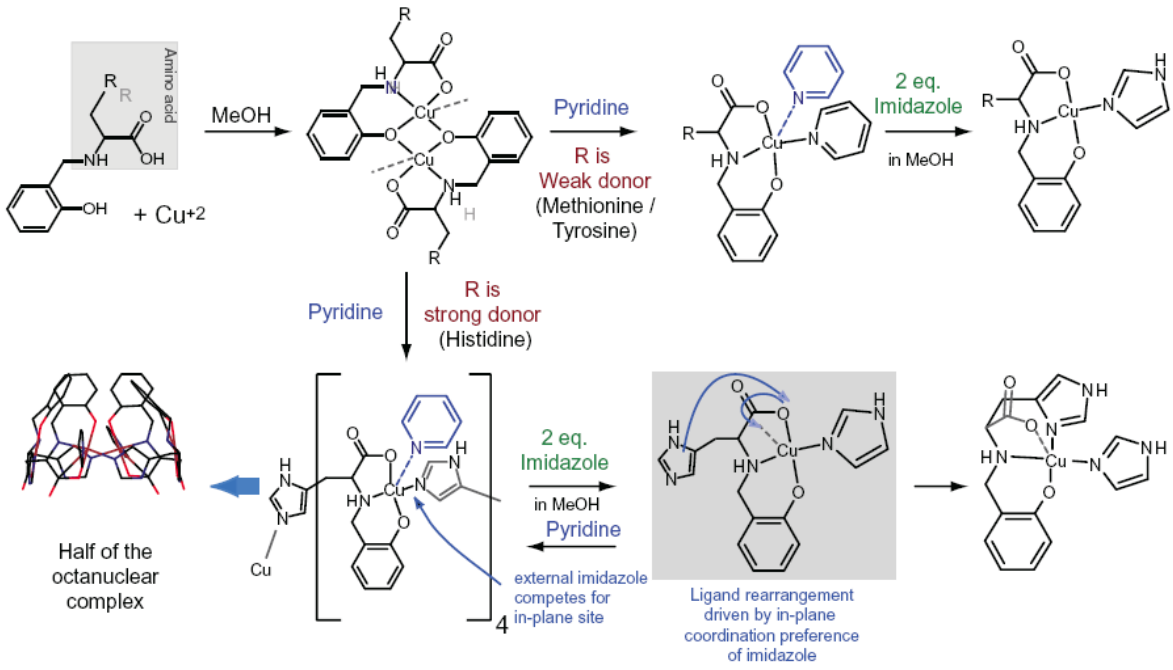

Scheme I. *Effect of amino acid, solvent, and imidazole on the formation mononuclear to octanuclear species.*

The solvent such as pyridine which can act as a ligand to Cu(II) are able to break the phenoxo bridge, forming a mononuclear complex. If the amino acid used is histidine, then replacement of the in-plane pyridine can lead to cyclic multinuclear complex formation. Methionine thioether and tyrosine phenol can neither break the phenoxo bridge or displace pyridine to form octanuclear complex.

Role of imidazole. As the formation of octanuclear occurred because of displacement of in-plane pyridine by the imidazole arm of histidine from another ligand, addition of excess imidazole competes with histidine imidazole and forms mononuclear complex. Imidazole, being a stronger ligand, tends to occupy the equatorial position rather than the axial position even at the expense of shifting other coligands to the axial position. This stronger preference of imidazole for the equatorial position switches the histidine containing ligand coordination

mode where carboxylate coordinates axially only in the imidazole complex.

We have identified that binding preference of histidine as in-plane ligand to Cu(II) is the most important factor in the formation of octanuclear capsule. Analyzing the networks and molecular units prepared in this section we have now several clues as how to control the network formation.

Chapter 3

Effect of aromatic ring substitution and ligand chirality on the formation of the capsule

Effect of aromatic ring substitution: We have prepared L-histidine derived ligand with methoxy substitution on the phenolic ring at 3 and 5 positions. The reason for keeping histidine has been discussed in the previous section. We were able to structurally characterize 5-methoxy derivative which shows formation of octanuclear capsule (Figure 1). In the case of 3-methoxy derivative, Electro Spray Ionization – Mass (ESI-Mass) supports the formation of similar octanuclear complex (Figure 1).

Characterization of these two new capsules signifies that substitution in the aromatic ring does not destabilize the capsule. The vertical size of the capsule increased from 13 Å to 19 Å in the 5-methoxy substituted capsule. Comparing this new structure with the earlier one without substitution we also found that organization of capsules in the lattice is different. Packing is tighter and crystals are more stable.

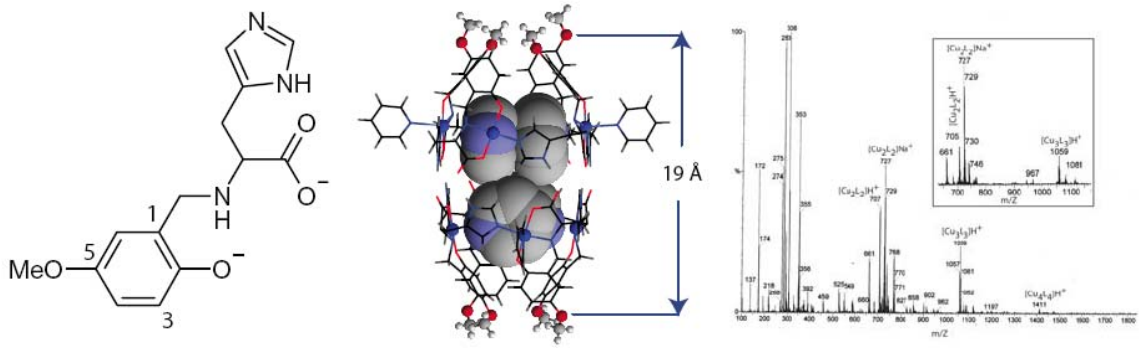

Figure 1. *The ligand, new capsular complex and the ESI-Mass of the 3-methoxy complex. The mass of of the corresponding 5-methoxy complex is shown as inset.*

Effect of ligand chirality: We have also studied the effect of ligand chirality on the capsule formation by trying to form Cu(II) capsule with L-histidine (1), D-histidine and DL-histidine derived ligand. With D-histidine we were able to get the capsule mirror image to that of L-histidine. There were two possibility with racemic ligand, either a racemic crystal will form with both type capsule in the lattice or spontaneous resolution will result in mixture of both D-type and L-type crystals, as is the case for numerous other chiral complexes. We obtained immediate precipitation of a green solid insoluble in any organic solvent or water. Same insoluble solid was precipitated when D and L version of the capsule mixed together. It is likely that the presence of mirror image units prevents the formation of C4 symmetric cycle necessary for capsule formation and

instead promotes polymerization (Scheme II). This result shows that ligand homochirality is a necessary condition for the formation of capsule.

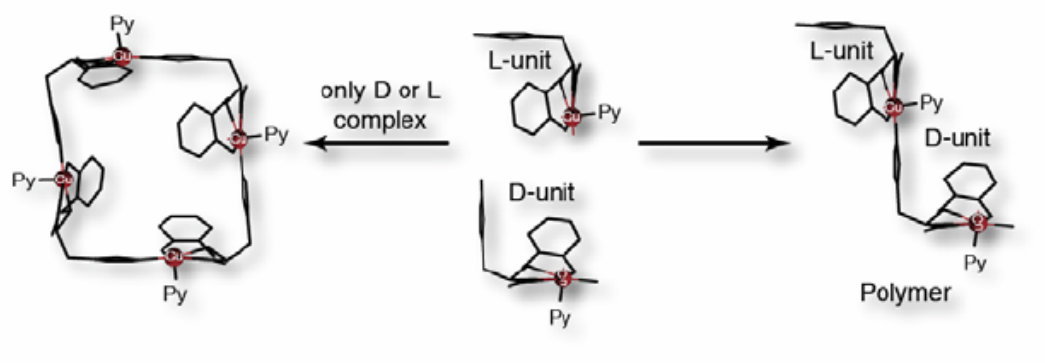

Scheme II. *Formation of the polymer when racemic ligand has been used*

Chapter 4

Effect of substitution on the pyridine ring and consequently formation of a series of Cu(II) complexes with chiral channels

In this chapter we have tried to understand the effect of substitution on the pyridine ring (guest) on the capsule formation. Methyl (sterically bulky) or hydroxo (H-bonding capable) substitution on the pyridine yielded monomeric Cu(II) complexes instead of the capsular assembly. Interestingly, the monomeric complexes showed formation of 1D chiral channels filled with removable water molecules in the crystals. Choosing substitution on the pyridine we were able to vary the size of the channels (Figure 2). A test on the removability of the waters molecules using TGA has been done. Crystals with channels are important class of compounds with various applications.

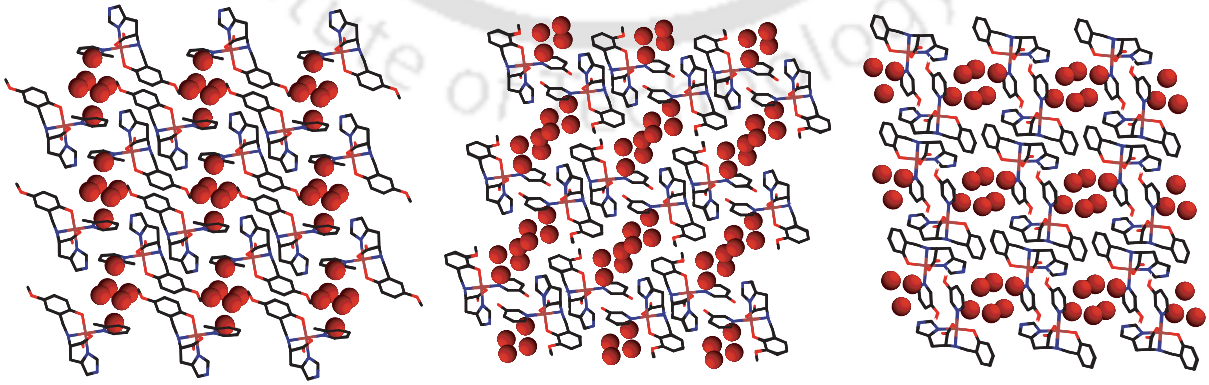

Figure 2. *1D chiral channels in the monomeric Cu(II) complexes*

Chapter 5

Effect of changing ligand denticity and metal: ligand ratio leading to the formation of a Trinuclear assembly of Cu(II)

In this chapter we have synthesized and structurally characterized a different type of capsule by using L-valine derived ligand (tridentate) and changing the metal: ligand ratio from 1:1 to 1:2. The new assembly consists of three mononuclear units of Cu(II), accommodating both cation and anion of a binary salt with general formula [K{Cu(HS-Val)$_2$}$_3$]ClO$_4$] (Figure 3).

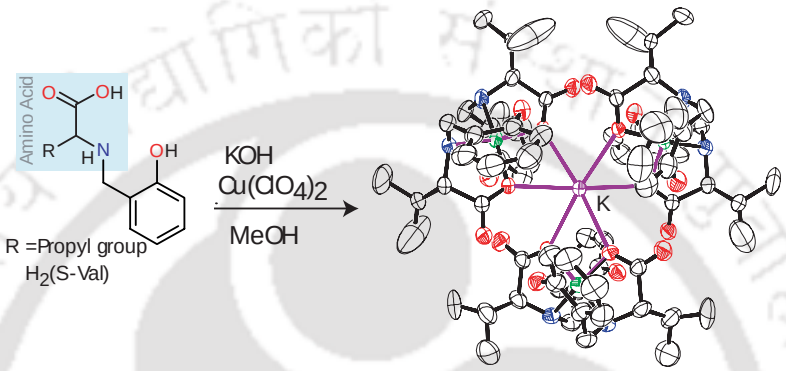

Figure 3. *Synthesis and molecular structure of trinuclear Cu(II) complex*

The three units of Cu(II) encapsulating the alkali metal ion in a hexadentate fashion while the oxo anions H-bonded to a chiral pocket on the surface of the capsule.
Six short (~2.5 Å) H-bonding between the Cu(II) units provide additional structural support to the capsule.

Chapter 6

Isolation of kinetically resolved conformational isomers of Ni(II) with L-tyrosine and L-tryptophan derived ligand

Continuing with tridentate amino acid derived ligands we have characterized Ni(II) complexes of L-tyrosine and L-tryptophan derived ligands. We had observed earlier that L-tyrosine derived ligand behaves as tridentate ligand (Chapter 2). Keeping the metal:Chiral ligand ratio intact 2:1 like previous chapter, but we added additional co-ligand phenanthroline in the reaction mixture. We wanted to check if this co-ligand is capable of replacing one of the chiral ligand and if it does then whether it is possible to organize it achirally within the crystal. The competition between chiral ligand and phenanthroline will show the relative strength of the ligand. If phenanthrolines do get incorporated in the crystal then due to the chiral nature of the complexes, phenanthrolines have to be organized achirally. Achiral arrangements of photoactive molecules are

important for the observation of non lineral optical property (NLO). Synthesis and structural characterization of the complexes showed: (a) octahedral Ni(II) complexes formed with two bidentate chiral ligands and phenanthroline where phenol groups of the chiral ligand were protonated form, (b) a set of structurally different isomers of Ni (II) complexes has been isolated from the same reaction due to the conformational change of the ligand due to rotation around single bond, (c) phenanthrolines units were organized achirally in the lattice (Figure 4).

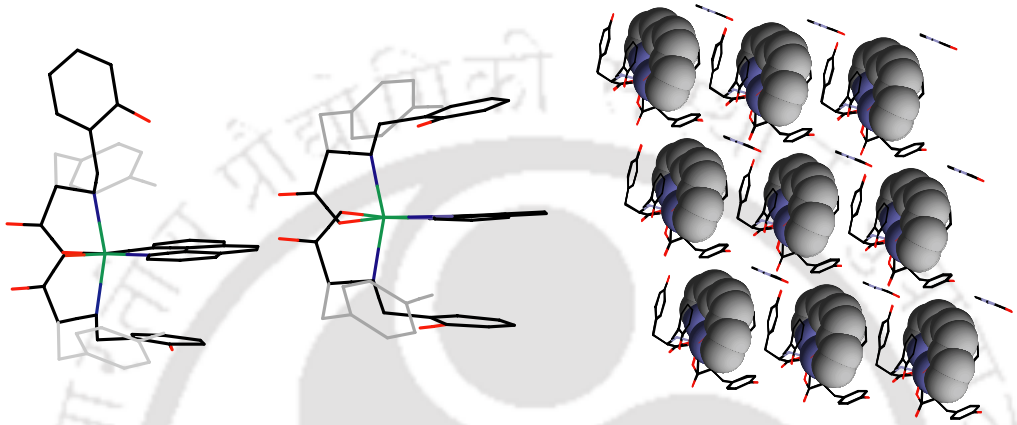

Figure 4. *Structurally different isomers (left) and the organization of phenanthroline in the lattice of one complex(extreme right)*

Chapter 7

Synthesis of aniline formaldehyde condensate (AFC) polymer as micron sized polymer sphere

As we have explained in the beginning that we intend to attach chiral complexes / receptors onto the polymer support, we choose to synthesize aniline polymers because of having amine group at the terminal end. It is easier to make derivatives of amines. In this chapter we have taken a known polymerization reaction between aniline and formaldehyde, forming usually a resinous sticky polymer used in the adhesive industry. We were able to form solid polymer instead of sticky substance by performing the synthesis in presence of simple alcohols. By lowering the reaction temperature and addition of alcohols like methanol, *t*-butanol, isopropanol and glycerine we have prepared solid polymers with different morphology (Figure 5). We have also characterized ~1 micron sized polymer spheres in bulk quantity (multi gram) using *t*-butanol in the synthesis. The polymers have been characterized using elemental analysis, MALDI-Mass, IR spectroscopy. To test the usefulness of the polymers and to probe the accessibility of the amine functional groups by external reagents, we measured metal removal property of

the polymers using Cr(VI) as a test case. All the polymers remove Cr(VI) from aqueous solution efficiently. Variation in metal removal capacity among the polymers also demonstrate that (a) the amine groups are accessible to outside reagent (b) the morphology plays a major role in the metal binding property (c) the template effect of *t*-butanol made the spheroids with free amine groups mostly in the inner surface. A mechanism for the formation of micron sized spheres has been proposed.

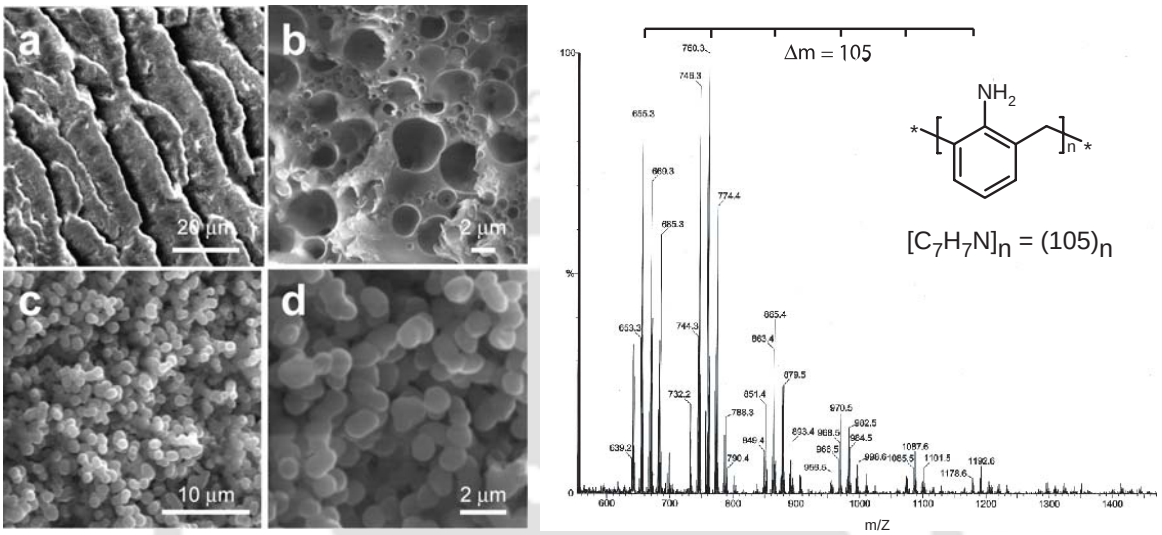

Figure 5. *SEM micrographs of polymers prepared in presence of (a) MeOH, (b) isopropanol (c) and (d) t-BuOH and MALDI-Mass of polymer (t-BuOH)*

Chapter 8

Synthesis of Schiff bases with oligoaniline having amines at both end

In this chapter we have focused on another aniline based polymer namely polyaniline. This is a linear polymer with amine as the terminal group. We started with synthesizing low molecular weight oligoaniline and their Schiff base derivative as these will be easier to characterize using usual molecular characterization techniques such as NMR and mass (Scheme III).

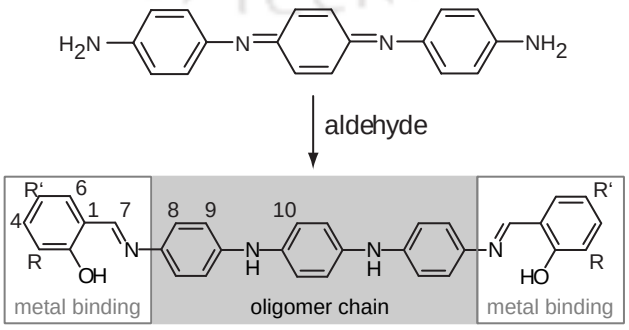

Scheme III. *Synthesis oligoaniline*

The chemistry can then be repeated with higher molecular weight polymers. We have synthesized a set of oligoanilines where Schiff base could be formed at the both end of the oligoaniline. We observed a reduction of the oligoaniline unit during Schiff base formation. This highlights the non innocent nature of the Schiff bases. Electrochemical properties of the ligands were explored using cyclic voltammetry. During the complexation reaction of the Schiff bases with Cu(II) we serendipitously discovered a new transformation from one of the Schiff base to a highly fluorescent, fluorescence active pyrido[1,2-a] quinoxalinylium derivative (Scheme IV). A mechanism of the reaction based on the reactions with different metal ions and oxidizers has been proposed. Metal complexation of the other Schiff bases has not been done.

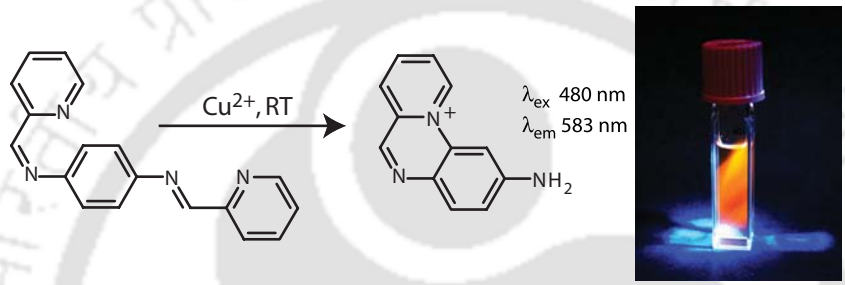

Scheme IV. *Synthesis of the new fluorescent dye*

Contents

1	Statement	ii
II	Certificate	iii
III	Course Certificate	iv
IV	Acknowledgements	v
V	Abstract	vii
VI	Contents	xv
VII	***Chapter 1–Introduction***	
	1.1 Non- covalent organic capsule based on resorcin[4]arene and Glycoluril derivative	2
	1.1.1 Metal-organic capsule based on Resorcin[4] arene-derived	3
	1.2 Metal-organic capsule or cage like structure based on heterocyclic multidentate ligand	6
	1.3 Chirality in the host design	9
	1.4 Complexes with amino acids based reduced Schiff base ligand	9
VIII	***Chapter 2- Effects of amino acid side chain, pyridine, and imidazole on the octanuclear Cu(II) assembly***	
	2.1 Experimental Section	15
	2.1.1 Solvents and Reagents	15
	2.1.2 Measurements	16
	2.2 Syntheses	16
	2.2.1 *S*-2-(2-Hydroxybenzylamino)-4-methylsulfanylbutyric acid. [H_2*S*-met] (1)	16
	2.2.2 *Rac*-2-(2-Hydroxybenzylamino)-4-methylsulfanyl butyric acid. [H_2*rac*-met] (2)	17
	2.2.3 [Cu_2 (*S*-met)$_2$] (1a)	17
	2.2.4 [Cu(*S*-met)·(imidazole)] (1b)	18
	2.2.5 [Cu_2 (*rac*-met)$_2$] (2a)	18
	2.2.6 [Cu (*rac*-met)(pyridine)$_2$] (2b)	18
	2.2.7 [Cu (*S*-tyr)(pyridine)$_2$] (3a)	18
	2.2.8 X-ray Data Collection, Structure Solution and Refinement	19
	2.3 Results and Discussion	20
	2.3.1 Syntheses and Selected Properties	21
	2.3.2 X-ray Structure of [Cu_2(*S*-met)$_2$] (1a)	22
	2.3.3 X-ray Structure of [Cu(*S*-met)(Imidazole)] (1b)	23
	2.3.4 X-ray Structure of [Cu(*Rac*-met)·(Pyridine)$_2$] (2b)	24
	2.3.5 X-ray Structure of [Cu(*S*-tyr)(Pyridine)$_2$] (3a)	24
	2.4 Effects of amino acid side chain, solvent (MeOH, Pyridine) and imidazole on the Cu(II) complexes	25

2.4.1 Complexation in MeOH with different amino acids 25

2.4.2 Role of pyridine 26

2.4.3 Role of Imidazole 26

2.4.4 Absorption Spectra and EPR spectral characteristics 27

Conclusion 30

References 34

IX ***Chapter 3 - Effect of aromatic ring substitution and ligand chirality on the formation of the capsule***

3.1 Experimental Section 35

3.1.1 Solvents and Reagents 35

3.2 Syntheses 35

3.2.1 *S*-2-(2-hydroxy-5-methoxy-benzylamino)-3 (1H-imidazol-4-ylpropanoicacid): [H_2*S*-5Omehis] (1) 35

3.2.2 *S*-2-(2-hydroxy-3-methoxy-benzylamino)-3- (1H-imidazol-4-ylpropanoicacid): [H_2*S*- 3Omehis] (2) 36

3.2.3 [Cu_8(*S*-5omehis)$_8$(Pyridine)$_8$] (1a) 36

3.2.4 [Cu_2(S-5OMehis)$_2$]·3H_2O (1b) 37

3.2.5 Complexation reaction with H_2 *S*-3omehis 37

3.2.6 [Cu_8(*R*-his)$_8$(Pyridine)$_{10}$] (3a) 37

3.2.7 Complexation reaction with (H_2*Rac*-his) 37

3.2.8 A note on elemental analysis 38

3.2.9 X-ray data collection, structure solution and refinement 38

3.3 Results and Discussion 40

3.3.1 Syntheses and Selected Properties 40

3.3.2 X-ray structure of [Cu_8(*S*-5omehis)$_8$(Pyridine)$_8$] (1a) 41

3.3.3 X-ray structure of [Cu_8(*R*-his)$_8$(Pyridine)$_{10}$] ·2Pyridine (3a) 45

3.3.4 ESI-MS analysis of the octanuclear complexes 45

3.3.5 Effect of ligand chirality 46

3..3.6 X-ray structure of [Cu_2(*S*-5omehis)$_2$]•3H_2O (1b) 47

3.3.7 Absorption and EPR spectra 49

Conclusions 52

References 52

X ***Chapter 4 – Effect of substitution on the pyridine ring and consequently formation of a series of Cu(II) complexes with chiral channels***

4. 1 Experimental Section 55

4.1.1 Solvents and Reagents 55

4.2 Syntheses of Cu(II) complexes 55

4.2.1 [Cu(S-his)(3-Hydpyridine)]·3H_2O (1a) 55

4.2.2 [Cu(S-5Omehis)(3-Hydpyridine)]·3H_2O (2a) 56

4.2.3 [Cu(S-5Omehis)(2-Mepyridine)]·3H_2O (2b) 56

4.2.4 [Cu(S-3Omehis)(3-Hydpyridine)]·4H2O (3a) 56

4.2.5 X-ray Data Collection, Structure Solution and refinement 56

4.3 Results and Discussion 58

4.3.1 Syntheses and Selected Properties 58

4.3.2 X-ray Structure of [Cu(S-his)(3Hydpy)]·3H_2O (1a) 59

4.3.3 X-ray Structure of [Cu(S-5OMehis)(3Hydpy)]·3H_2O (2a) 60

4.3.4 X-ray Structure of [Cu(S-5OMehis)(2Mepy)]·3H_2O (2b) 60

4.3.5 X-ray Structure of [Cu(S-3OMehis)(3Hydpy)]·4H_2O (3a) 64

4.3.6 Absorption and EPR Spectral Characteristics 64

Conclusion 67

References 67

XI ***Chapter 5 – Effect of changing ligand denticity and metal: ligand ratio leading to the formation of a Trinuclear assembly of Cu(II)***

5.1 Experimental Section 69

5.1.1 Solvents and Reagents 69

5.2 Syntheses 69

5.2.1 2-(2-Hydroxy-benzylamino)-3-methyl-butyric acid: [H_2S-Val] (1) 69

5.2.2 [K{Cu(HS-Val)$_2$}$_3$]ClO_4]·(CH_3CN)$_2$(1a) 70

5.2.3 X-ray data collection, structure solution and refinement 70

5.3 Results and Discussion 70

5.3.1 Synthesis and Selected Properties 70

5.3.2 [K{Cu(HS-Val)$_2$}$_3$]ClO_4] (CH_3CN)$_2$ (1a) 71

5.3.3 Absorption and EPR spectral study 74

Conclusion 75

References 75

XII ***Chapter 6 – Isolation of kinetically resolved conformational isomers of Ni(II) with L-tyrosine and L-tryptophan derived ligand***

6.1 Experimental Section 77

6.1.1 Solvents and Reagents 77

6.2 Syntheses 78

6.2.1 2-(2-Hydroxy-benzylamino)-3-(1H-indol-7-yl)-propionic acid [H_2*S*-trypt] (2) 78

6.2.2 [Ni(*S*Htyr)$_2$(Phen)]·(DMF)$_2$](1a)and [Ni(*S*Htyr)$_2$(Phen)]·(DMF)·(H_2O)$_4$] (1b) 78

6.2.3 [Ni(H*S*-trypt)$_2$(Phen)]·CH_3OH (2a) 79

6.2.4 X-ray Data Collection, Structure Solution and refinement 80

6.3 Results and Discussion 80

6.3.1 Syntheses and Selected Properties 80

6.3.2 Crystal structure of [Ni(*S*-Htyr)$_2$(Phen)]·(DMF)$_2$ (1a) 83

6.3.3 Crystal structure of [Ni(*S*-Htyr)$_2$(Phen)]·4H_2O·DMF (1b) 83

6.3.4 Crystal structure of [Ni(*S*-Htryp)$_2$(Phen)]·H_2O·CH_3OH (2a) 86

6.3.5 UV-Visible spectrum 87

Conclusion 88

References 89

XIII ***Chapter 7 – Synthesis of aniline formaldehyde condensate (AFC) polymer as micron sized polymer sphere***

7.1 Experimental Section 91

7.1.1 Solvents and Reagents 92

7.1.2 Measurements 92

7.2 Syntheses 92

7.2.1 General Synthesis of the polymers 92

7.2.2 Synthesis of Polymer in presence of t-butanol 93

7.3 Results and Discussion 93

7.3.1 Synthesis and characterization 93

7.3.2 MALDI-TOF Mass spectral analysis 94

7.3.3 Stability of the polymers 96

7.3.4 Scanning Electron microscopy 96

7.3.5 Chromium removal property 99

Conclusion 100

References 101

XIV *Chapter 8-Synthesis of Schiff bases with oligoaniline having amines at both end*

8.1 Experimental Section 103

8.1.1 Solvents and Reagents 103

8.1.2 Measurements 104

8.2 Syntheses 104

8.2.1 N,N′-Bis(4′-Aminophenyl)-1,4-Qunonenediimine (1) 104

8.2.2 Schiff Base with Salicylaldehyde (2) 105

8.2.3 Schiff Base with *3*-OMe-Salicylaldehyde (3) 105

8.2.4 Schiff Base with *5*-OMe-Salicylaldehyde (4) 105

8.2.5 N,N'-Bis-pyridine-2-ylmethylene-benzene-1,4-diamine (5) 106

8.2.6 2-Amino-pyrido[1,2-a]quinoxalin-11-ylium perchlorate ([6]ClO_4) 106

8.2.7 2-Amino-pyrido[1,2-a]quinoxalin-11-ylium thiocyanate ([6]SCN) 106

8.2.8 Reactions of 5 with $(NH_4)_2Ce(NO_3)_6$ and $(NH_4)_2S_2O_8$ 106

8.2.9 Reactions of 5 with $HClO_4$ 107

8.2.10 X-ray data collection structure solution and refinement 107

8.3 Results and Discussion 108

8.3.1 Synthesis and characterization of oligoaniline Schiff bases 108

8.3.2 Electrochemical Properties 109

8.3.3 Synthesis of 2-Amino-pyrido[1,2-a]quinoxalin-11-ylium perchlorate $([6])^+$ 110

8.3.4 Structure of pyrido[1,2-a] quinoxalinylium ion ($[6]^+$) 110

8.3.5 Proton NMR of [6]ClO_4 114

8.3.6 Electronic and fluorescence spectroscopic properties of [6]ClO_4 115

8.3.7 Mechanism of the formation of $[6]^+$ 116

Conclusion 118

References 119

XV. **Findings of the thesis** 121

XVI **List of Publications** 125

XVII **Appendix** A

Chapter 1

The term, *confined space* may be defined as space within a lattice of the molecular crystal that permits to accommodate different size and shape of the molecules and also to do chemistry within the space of the cavity.[1] From the scientific point of view and technological interest the molecules with confined space are enormously important because of their ability to act as reaction container with catalysis by offering high concentration of reactant inside the confined space, gas storage, molecular recognition and to more advanced technological applications as chemical sensors, electrodes, data imaging and storage materials, and even lasers. For example, Rebek *et al*. showed that the rate of reactivity of Diels-Alder reaction accelerated nearly 200-fold inside the dimeric capsule, based upon glycoluril subunit.[2] K. N. Raymond *et al*. reported a highly charged, water-soluble, metal-ligand assembly with a hydrophobic interior cavity that thermodynamically stabilizes protonated substrates and consequently catalyzes the normally acidic hydrolysis of orthoformates in basic solution, with rate accelerations of up to 890-fold.[3] K. Kim *et al*. prepared a homochiral metal-organic porous material that allows the enantioselective inclusion of metal complexes in its pores and catalyses the trans esterification reaction in an enantioselective manner.[4] Aoyama *et al.* reported selective crystalline-phase guest addition, removal and exchange within the cavity, formed by anthracene-bis(resorcinol) derivatives.[5] Hulliger *et al* demonstrated organic photorefractive materials which have potential application in the fields of high-density optical storage and image-processing techniques.[6] Schuth *et al.* have aligned and elongated highly polarisable pyridinium perchlorate derivative within the parallel channels of molecular sieve $AlPO_4$-5 which demonstrated laser action upon exciting the frequency.[7] Stang *et al* developed organic square molecule including chiral square as well as their application to catalysis, porous sensing and filtering materials.[8] Thus synthesizing molecules with confined space of different shape like cages, squares and capsule are challenging to a chemist.

Syntheses of a diverse set of molecules or molecular assemblies containing empty space capable of accommodating guest molecules have been reported in the recent literature. These can be broadly classified into two sets; (a) those using resorcinarene and calixarene derivatives where large organic molecule determines the frame of the host and (b) those using metal complexes of smaller multidentate heterocyclic ligands where metal ion helps in the assembly and provides rigidness to the host.[9]

1.1 Non- covalent organic capsule based on resorcin[4]arene and Glycoluril-derivative

This section focuses on larger resorcin[4]arene and pyrogallol[4]arene nanocapsules. Rebek and co-workers have published an outstanding series of non-covalent dimeric capsules based upon the dimerization of glycoluril derivatives **1** (Figure 1.1) through its intrinsic curvature and multiple hydrogen- bonding groups some of which are known as 'tennis balls' or 'softballs' **2** (Figure 1.1). By variation of the spacer in the glycoluril units Rebek *et al.* controlled the volume of the cavity and encapsulated large guest molecules **3** (Figure 1.1).[2,10] Recently they demonstrated the broad series of elegant solution phase studies outline the behavior of encapsulated species within this cylindrical capsules. [11]

Gibb and co-workers have invested considerable effort into the extension of the upper rim of cavitands, thereby affording new classes of 'deep-cavity' cavitands **4** (Figure 1.1). They have also shown how these molecules self-assemble into dimeric species that have hydrophobic pockets capable of controlling photophysical properties of aromatic molecules.[12] These water-soluble capsules are even capable of sequestering and separating hydrocarbon gases that are present in the headspace above the aqueous phase.[13]

Recently, Ananchenko *et al.* has described a series of van der Waals capsular **6** assemblies formed by a series of p-alkanoylcalix[4]arenas **5** (Figure 1.1).[14] The particular novelty associated with these assemblies is the ability to exchange the encapsulated guest species within a single crystal.[15] They also exhibited phototransformation of cis and trans stilbene.[16]

Böhmer and co-workers have studied a series of 'tetra-urea' calixarenes **7** (Figure 1.2) that form dimeric capsules **8** (Figure 1.2).[17,18] These capsules can be used to form monolayer on gold surfaces, and the complimentarily of these molecules has been adapted to form cores for dendrimes that are based on tris-complementary type core species linked to 'tetra-urea' calixarenes.[19]

1.1.1 Metal-organic capsule based on Resorcin[4]arene-derivative

Atwood *et al.* reported self-assembly of hydrogen-bonded nano-capsules based on C-methylresorcin [4] arene or the C-alkylpyrogallol [4] arenes, by changing the upper or lower rim of the corresponding units.[20,9] They have also reported a chiral hexameric capsule in the solid state.[21] Recently, they have focused on quantitative conversion of pyrogallol[4]arene monomers into corresponding hexameric nano-capsules and also the

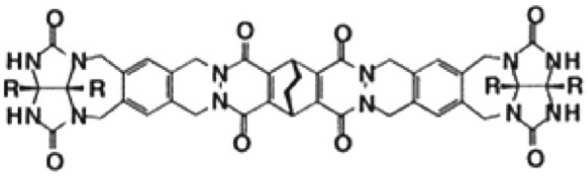

1

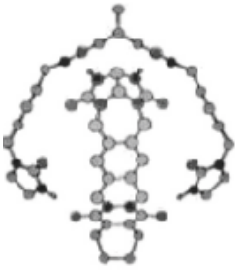

"softball"

2

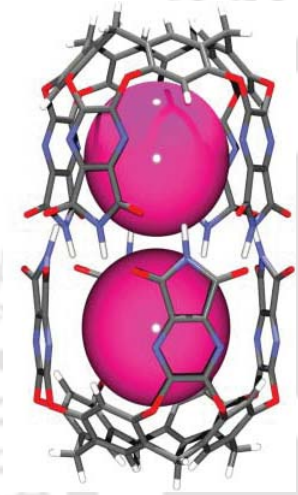

3

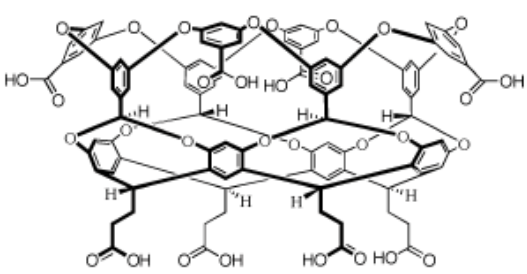

4

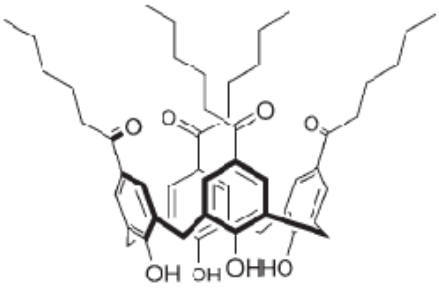

para-hexanoylcalix[4]arene

5

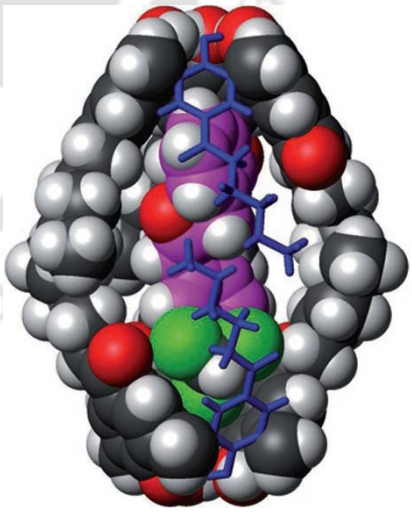

6

Figure 1.1. *Non-covalent organic capsules*

assembly of metal–organic nano-capsules (MONC's) (Cu, Ga) based on preformed capsule as template (Figure 1.3).[22] The capsule **9** contains total 24 Cu metal centers into

all of the theoretical square planar binding sites. This capsule further assemble through coordination of the propanol tails to Cu centres of neighbouring MONC's, the result being an insoluble coordination polymer. They also investigated to encapsulate the probe molecules within these large assemblies with a view to reporting on the interior of this voluminous capsules.[23, 9]

Harrison and co-workers have synthesized a series of resorcin[4]arene-based cavitands **10** (Figure 1.3) that possess 'upper rim' functionalized with iminodiacetate groups as well as dipyridylimino groups which were useful for metal complexation with copper, iron and cobalt **11** (Figure 1.3) for example.[24] They also showed a series of elegant structures based on dimeric tetra-metallated capsules that can be pH dependent, and that can reversibly capture organic molecules from water.[25]

Dalcanale and co-workers have synthesized a series of coordination cages based on cavitands possessing 'upper-rim' nitrile functionality **12** (Figure 1.3).[26] These building blocks, when combined with square planar metal centres for directed self-assembly,

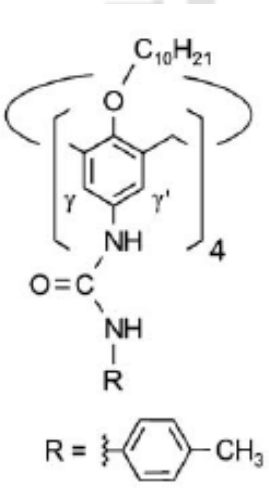

7

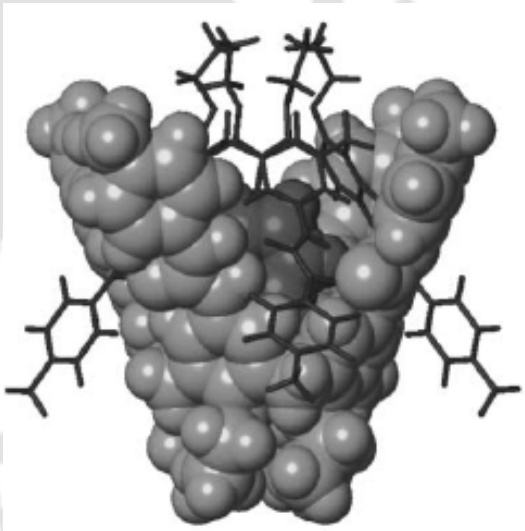

8

Figure 1.2. *Non-covalent calixarene based dimeric capsule*

afford dimeric capsules **13** (Figure 1.3) that have varied anion encapsulation properties that have been studied extensively. By extending the 'upper-rim' functionality to 'benzonitrile', they used the same methodology to assemble a metal-organic capsule

containing large equatorial portals.[27] This alteration to the system results in a large increase in the estimated internal volume (over four times greater).

1.2 Metal-organic capsule or cage like structure based on heterocyclic multidentate ligand:

Fujita *et al.* have shown that the combination of the square planer geometry of palladium and platinum with pyridine-based bridging ligand for the construction of highly symmetric supramolecular cages and capsules.[28] The positive charges on the metal centers make the compound highly water soluble; the hydrophobic pocket provided by the ligand is capable of efficient for binding the variety of guest molecule. The triangular tridentate **14** (Figure 1.4), was assembled into a bowl-like M_6L_4 square –pyramidal cone **15** (Figure 1.4) in presence of ethylenediamine-procted Pd(II) complex which was further assembled in to a dimeric capsule **16** (Figure 1.4) in aqueous media, that accommodates as many as six neutral organic molecules.[29] Almost coplanar triangle hexadentate ligand, **17** (Figure 1.4) was combined with $[(en)Pd(NO_3)_2]$ formed almost fully closed shell molecule but it is unable to allow entry or escape of organic guest molecule during assemble. There is no direct metal-ligand bonding between the supramolecular cages or capsules that comprise the capsule halves. To demonstrate the potential of some of these large metal-organic assemblies, Fujita and co-workers are currently investigating these frameworks for uses that include chirality enrichment through enantiomer recognition.[30]

Stang and co-workers have also used pyridyl-based ligands **19** (Figure 1.4) with platinum metal centers to synthesize an impressive series of discrete metallo-supramolecular assemblies. They have used *cis* $Pt(PMe_3)_2(OTf)_2$ as a V-shaped building unit, and react the metal centers with triangular shaped ligands (such as 1,3,5- tris(4-pyridyl-*trans*-ethenyl)benzene) in a 3:2 ratio to build the discrete architectures in near quantitative yield **20** (Figure 1.4).[31] A series of self-assembled coordination cages of D_{3h} symmetry were also assembled by similar methods using slightly varied platinum subunits and tripodal pyridyl-based ligands.[32]

Raymond and co-workers have used catechol-based ligands **21** (Figure 1.5) and reacting with iron and gallium centres, the chelating effect and the presence of particular (naphthalene and pyrene) organic spacers between the catechols drives the formation of M_4L_6, **22** (Figure 1.5) cluster type assemblies (where M= Fe or Ga, and L = catechol-based ligand).[33] They have shown that a chiral self-assembled M_4L_6 supramolecular tetrahedron can encapsulate a variety of cationic guests with varying degrees of

stereoselectivity. Recently, they encapsulated reactive iridium guests and the C-H bond activation of aldehydes occurs with the host cavity controlling the ability of substrates to interact with the metal center based upon size and shape. In addition, the host container can act as a catalyst itself by restricting reaction space and preorganizing the substrates into reactive conformations.[34]

Saalfrank and co-workers used the tris-bidentate 4-acyl-2-pyrazolin-5-one ligand **23** (Figure 1.5) with gallium centres to assemble M_6L_6 clusters **24** (Figure 1.5**)** that they describe as a 'cylinder'[35] Further modification of the trigonal ligand framework so as to generate tris-malonate-based chelator ligands, followed by combination with iron chloride, resulted in the formation of tetra- and hexa-nuclear metal clusters depending on particular functionalities (O-tBu or O-tolyl, respectively) placed on the ligand framework[36]

1.3 Chirality in the host design.

Chirality and porosity play important role in chemistry and biology. Enantiopure capsular assembly or cages have the potential to discriminate between the enantiomer enrichment and even resolution inside a cavity. These can be employed for chiral sensor, enantiopure drug synthesis, stereo specific synthesis etc. Thus it is important and challenging to design chiral hosts. Incorporation of chirality however is not trivial and fewer reports on chiral host are available. K. Kim *et al.* reported chairal nanoporus channel which is used for preferred binding of an enantiomer.[4] Rebek *et al* showed chiral polymers changing frequency of a quoted crystal with one enantiomer and diastereomeric encapsulation using chiral capsules.[37] Rosseinsky group reported homochiral permanently microporous material with three dimensional channel system that retains crystallinity upon guest loss and displays enantioselective sorption of guests.[38] Sansone group reported chiral dimeric capsules from N, C-Linked Peptidocalix[4]arenas, self-assembled through an antiparallel β-sheet-like motif and characterized these capsules by NMR and ESI-Ms. The importance of the capsule is the robustness of the cage that can be modulated by changing length, nature, and number of the peptide chains up to the formation of α-helices.[39]

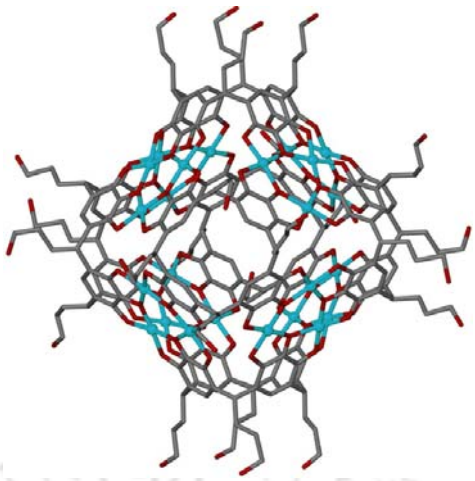

9

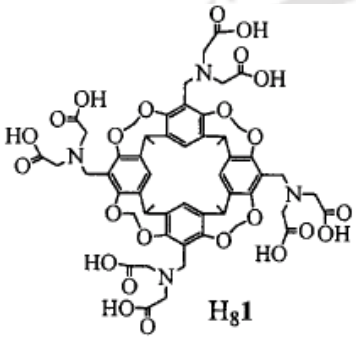

10

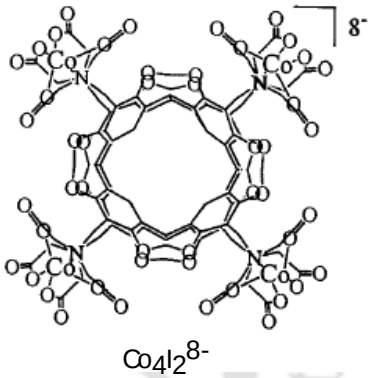

$Co_4I_2^{8-}$

11

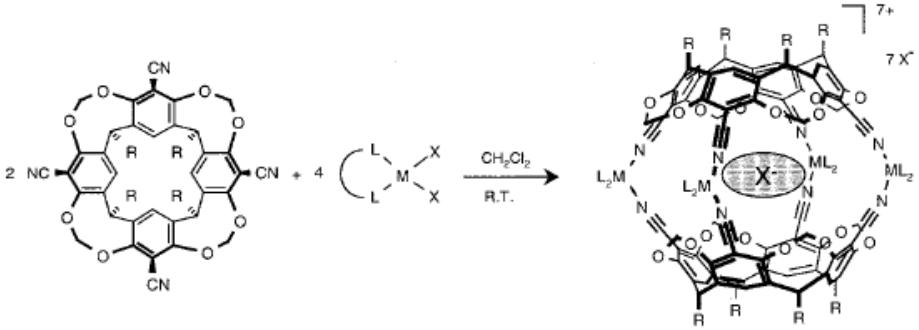

12

13

Figure 1.3. *Resorcin[4]arene-derived metallo-organic capsules*

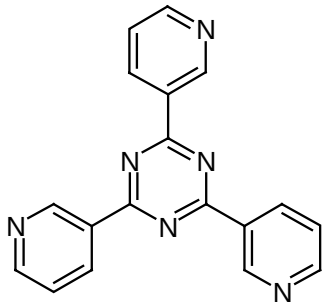

14

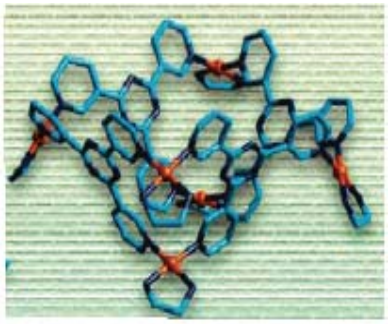

15

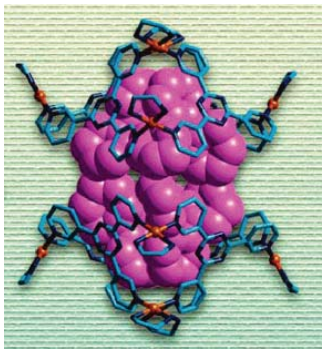

16

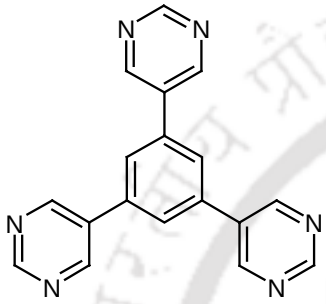

17

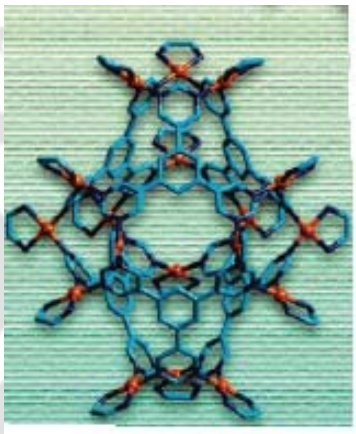

18

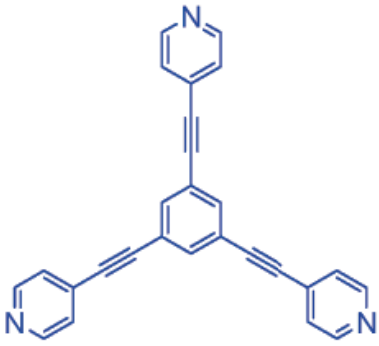

19

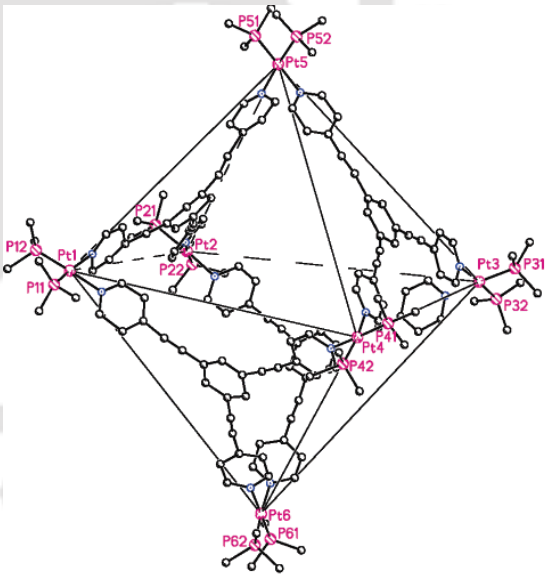

20

Figure 1.4. *Complexes (cages or capsules) based on tris(pyridine) based ligand*

1.4 Complexes with amino acids based reduced Schiff base ligand

Earlier our group reported synthesis and characterization of a octanuclear Cu(II) complex **25** with L-histidine derived reduced Schiff base ligand **26** which accommodated four pyridine inside its capsular cavity (Scheme 1.1).[40] It was one of a kind having chirality, H-bonding and labile metal centre within the same molecule. Using the same ligand our group also reported hydroxo bridged one dimensional water removable channel using the Fe(III) metal ion **27** (Scheme 1.1).[41]

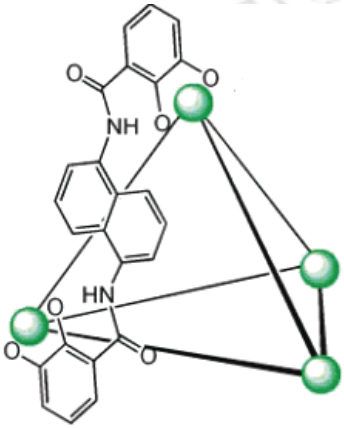

21

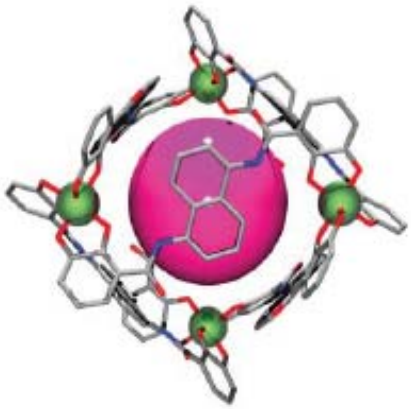

= Fe, Ga Metal

22

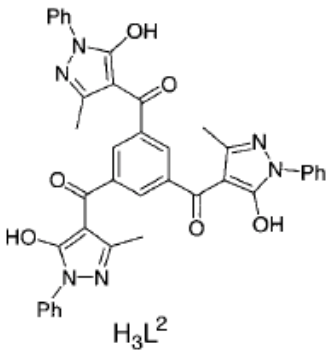

23

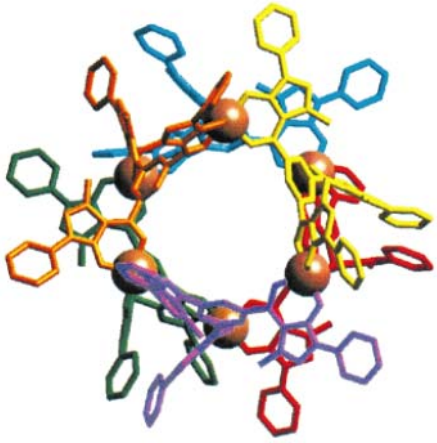

24

Figure 1.5. *Metalo-organic clusters with multidentate heterocyclic ligand*

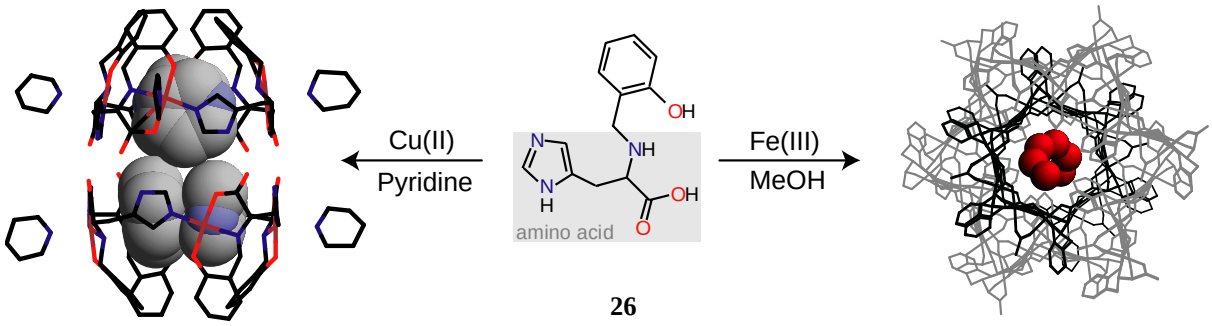

25 **26** **27**

Scheme 1.1. *Formation of octanuclear Cu(II) and hydroxo bridged water removable channel of Fe(III)*

\

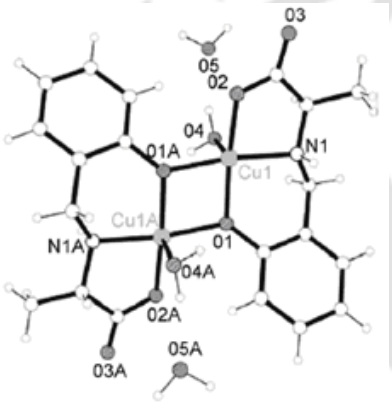

28

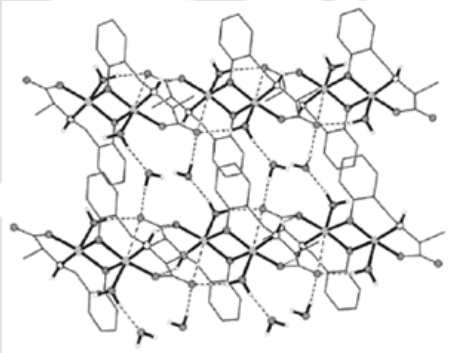

29

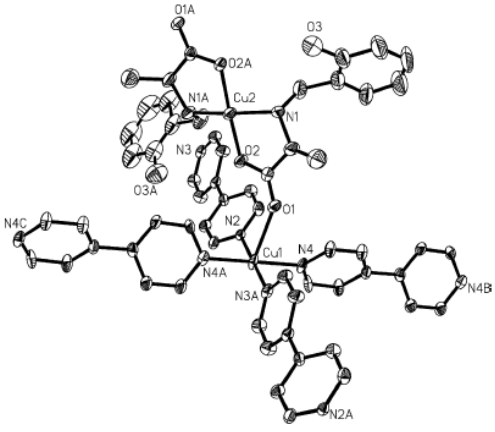

30

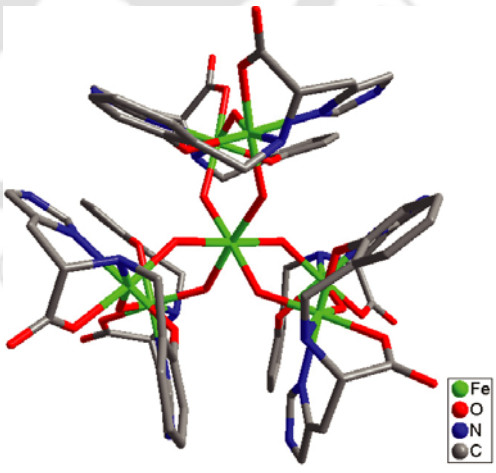

31

Figure 1.6. *Metal complexes with reduced amino acid Schiff base ligand*

This kind of ligands (amino acid derived reduced Schiff base) have employed by several groups. For example, Ranford group reported several Cu(II) complexes with this type of ligands as models for the intermediate species in biological racemization and transamination reactions.[42] Using reduced Schiff base ligands derived from salicylaldehyde as well as various substituted salicylaldehydes with amino acids Vittal *et al* reported phenoxobridge binuclear complex **28** (Figure 1.6) and their diversity in networked structure **29** (Figure 1.6) using either water and methanol as solvent in which metal ligand ratio 1:1. [43]

Hong *et al* reported a chiral supramolecular architecture by alanine derived reduced Schiff base ligand and 4, 4′-bipirydine, **30** (Figure 1.6) $[Cu_2(4,4'\text{-bipy})_2(s\text{-}ala)_2]_n.4.5nH_2O]$ (sala = N-(2-hydroxybenzyl)-L-alanine anion).[44] X-ray single crystal diffraction analysis reveals that complex **28** has a 3D extended structure in which the mononuclear anions $[Cu(s\text{-}ala)_2]_2$ are bonded to $[Cu(4,4'\text{-bipy})_2]$ cations through Cu–O bond. Recently, Yan *et al* reported chiral heptanuclear Fe(III) cluster **31**(Figure 1.6) using histidine derived reduced Schiff base ligand.[45]

From these reports we have noticed that using similar reduced Schiff base ligand, complexes with different nuclearity have been formed by changing the solvent.[40-43] However, systematic studies on the effects of substitution of the ligand, external ligand like imidazole, substituted pyridine and different metal/ligand ratio on the formation of octanuclear assembly of Cu(II) **25** has not been studied in details. Thus we felt the necessity to explore the coordination chemistry of these ligands with different metal ions to understand the factors responsible for the formation of complexes with different nuclearity. For this we chose the octanuclear Cu(II) assembly and systematically varied (a) the amino acid and solvent (Chapter 2), (b) substitution on the aromatic ring (Chapter 3), (c) substitution on the pyridine (Chapter 4), (d) ligand:metal ratio (Chapter 5) and (e) use of additional bidentate ligand (Chapter 6) to explore the effect on the formation of the assembly.

Additionally, as we intend to attach the chiral hosts on to a solid surface for chiral discrimination in future, we have chosen to synthesize polymers with functional groups. In this section we have focused on synthesis and characterization of (a) aniline formaldehyde condensate polymer (Chapter 7) and (b) functionalized oligoaniline as polyaniline precursor (Chapter 8).

References

1. Davis, M. E. *Nature*. **2002**, *417*, 813.

2. (a) Meissner, R.S. ; Rebek, J. Jr., Mendoza, D. J. *Science*, **1995**, *270*, 1485. (b) Kang, J.; Rebek, J. Jr. *Nature*, **1997**, *385*, 50.

3. Pluth, M. D.; Bergman, R. G.; Raymond, K. N. *Science*, **2007**, *316*, 85.

4. Seo, J. S.; Whang, D.; Lee, H.; Jun, S. I.; Oh, J.; Jeon, Y. J.; Kim, K. *Nature*, **2000**, *404*, 982.

5. Endo, K.; Kpoke, T.; Sawaki, T.; Hayashida, O.; Masuda, H.; Aoyama, Y. *J. Am. Chem. Soc.*, **1997,** *119*, 4117.

6. Langley, P. J.; Hulliger, *J. Chem. Soc. Rev*., **1999**, *28*, 279.

7. Ihlein, G.; Schuth, F.; Krauss, O.; Vietze, U.; Laeri, F. *Adv. Mater*., **1998**, *10*, 1117.

8. Leininger, S.; Olenyuk, B.; Stang, P. J. *Chem. Rev.*, **2000**, *100*, 853.

9. Dalgarno, S. J.; Power, N. P.; Atwood, J. L. *Coord. Chem. Rev*. **2008**, *252*, 825.

10. Rebek, J. JR.; *Acc. Chem. Res*. **1999**, *32*, 278.

11. Biros, S. M.; Rebek, J. Jr.; *Chem. Soc. Rev*., **2007**, *36*, 93.

12. Kaanumalle, L. S.; Gibb, C. L. D.; Gibb, B. C.; Ramamurthy, V. *J. Am. Chem. Soc.* **2005**, *127*, 3674.

13. Gibb, C. L. D.; Gibb, B. C. *J. Am. Chem. Soc*. **2006**, *128*, 16498.

14. Ananchenko, G. S.; Udachin, K. A.; Dubes, A.; Ripmeester, J. A.; Perrier, T.; Coleman, A. W. *Angew. Chem. Int. Ed.*, **2006**, *45*, 1585.

15. Ananchenko, G. S.; Udachin, K. A.; Pojarova, M.; Dubes, A.; Ripmeester, J. A.; Jebors, S.; Coleman, A. W. *Cryst. Growth Des*. **2006**, *6*, 2141.

16. Ananchenko, G. S.; Udachin, K. A.; Ripmeester, J. A.; Perrier, T.; Coleman, A. W. *Chem. Eur. J.*, **2006,** *12*, 2441.

17. Vysotsky, M. O.; Thondorf, I.; Böhmer, V. *Angew. Chem. Int. Ed*. **2000**, *39*, 1264.

18. Ziganshin, M .A.; Yakimova, L. S.; Khayarov, K. R.; Gorbatchuk, V. V.; Vysotsky, M. O.; Böhmer, V. *Chem. Commun.* **2006,** 3897.

19. Rudzevich, Y.; Rudzevich, V.; Moon, C.; Schnell, I.; Fischer, K.; Böhmer, V. *J. Am. Chem. Soc.* **2005,** *127*, 14168.

20. Atwood, J. L.; Barbour, L. J.; Hardie, M. J.; Raston, C. L. *Coord. Chem. Rev.* **2001**, *222*, 3.

21. MacGillivray, L. R.; Atwood, J. L. *Nature*, **1997**, 389, 469.

22. Dalgarno, S. J.; Power, N. P.; Warrenc, J. E.; Atwood, J. L. *Chem. Commun*. **2008**, 1539.

23. Dalgarno, S. J.; Tucker, S. A.; Bassil, D. B.; Atwood, J. L. *Science*, **2005**, *309*, 2037.

24. Fox, O.D.; Dalley, N. K.; Harrison, R. G. *J. Am. Chem. Soc*. **1998,** *120*, 7111.

25. Fox, O. D.; Leung, J. F. Y.; Hunter, J. M.; Dalley, N. K.; Harrison, R. G. *Inorg. Chem.* **2000,** *39*, 783.

26. Biavardi, E.; Battistini, G.; Montalti, M.; Yebeutchou, R. M.; Prodi, L.; Dalcanale, E. Chem. Commun. **2008,** 1638.

27. Zampolli, S.; Betti, P.; Elmia, I.; Dalcanale, E. *Chem. Commun*. **2007**, 2790.

28. Fujita, M.; Nagao, S.; Ogura, K. *J. Am. Chem. Soc*. **1995**, *117*, 1649.

29. Fujita, M.; Tominaga, M.; Hori, A.; Therrien, B. *Acc. Chem. Res*. **2005**, *38*, 371.

30. Yoshizawa, M.; Tamura, M.; Fujita, M. *Angew. Chem. Int. Ed.* **2007**, *46*, 3874.

31. Schweiger, M.; Yamamoto, T.; Stang, P. J.; Bläser, D.; Boese, R. *J. Org. Chem.* **2005,** *70*, 4861.

32. Kuehl, C. J.; Kryschenko, Y. K.; Radhakrishnan, U.; Seidel, S. R.; Huang, S. D.; Stang, P. J. *Proc. Natl. Acad. Sci. U.S.A.* **2002,** *99*, 4932.

33. (a) Pluth, M. D.; Bergman, R. G.; Raymond, K. N. *Science*, **2007**, *316*, 85. (b) Caulder, D. L.; Powers, R. E.; Parac, T. N.; Raymond, K. N. *Angew. Chem. Int. Ed.*

1998, *37*, 1840. (c) Terpin, A. J.; Ziegler, M.; Johnson, D. W.; . Raymond, K. N. *Angew. Chem. Int. Ed*. **2001**, *40*, 157.

34. (a) Pluth, M. D.; Raymond, K. N. *Chem. Soc. Rev.*, **2007**, *36*, 161. (b) Fiedler, D. ; Leung, D. H.; Bergman, R. G. ; Raymond, K. N. *Acc. Chem. Res*. **2005**, *38*, 351.

35. Johnson, D. W.; Xu, J.; Saalfrank, R. W.; Raymond, K. N. *Angew. Chem. Int. Ed*. **1999**, *38*, 2882.

36. Saalfrank, R. W.; Glaser, H.; Demleitner, B.; Hampel, F.; Chowdhry, M. M.; Schünemann, B.; Trautwein, A. X.; Vaughan, G. B. M.; Yeh, R.; Davis, A. V.; Raymond, K. N. *Chem. Eur. J*. **2002**, *8*, 493.

37. (a) Castellano, R. K.; Clark, R.; Craig, S. L.; Nuckolls, C.; Rebek, J. Jr. *Proc. Natl. Acad. Sci. USA* **2000**, *79*, 12418. (b) Rivera, J. M.; Martin, T.; Rebek, J. Jr. *J. Am. Chem. Soc*. **2001**, *123*, 5213.

38. Bradshaw, D.; Prior, J. T.; Cussen, E. J.; Claridge, J. B.; Rosseinsky, M. J. *J. Am. Chem. Soc*. **2004**, *126*, 6106.

39. Sansone, F.; Baldini, L.; Casnati, A.; Chierici, E.; Faimani, G.; Ugozzoli, F.; Ungaro R. *J. Am. Chem. Soc.* **2004**, *126*, 6204.

40. Alam, M. A.; Nethaji, M.; Ray, M. *Angew. Chem. Int. Ed.* **2003,** *42*, 1940.

41. Alam, M. A.; Nethaji, M.; Ray, M. Inorg. Chem. **2005**, *44*, 1302.

42. Koh, L. L.; Ranford, J. D.; Robinson, W. T.; Stevenson, J. O.; Tan, A. L. C.; Wu, D. *Inorg. Chem.*, **1996,** *35*, 6466.

43. Ganguly, R.; Sreenivasulu, B.; Vittal, J. J. *Coord. Chem. Review*, **2008,** *252*, 1027.

44. Lou, B. Y.; Yuan, D. Q.; Gao, S.; Xu, Y.; Wang, R. H.; Xu, Y. Ham, L.; Hong, M. C. *J. Mol. Struct.* **2004**, *707*, 231.

45. Ma, X. F.; Tian, J. L.; Gu, W. ; Gao, S. ; Yan, S. P.; Liao, D. Z. *Inorg. Chem. Commun.* **2008**, *11*, 256.

Earlier our group communicated the synthesis of a enantiopure octameric capsule shaped Cu(II) complex capable of trapping four pyridine molecules inside the cavity.[1] Using the same L-histidine derived ligand our group had also reported the water removable helical channel with Fe(III).[2] Using similar type of ligand Vittal and coworkers reported the isolation of mostly binuclear Cu(II) complexes from MeOH with similar amino acid derived ligands.[3] Thus we felt the necessity to understand the factors responsible for the formation of complexes with different nuclearity by exploring the co-ordination chemistry of this type of ligands with Cu(II) ion. In this chapter we have synthesized, characterized and structurally isolated a set of Cu(II) complexes of different nuclearity by varing amino acids, solvent and external monodentate ligand to understand the factors responsible for the structural diversity.

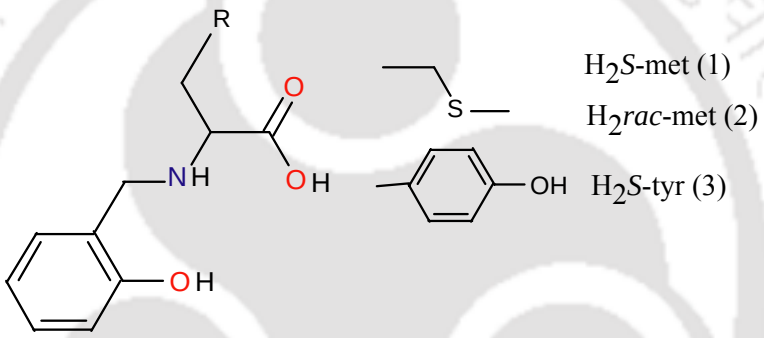

Scheme 2.1. *Ligands used in this chapter*

2.1 Experimental section

2.1.1 Solvents and reagents

Solvents and reagents were obtained from commercial sources and used without further purification unless otherwise stated. Methanol was distilled over magnesium methoxide [$Mg(OCH_3)_2$].[4] Diethyl ether (Et_2O) was dried first with anhydrous calcium chloride ($CaCl_2$) and then refluxed with sodium metal using benzophenone (as an indicator) and distilled over sodium metal wire.[4] Pyridine (Py) was refluxed over KOH and then distilled with careful exclusion of moisture and *N, N*-Dimethylformamide (DMF) was purified first by azeotropic distillation with benzene followed by shaking with alumina (neutral) and finally by vacuum distillation.[4] Tetra-n-butylammonium perchlorate (TBAP), salicylaldehyde were purchased from Fluka Aldrich Chemical Co. All amino acids were brought from Sisco Research Laboratories Pvt. Ltd. (SRL), India,

and used as received. The ligand H_2*S*-tyr (3)[3a], the complex $[Cu_8(S\text{-his})_8(pyridine)_{10}]$[1] and Cu(*S*-his)(imidazole)[5] were synthesized as before.

2.1.2 Measurements

The IR spectra were recorded on either Nicolet Impact 410 or Perkin-Elmer Spectrum One FT-IR spectrophotometer with KBr discs in the range 4000-400 cm^{-1} and electronic spectra on either a Shimadzu U-2001 or perkin-Elmer Lambda 25 UV-vis spectrophotometer. Solid-state magnetic susceptibility of the complexes at room temperature was recorded using Sherwood Scientific balance MSB-1. Solution electrical conductivity measurements were made with a Systronics Conductivity Meter 306 by using 0.01N KCl solution as calibrate. Elemental analyses were done using a Carlo Erba 1108 and also by using a Micromass Quattro II mass spectrometer. X-Band EPR spectra were recorded with a Jeol JES-FA series spectrometer fitted with a quartz dewar for measurements at liquid nitrogen temperature. The spectra were calibrated with DPPH (g = 2.0037).

Caution! Perchlorate salts are potentially dangerous as explosives and should only be handled in small quantities, although we have worked with these ClO_4^- salts without any incident.

2.2 Syntheses

2.2.1 *S*-2-(2-Hydroxybenzylamino)-4-methylsulfanylbutyric acid. [H_2*S*-met] (1)

A mixture of L-methionine (1.00 gm, 6.71 mmol) and $LiOH.H_2O$ (0.284 gm, 6.77 mmol) in methanol (dry, 30 ml) was stirred for 30 min. Salicylaldehyde (0.820 gm, 6.72 mmol) in methanol was added slowly drop by drop. After stirring for 20 min. clear yellow color solution was obtained. The solution was treated with sodium borohydride (0.248 gm, 6.71 mmol) with constant stirring upon which the solution became colorless. The solvent was evaporated using a rotary evaporator. The resulting sticky mass was dissolved in water. Clear solution was obtained, which was then acidified with dilute HCl and solution pH was maintained between 5-7. The ligand as white solid was precipitated out. The solid was filtered and thoroughly washed with water. The solid was dried under reduced pressure inside a desiccator. Yield 1.45 gm (80%). IR (KBr, cm^{-1}) $\upsilon(COO)_{asym}$ 1615(s), $\upsilon(COO)_{sym}$ 1430(m). $[\alpha]_D^{25^\circ}$ = -42º in MeOH, c = 1.00 gm/100ml, in presence of 2 equivalent $LiOH.H_2O$. ^{1}H NMR Li_2*S*-met (CD_3OD, 300 MHZ. ppm): 2.06 (s, 3H, -CH_3-

S), 2.57 (m, 2H, -C**H**H-S), 1.97 (m, 1H, CHCH**H**), 1.86 (m, 1H, -CHC**H**H), 3.19 (dd, 1H, -C**H**), 3.83 (d, 1H, -CH**H**-phenolate), 3.44 (d, 1H, -C**H**H-phenolate), 6.44 (t, 1H, *p*-phenolate), 6.97 (m, 2H, *m*-phenolate), 6.65 (d, 1H, *o*-phenolate). ESI-Mass (-ve) for **1** at at 254 (calcd. 254.32).

2.2.2 *Rac*-2-(2-Hydroxybenzylamino)-4-methylsulfanylbutyric acid. [H_2*rac*-met] (2)

This was synthesized following the same procedure as described for H_2*S*-met (**1**) starting with racemic methionine (2.00 gm, 13.40 mmol). Yield 2.85 gm (83%). IR (KBr, cm^{-1}) $\upsilon(COO)_{asym}$ 1615(sh), 1594, $\upsilon(COO)_{sym}$ 1387(m). $[\alpha]_D^{25^o}$ = 0º in MeOH, c = 1.00 gm/100ml, in presence of 2 equivalent LiOH.H_2O. ^{1}H NMR Li$_2$*rac*-met (D_2O, 300 MHZ. ppm): 2.08 (s, 3H, -CH_3-S), 2.27 (q, 2H, - CHC**HH**), 2.66 (m, 1H, -C**H**$_2$-S), 4.14 (t, 1H, -C**H**), 4.36 (s, 2H, -CH**H**-phenolate), 6.99 (m, 2H, *m*-phenolate), 7.34-7.41 (m, 2H, *o,p*-phenolate). ESI-Mass (-ve) for **1** at at 254 (calcd. 254.32).

2.2.3 [Cu_2 (*S*-met)$_2$] (1a)

A methanolic solution of $Cu(ClO4)_2$•$6H_2O$ (0.294 gm, 1.19 mmol) was added drop wise to a clear solution of H_2*S*-met (0.294 gm, 1.19 mmol) and KOH (0.090 gm, 2 .39 mmol) in 25 ml of dry methanol . The resulting dark green color solution along with some undissolved white particles was stirred for 20 min. The solution was filtered through a medium-porosity frit, after which the volume of the filtrate was reduced to ~ 10 ml by rotary evaporation and the complex was precipitated by the addition of diethyl ether. The resulting light green powder was filtered off and washed with diethyl ether prior to drying under vacuum in a desiccator (yield: 0.380 gm, 103 %, yield is very high because $KClO_4$ present as a impurity). IR (KBr, cm^{-1}) $\nu(COO)_{asym}$ 1633, 1600, $\nu(COO)_{sym}$ 1383, $\nu(ClO_4^-)$ 1100.

Purification and Recrystallization: Diffusion of diethyl ether into the solution of the complex in dimethylformamide afforded dark green crystals free from ClO_4^- suitable for X-ray analysis. The single crystal X-ray analysis revealed that the crystal contains binuclear Cu(II) complex and the elemental analysis agreed with the chemical formula [$Cu_2(C_{12}H_{17}NO_3S)_2$], yield: 51 %. Anal. Calcd (%) for [$Cu_2(C_{12}H_{17}NO_3S)_2$] (**1a)**: C, 45.71; H, 4.47; N 4.44. found: C, 45.18; H, 4.91; N, 4.55. IR (KBr, cm^{-1}) $\nu(COO)_{assym}$ 1633(sh), 1600, $\nu(COO)_{sym}$ 1383(s).

2.2.4 [Cu(*S*-met)(imidazole)] (1b)

The complex **1b** was synthesized from binuclear complex **1a** (0.100 g, 0.156 mmol) taken in 15 ml methanol followed by addition of excess imidazole (0.021 g, 0.308 mmol). The reaction mixture was stirred for 30 min. After that the reaction mixture was filtered to remove undissolved particle. The solution was kept for slow evaporation at room temperature. After 24 hours yielded green crystals of **1b** and elemental analysis agreed with the chemical formula $[Cu(C_{12}H_{17}NO_3S)(C_3H_4N_2)]$, yield 55 %. Anal. Calcd (%) for [Cu $(C_{12}H_{17}NO_3S)$ $(C_3H_4N_2)$] (**1b**): C, 46.87; H, 4.99; N 10.94. found: C, 46.70; H, 3.99; N, 10.80.IR (KBr, cm^{-1}) $\nu(COO)_{assym}$ 1618, 1599(sh), $\nu(COO)_{sym}$ 1384(s).

2.2.5 [Cu_2 (*rac*-met)$_2$] (2a)

This compound has been prepared by following the same procedure like **1a** using **2** (H_2*rac*-met) as ligand. Diffusion of diethyl ether into the solution of the complex in dimethylformamide afforded dark green microcrystal and the elemental analysis matched with the formula $[Cu_2(C_{12}H_{17}NO_3S)_2]$, yield: 50 %. Anal. calcd (%) for $[Cu_2(C_{12}H_{17}NO_3S)_2]$ (**2a)**: C, 45.71; H, 4.47; N 4.44. found: C, 45.26; H, 4.80; N, 4.28.IR (KBr, cm^{-1}) $\nu(COO)_{assym}$ 1626(sh), 1599, $\nu(COO)_{sym}$ 1385(s).

2.2.6 [Cu (*rac*-met)(pyridine)$_2$] (2b)

This compound has been prepared by recrystallizing (**2a**) from pyridine. Diffusion of diethyl ether into the solution of the complex in pyridine afforded dark green crystals suitable for X-ray analysis. The single crystal X-ray analysis revealed that the crystal contains mononuclear Cu(II) complex and elemental analysis agreed with the chemical formula $[Cu(C_{12}H_{17}NO_3S)(C_5H_5N)_2]$, yield: 50 %. Anal. calcd (%) for $[Cu(C_{12}H_{17}NO_3S)(C_5H_5N)_2]$ (**2b**): C, 55.45; H, 5.71; N 8.82. found: C, 55.30; H, 4.95; N, 8.61.IR (KBr, cm^{-1}) $\nu(COO)_{assym}$ 1645(sh), 1592, $\nu(COO)_{sym}$ 1380(s).

2.2.7 [Cu (*S*-tyr)(pyridine)$_2$] (3a)

A methanolic solution of $Cu(ClO4)_2.6H_2O$ (0.168g, 0.697 mmol) was added dropwaise to a clear solution of H_2*S*-tyr (0.200g, 0.697 mmol) and Et_3N (0.141g, 1.39 mmol) in 25 ml of methanol. The resulting dark green solution along with undissolved white particles was filtered through a medium porosity frit. Then the volume of the filtrate was reduced to ~10 ml by rotary evaporation, and the complex was precipitated by

the addition of diethyl ether prior to drying under vacuum in a desiccator ($KClO_4$ present as a impurity). IR (KBr, cm^{-1}) ν(COO)asym 1630, ν(COO)sym 1394, ν(ClO_4^-) 1100.

Purification and recrystallization: Diffusion of diethyl ether into complex solution of pyridine afforded dark green crystal of pure compound **3a**. The single crystal X-ray analysis showed that the crystal contains mononuclear Cu(II) complex and the elemental analysis matched with the chemical formula [Cu ($C_{16}H_{15}NO_4$)(C_5H_5N)$_2$] , yield: 50 %. Anal. calcd (%) for [Cu($C_{16}H_{15}NO_4$)(C_5H_5N)$_2$] (**3a**): C, 61.65; H, 4.98; N 8.30. found: C, 61.30; H, 4.70; N, 8.30. IR (KBr, cm^{-1}) $\nu(COO)_{assym}$ 1623, 1606(sh), $\nu(COO)_{sym}$ 1394(s).

2.2.8 X-ray Data Collection, Structure Solution and Refinement

The crystal structures of [Cu_2(*S*-met)$_2$] (**1a)**, [Cu(*S*-met)(imidazole)] (**1b**) [Cu(*Rac*-met)(Pyridine)$_2$] (**2b**) and [Cu(*S*-tyr)(Pyridine)$_2$] (**3a)** were obtained by single crystal X-ray diffraction technique. Single crystal of **1a** was obtained by slow diffusion of diethyl ether into the dimethyl formamide solution of the complex. Single crystal of **1b** was grown by slow evaporation of the methanolic solution of the complex. Single crystal of **2b** and **3a** were grown by slow diffusion of diethyl ether into the pyridine solution the complex. The selected crystallographic data of **1a**, **1b**, **2b** and **3a** are given Table 2.A. The crystals of **1a**, **1b**, **2b** and **3a** were mounted on glass fiber. All geometric and intensity data for the crystals were collected at room temperature using a Bruker SMART APEX CCD diffractometer equipped with a fine focus 1.75 kW sealed tube Mo Kα (λ = 0.71073 Å) X-ray source, with increasing ω (width of 0.3° per frame) at a scan speed of 3 s/frame. The SMART software was used for data acquisition and the SAINT software for data extraction. Structures were solved and refined using SHELX97.[6] All non-hydrogen atoms were located from the difference Fourier maps and were refined isotropically.

2.3 Results and discussion

2.3.1 Synthesis and Selected Properties

The complexes [Cu_2(*S*-met)$_2$] **(1a),** [Cu_2(*rac*-met)$_2$] (**2a)** and [Cu(*S*-tyr)(pyridine)$_2$] (**3a)** were synthesized using the H_2*S*-met, H_2*Rac*-met and H_2*S*-tyr with two equivalents of KOH and one equivalent of $Cu(ClO_4)_2$•$6H_2O$ in MeOH and purified as well as recrystallized the complexes from dimethylformamide for **1a, 2a** and **3a** from pyridine under the diffusion of diethyl ether. The complexes [Cu(*S*-met)(imidazole)] (**1b)** and [Cu(*rac*-met)(pyridine)$_2$] **(2b)** were synthesized from their corresponding binuclear

complex. All the complexes showed the sharp band in the region 3157-3240 cm^{-1}, has been assigned to N-H stretching mode. The carboxylate stretches were observed at ~ 1640 and at 1380 cm^{-1} for ν_{assym} and ν_{sym} respectively.[7] The band around 1266-1296 cm-1 might be assigned to ν(C-O) of phenolic group.[7] The elemental analyses support the formulation of the complexes. The non-electrolytic nature of the complexes were confirmed by conductance measurement in MeOH and DMF.[8] The room temperature magnetic moment of the monomers **1b**, **2b** and **3a** are 2.05, 1.73 and 1.84 μ_B respectively closer to the spin only value of 1.73 for Cu(II) expected for monomeric complexes.[9] The room temperature magnetic moments of the binuclear **1a** and **2a** are 1.38 and 1.15 μB/Cu respectively, considerably lower than 1.73 B.M expected for a S=1/2 system (Table 2.A) supporting the antiferromagnetically coupled binuclear nature of the complexes. This has been observed by similar phenoxo bridged dimeric Cu(II) complexes.[3a]

2.3.2 X-ray Structure of $[Cu_2(S\text{-met})_2]$ (1a)

The complex **1a** is a phenoxo bridged binuclear complex of Cu(II) having NO_4 coordination environment, crystallized in the space group $P2_1$ with two independent binuclear unit in the unit cell. Both the binuclear units were numbered similarly but with different subscript (Cu1 with subscript 3, Cu2 with subscript 4).The ORTEP figure of one of the binuclear unit,[10] selected bond lengths and angles of both the units are given in Figure 2.1 and Table 2.B respectively.

The in-plane coordination of each copper (II) is satisfied by phenolate, amine and carboxylate and the axial coordination is provided by non-coordinated carboxylate oxygen from another dimeric unit forming a planar coordination polymer network (Figure 2.2). The in-plane Cu-N and Cu-O bond lengths are similar to that found for $[Cu_8(S\text{-his})_8(Py)_{10}]$ and are typical for Cu(II) complexes.[2,3,11] The thioether arm of the ligand remains non-coordinated. The other independent dimeric unit forms a similar planar coordination network. Both networks interpenetrate each other to form the crystal, devoid of any void space. The geometry around the two copper centers in each binuclear unit is different. While one is closer to the ideal square pyramidal geometry and the other copper centre is distorted toward TBP which can be described as τ (Table 2.C) [$\tau = (\beta-\alpha)/60$, with α and β being the two largest coordination angles]. In a perfect square-pyramidal geometry τ is equal to 0, while it is 1 in a perfect trigonal-bipyramidal geometry.[12] In this

complex τ value is 0 for square- pyramidal geometry and Cu(II) is 0.21 Å above the mean plane formed by N1, O1, O3a, O3, for TBP geometry τ value is 0.38.

Table 2.A. Selected crystallographic data for the complexes

Complexes	**1a**	**1b**	**2b**	**3a**
Empirical formula	$C_{48}H_{55}Cu_4N_4O_{12}S_4$	$C_{15}H_{19}CuN_3O_3S$	$C_{22}H_{25}CuN_3O_3S$	$C_{26}H_{25}CuN_3O_4$
Formula weight	1262.44	384.93	475.07	507.04
Wavelength (Å)	0.71073	0.71073	0.71073	0.71073
Crystal system	Monoclinic	Monoclinic	Triclinic	Orthorhombic
Space group	$P2_1$	$P2_1$	P-1	$P2_12_12_1$
a, Å	13.337(8)	6.9706(7)	8.988(3)	9.2596(4)
b, Å	8.622(5)	21.827(2)	10.602(3)	9.7379(4)
c, Å	23.425(16)	11.0363(12)	13.550(4)	26.6724(4)
α, deg	90.00	90.00	69.213	90.00
β, deg	106.032(9)	100.638(7)	84.875(5)	90.00
γ, deg	90.00	90.00	67.454(4)	90.00
Volume, $Å^3$	2589(3)	1650.3(3)	1113.3(6)	2405.03(19)
Z	2	4	2	4
ρ, Mg/m^3	1.619	1.549	1.417	1.400
μ, mm^{-1}	1.847	1.467	1.103	0.945
Reflections collected	20081	15588	12969	23040
Reflections indep	10275	6972	9874	3979
Flack parameter	0.041 (16)	0.017(14)	achiral	0.000(10)
GOF	1.174	1.248	1.466	1.184
Final R indices [*I*>2sigma(*I*)]	R1 = 0.0550 wR2 = 0.1625	R1 = 0.0509 wR2 = 0.1064	R1 = 0.0733 WR2 = 0.1498	R1 = 0.0314 wR2 = 0.0497
R indices (all data)	R1 = 0.0586 wR2 = 0.1664	R1 = 0.0806 wR2 = 0.1149	R1 = 0.1137 wR2 = 0.1603	R1 = 0.0456 wR2 = 0.0513

Table 2.B. Selected bond distances and angles of complex **1a**

Atoms	Cu1	Cu2	Cu3	Cu4
Cu-Cu	3.0009(17)		2.986(2)	
$Cu\text{-}O_{acetate}$	1.938(4)	1.988(5)	1.949(5)	1.976(5)
$Cu\text{-}O_{phenolate}{}^{a}$	1.960(4)	1.972(4)	1.948(4)	1.951(4)
$Cu\text{-}O_{phenolate}$	1.952(4)	1.938(4)	1.956(4)	1.976(4)
$Cu\text{-}N_{amine}$	1.976(5)	1.970(5)	1.968(5)	1.967(5)
$Cu\text{-}O_{acetate}{}^{a}$	2.378(5)	2.285(5)	2.378(6)	2.239(6)
$N_{amine}\text{-}Cu\text{-}O_{phenolate}$	92.99(18)	94.03(19)	94.3(2)	94.4(2)
$O_{phenolate}\text{-}Cu\text{-}O_{phenolate}{}^{a}$	79.74(16)	79.79(16)	80.87(18)	80.32(17)
$O_{phenolate}{}^{a}\text{-}Cu\text{-}O_{acetate}$	100.06(18)	102.87(19)	98.2(2)	101.9(2)
$O_{acetate}\text{-}Cu\text{-}N_{amine}$	84.5(2)	83.3(2)	84.2(2)	83.9(2)
$O_{phenolate}{}^{a}\text{-}Cu\text{-}O_{acetate}{}^{a}$	93.29(18)	109.8(2)	95.0(2)	107.6(3)
$O_{acetate}{}^{a}\text{-}Cu\text{-}N_{amine}$	99.2(2)	87.1(2)	96.3(2)	86.7(2)
$N_{amine}\text{-}Cu\text{-}O_{phenolate}{}^{a}$	165.57(19)	173.6(2)	167.6(2)	174.2(2)
$O_{phenolate}\text{-}Cu\text{-}O_{acetate}$	168.2(2)	150.6(2)	167.8(2)	148.7(2)
τ	0.04	0.38	0.00	0.43

[a]Atoms of the ligand coordinated to neighboring Cu atom

Table 2.C. Selected bond distances and angles of complex **1b**

Atoms	Distance/Angles	Atoms	Distance/Angles
Cu1-N1	1.984(4)	Cu2-N1a	2.004(4)
Cu1-O1	1.925(3)	Cu2-O1a	1.906(4)
Cu1-N2	1.941(5)	Cu2-N2a	1.954(4)
Cu1-O2	1.958(4)	Cu2-O2a	1.945(4)
N1-Cu1-O1	93.95(15)	N1a-Cu2-O1a	94.33(16)
O1-Cu1-N2	91.17(16)	O1a-Cu2-N2a	90.72(17)
N2-Cu1-O2	91.29(16)	N2a-Cu2-O2a	92.28(17)
O2-Cu1-N1	84.02(16)	O2a-Cu2-N1a	83.57(16)
N1-Cu1-N2	170.23(16)	N1a-Cu2-N2a	172.58(18)
O1-Cu1-O2	176.31(16)	O1a-Cu2-O2a	170.84(17)
τ	0.10		0.03

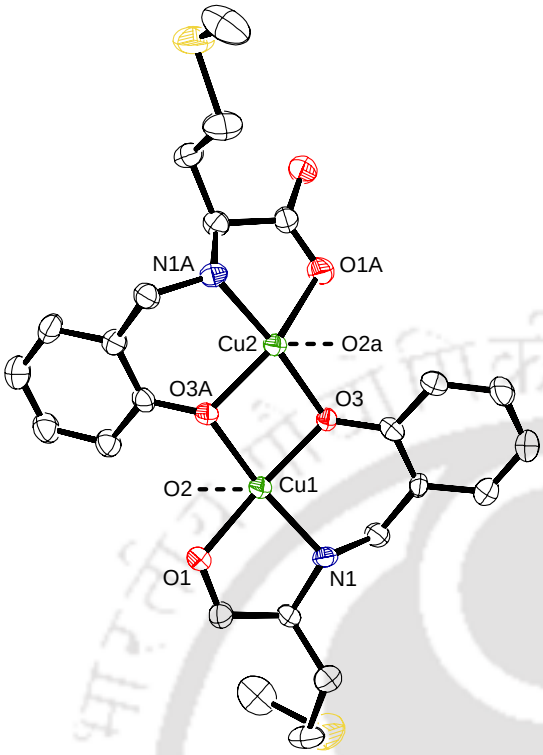

[Cu_2(S-met)$_2$] **1a**

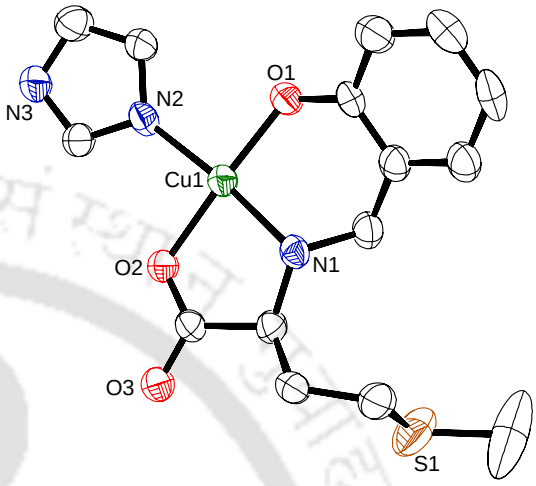

[Cu(S-met)·(imidazole)] **1b**

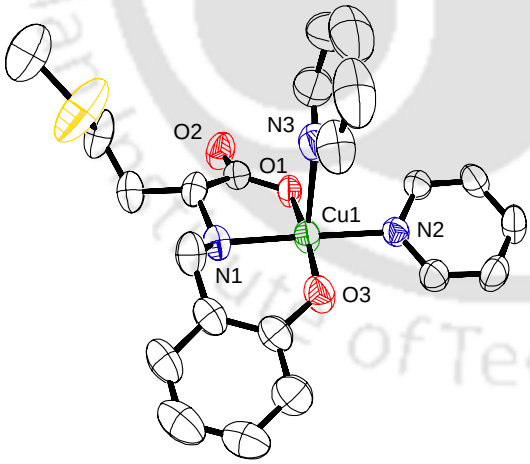

[Cu(rac-met)(Pyridine)$_2$] **2b**

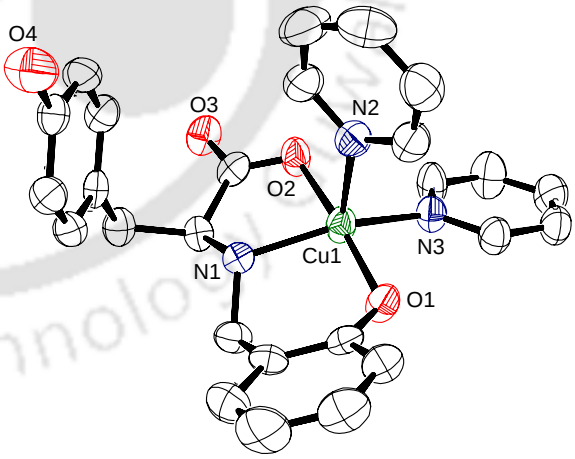

[Cu(S-tyr)(Pyridine)$_2$] **3a**

Figure 2.1. *The ORTEP diagram of Cu(II) complexes*

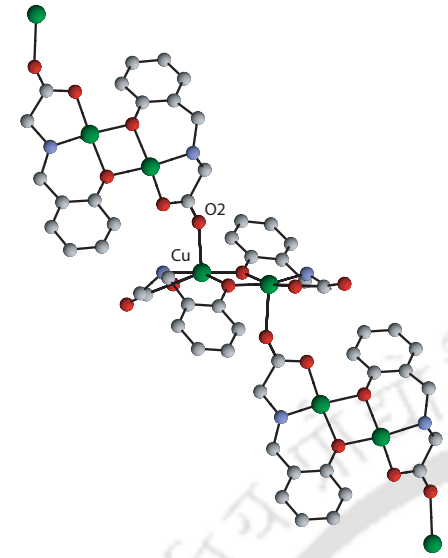

[Cu_2(*S*-met)$_2$]**(1a)**

1

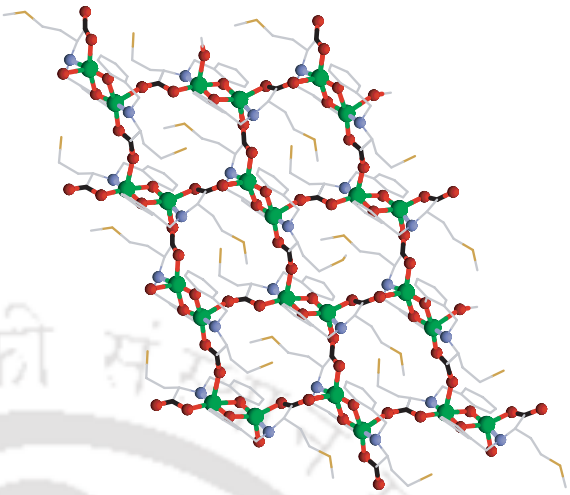

(1a)

2

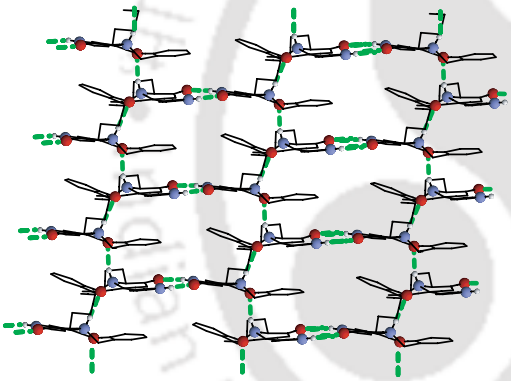

[Cu(*S*-met)·(Imidazole)]**(1b)**

3

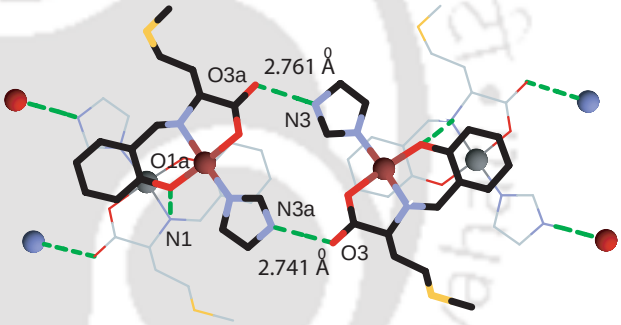

1b

4

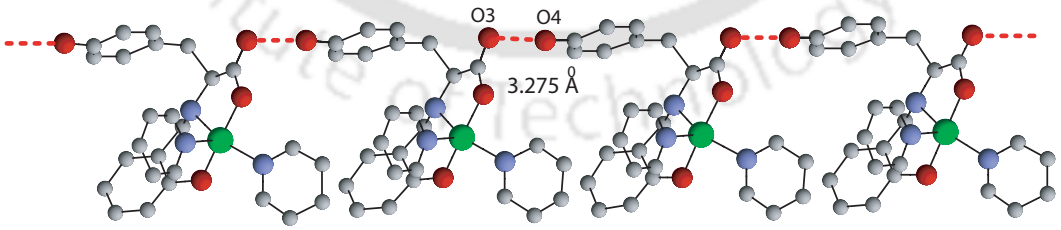

[Cu(*S*-tyr)·(Pyridine)$_2$]**(3a)**

5

Figure 2.2. *Network diagram of complexes **1a**, **1b** and **3a**.*

2.3.3 X-ray Structure of [Cu(*S*-met)(Imidazole)] (1b)

The complex **1b** was crystallized in the space group $P2_1$ with two independent mononuclear units in the unit cell. The ORTEP figure of one of the monomer unit, selected bond lengths and angles for both monomers are given in Figure 2.1 and Table 2.C respectively.

The geometry of the Cu(II) in complex 1b is square planar with τ value of 0.02, the phenolate, amine and carboxylate donors from the ligand and external imidazole completes the coordination site. The lattice diagram shows the 2D honeycomb (**3**, Figure 2.2) network formed by a complementary H-bonding of uncoordinated carboxylate oxygen and imidazole NH (N3A-O3, 2,741Å, N3-O3a, 2.761Å) and vertical H-bonding of amine and phenolate (N1-O1A, 3.061Å, N1A-O1, 3.153Å) both are within expected range (**4**, Figure 2.2).[13]

2.3.4 X-ray Structure of [Cu(*Rac*-met)·(Pyridine)$_2$] (2b)

The complex **2b** is a mononuclear Cu(II) complex with N_3O_2 coordination environment and crystallized in the space group *P1*. The perspective view of the complex **2b** has shown as ORTEP diagram in Figure 2.1. The coordination geometry around the copper center in **2b** is square pyramidal geometry (τ=0.01) with three of the in-plane coordination from ligand, similar to that in **1a**, and rest of the two coordination by two pyridine from solvent. The bond lengths and angles are well within expected limits which are summarized in Table 2.D.[2,11]

2.3.5 X-ray Structure of [Cu(*S*-tyr)(Pyridine)$_2$] (3a)

The complex **3a** was crystallized in the space group of $P2_12_12_1$.The ORTEP diagram, selected bond lengths and angles are given in Figure 2.1 and Table 2.D. The Cu(II) in **3a**, coordinated with three of the in-plane coordination from ligand and rest of the two coordination by two pyridine from the solvent. Unlike **2b**, the distortion towards TBP is significant with a τ value of 0.32.

In lattice only one H-bond is present between tyrosine phenol (protonated) and uncoordinated carboxylate oxygen (O4….O3 2.751Å) forming a 1D network (Figure 2.2).

Table 2.D. Selected bond distances (Å) and angles (°) of complex **2b** and **3a**

Complexes	**2b**	**3a**
$Cu\text{-}O_{carboxylate}$	1.965 (3)	1.952 (18)
$Cu\text{-}N_{amine}$	1.997 (3)	2.012 (2)
$Cu\text{-}O_{phenolate}$	1.910 (3)	1.910 (18)
$Cu\text{-}N_{pyridine}$ [e]	2.018 (3)	2.024 (2)
$Cu\text{-}N_{pyridine}$ [a]	2.429 (4)	2.280 (2)
$O_{carboxylate}\text{-}Cu\text{-}N_{amine}$	82.08 (12)	82.40 (8)
$N_{amine}\text{-}Cu\text{-}O_{phenolate}$	93.97 (13)	93.92 (8)
$O_{phenolate}\text{-}Cu\text{-}N_{pyridine}$ [e]	91.53 (12)	90.82 (8)
$N_{pyridine}$ [e]$\text{-}Cu\text{-}O_{carboxylate}$	91.59 (11)	90.75 (8)
$O_{carboxylate}\text{-}Cu\text{-}N_{pyridine}$ [a]	92.18 (14)	92.13 (8)
$N_{pyridine}$ [a]$\text{-}Cu\text{-}N_{amine}$	96.90 (13)	100.94 (9)
$N_{amine}\text{-}Cu\text{-}N_{pyridine}$ [a]	171.52 (13)	155.32 (9)
$O_{carboxylate}\text{-}Cu\text{-}O_{phenolate}$	171.38 (12)	174.32 (8)
τ	0.00	0.32

[e,a]Pyridine coordinate to Cu atom equatorially and axially.

2.4 Effects of amino acid side chain, solvent (MeOH, Pyridine) and imidazole on the Cu(II) complexes

2.4.1 Complexation in MeOH with different amino acids

To understand the effect of amino acid side arm on the Cu(II) complexation, we have chosen to synthesize complexes of the methionine and tyrosine derivative of the ligands **1** to **3.** These choices are based on having amino acids with weaker donor to compare with stronger donor histidine derived ligand.[1] As number of donor atom provided by this ligand is not sufficient to coordinatively saturate the Cu(II), it is likely that having or not having a coordinating solvent will effect the type of complexes formed. Thus we attempted to isolate the complexes from MeOH. Addition of *S*-Met (**1**), *Rac*-Met (**2**) with Cu(II) in MeOH resulted in green crystalline complexes **1a** and **2a** respectively with identical formulation of $[Cu_2(\mathbf{1} \text{ or } \mathbf{2})_2]$. The single crystal of **1a** was grown from DMF and the structural identity was found to be a bis-phenoxo-bridged binuclear complex using

single crystal X-ray diffraction (Section 2.3). On the other hand Vittal and co-workers have structurally characterized a number of Cu(II) complexes of related ligands with alanine, valine, glycine, tryptophan, and tyrosine.[3a] All the reported complexes isolated either from water or alcohols have a phenoxo-bridged binuclear structure like that of **1a**.[3a] Thus all the Cu(II) complexes of reduced Schiff bases of amino acid-salicylaldehyde ligands isolated from alcohol or water irrespective of amino acids used are phenoxo-bridged binuclar complexes. Although crystals of **1a** were isolated from DMF still it is binuclear structure, as DMF is not a strong ligand.

We conclude that in absence of a strong ligand in the form of solvent and in the amino acid side arm the formation of phenoxo bridged binuclear complex is favored irrespective of amino acid used. The ligands **1** - **3** being non-planar ligand, phenoxo bridged binuclear complex formation satisfies the coordination requirements on the Cu(II). This indicates that the solvent such as pyridine which can act as ligand to Cu(II) might be able to break the phenoxo bridge forming mononuclear complex.

2.4.2 Role of pyridine

The pyridine coordinated mononuclear complexes **2b** and **3a** were isolated by crystallizing corresponding binuclear species from pyridine (Figure 2.1, Section 2.3). The crystal structure of **2b** and **3a** shows that the pyridine, being preferred ligand for Cu(II) compared to phenolate, is capable of breaking the phenoxo bridge of the binuclear complex to form mononuclear complexes where pyridine occupy both axial and equatorial position. Thus pyridine breaks the phenoxo bridged binuclear complexes into mononuclear bis-pyridine adducts if a stronger ligand such as imidazole is absent in the amino acid. The presence of histidine, the imidazole in $[Cu_8(S\text{-his})_8(Pyridine)_{10}]^1$ probably displaces the in-plane pyridine ligand to form the cyclic capsular complex.

2.4.3 Role of Imidazole

Previously, we observed that formation of octanuclear complexed $[Cu_8(S\text{-his})_8(Pyridine)_{10}]^1$ occurred most likely because of displacement of in-plane pyridine by imidazole arm of histidine from another ligand.[2] Also, addition of excess imidazole influences carboxylate to coordinate axially in [Cu(*S*-his)(Imidazole)].[5] One possibility is that imidazole being a stronger ligand tends to occupy equatorial position rather than axial position even at the expense of shifting other co-ligands to the axial position.[14] This

stronger preference of imidazole for the equatorial position is driving the ligand coordination mode switching in [Cu(*S*-his)(Imidazole)].[5] This has been further substantiated by the synthesis and structural characterization of square planar **1b** [Cu(*S*-met)(Imidazole)] from the corresponding binuclear **1a** [(Cu_2(*S*-met)$_2$] upon addition of 2 equivalent of imidazole. In **1b**, the imidazole coordinates as in-plane ligand only (Figure 2.1). Addition of up to 4 equiv of imidazole did not yield any five-coordinated complex with axially coordinated imidazole. The isolation and structural characterization of this complex substantiate that the tendency of imidazole to coordinate in-plane was responsible for (a) capsule formation by displacing a pyridine in [Cu_8(*S*-his)$_8$(Pyridine)$_{10}$][1] and axial carboxylate coordination in [Cu(*S*-his) (Imidazole)][5] where both externally added imidazole and histidine imidazole occupied two in-plane positions.

Overall, these complexes preferably form bis-phenoxo binuclear complexes in weakly coordinating solvent. Solvents or reagents with better binding ability to Cu(II) compared to phenolate such as pyridine will break the phenoxo bridge and form mononuclear complexes. If the amino acid used is histidine, then replacement of the in-plane ligand can lead to cyclic multinuclear complex (tetramer in [Cu_8(*S*-his)$_8$(Pyridine)$_{10}$][1]) formation. The generalized process is shown in Scheme 2.2.

2.4.4 Absorption Spectra and EPR spectral characteristics

The UV-visible spectral characteristic data of all the complexes are given in Table 2.E and the spectra figure of **1a** and **1b** are shown in Figure 2.3. The absorption maxima at ~ 400 nm is due to LMCT, origin evident from high ε value (ε 500 dm^3 $mol^{-1}cm^{-1}$/Cu). The absorption maxima between 600 – 700 nm with ε value ~150 dm^3 $mol^{-1}cm^{-1}$ are of ligand field origin. Several other square-pyramidal Cu(II) complexes with N/O donor environment have similar spectral characteristics. [3, 15] The spectral characteristics of **1a**, **2a**, **2b** and **3a** are almost identical. The complex **1b**, being the only complex with four coordination, has ligand-field transition at 632 nm, quite different from the others at 650 nm or above. This suggests retention of square planar geometry in solution.

The EPR spectral characteristic of all the complexes are shown in Figure 2.4 and the data at 77 K are shown in Table 2.E. The complexes **1a**, **2a**, **2b** and **3a** shows a typical square pyramidal EPR spectra as is evident from their $A_\parallel$ values ~175G and g values.[16] The complex **1b** however shows higher $A_\parallel$ and lower g values due to square planar geometry.[17]

Table 2.E. UV-Visible and EPR data of complexes

Complex	λ/nm(ε/cm^{-1} M^{-1})	EPR, g	$A_{\parallel}$/G
1a[a]	362 (1560), 660 (180)	2.271, 2.061	174
1b[b]	389 (660), 632 (142)	2.192, 2.00	182
2a[a]	358 (1300), 658 (180)	2.271, 2.061	174
2b[c]	423 (770), 678 (260)	2.253, 2.071	174
3a[c]	417 (592), 667 (177)	2.230, 2.011	174

Solvent used for spectral analysis [a]DMF, [b]MeOH and [c]Pyridine

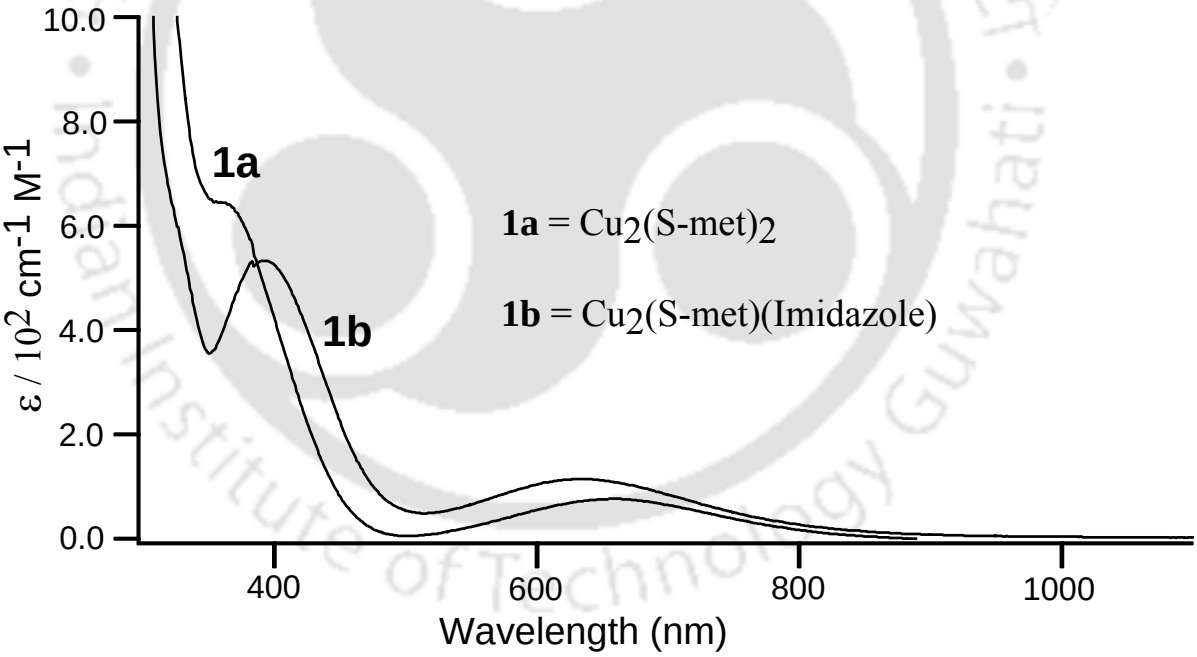

Figure 2.3. *UV-Visible spectrum of complex **1a** and **1b***

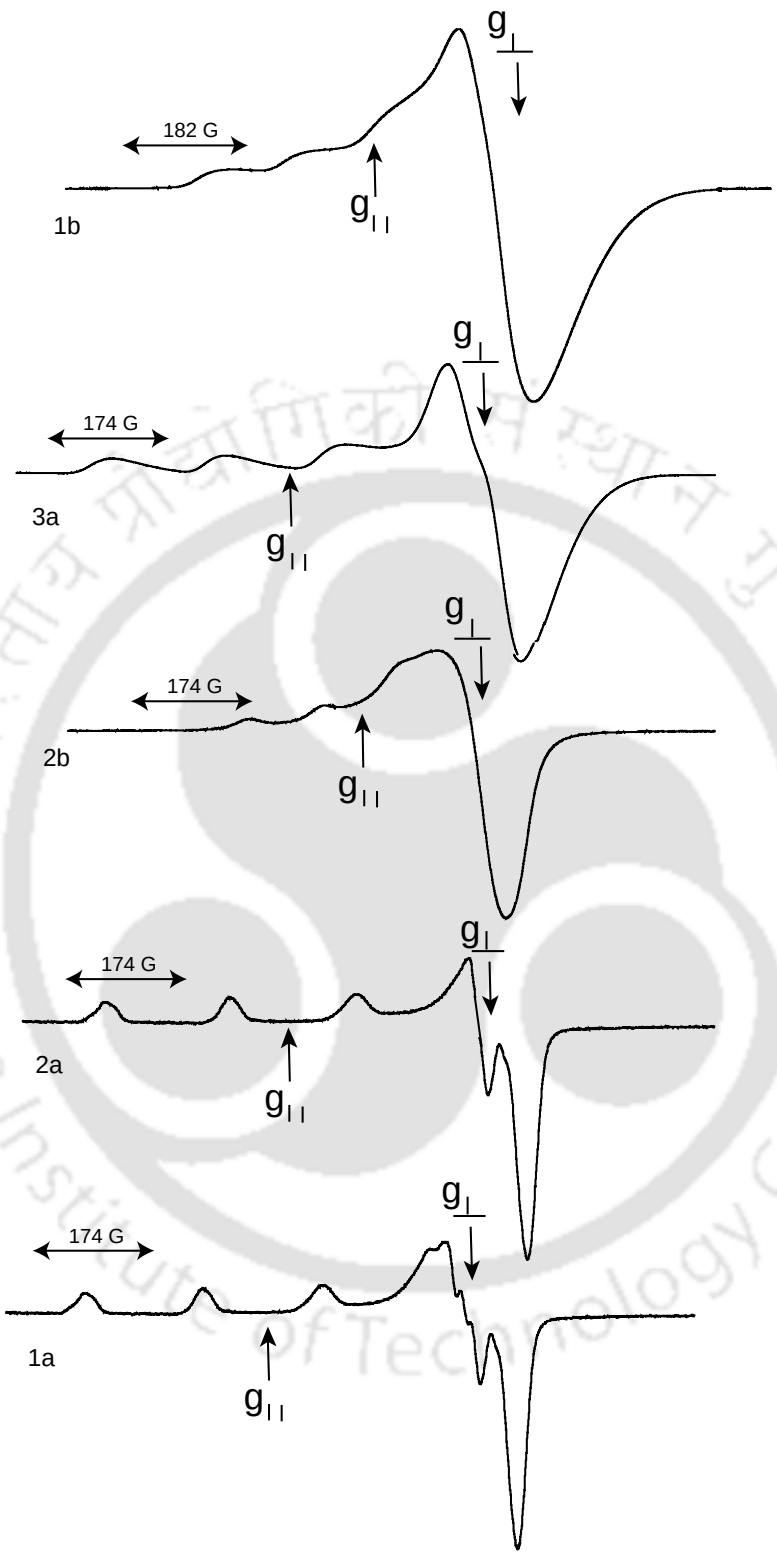

Figure 2.4. *EPR spectrum of Cu(II) complexes*

Conclusion

In this chapter we have attempted to rationalized the effect of amino acid side arm, solvent, imidazole and coordination chemistry of Cu(II) on different nuclearity. Based on these complexes, interconvertion between them as well as comparison with complexes reported by Alam *et al* and Vittal *et al* we are proposing a general mechanism of formation of these complexes (Scheme 2.2).

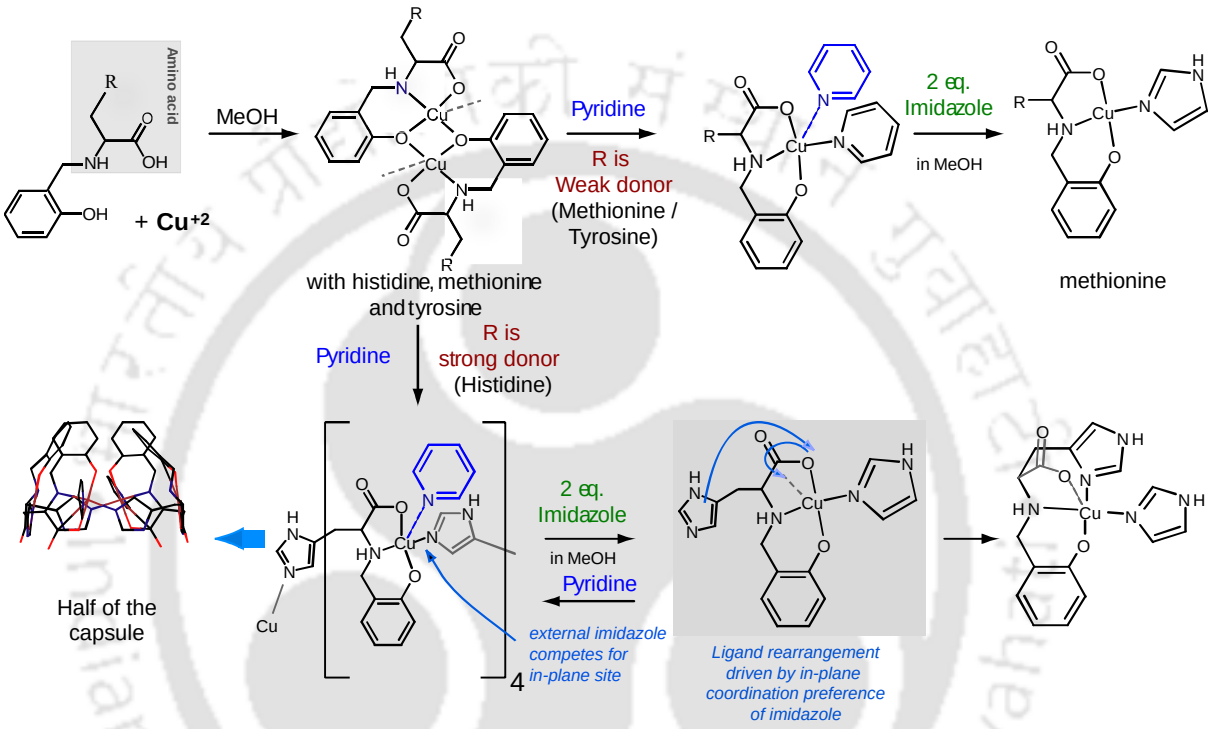

Scheme 2.2. *Effect of amino acid, solvent, and imidazole on the formation mononuclear to octanuclear species.*

The major finding in this section are that (a) in MeOH or weak coordinating solvent (DMF) the ligands preferentially form phenoxo bridged species (b) in presence of pyridine, cleavage of the phenoxo bridge takes place, leading toformation of mononuclear complex in which pyridine binds both equatorial and axial positions (c) in histidine-derived ligand, presence of stronger donor (imidazole) leads to octanuclear species, most likely because of displacement of in-plane pyridine by imidazole arm of histidine from another ligand (d) the imidazole prefers to act as in-plane ligand in Square pyramidal Cu(II) complexes. The complex **1b** was synthesized solely to confirm this point.

Systematic isolation and structural characterization of the complexes in this section provided an opportunity to identify the factors governing the network formation in metal

complexes of amino acid derived ligands, which so far generated a large number of interesting structures at random. Figure 2.5 arranges the H-bonded networks found in the

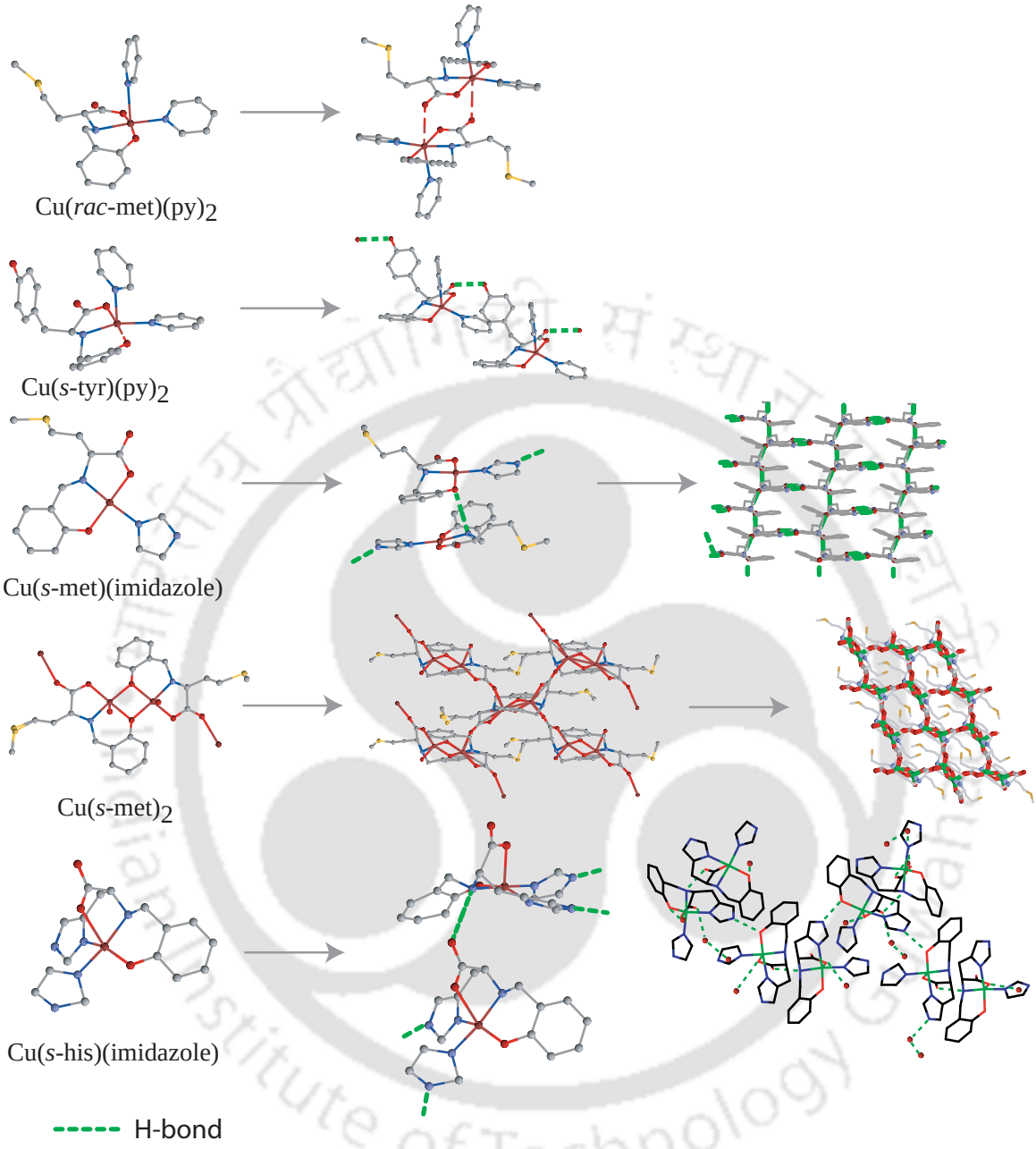

Figure 2.5. *Structural motifs generated through coordination preferences of Cu(II) with the ligands and the way lead to different type of networks.*

structures from simple to more complex pattern. We observed that (a) pyridine adduct complexes contain less number of H-bond resulting in simpler network (b) gradual substitution of pyridine with imidazole introduced new H-bonding which lead to complex

network. (c) the network in the binuclear complex is entirely different as carboxylate coordination to neighboring Cu(II) predominates over H-bond formation.

Identification of the factors governing the nuclearity and geometry of the Cu(II) complexes along with choice of amino acid might help designing metal complexes and networks with this type of ligands in a more rational way in future.

References

1. Alam, M. A.; Nethaji, M.; Ray, M. *Angew. Chem., Int. Ed.* **2003**, *42*, 1940.
2. Alam, M. A.; Nethaji, M.; Ray, M. *Inorg. Chem*. **2005**, *44*, 1302.
3. (a)Yang, C. T.; Vetrichelvan, M.; Yang, X; Keith, B. M.; Murray, S.; Vittal, J. J. *J. Chem. Soc., Dalton Trans.* **2004**, 113. (b) Yang, C. T.; Moubaraki, B.; Murray, K. S.; Ranford, J. D.; Vittal, J. J. *Inorg. Chem.* **2001**, *40*, 5934. (c) Xiandong, Y.; Daqing, W.; Ranford, J. D.; Vittal, J. J. *Cryst. Growth Des.* **2005**, *5*, 41. (d) Xiandong, Y.; Ranford, J. D.; Vittal, J. J. *Cryst. Growth Des.* **2004**, *4*, 781. (e) Ranford, J. D.; Vittal, J. J.; Wu, D. *Angew. Chem., Int. Ed.* **1998**, *37*, 1114. (f) So, K. W.; Yang, C T.; Vittal, J. J.; Ranford, J. D. *Inorg. Chim. Acta*. **2003**, *349*, 135. (g) Wang, X.; Ding, J.; Vittal, J. J. *Inorg. Chim. Acta*, **2006**, *359*, 3481.
4. Furniss, B. S.; Hannaford, A. J.; Rogers, V.; Smith, P. W. G.; Tatchell, A. R. *Vogel's Textbook of Practical Organic Chemistry*, 4th ed, English Language Book Society/Longman, England, 1978, 661.
5. Alam, M. A. *Synthesis of Enantiomerically Pure Chiral Hosts using Amino Acid Derived Ligands with Fe(III), Ni(II) and Cu(II) ions,* 2004, IIT-Guwahati.
6. Sheldrick, G. M. SHELXL-97, Program for the Solution of Crystal Structures; University of Go¨ttingen: Go¨ttingen, Germany.
7. Nakamoto, K. Infrared and Raman Spectra of Inorganic Compounds, 5th ed.; WileInterscience: New York, 1997; Part B.
8. Geary, W. J. *Coord. Chem. Rev*. **1971**, *7*, 81.
9. a) Earnshaw, A. Introduction to Magnetochemistry; Academic Press: London, 1968. (b) Figgis, B. N.; Lewis, J. Prog. *Inorg. Chem*. **1964**, *6*, 37.
10. Johnson, C. K. *ORTEP, Report ORNL-3794*; Oak Ridge National Laboratory: Oak Ridge, TN, 1976.
11. a) Anderson, O. P.; Packard, A. B. *Inorg. Chem.* **1980**, *19*, 2123. (b) Barclay, G. A.; Kennard, C. H. L. *J. Chem. Soc.* **1961**, 5244. (c) Tables of Interatomic

Distances and Configuration in molecules and Ions. Spec. Publ. - Chem. Soc. 11; Sutton, L. E., Ed.; 1958.

12. Addision, A. W.; Rao, T. N.; Reedijk, J.; van Rijn, J.; Verschoor, G. C. *J. Chem. Soc., Dalton Trans.* **1984**, 1349.
13. N(H)…O range: 2.69 to 2.89 Å. (a) Couchman, S. M.; Jeffery, J. C.; Ward, M. D. *Polyhedron* **1999**, *18*, 2633. (b) Kuduva, S. S.; Bläser, D.; Boese, R.; Desiraju, G. R. *J. Org. Chem.* **2001**, *66*, 1621. (c) Alam, M. A.; Nethaji, M.; Ray, M. *Inorg. Chem*. **2005**, *44*, 1302.
14. (a) Morehouse, S. M.; Suliman, H.; Haff, J.; Nguyen, D. *Inorg. Chim. Acta*. **2000,** *297*, 411. (b) Iskander, M. F.; Khalil, T. E.; Werner, R.; Haase, W.; Svoboda, I.; Fuess, H. *Polyhedron*, **2000**, *19*, 1181.
15. Admas, H.; Bailey, N. A.; de Barbarin, C. O. R.; Fanton, D. E. *J. Chem. Soc., Dalton Trans.* **1995**, 2323.
16. Yokoi, H.; Addison, A. W. *J. Chem. Soc., Dalton Trans.* **1977**, *16*, 1341.
17. Sakaguchi, U.; Addison, A. W. *J. Chem. Soc., Dalton Trans.* **1979**, 600.

In the previous chapter we have discussed the effect of amino acid side arm, solvent (MeOH, Pyridine) and imidazole on the assembly of octanuclear Cu(II) complex (capsule). In this chapter we have explored the effect of substitution on the aromatic ring and chirality of the ligand on the formation of octanuclear assembly or capsular like complex. The aromatic ring substitution might help us change the size and shape of the capsule. The substitution of the ligand might also change the solubility of the capsular complexes helping solution studies. This chapter presents the synthesis and characterization of Cu(II) complexes with *S*-5OMehis, *S*-3OMehis, *R*-his and *dl*-his.

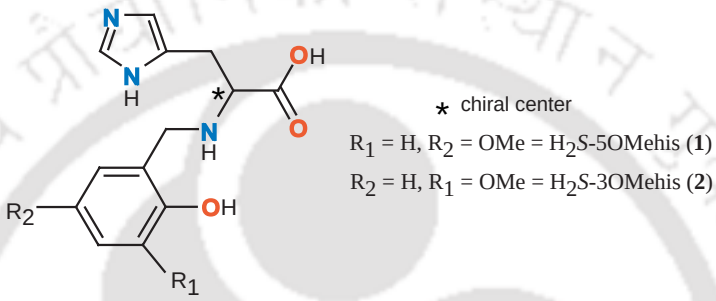

Scheme 3.1. *Ligands used in this chapter*

3.1 Experimental Section

3.1.1 Solvents and Reagents

Details of the solvent purification and analytical measurements have already discussed in chapter 2. 2-hydroxy 5-methoxy bezaldehyde and 2-hydroxy 3-methoxy bezaldehyde were purchased from Aldrich Chemical Co. The ligand H_2*R*-his(**3**),[1] was synthesized and characterized as before.

3.2 Syntheses

3.2.1 *S*-2-(2-hydroxy-5-methoxy-benzylamino)-3-(1H-imidazol-4-ylpropanoicacid): [H_2*S*-5Omehis] (1)

L-histidin monohydrocholoride (0.800g, 3.81 mmol) was dissolved in methanol in presence of LiOH (0.323g, 7.70 mmol) .To this solution, 2-hydroxy 5-methoxy bezaldehyde (0.580g, 3.81 mmol) was added dropwaise with constant stirring. Small quantity of precipitate which came initially was dissolved automatically and formed a bright yellow color solution. Into the solution $NaBH_4$ (0.072g, 1.91 mmol) was added and the solution became colorless. After completion of the reaction, the solvent was evaporated in rotary evaporator to get sticky white material. The white material was

dissolved with water and acidified with dil HCl (pH5~7) resulting the precipitation of the ligand as a white solid which was filtered off and dried under vacuum. Yield 70%. IR (KBr, cm^{-1}) ν(COO) $_{(assym)}$ 1610, ν$(COO)_{sym}$ 1399. $[\alpha]_D^{25^\circ}$ = -40° in MeOH, c = 1.00 (c = gm/100ml) , in presence of 2 equivalent $LiOH.H_2O$. ^{1}H NMR Li_2*S*-5-OMehis (CD_3OD, 400 MHZ. ppm): 2.59 (dd, 1H, J = 9.2, 14.2 -C**H**H-imidazole), 2.87 (dd, 1H, J = 4, 14.4-CH**H**-imidazole), 3.12 (m, 1H, -C**H**CHH), 3.26 (d, 1H, J = 12.8 -C**H**H-phenolate), 3.48 (s, 3H, -OC**H**$_3$), 3.63 (d, 1H, J = 12.8 -CH**H**-phenolate), 6.44-6.38 (m, 3H, -phenolate), 6.67 (s, 1H, imidazole), 7.40 (s, 1H, imidazole). (All J values are in Hz.). ESI-Mass (-ve) for **1** at at 290 (calcd. 290.11).

3.2.2 *S*-2-(2-hydroxy-3-methoxy-benzylamino)-3-(1H-imidazol-4-ylpropanoicacid): [H_2*S*-3Omehis] (2)

This was synthesized following the same procedure as described for [H_2*S*-5omehis] (**1**) starting with 2-hydroxy-3-methoxy bezaldehyde (2.00gm, 13.40 mmol). Yield 83 %. IR (KBr, cm^{-1}) υ$(COO)_{asym}$ 1615(sh), 1594, υ(COO) $_{sym}$ 1386(m). $[\alpha]_D^{25^\circ}$ = -38º in MeOH, c = 1.00 (c = gm/100ml). ^{1}H NMR *S*-3OMehis (CD_3OD, 400 MHZ. ppm): 2.96 (dd, 1H, J = 8, 15.2 -C**H**H-imidazole), 3.17 (dd, 1H, J = 15.4, 4 -CH**H**-imidazole), 3.56 (qt, 1H, J = 4.0 -C**H**CHH), 3.82 (s, 3H, -OC**H**$_3$), 3.96 (d, 1H, J = 13.2 -C**H**H-phenolate), 4.14 (d, 1H, J = 13.2 -CH**H**-phenolate), 6.73-6.75 (m, 1H, -phenolate), 6.88 (s, 1H, imidazole), 6.89-6.91 (m, 2H, -phenolate), 7.57 (s, 1H, imidazole). ESI-Mass (-ve) for **2** at 290 (calcd. 290.11).

3.2.3 $[Cu_8$(*S*-5omehis)$_8$(Pyridine)$_8]$ (1a)

This was prepared following the procedure reported for the unsubstituted capsular complex $[Cu_8$(*S*-his)$_8$(Pyridine)$_{10}]$.[2] The detailed procedure is described below.

A methanolic solution of $Cu(ClO_4)_2$•$6H_2O$ (0.190 g, 0.515 mmol) was added drop wise to a clear solution of H_2*S*-5OMehis (0.150 g, 0.515 mmol) and KOH (0.058 gm, 1 .03mmol) in 25 mL of dry methanol . The resulting green color solution along with some undissolved white particles was stirred for 30 min. The solution was filtered through a medium-porosity frit, after which the volume of the filtrate was reduced by rotary evaporation and the complex was precipitated by the addition of diethyl ether. The resulting light green powder was filtered off and washed with diethyl ether prior to drying under vacuum in a desiccator (yield: 103 %, yield is very high because $KClO_4$ present as impurity). IR (KBr, cm^{-1}) ν$(COO)_{asym}$ 1598, ν$(COO)_{sym}$ 1403, ν(ClO4) 1100.

Purification and Recrystallization: Diffusion of diethyl ether into the solution of the complex in pyridine, afforded dark green crystals free from ClO_4^- suitable for X-ray analysis. Yield: 65%. IR (KBr, cm^{-1}): $\nu(COO^-)_{assym}$ 1615(sh), 1598, $\upsilon(COO^-)_{sym}$ 1388s, υ(phenolic CO) 1264. ESI-Mass (+ve) for **1a** at 705 and 1059 (calcd. 705.07, 1059.15 for $\{Cu_2(\mathbf{1})_2+H^+\}$) and $Cu_3(\mathbf{1})_3+H^+\}$) respectively.

3.2.4 $[Cu_2(S\text{-}5OMehis)_2]\cdot 3H_2O$ (1b)

Complex **1a** (0.010 g, 0.066 mmol), grinded to fine powder, was stirred in 20 mL of water and filtered to remove largely undissolved complex. The filtrate was kept standing at room temperature. Within two days green crystals suitable for X-ray analysis was isolated. IR (KBr, cm^{-1}): $\nu(COO^-)_{assym}$ 1640, 1620 (sh), $\upsilon(COO^-)_{sym}$ 1350 s, υ(phenolic CO)1274. Poor solubility of **1a** made it difficult to scale up the reaction. Analysis and magnetic susceptibility on this sample has not been attempted.

3.2.5 Complexation reaction with H_2 *S*-3omehis (2a)

The complexation procedure was similar to **1a**. The deprotonation of the ligand with base followed by addition of Cu(II) in MeOH resulted in a green powder contaminated with perchlorate. Attempt to purify from pyridine as before (Section 3.2.3) resulted in isolation of green solid (**2a**) free of perchlorate (from FTIR). Repeated attempt to crystallize **2a** was unsuccessful. IR (KBr, cm^{-1}): $\nu(COO^-)_{assym}$ 1609sh, 1598 s, $\nu(COO^-)_{sym}$ 1388 s, ν (phenolic CO) 1264 s. ESI-Mass (+ve) for **2a** at 705, 1059, 1411 (calcd. 705.07, 1059.15 and 1411.19 for $\{Cu_2(\mathbf{2})_2+H^+\}$), $\{Cu_3(\mathbf{2})_3+H^+\}$ and $\{Cu_4(\mathbf{2})_4+H^+\}$) respectively.

3.2.6 $[Cu_8(R\text{-}his)_8(Pyridine)_{10}]$ (3a)

The complex **3a**, as crystals was synthesized (55% yield) following the procedure described for **1a** using the *D*-histidine derived ligand (R-H_2L).[1] Yield: 55%. IR (KBr, cm^{-1}): $\nu(COO^-)_{assym}$ 1609, $\nu(COO^-)_{sym}$ 1388 s, ν (phenolic CO) 1264 s. ESI-Mass (+ve) for **3a** at 645 and 969 (calcd. 645.08, 969.11 for $\{Cu_2(\mathbf{3})_2+H^+\}$) and $Cu_3(\mathbf{3})_3+H^+\}$) respectively.

3.2.7 Complexation reaction with (H_2*Rac*-his)

The racemic ligand was prepared from equimolecular mixture of D and L-histidine derived ligand. The optical rotation of the mixture was checked and found to be nil. The complexation proceeded similar to **1a**. The deprotonation of the ligand with base followed by addition of Cu(II) resulted in a immediate precipitation of a green solid insoluble in common organic solvent including DMF, pyridine and DMSO. The synthesis of this type of complex in MeOH tends to contaminated with perchlorate ion (Section 3.2.3) and phenoxo bridged complex (Chapter 2, Scheme 2.2). Thus we have further attempted to form the racemic complex by mixing both D and L enantiopure capsular complexes together in pyridine where the capsular form is stable (Chapter 2, Scheme 2.2). The mixing of **3a** and $[Cu_8(S\text{-his})_8(Pyridine)_{10}]^{2}$ in equimolecular ratio resulted in a almost quantitative precipitation of a insoluble green solid. IR (KBr, cm^{-1}) $\nu(COO)_{assym}$ 1597(s), $\nu(COO)_{sym}$ 1352(s), ν(phenolic CO) 1251 (s), $\nu(ClO_4^{-1})$ 1120, 1088. No further characterization was attempted.

3.2.8 A note on elemental analysis

We had faced difficulty in matching elemental analysis of the multinuclear complexes reported in this chapter. The presence of extensive H-bonding, disordered solvents and empty spaces within the lattice (Section 3.3) make all of these capsular complexes susceptible to loss of pyridine and absorption of indefinite amount of water. As the elemental analysis were inconclusive we have used the formula based on the structural analysis Cu(II) complexes being labile and subjected to fragmentation, ESI-Mass support the presence of Cu_4L_4 cage but not the entire formula.

3.2.9 X-ray data collection, structure solution and refinement

The crystal structures of $[Cu_8(S\text{-5OMehis})_8(Py)_8]$ (**1a**), $[Cu_2(S\text{-5OMehis})_2].3H_2O$ (**1b**) and $[Cu_8(R\text{-his})_8(Py)_{10}]$ (**3a**) were obtained by single crystal X-ray diffraction technique. Single crystal of **1a** and **3a** were obtained by slow diffusion of diethyl ether into the pyridine solution of the complex. Single crystal of **1b** was grown by slow evaporation of the water solution of the complex. The data collection and structure refinement method are discussed in chapter 2. Due to desolvation especially in complex **3a** out of 5 frame collected data, 3 were very poor so, we were unable to refine all the atom anisotropically and thermal ellipsoid parameters of some of the atoms in complex **1a** and **3a** are very

high. The selected crystallographic data of complexes **1a**, **1b** and **3a** has given in Table 3.A.

Table 3.A. Selected crystallographic data for complexes **1a**, **1b** and **3a**

Complexes	**1a**	**1b**	**3a**
Empirical formula	$C_{76}H_{75}Cu_4N_{16}O_{16}$	$C_{28}H_{30}Cu_2N_6O_{11}$	$C_{163}H_{164}Cu_8N_{36}O_{27}$
Formula weight	1722.72	751.65	3567.64
Wavelength (Å)	0.71073	0.71073	0.71073
Crystal system	Orthorhombic	Orthorhombic	Triclinic
Space group	$C222_1$	$C222_1$	P_1
a, Å	24.769(5)	11.3790(4)	16.8174(15)
b, Å	25.780(5)	15.5705(4)	18.1057(18)
c, Å	32.508(6)	17.9156(6)	19.8038(18)
α, deg	90.00	90.00	90.648(6)
β, deg	90.00	90.00	112.891(5)
γ, deg	90.00	90.00	105.670(5)
Volume, Å^3	2075.8(7)	3174.23(17)	5302.5(9)
Z /ρ / μ	4 / 1.102 / 0.866	4 / 1.640 / 1.416	1 / 1.151 / 0.852
Collected/ indep reflns	43774 / 11856	14313 / 2557	30170 / 14579
Flack parameter	0.004(19)	-0.003(16)	0.00
GOF	1.098	0.816	1.527
Final R indices [*I*>2sigma(*I*)]	R1 = 0.0671 wR2 = 0.1928	R1 = 0.0338 wR2 = 0.0976	R1 = 0.1640 wR2 = 0.3977
R indices (all data)	R1 = 0.0846 wR2 = 0.2106	R1 = 0.0379 wR2 = 0.1019	R1 = 0.2491 wR2 = 0.4539

Table 3.B. Selected bond distances (Å) and angles (°) of complex **1a** and **1b**

Complexes	**1a**				**1b**
	Cu1	Cu2	Cu3	Cu4	Cu1
Cu-O1$_{acetate}$	1.987 (6)	1.995 (6)	1.978 (7)	1.901 (7)	1.970 (5)
Cu-O3$_{phenolate}$	1.904 (6)	1.928 (6)	1.898 (8)	1.957 (6)	1.900 (5)
Cu-N$_{amine}$	2.008 (7)	2.034 (7)	2.007 (8)	1.988 (7)	1.928 (6)
Cu-N$_{imidazole}$	1.990 (8)	1.975 (8)	1.991 (8)	1.994 (8)	1.956 (6)
Cu-N$_{pyridine}$	2.422 (11)	2.349 (8)	2.344 (10)		
N$_{amine}$-Cu-O$_{acetate}$	82.4 (3)	81.7 (3)	84.3 (3)	82.4 (3)	82.5 (3)
O$_{acetate}$-Cu-N$_{imidazole}$	91.9 (3)	92.5 (3)	91.0 (3)	92.8 (3)	91.1 (3)
N$_{imidazole}$-Cu-O$_{phenolate}$	92.2 (3)	91.0 (3)	89.4 (4)	90.6 (3)	93.9 (3)
O$_{phenolate}$-Cu-N$_{amine}$	92.3 (3)	93.7 (3)	92.7 (3)	94.0 (3)	93.8 (3)
N$_{amine}$-Cu-N$_{imidazole}$	167.2 (3)	162.2 (3)	162.0 (3)	174.1 (3)	168.6 (3)
O$_{acetate}$-Cu-O$_{phenolate}$	172.4 (3)	174.5 (3)	171.4 (4)	176.3 (3)	170.8 (2)
N$_{pyridine}$-Cu-N$_{amine}$	96.3 (4)	98.8 (3)	95.9 (3)		
N$_{pyridine}$-Cu-N$_{imidazole}$	95.5 (4)	97.9 (3)	101.6 (3)		
τ	0.09	0.21	0.16	0.03	0.02

3.3 Results and Discussion

3.3.1 Synthesis and Selected Properties

The complexes **[**Cu_8(*S*-5OMehis)$_8$(Pyridine)$_8$] (**1a)** and [Cu_8(*R*-his)$_8$(Pyridine)$_{10}$] (**3a)** were synthesized following the protocol used for [Cu_8(*S*-his)$_8$(Pyridine)$_{10}$].[2] The crystals of **[**Cu_2(*S*-5OMehis)$_2$]·3H_2O (**1b)** was isolated from aqueous solution of **1a**. In IR spectrum carboxylate stretches for **1a**, **3a**, **1b** and the complexes obtained from 3-OMe substituted ligand (Section 3.2.5) and racemic ligand (Section 3.2.7) were observed at ~1610 and ~1380 cm^{-1} for υ_{assym} and υ_{sym} respectively.[3] The band around 1250-1270 cm^{-1} might be assigned to υ(C-O) of phenolic group.[3] Conductance of all the complexes except **1b** (insoluble) in DMF showed non-electrolyte nature of the complexes.[4] The room temperature magnetic moments for **1a** and **3a** at 1.70 and 1.62 B.M./Copper respectively are less than expected for a S = ½ system 1.73 B.M. This indicates the presence of

antiferromagnetic coupling between the Cu(II) centers.[5] Susceptibility measurements on **1b** were not performed due to the lack of sufficient quantity (Section 3.2.4).

3.3.2 X-ray structure of [Cu_8(*S*-5omehis)$_8$(Pyridine)$_8$] (1a)

The complex **1a** was crystallized in the chiral space group of $C222_1$ containing two slightly different tetranuclear units (**a** and **b**) in the unit cell held together by H-bond in the solid state and the substituent OMe groups are arranged in such a way at the top and bottom of the capsule that formed a crown shape (Figure 3.1). Four pyridine molecules are trapped inside the cavity similar to the capsule formed by L-histidine derived ligand [Cu_8(*S*-his)$_8$ (Pyridine)$_{10}$] [2] The ORTEP [6] view and selected bond distances along with angles of complex **1a** are listed in Figure 3.2 and Table 3.B.

The octanuclear capsular complex has been formed by two tetranuclear unit joined by eight H-bonds between the carboxylate oxygen and imidazole N-H.[7] The tetranuclear units has been formed by four mononuclear Cu(II) complex where the histidine arm from one of the ligand coordinated to the next Cu(II) unit and so on.

Thus two tetranuclear units connected by coordinate bond has been joined again through H-bonds formed the cage. Each Cu(II) is coordinated by three donor (amine, phenol and carboxylate) from one ligand, one histidine from the neighboring ligand and a pyridine in the fifth axial site. Out of eight axial pyridine coordinated to eight Cu(II), four are inside the cage.

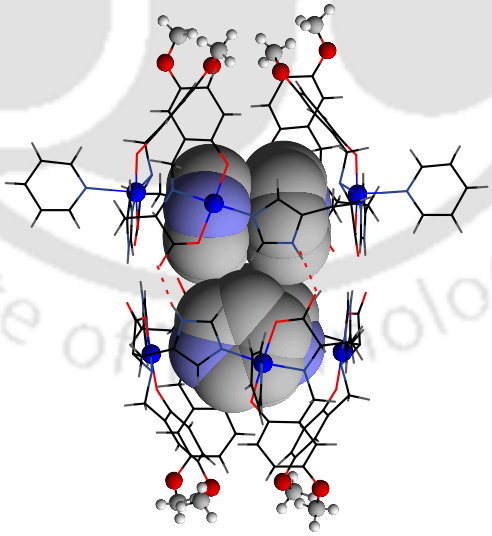

Figure 3.1. *Crown shaped molecular structure of [Cu_8(S-5OMehis)$_8$·(Pyridine)$_8$] **(1a)***

The two of the pyridine inside the cage are coordinated to the Cu(II) with a longer bond (>3Å) simultaneously forming a H-bond with the amine N-H (<3Å) (Figure 3.3). This unusual structural feature was reported for [Cu_8(*S*-his)$_8$(Pyridine)$_{10}$] as well.[2] The

coordination around the each Cu(II) centre in both the units is N_3O_2 donor environment. The geometry of Cu(II) centers are best described as square pyramidal in unit **1a** and trigonal bipyramidal geometry in **1b** according to τ value.[8] The conformation at the chiral carbon of the ligand is *S* since the ligand was synthesized from *S*-isomer of the histidine and the coordination of amine nitrogen to the metal centre gives rise to asymmetric secondary nitrogen atom, which has the *R* absolute configuration. Thus substitution at the fifth position of the aromatic ring of the ligand forms structurally similar octanuclear capsular complex. Substitution increases the overall size the cage at the both end from 13Å to 19Å (Figure 3.4).

Table 3.C. Selected bond distances (Å) and angles (°) of complex 3a.

Atoms	Cu1	Cu2	Cu3	Cu4	Cu5	Cu6	Cu7	Cu8
$Cu\text{-}O1_{acetate}$	2.0023	1.9855	1.9619	1.9851	1.8742	2.0013	1.9436	1.9513
$Cu\text{-}O3_{phenolate}$	1.8777	1.8574	1.9120	1.8643	1.8285	1.9404	1.8738	1.9081
$Cu\text{-}N3_{amine}$	1.9820	1.9867	1.9664	2.0175	2.0545	2.0303	1.9428	2.0306
$Cu\text{-}N1_{imidazole}$	1.9671	1.9260	1.9273	1.9881	1.9573	1.9703	1.9367	1.9513
$Cu\text{-}N4_{pyridine}$	2.4708		2.4188	2.4708	2.4155	2.3569	2.3286	
$N3_{amine}\text{-}Cu\text{-}O1_{acetate}$	81.9	83.6	82.1	80.7	82.0	82.4	83.2	81.2
$O1_{acetate}\text{-}Cu\text{-}N1_{imidazole}$	88.4	93.2	92.2	94.3	93.4	92.1	94.3	92.6
$N1_{imidazole}\text{-}Cu\text{-}O3_{phenolate}$	94.8	89.8	89.9	91.4	94.0	92.9	88.1	94.2
$O3_{phenolate}\text{-}Cu\text{-}N3_{amine}$	94.4	93.4	94.8	92.6	99.6	90.9	92.9	90.7
$N3_{amine}\text{-}Cu\text{-}N1_{imidazole}$	159.1	176.8	167.4	167.2	166.1	161.8	165.8	158.0
$O1_{acetate}\text{-}Cu\text{-}O3_{phenolate}$	176.3	173.3	174.0	172.2	169.0	172.0	172.9	171.7
$N4_{pyridine}\text{-}Cu\text{-}N3_{amine}$	98.1		97.1	98.9	90.0	100.6	93.9	
$N4_{pyridine}\text{-}Cu\text{-}N1_{imidazole}$	100.1		94.5	93.1	102.4	97.1	100.1	
τ	0.29	0.06	0.11	0.08	0.05	0.17	0.12	0.23

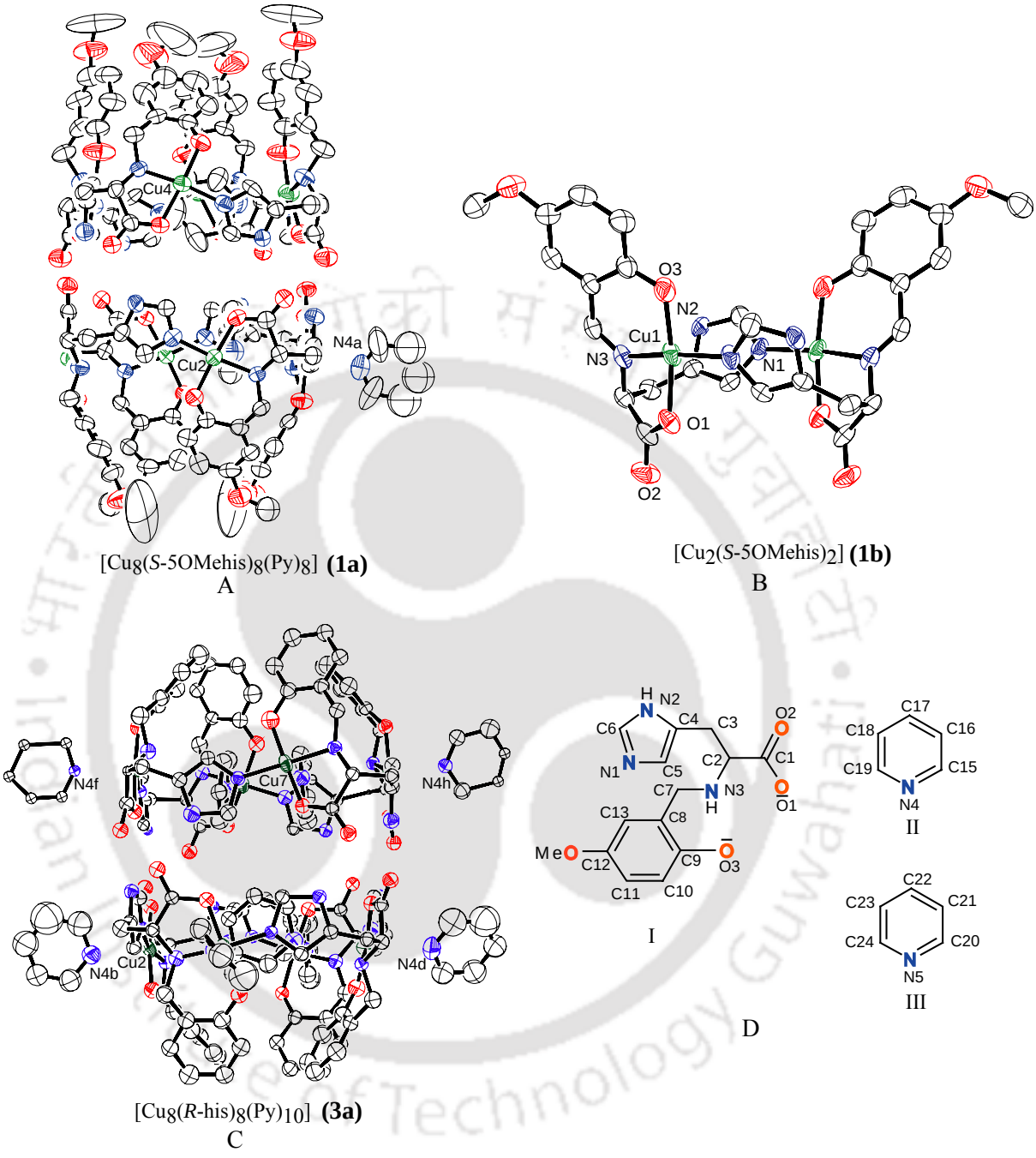

Figure 3.2. *(A), (B) and (C) are the ORTEP figure of complex **1a, 1b** and **3a** (probability set to 50% for **1a** and **1b**, 30 % for **3a**). (D) Numbering scheme of (I) ligand for complex **1a** and **3a**. (II) and (III) are pyridine outside the cavity and inside the cavity respectively.*

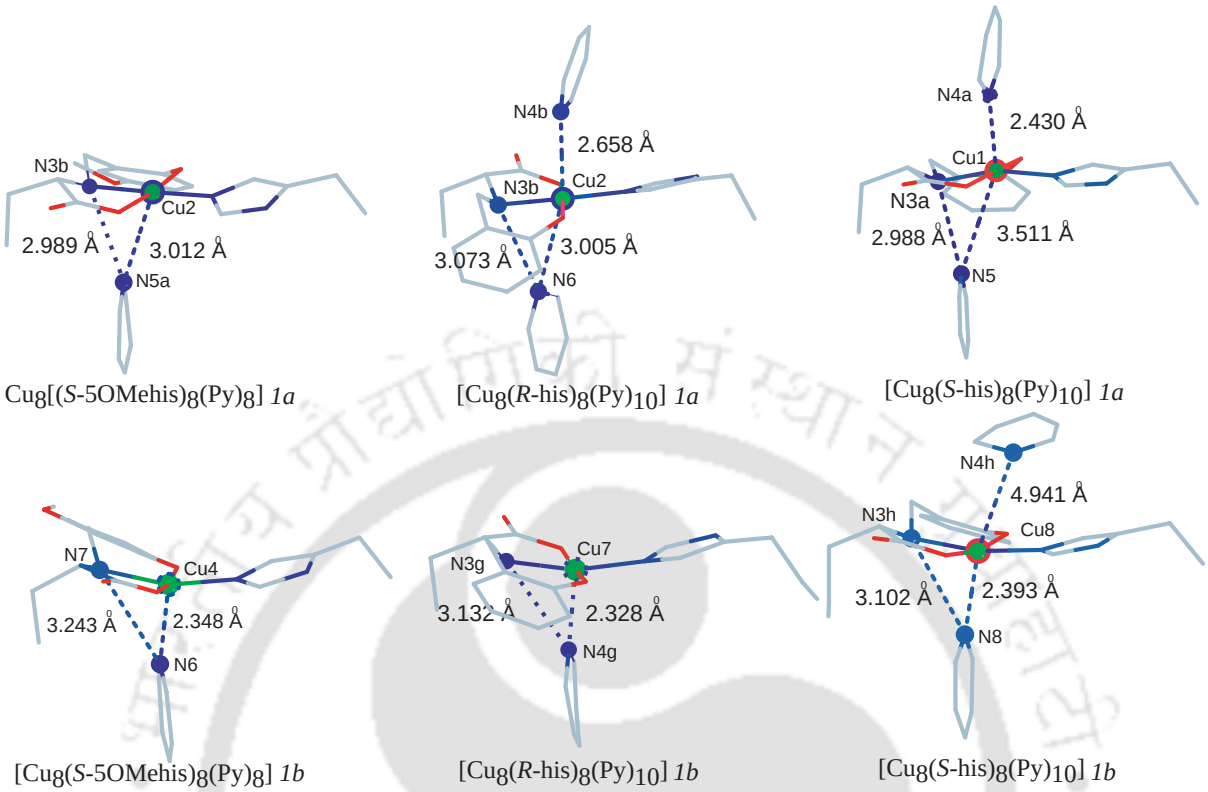

Figure 3.3. *Interdependence of H-bond and Cu(II) coordination observed in the binding of pyridine inside and outside the capsule. [1a and 1b denotes to Cu(II) of different unit]*

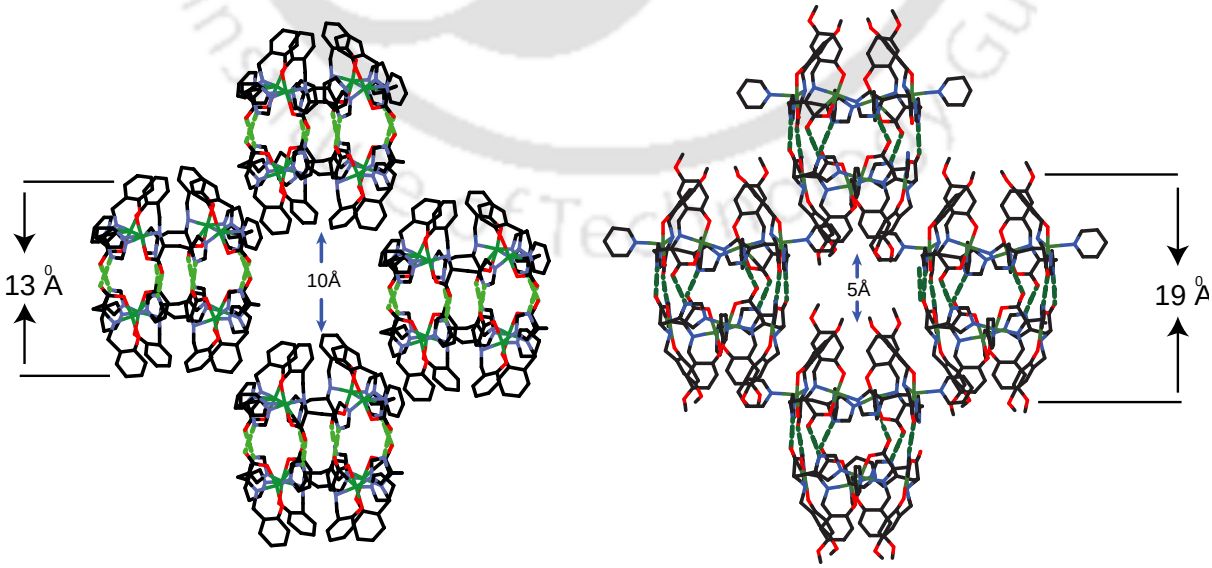

[Cu8(*R*-his)8(Pyridine)8] (**3a**) [Cu8(*S*-5OMehis)8(Pyridine)8] (**1a**)

Figure 3.4. *Comparison of lattice between **1a** and **3a***

3.3.3 X-ray structure of $[Cu_8(R\text{-his})_8(Pyridine)_{10}]\cdot 2Pyridine$ (3a)

Structurally, **3a** is the mirror image of the octanuclear complex $[Cu_8(S\text{-his})_8(Pyridine)_{10}]$[2] reported earlier except amount of solvent in the lattice. The ORTEP[6] figure, selected bond distances and angles are given in Figure 3.2 and Table 3.C respectively. The crystal is more susceptible to desolvation compared to **1a**. Large size, desolvation, especially loss of pyridine and moisture acquiring tendency of these cages poses difficulty in getting a reasonable analysis (Section 3.2.9) as well as structural analysis. The lattice of **3a** and **1a** shows formation of large channels.

3.3.4 ESI-MS analysis of the octanuclear complexes

We were able to crystallize the octanuclear **1a** (Section 3.3.2) and **3a** (Section 3.3.3) but could not isolate crystals from the ligand **2**. In order to investigate whether a similar octanuclear complex formation occurred or not, we have utilized electro spray ionization mass spectral (ESI-Mass) analysis. Earlier ESI-Mass of $[Cu_8(S\text{-his})_8(Pyridine)_{10}]$ in MeOH showed molecular ion peak of $Cu_4L_4H^+$ along with $Cu_2L_2H^+$ and $Cu_3L_3H^+$ (L = *S*-his).[2] This was not surprising as the H-bonds between the two Cu_4L_4 unit in the octanuclear complex can be fragmented in polar MeOH. Also the lability of Cu(II) and loosely bound axial pyridines can lead to fragmentation.

The ESI-MS of $[Cu_8(S\text{-5OMehis})_8(Pyridine)_8]$ **(1a)** in MeOH shows molecular ion peak maximum at 1059, 727 and 705 for $Cu_3(S\text{-5OMehis})_3H^+$ (calcd 1059.15), $Cu_2(S\text{-5OMehis})_2Na^+$ (calcd 727.06) and $Cu_2(S\text{-5OMehis})_2H^+$ (calcd 705.08) respectively (Figure 3.5 inset). The $[Cu_8(R\text{-his})_8(Pyridine)_{10}]$ **(3a)** shows molecular ion peak maximum at 645 and 969 for $Cu_3(R\text{-his})_3H^+$ (calcd 645.08) and $Cu_2(R\text{-his})_2H^+$ (calcd 969.01). The isotopic distribution pattern for the entire ion matched with that of the calculated pattern. The complex **(2a)** shows molecular ion peak maximum at 1411, 1059, 727 and 705 for $Cu_4(S\text{-3OMehis})_4H^+$ (calcd 1411.19), $Cu_3(S\text{-3OMehis})_3H^+$ (calcd 1059.15), $Cu_2(S\text{-3OMehis})_2Na^+$ (calcd 727.06), and $Cu_2(S\text{-3OMehis})_2H^+$ (calcd 705.08) respectively (Figure 3.5). Even though the identity of the **1a** and **3a** as octanuclear species were confirmed from the structural analysis, the absence of $Cu_4L_4H^+$ peak in the mass spectral results shows that $Cu_4L_4H^+$ ion may not be very stable. However, the $Cu_4(S\text{-3OMehis})_4H^+$ for **2a** has been observed indirectly confirming the formation of octanuclear capsular complex with ligand **2**. Overall, the structural characterization of **1a** and ESI-Mass results supports formation of octanuclear capsular complex with both 3-methoxy and 5-methoxy derivative of the ligand.

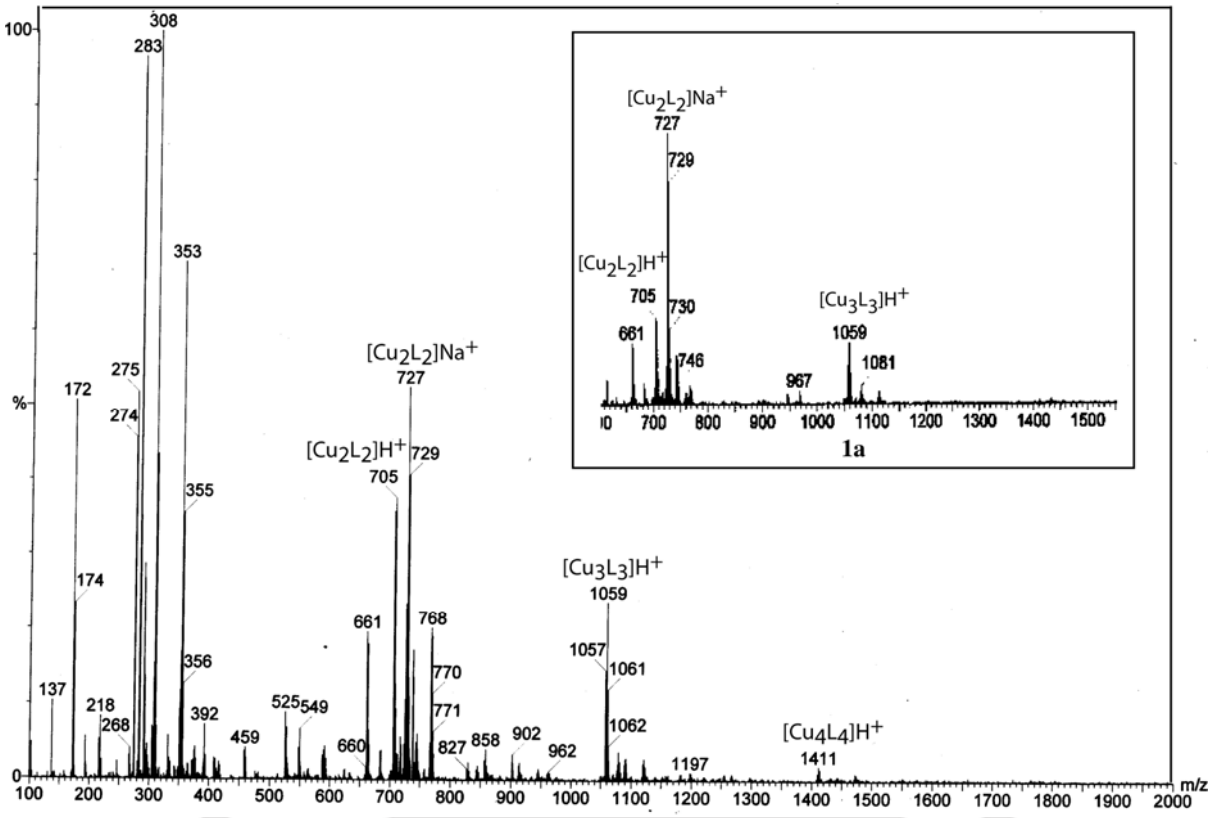

Figure 3.5. *ESI-MS spectrum of complex **2a** with **1a** as inset*

3.3.5 Effect of ligand chirality

We have studied the effect of ligand chirality on the formation of Cu(II) capsule using L-histidine, D-histidine and DL-histidine derived ligands. With D-histidine we were able to get the octanuclear capsular complex (**3a**) mirror image isomer of the octanuclear cage of L-histidine. For the complexation with DL (racemic) ligand we expected to get either (a) racemic crystal with both type capsule or (b) spontaneously resolved both D-type and L-type crystals as racemic mixture. Reaction of racemic ligand with Cu(II) in MeOH resulted in a insoluble solid (Section 3.2.7) contaminated with perchlorate salts. Mixing crystals of octanuclear complexes, prepared with D-type (**3a**) and L-type ligands separately, in pyridine yielded insoluble solid within minutes. FTIR spectra of this solid and that of capsular complexes are nearly identical. Thus the gross structure of the CuL unit is unlikely to be very different. We assume that the presence of mirror image units might have prevented the formation of C_4 symmetric cycle necessary for capsule formation and instead promotes polymerization (Figure 3.6). This result shows the

importance of ligand chirality in the formation of chiral capsular cages formed by self assembly process.

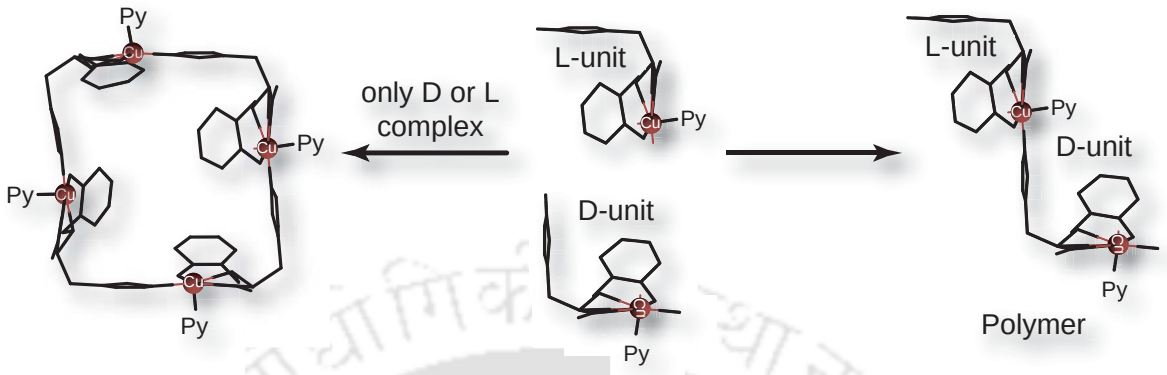

Figure 3.6. *Effect of ligand chirality on the formation of capsule or polymer*

3.3.6 X-ray structure of $[Cu_2(S\text{-}5omehis)_2]\cdot 3H_2O$ (1b)

The complex **1a** is sparingly soluble in water. We were able to isolate few crystals of **1b** with great difficulty from the dilute aqueous solution of **1a**. Crystals of **1b** once formed are insoluble even in DMF. Synthesis of either **1a** or **1b** directly from ligand and metal ion does not work. This dependency on solvent has been explained in the Chapter II on the basis of phenoxo bridge formation in the initial stage (Scheme 2.2). Thus studies of **1b** are restricted to structural study only.

The complex **1b** was crystallized in the chiral space group ***C222₁*** in the orthorhombic crystal system. The ORTEP diagram, selected bond distances and angles are given in Figure 3.2 and Table 3.B respectively.

The structural identity of the complex **1b** was found to be a binuclear complex of Cu(II). The complex $[Cu_2(S\text{-}5omehis)_2]\cdot 3H_2O$ (**1b)** consists of two Cu(II) unit of square planar geometry bridged by imidazole group, side arm of the ligand. The co-ordination geometry around the each Cu(II) center is N_2O_2 donor environment, three from one ligand [amine N, carboxylate O and Phenolate O] and one imidazole N from another ligand. The in-plane bond lengths Cu-N and Cu-O are matched with complex **1a** and is typical for Cu(II) complexes.[9]

The conformation at the chiral carbon of the ligand in **1b** is *S*. In addition to the asymmetric carbon centre in the ligand, the coordination amine N to the Cu(II) gives rise

to an asymmetric secondary nitrogen atom, N2 which has the *R* configuration.

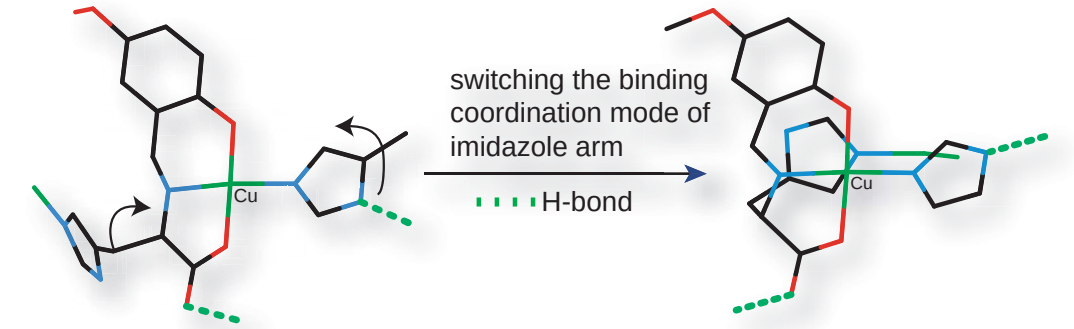

[Cu_8(*S*-5OMehis)$_8$.(Pyridine)$_8$] **1a** [Cu_2(*S*-5OMehis)$_2$] **1b**

1A

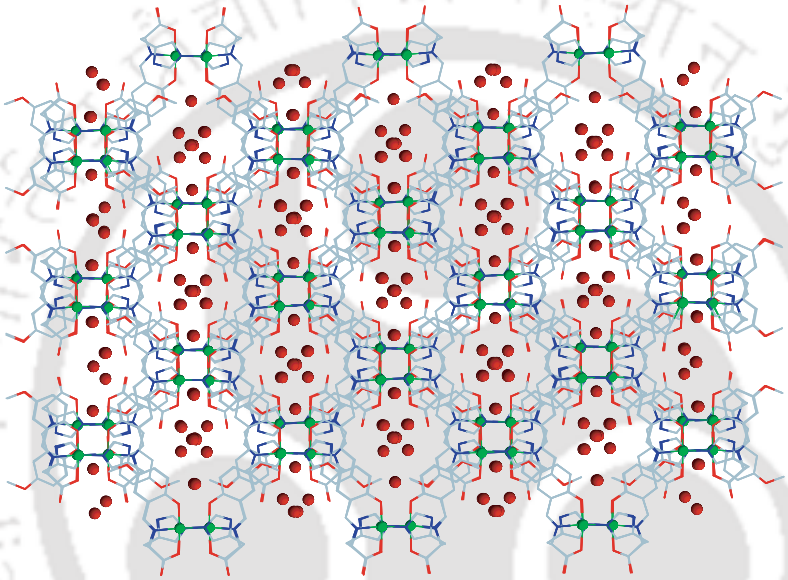

1B

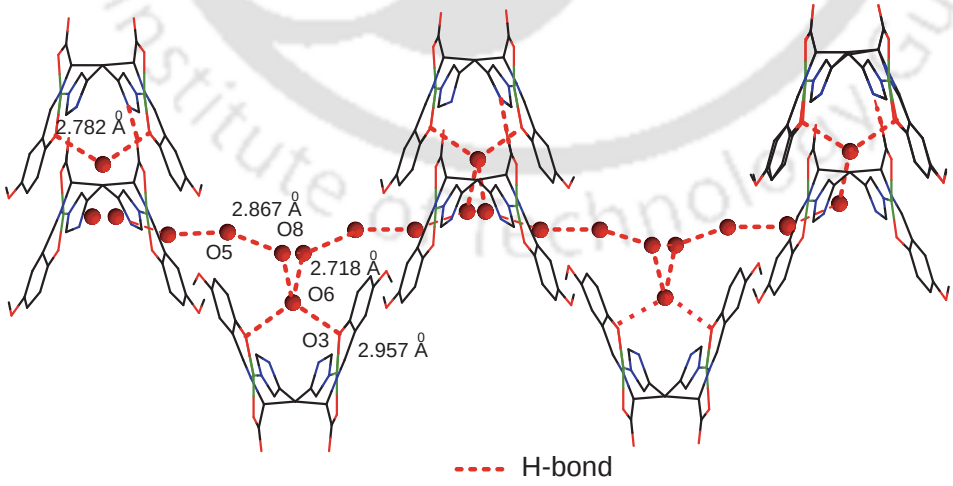

1C

Figure 3.7. *(1A) comparison of bonding mode between* ***1a*** *and* ***1b****. (1B) water filled one dimentional channel. (1C) H-bonding network in crystal lattice.*

In comparison to molecular structure of **1a** in which ligand coordinated in such a manner that non-coordinated carboxylate O and imidazole NH are oriented in syn direction but in complex **1b** imidazole arm switched in opposite direction resulted the carboxylate O and imidazole NH in anti direction (1A Figure 3.7).

All the potential H-bond donors (amine, imidazole) and acceptors (phenolate oxygen, two carboxylate oxygen) from the ligand and three water molecules in lattice take part in inter-molecular H-bond formation, forming a extensive H-bonded network with large one dimensional channel filled with water (dia: ~10 Å) in the crystal lattice (1B Figure 3.7). In the lattice, binuclear units are connected by H-bonding through uncoordinated carboxylate O of the ligand from one binuclear unit and imidazole NH of different binuclear unit at a distance of 2.782 Å.[7] Out of the three H-bonded water molecules present in the lattice, one of the water molecules labeled O6 bridged two coordinated phenolate O through H-bonding at a distance of 2.957 Å in the binuclear unit and other two water molecules labeled O5 and O8, are H-bonded with themselves and also with O6 to form a chain of water in lattice. The distances of O6…O8, O8…O5 and O5…O5 are 2.718, 2.867 and 2.838 respectively (1C Figure 3.7). All the O..O H-bonds showed here are within literature limits.[10]

3.3.7 Absorption and EPR spectra

The UV-visible spectral characteristic data of the complexes $[Cu_8(S\text{-}5OMehis)_8(Pyridine)_8]$ (**1a)**, complex isolated in section 3.2.5 (**2a)** and $[Cu_8(R\text{-his})_8(Pyridine)_{10}]$ (**3a)** solvent are given in Table 3.D and spectral figure are shown in Figure 3.8. The absorption maxima at ~400 nm are likely to be LMCT origin evident from high ε value (≥ 500 dm^3 mol^{-1} cm^{-1}/Cu). The absorption maxima between 600 – 700 nm with ε value in between 100 – 200 (dm^3 mol^{-1} cm^{-1}/Cu) are of ligand field origin (*d-d* transition). The ε values of **2a** are calculated according to $[Cu_4(S\text{-}3OMehis)_4]$ unit. The EPR spectral characteristic of all the complexes are shown in Figure 3.9 and the data at 77 K in methanol are shown in Table 3.D. The complexes **1a , 2a** and **3a** show a typical square pyramidal EPR spectra as is evident from their $A_{\parallel}$ values ~178G and g values.[11]

Table 3.D. UV-Visible and EPR spectral data of complexes **1a**, **2a** and **3a**

Complexes	λ/nm (ε/cm^{-1} M^{-1})/ Cu	EPR, g	$A_{\parallel}$/G
1a	420 (625), 620 (199)	2.23, 2.04	178
2a*	404 (698), 643 (120)	2.23, 2.04	178
3a	401 (548), 626 (138)	2.24, 2.04	178

*Complex isolated in Section 3.2.5

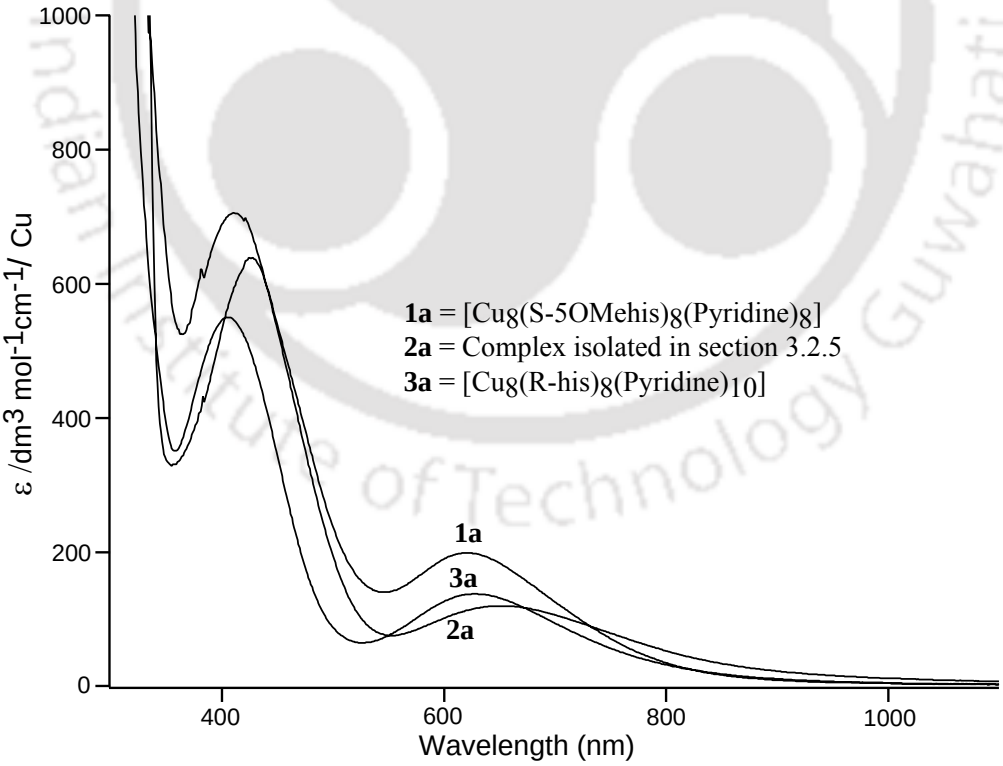

Figure 3.8. *UV-Visible spectra of complexes*

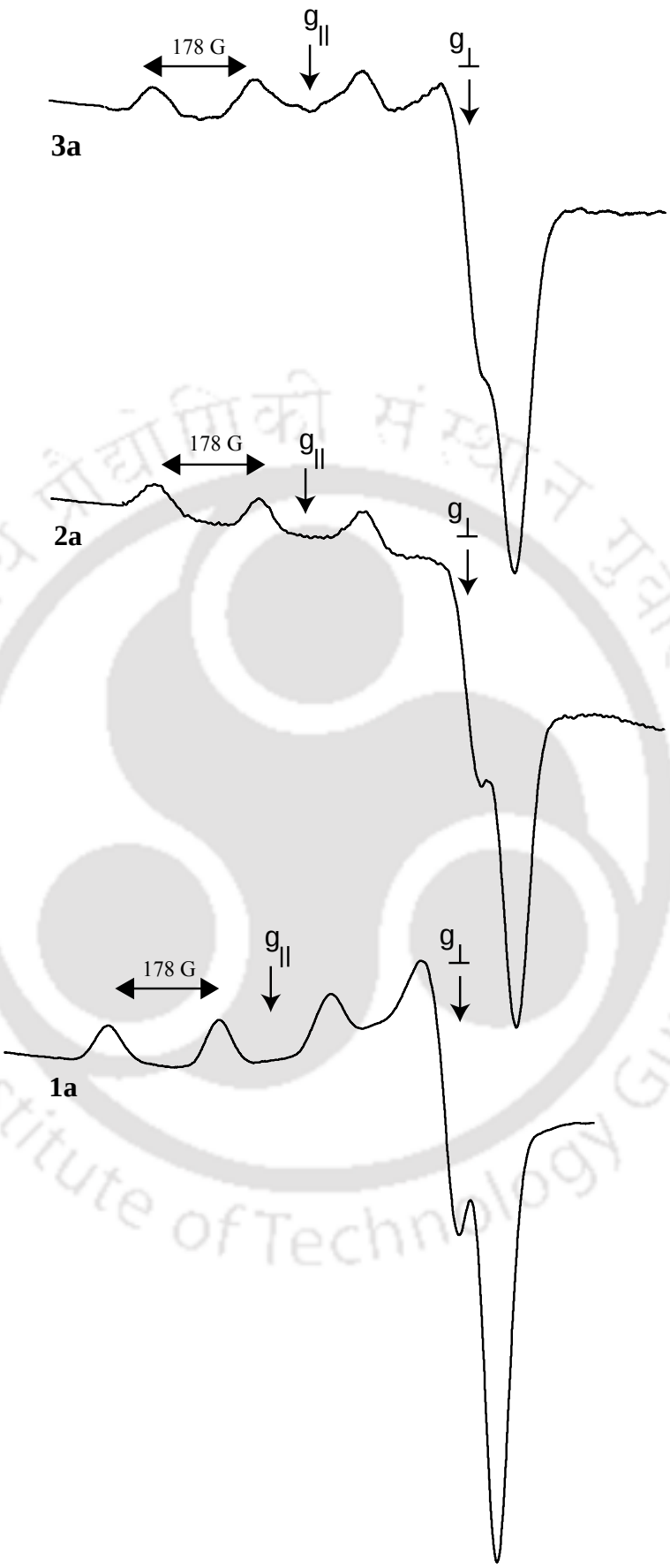

Figure 3.9. *EPR spectra of complexes **1a**, **2a** and **3a***

Conclusions

In this chapter we have reported synthesis, characterization and structural analysis of octameric Cu(II) capsule using substitution of aromatic ring and different chiral form (D, and DL) of ligand. We are also able to isolate and structurally characterized a new binuclear complex $[Cu_2(S\text{-}5OMehis)_2]$ (**1b)**, with one dimensional water filled channel during the solution study from complex $[Cu_8(S\text{-}5OMehis)_8(Pyridine)_8]$ (**1a**). Structural characterization of these two new capsules signifies that substitution in the 3 and 5 position of the aromatic ring does not destabilize the capsule and homochirality is strongly necessary for the formation of capsular complex. The vertical size of the capsule increased from 13 Å to 19 Å in the 5-methoxy substituted capsule (Figure 3.4). Comparing this new structure with the earlier one without substitution we also found that organization of capsules in the lattice is different. Packing is tighter and crystals are more stable (Figure 3.4).

In addition, a comparison of the binding of pyridine inside the capsule has been compared (Figure 3.3). It shows the binding of inside and outside pyridines with Cu(II) and the associated H-bond with amine NH are interdependent in such a way that strengthening of one weakens the other. Shorter Cu-N_{inner} pyridine bond lengths ($\leq$ 3Å) resulting in loss of externally bound pyridine. Pyridines bound in 5-methoxy substituted capsules $[Cu_8(S\text{-}5OMehis)_8(Pyridine)_8]$ (**1a**) are strongly bonded compared to $[Cu_8(R\text{-}his)_8(Pyridine)_{10}]$ (**3a**) and $[Cu_8(S\text{-}his)_8(Pyridine)_{10}]$[2] capsules.

References

1. Alam, M. A.; Nethaji, M.; Ray, M. *Inorg. Chem.* **2005**, *44*, 1302.

2. Alam, M. A.; Nethaji, M.; Ray, M. *Angew. Chem. Int. Ed.* **2003,** *42*, 1940.

3. Nakamoto, K. Infrared and Raman Spectra of Inorganic Compounds, 5th ed.; Wiley-Interscience: New York, 1997; Part B.

4. Geary, W. J. *Coord. Chem. Rev*. **1971**, *7*, 81.

5. (a) Earnshaw, A. Introduction to Magnetochemistry; Academic Press: London, 1968. (b) Figgis, B. N.; Lewis, J. *Prog. Inorg. Chem*. **1964**, *6*, 37.

6. Johnson, C. K. ORTEP, Report ORNL-3794; Oak Ridge National Laboratory: Oak Ridge, TN, 1976.

7. The (imidazole) NH…O (carboxylate) distance range 2.69- 2.98 Å ; Couchman, S. M.; Jeffery, J. C.; Ward, M. D. *Polyhedron*, **1999**, *18*, 2633.

8. Addision, A. W.; Rao, T. N.; Reedijk, J.; van Rijn, J.; Verschoor, G. C. *J. Chem. Soc., Dalton Trans.* **1984**, 1349.

9. (a) Koh, L. L.; Ranford, J. O.; Robinson, W. T.; Svensson, J. O.; Tan, A. L. C.; Wu, D. *Inorg. Chem.,* **1996**, *35*, 6466. (b) Vittal, J. J.; Wang, X.; Ranford, J. J. *Inorg.Chem.*, **2003**, *42*, 3390.

10. (a) Desiraju, G. R. *Perspective in Supramolecular Chemistry*, Wiley, *Vol 7*. (b) Miyake, R.; Tashiro, S.; Shiro, M.; Tanaka, K.; Shionoya, M. *J.Am. Chem. Soc*. **2008**, *130*, 5646. (c) Wang, X.; Vittal, J. J. *Inorg. Chem.* **2003**, *42*, 5135. (d) Yang, C. T.; Moubaraki, B.; Murray, K. S.; Vittal, J. J. *Dalton Trans*, **2003**, 880. (e) Mckinlay, R. M.; Thallapally, P. K.; Cave, G. W. V.; Atwood, J. L. *Angew. Chem*, **2005**, *44*, 5733.

11. Yokoi, H.; Addision, A. W. *Inorg. Chem.* **1997**, *16,* 1341.

In previous chapter we have noticed that substitution on aromatic ring of the ligand does not inhibit the formation of capsular complex. In this chapter we have tried to sec if anything other than pyridine can be inserted in the cage or not. Thus, we have synthesized and structurally characterized a set of Cu(II) complexes with Methyl and hydroxo (H-bonding capable) substituted pyridine using substituted and unsubstituted amino acid derived ligands. The results showed that using substituted pyridine yielded monomeric Cu(II) complexes instead of the capsular assembly. Interestingly, the monomeric complexes showed formation of 1D chiral channels filled with removable water molecules in the crystals.

4.1 Experimental Section

Details of the solvent purification, analytical measurements have already discussed in chapter 2 and chapter 3. The starting materials 3-Hydroxy pyridine (3-Hydpy) and 2-Methyl pyridine (2-Mepy) were brought from Merck. The ligand [*S*-H_2salhis] was synthesized before.[1] The starting materials other than that stated above already been discussed in previous chapter 3.

4.2 Syntheses of Cu(II) complexes

4.2.1 [Cu(*S*-his)(3-Hydpyridine)]·3H_2O (1a)

Complex Cu_8(*S*-His)$_8$(pyridine)$_{10}$][1] (0.200 g, 0.066 mmol) was taken in 20 mL of dry methanol followed by addition of 3-hydroxypyridine (0.100 g, 1.47 mmol) to the methanolic solution which was kept for slow evaporation at room temperature. After 2 days green crystals were formed. The crystals were filtered and washed with methanol and dried in vacuum desiccator. Yield: 50 %. IR (KBr, cm^{-1}) ν(COO)asym 1601, ν(COO)sym 1396.

Alternatively the complex **1a** can be prepared directly from the ligand following the procedure given below.

Ligand H_2S-his 0.202 g (0.771 mmol) was deprotonated with KOH 0.087 g (1.54 mmol) in 10 ml MeOH. $Cu(NO_3)_2.3H_2O$ 0.186 g (0.771 mmol) was dissolved in 3 ml dry MeOH and was added dropwise into the deprotonated ligand solution. Color of the reaction mixture became green with white particles of KNO_3 precipitated out from the solution. Excess 3-hydroxypyridine 0.145 g (1.53 mmol) was added to this solution. The color of the solution was turned deep green immediately. Reaction mixture was filtered

and kept in open atmosphere for crystallization. After 3-4 days green crystal was formed. Crystals were filtered and washed with cold MeOH. The IR of **1a** prepared this way was identical with that of prepared from octanuclear Cu(II) complex.[1] Yield (57%). $Cu(C_{13}H_{13}N_3O_3)$ $(C_5H_5NO)\bullet 3H_2O$ Anal. Calcd (%) for C 45.81, H 5.12, N 11.88; found C 44.93, H 5.41, N 11.40. IR (KBr, cm^{-1}) ν(COO)asym 1601, ν(COO)sym 1396.

4.2.2 [Cu(*S*-5Omehis)(3-Hydpyridine)]·3H$_2$O (2a)

This compound has been prepared by following the procedures described for **1a** using the H_2*S*-5Ome ligand. Yield 50 %. $Cu(C_{14}H_{15}N_3O_4)(C_5H_5NO)\bullet 3H_2O$ Anal. Calcd (%) for C 45.46, H 5.22, N 11.16; found C 45.91, H 5.68, N 11.29. IR (KBr, cm^{-1}) ν(COO)asym 1616, ν(COO)sym 1382.

4.2.3 [Cu(*S*-5Omehis)(2-Mepyridine)]·3H$_2$O (2b)

Complex $[Cu_8(S\text{-}5omeHis)_8\bullet(pyridine)_4]$ (0.200 g, 0.066 mmol) was dissolved in 10 mL of 2-Methylpyridine. After 2 days green crystals were formed by slow diffusion of diethyl ether into the complex solution. Yield 50 %. $Cu(C_{14}H_{15}N_3O_4)(C_6H_7N)\bullet 3H_2O$ Anal. Calcd (%) for C 48.04, H 5.64, N 11.20; found C 46.51, H 5.15, N 11.25. IR (KBr, cm^{-1}) ν(COO)asym 1612, ν(COO)sym 1386.

4.2.4 [Cu(*S*-3Omehis)(3-Hydpyridine)]·4H2O (3a)

This compound has been prepared by following the same procedure like **1a** using H_2*S*-3-Omehis **(3)** as ligand. Yield: 56 %. $Cu(C_{14}H_{15}N_3O_4)(C_5H_5NO)\bullet 4H_2O$ Anal. Calcd (%) for C 43.88, H 5.42, N 10.77; found C 42.90, H 4.95, N 10.52. IR (KBr, cm^{-1}) ν(COO)asym 1606(sh), 1591ν. (COO)sym 1363(s), ν(phenolic CO) 1286.

4.2.5 X-ray Data Collection, Structure Solution and Refinement

The crystal structures of [Cu(*S*-his)(3-Hydpy)]·3H_2O (**1a**), [Cu(*S*-5OMehis)(3-Hydpy)]·3H_2O (**2a**), [Cu(*S*-5OMehis)(2-Mepyridine)]·3H_2O (**2b**) and [Cu(*S*-3Omehis)(3-Hydpy)]·4H_2O (**3a**) were obtained by single crystal X-ray diffraction technique. Single crystal of **1a, 2a** and **3a** were obtained by slow evaporation of the methanolic solution of the complex. Single crystal of **2b** was grown by slow diffusion of diethyl ether into the 2-Mepyridine solution the complex. The data collection and structure refinement method are discussed in chapter 2. The hydrogen atoms wherever possible were located from the

difference Fourier maps and were refined isotropically. The selected crystallographic data of all these complexes has given in Table 4.A.

Table 4.A. Selected crystallographic data of Cu(II) complexes

Complexes	**1a**	**2a**	**2b**	**3a**
Empirical formula	$C_{18}H_{18}CuN_4O_7$	$C_{19}H_{20}CuN_4O_8$	$C_{20}H_{28}CuN_4O_7$	$C_{19}H_{20}CuN_4O_9$
Formula weight	465.91	495.94	500.00	511.93
Wavelength (Å)	0.71073	0.71073	0.71073	0.71073
Crystal system	Monoclinic	Monoclinic	Monoclinic	Monoclinic
Space group	$P2_1$	$P2_1$	$P2_1$	$P2_1$
a, Å	10.9255(6)	10.8028(5)	10.651(2)	11.361(7)
b, Å	9.2418(5)	9.2593(4)	9.2136(19)	9.240(5)
c, Å	11.4207(6)	11.3456(5)	11.284(3)	12.466(7)
α, deg	90.00	90.00	90.00	90.00
β, deg	95.844(3)	96.986(3)	97.089(15)	99.22(4)
γ, deg	90.00	90.00	90.00	90.00
Volume, $Å^3$	1147.17(11)	1126.43(9)	1098.8(4)	1291.8(12)
Z	2	2	2	2
ρ, Mg/m^3	1.418	1.383	1.511	1.291
μ, mm^{-1}	1.001	1.010	1.044	0.891
Reflections collected	2993	3066	18838	3122
Reflections indep	2276	2547	7672	2095
Flack parameter	0.02(3)	0.01(2)	-0.005(9)	-0.03(3)
GOF	1.283	0.837	1.002	0.850
Final R indices [*I*>2sigma(*I*)]	R1 = 0.0490 wR2 = 0.1149	R1 = 0.0445 wR2 = 0.1132	R1 = 0.0398 wR2 = 0.0862	R1 = 0.0535 wR2 = 0.1391
R indices (all data)	R1 = 0.0713 wR2 = 0.1223	R1 = 0.0549 wR2 = 0.1188	R1 = 0.0637 wR2 = 0.0957	R1 = 0.0850 wR2 = 0.1546

Table 4.B. Selected bond lengths (Å) and angles (°) of complexes

Complexes	**1a**	**2a**	**2b**	**3a**
Cu1-O3	1.927(5)	1.916(4)	1.9480(17)	1.905(6)
Cu1-N2	1.986(5)	2.027(5)	2.045(2)	1.994(8)
Cu1-N1	1.999(5)	2.031(4))	2.0379(17)	2.030(6)
Cu1-N4	2.013(5)	2.004(4)	2.0218(18)	1.994(7)
Cu1-O1	2.295(5)	2.301(4)	2.2753(16)	2.285(6)
O3-Cu1-N1	93.6(2)	93.58(16)	92.47(8)	93.7(3)
N1-Cu1-N2	89.3(2)	89.47(17)	90.66(7)	89.7(3)
N2-Cu1-N4	91.6(2)	90.88(19)	88.71(8)	91.2(3)
N4-Cu1-O3	88.5(2)	88.92(18)	88.71(8)	87.7(3)
O3-Cu1-O1	112.6(2)	113.77(17)	106.74(7)	110.6(3)
O1-Cu1-N1	77.2(2)	76.61(16)	76.92(6)	78.2(2)
N1-Cu1-N4	172.4(3)	172.7(2)	177.72(8)	173.6(3)
N2-Cu1-O3	157.2(2)	157.19(19)	164.77(8)	158.8(3)
τ	0.25	0.26	0.22	0.25

4.3 Results and discussion

4.3.1 Synthesis and Selected Properties

All the complexes were synthesized from their corresponding multinuclear complexes as well as directly from the ligand by addition of excess 3-hydroxopyridine and Me-pyridine. The complexes [Cu(*S*-his)(3-Hydpyridine)]·3H_2O **(1a)**, [Cu(*S*-5Omehis)(3-Hydpyridine)]·3H_2O **(2a)** and [Cu(*S*-3OMehis)(3-Hydpyridine)]·4H_2O **(3a)** were crystallized by slow evaporation of compound solution of methanol. The complex [Cu(*S*-5Omehis)(2-Mepyridine)]·3H_2O **(2b)** was crystallized by slow diffusion of diethyl ether into complex solution of 2-Mepyridine. The complexes **1a**, **2a**, **2b** and **3a** showed absorption band at ~1600 and ~1380 cm^{-1} were identified as asymmetric and symmetric carboxylate stretches respectively.[2] The elemental analysis of all the complexes were done but could not matched exactly due to H-bonded solvent water molecules in the lattice (Section 4.2.1- 4.2.4). The thermogravimetric analysis (TGA) of the complexes **1a** and **2b** were performed to prove the presence of solvent. The TGA between 50 - 80ºC shows weight loss of 11.09%, 11.10%, for **1a** and **2b** against the calculated values of

11.46% and 10.80% respectively for $3H_2O$. The conductance values in DMF revealed non-electrolyte nature of the complexes.[3] The room temperature magnetic moment of **1a**, **2a**, **2b** and **3a** are 1.73, 1.78, 1.80, 1.85 B.M. respectively closer to spin only value 1.73 B.M. of expected monomeric Cu(II) complex.[4]

4.3.2 X-ray Structure of [Cu(*S*-his)(3Hydpy)]·3H$_2$O (1a)

The crystals of the complex **1a** were obtained from slow evaporation of methanol afforded green crystals of [Cu(*S*-his)(3Hydpy)]·$3H_2O$ (Hydpy = 3-Hydroxy Pyridine) with space group $P2_1$. The ORTEP[5] figure of the complex has shown in Figure 4.1 and selected bond distances and angles are given in Table 4.B.

The **1a** is mononuclear complex of Cu(II) coordinated with four donors from *S*-his^{-2} and one from 3-Hydroxypyridine, forming a N_3O_2 type donor environment. The coordination geometry at the Cu(II) center is best described as distorted TBP with τ value of 0.23. In a perfect square-pyramidal geometry τ equal to 0, while it is 1 in a perfect trigonal-bipyramidal geometry.[6] The in-plane Cu-N and Cu-O bond lengths are in matched with Cu_8(*S*-His)$_8$(pyridine)$_{10}$][1] and is typical for Cu(II) complexes (Table 4.B).[7] The axial Cu-O(carboxylate) bond distance in 1a is 2.296 Å, longer than expected with compared to other axial Cu-O(carboxylate) bond observed in similar Cu(II) complexes due to Jahn-Teller distortion. For example, [Cu(*S*-bal)(phen)][8] the Cu-O(carboxylate) bond distance is 2.185 Å , in [Cu(bpa)](SO_3CF_3).H_2O[9] is 2.279 Å (bpa^{1-} = *N*,*N*-di-(2-pyridylmethyl)alanine) and in [Cu(bpg)](NO_3).H_2O[9] is 2.195 Å (bpg^{1-} = *N*,*N*-di-(2-pyridylmethyl)glycine).

All the potential H-bond donors (amine, imidazole, hydroxyl group in pyridine) and acceptors (phenolate oxygen, two carboxylate oxygen) from the ligand and three water molecules in lattice take part in inter-molecular H-bond formation, forming a nice H-bonded network with one dimensional channel filled with water (dia: ~7 Å) (Figure 4.4) in the crystal lattice.

In lattice the monomeric units are connected by H-bonding through non-coordinated carboxylate O of the ligand from one monomeric unit with secondary amine NH (O2…N1 2.889 Å) and also non-coordinated carboxylate O from another monomeric unit with phenolic OH of pyridine moiety (O4..O2 2.600 Å) (Figure 4.2).

H-bonded water molecules are oriented in zigzag fashion through H-bonding of coordinated carboxylate O from one unit with coordinated phenolate oxygen of another

unit and also imidazole NH from different unit. The NH..O and O..O distances are within H-bonded range and also shown in Figure 4.2.[10,11]

4.3.3 X-ray Structure of [Cu(*S*-5OMehis)(3Hydpy)]·3H_2O (2a)

The mononuclear complex, [Cu(*S*-5OMehis)(3Hydpy)]·3H_2O **(2a)** was crystallized in the space group of $P2_1$. The ORTEP[5] representation of the complex 2a has shown in Figure 4.1 and selected bond lengths and angles are given in Table 4.B. The coordination environment of Cu(II) in **2a** is same like N_3O_2 type, four from ligand and one from hydroxo pyridine. The angular structural parameter (τ) suggests trigonal bipyramidal geometry (τ = 0.26) of Cu(II).[6] The in-plane bond lengths Cu-N and Cu-O are matched with complex **1a** and is typical for Cu(II) complexes (Table 4.B).[7] The long axial Cu-O (carboxylate) bond length (2.302 Å) is similar to that found for **1a** and other as well.[8,9] In crystal lattice all the potential H-bond donors and acceptors of the ligand (except imidazole NH) and three water molecules form nice H-bonded network with water filled one dimensional channel (dia: ~7.6 Å) (Figure 4.3).

In network the monomeric units are connected by three different type of H-bond which helped to form the network; (i) non-coordinated carboxylate oxygen from one monomer to secondary amine NH from another unit (O2..N1 2.861 Å), (ii) phenolic OH of pyridine moiety from one unit with non-coordinated carboxylate of different unit (O5..O2 2.594 Å), (iii) coordinated phenolic OH from one unit to methoxy group of different unit through two hydrogen bonded water molecule labeled as O8 and O6 (O3..O8..O6..O4 2.773, 2.774, 2.998 Å). Unlike in complex **1a**, water molecules form H-bonded column of water in the lattice of complex **2a** (Figure 4.2).

4.3.4 X-ray Structure of [Cu(*S*-his)(2Mepy)]·3H_2O (2b)

The complex [Cu(*S*-5Omehis)·(2Mepy)]·3H_2O **(2b)** (2-MePy = 2-Methyl pyridine) is mononuclear Cu(II) complex with N_3O_2 type donor environment, four from the ligand 5-OMehis^{-2} and one from 2-Mepyridine. The ORTEP[5] view of the complex and selected bond distances and angles are given in Figure 4.1 and Table 4.B respectively. The complex **3a** is crystallized in the same space group $P2_1$ like **1a** and **2a**. The geometry around the Cu(II) centre distorted towards TBP structure with τ value of 0.22. The in-plane and axial bond lengths are matched with complex **1a**, **2a**.

The complex **2b** also forming one dimensional channel (dia: ~7.4 Å) filled with water. (Figure 4.3). Among the three water molecules in lattice two water molecules labeled as O5 and O7 are arranged like a rhombus (Figure 4.4) with distances of 2.851 and 2.965 Å for vertical and parallel length respectively. In addition the non-coordinate carboxylate O forming H-bond with secondary amine NH with distance of 2.864 Å. The imidazole (NH) H-bonded with O5 and O6 water molecule (N3..O5 3.059 Å, N3..O6 3.011 Å).

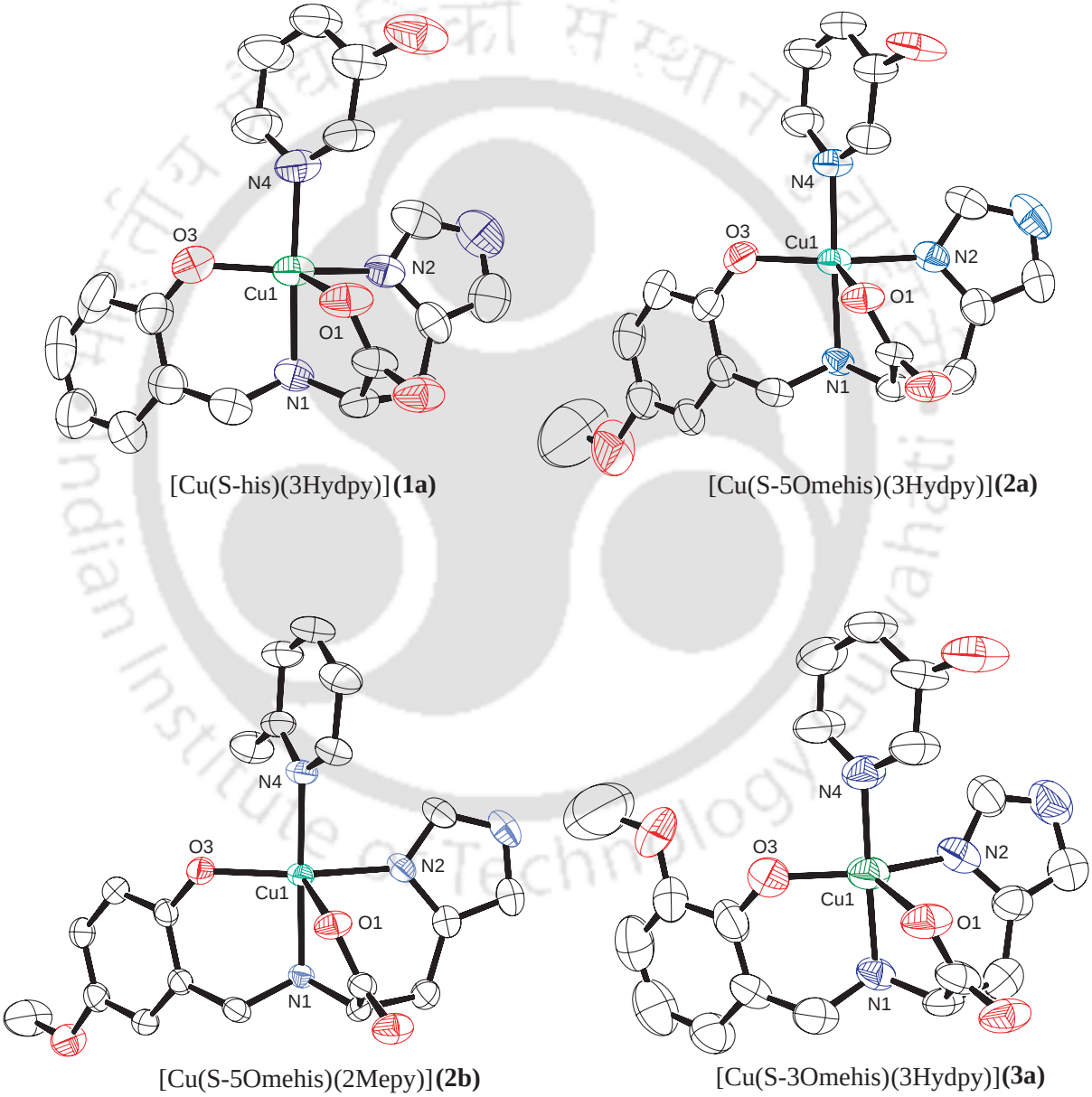

Figure 4.1: *The ORTEP figures of complexes (probability set to 50 %). Solvent molecules are omitted for clarity*

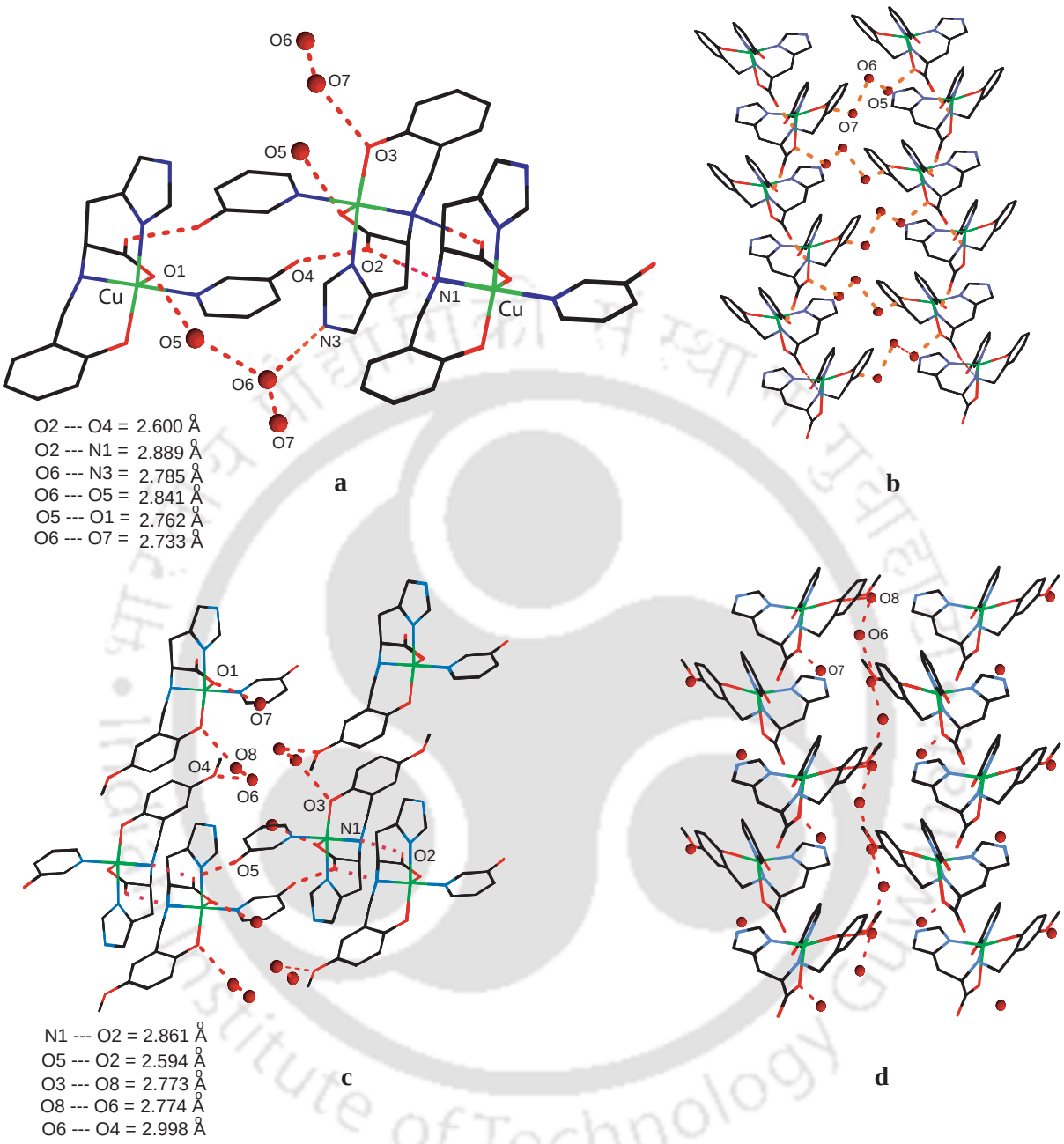

Figure 4.2. (*a) and (b) are intermolecular H-bonding and arrangement of water in crystal lattice respectively of complex [Cu(S-his)(3hydpy)].3H2O (1a). (c) and (d) also showing the intermolecular H-bonding and orientation of water in lattice of complex [Cu(S-5Omehis)(3hydpy)].3H2O (2a)*

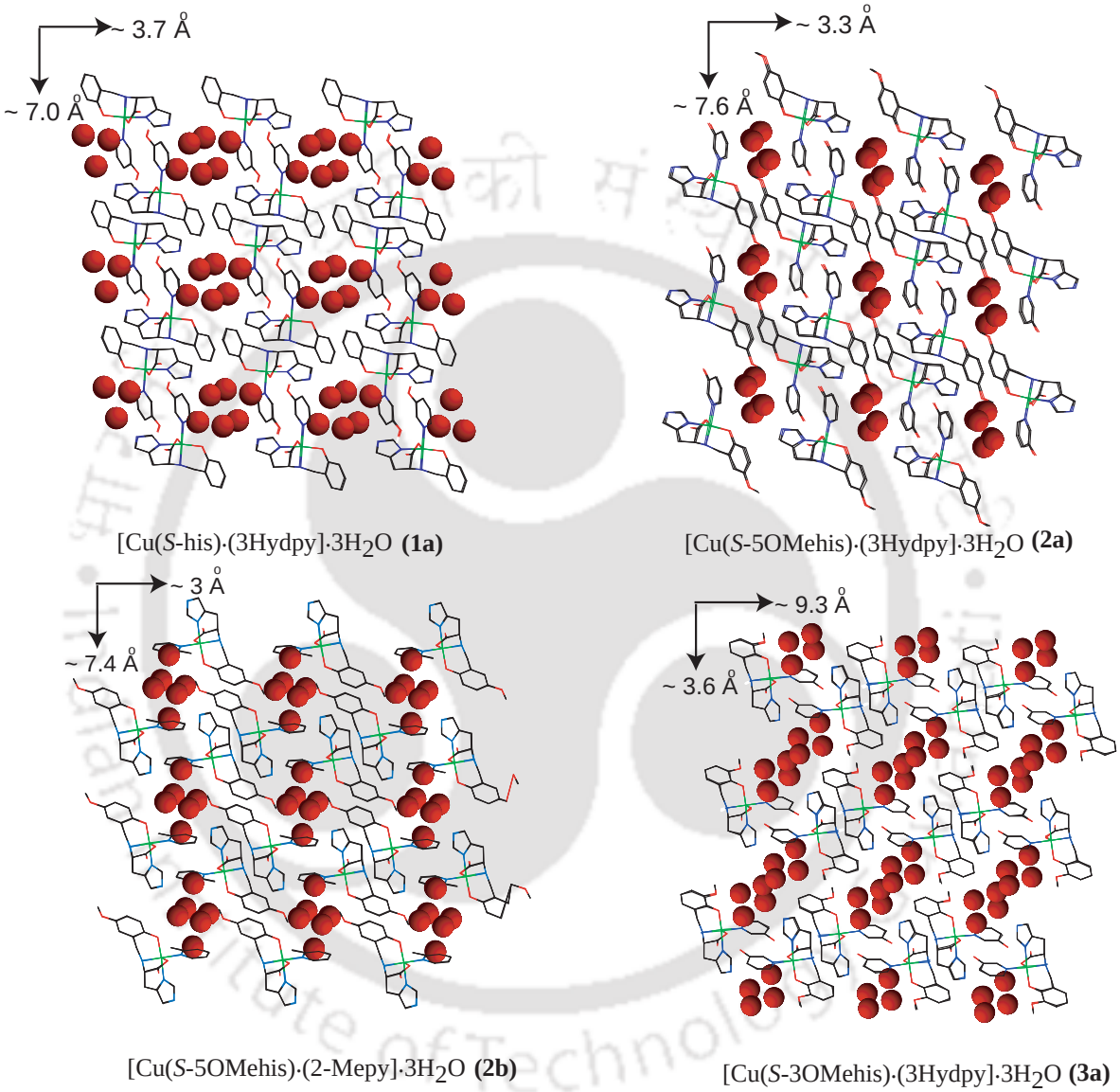

Figure 4.3. *Water filled channel of complexes*

4.3.5 X-ray Structure of [Cu(*S*-3OMehis)(3Hydpy)]·4H_2O (3a)

The crystallization of the complex **3a** from methanol formed the crystals of [Cu(*S*-3OMehis)(3Hydpy)]·4H_2O with same space group. The ORTEP[5] figure of the complex and selected bond distances and angles are given in Figure 4.1 and Table 4.B respectively. The co-ordination geometry of Cu(II) with in-plane and axial bond lengths are similar to complexes of **1a**, **2a** and **2b**. The nice H-bonded network (Figure 4.4) using different H-bond donors and acceptors with one dimensional channel (Figure 4.3) was observed in the crystal lattice of complex **3a** but in larger dimension (dia: ~9.3 Å) compare to others.

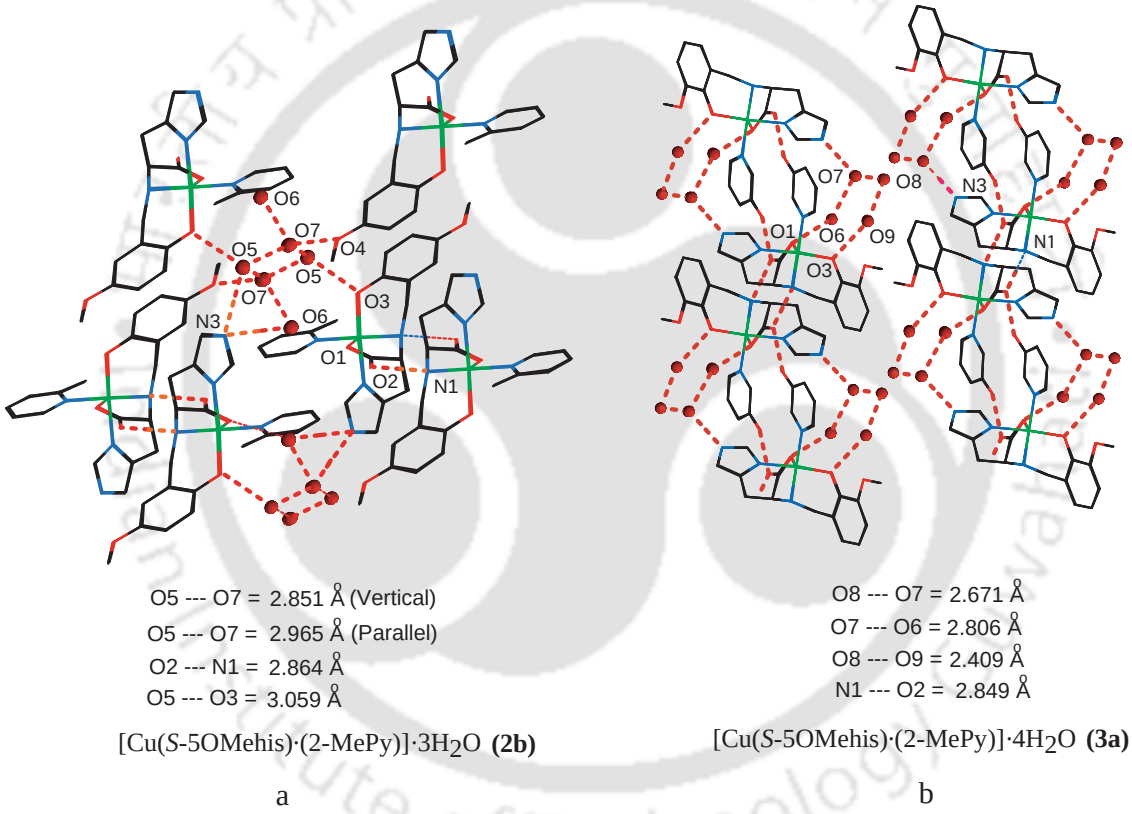

Figure 4.4. (*a) and (b) are intermolecular H-bonding and arrangement of water in crystal lattice of complex [Cu(S-5OMehis)(2Mepy)].3H_2O (2b) and [Cu(S-3OMehis)(3hydpy)].3H_2O (3a) respectively.*

4.3.6 Absorption and EPR Spectral Characteristics

The UV-visible spectral characteristic data of all the complexes are given in Table 4.C and the spectrum figure of **1a** and **2a** are shown in Figure 4.5. These spectra were recorded in DMF solution. The absorption bands observed in the range 400-430 nm are due to ligand to metal charge transfer. The absorption maxima between 615-680 nm

correspond to d-d transition. The absorption band in the range of 356-401 nm are generally due to phenolate to Cu(II) charge transfer.[12]

The EPR spectral characteristic of all the complexes are shown in Figure 4.6 and the data at 77 K in methanol are shown in Table 4.C. The complexes 1,2, 3 and 4 shows a typical square pyramidal EPR spectra as is evident from their $A_{\parallel}$ values ~178G and g values.[13]

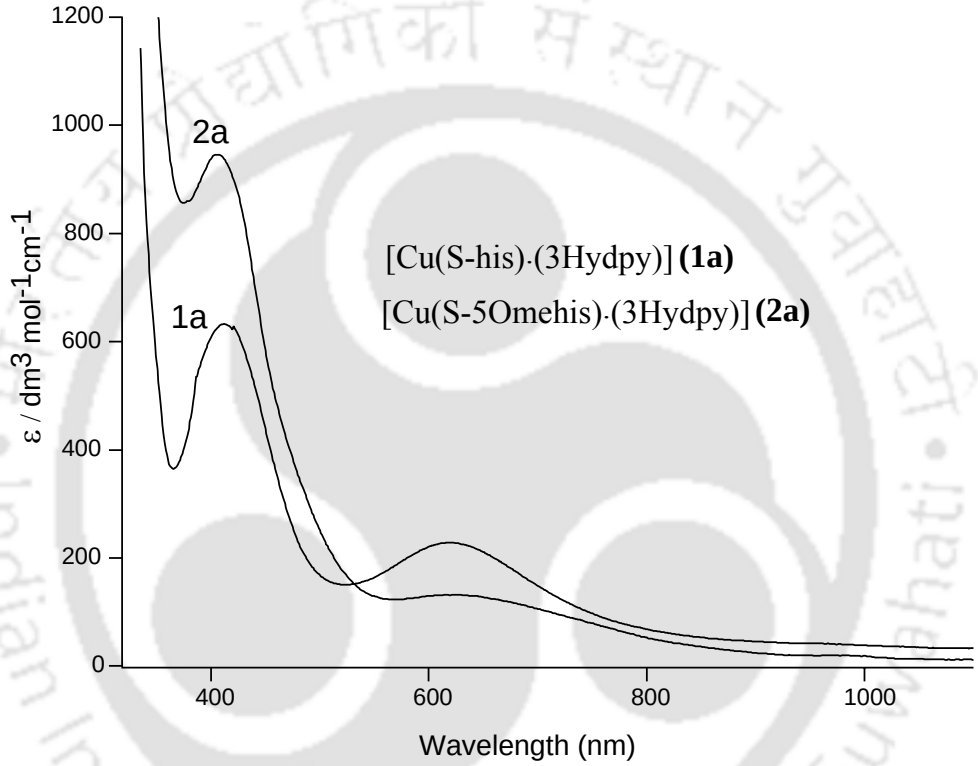

Figure 4.5. *UV-Visible spectra of complex **1a** and **2a***

Table 4.C. The UV-Visible and EPR spectral data of Cu(II) complexes

Complex	λ/nm (ε/cm^{-1} M^{-1})	EPR, g	$A_{\parallel}$/G
1a	409 (630), 620 (228)	2.24, 2.05	178
2a	400 (938), 625 (133)	2.24, 2.04	178
2b	410 (594), 634 (178)	2.24, 2.05	175
3a	420 (678), 649 (185)	2.23, 2.04	178

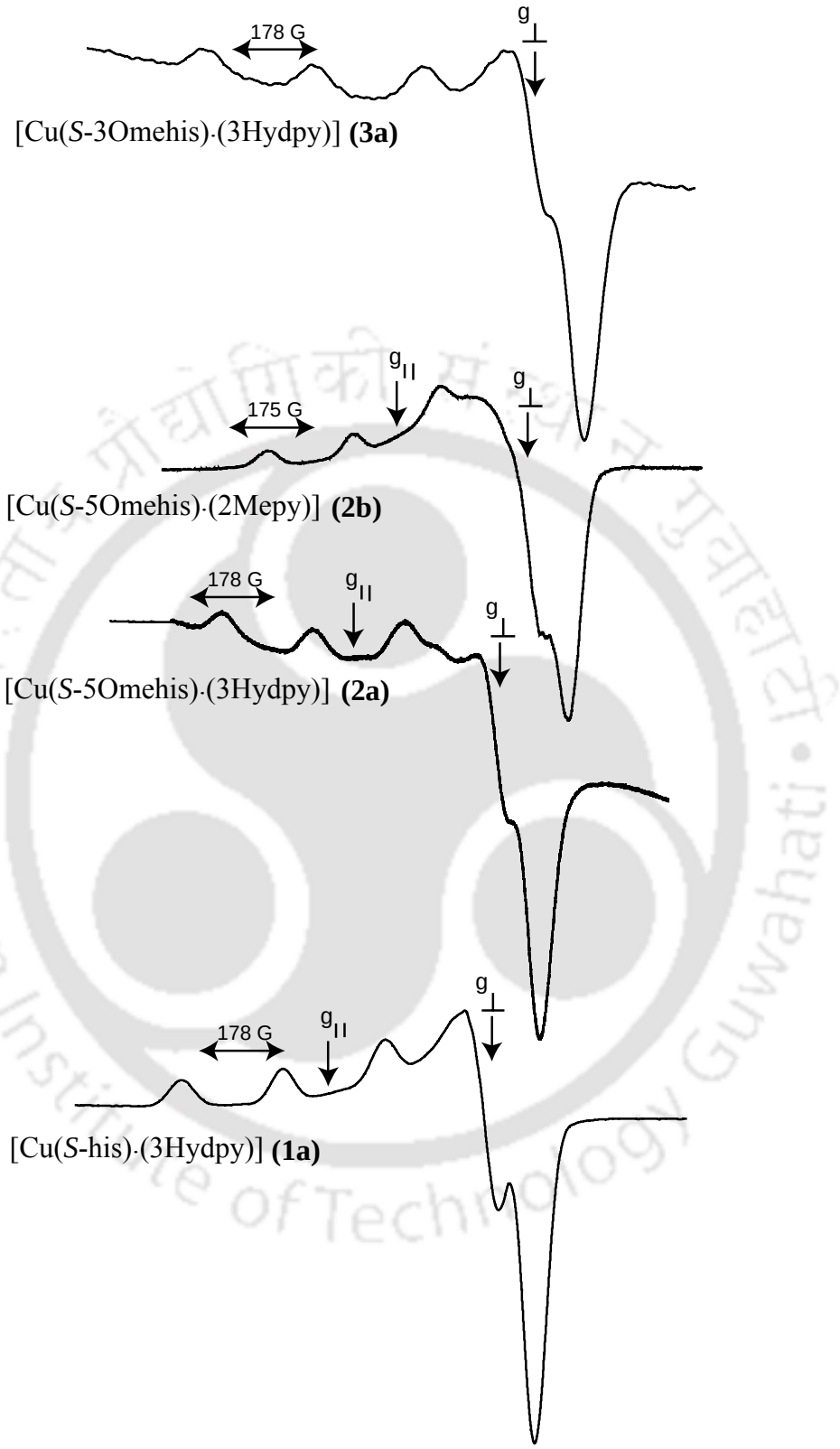

Figure 4.6. *EPR spectra of Cu(II) complexes*

Conclusion

In this chapter, the characterization data and structural analysis on the effect of substituted pyridine on the formation of octanuclear Cu(II) complex revealed that the stability of the cage greatly depends on the substitution on the pyridine as well. In fact substitution on pyridine prevents formation of cage. All the complexes form mononuclear species having one dimensional channel of different sizes (~7-9 Å) filled with H-bonded water. These compounds with channels have many potential application.[14-16]

References

1. Alam, M. A.; Nethaji, M.; Ray, M. *Angew. Chem., Int. Ed.* **2003**, *42*, 1940.
2. Nakamoto, K. Infrared and Raman Spectra of Inorganic Compounds, 5th ed.; WileInterscience: New York, 1997; Part B.
3. Geary, W. J. *Coord. Chem. Rev*. **1971**, *7*, 81.
4. (a) Earnshaw, A. Introduction to Magnetochemistry; Academic Press: London, 1968. (b) Figgis, B. N.; Lewis, J. Prog. *Inorg. Chem*. **1964**, *6*, 37.
5. Johnson, C. K. *ORTEP, Report ORNL-3794*; Oak Ridge National Laboratory: Oak Ridge, TN, 1976.
6. Addision, A. W.; Rao, T. N.; Reedijk, J.; van Rijn, J.; Verschoor, G. C. *J. Chem. Soc., Dalton Trans.* **1984**, 1349.
7. (a) Anderson, O. P.; Packard, A. B. *Inorg. Chem.* **1980**, *19*, 2123. (b) Barclay, G. A.; Kennard, C. H. L. *J. Chem. Soc.* **1961**, 5244. (c) Tables of Interatomic Distances and Configuration in molecules and Ions. *Spec. Publ. - Chem. Soc*. *11*; Sutton, L. E., Ed.; 1958.
8. Yang, C. T.; Mubaraki, B.; Murray, K. S.; Randford, J. D.; Vittal, J. J. *Inorg. Chem.* **2001**, *40*, 5934.
9. So, K. W.; Yang, C. T. Vittal, J. J.; Randford, J. D. *Inorg. Chim. Acta.* **2003,** *349*, 135.
10. N(H)…O range: 2.69 to 2.89 Å. (a) Couchman, S. M.; Jeffery, J. C.; Ward, M. D. *Polyhedron* **1999**, *18*, 2633. (b) Kuduva, S. S.; Bläser, D.; Boese, R.; Desiraju, G. R. *J. Org. Chem.* **2001**, *66*, 1621. (c) Alam, M. A.; Nethaji, M.; Ray, M. *Inorg. Chem*. **2005**, *44*, 1302.
11. (a) Desiraju, G. R. *Perspective in Supramolecular Chemistry*, Wiley, *Vol 7*. (b) Miyake, R.; Tashiro, S.; Shiro, M.; Tanaka, K.; Shionoya, M. *J.Am. Chem. Soc*.

2008, *130*, 5646. (c) Wang, X.; Vittal, J. J. *Inorg. Chem.* **2003**, *42*, 5135. (d) Yang, C. T.; Moubaraki, B.; Murray, K. S.; Vittal, J. J. *Dalton Trans*, **2003**, 880. (e) Mckinlay, R. M.; Thallapally, P. K.; Cave, G. W. V.; Atwood, J. L. *Angew. Chem*, **2005**, *44*, 5733.

12. Admas, H.; Bailey, N. A.; de Barbarin, C. O. R.; Fanton, D. E. *J. Chem. Soc., Dalton Trans.* **1995**, 2323.
13. Yokoi, H.; Addison, A. W. J. Chem. Soc., *Dalton Trans.* **1977**, *16*, 1341.
14. (a) Ludwig, R. Angew. Chem., Int. Ed. 2003, 42, 3458. (b) Pal, S.; Sankaran, N. B.; Samanta, A. Angew. Chem., Int. Ed. 2003, 42, 1741. (c) Mukherjee, A.; Saha, M. K.; Nethaji, M.; Chakravarty, A. R. Chem. Commun. 2004, 716. (d) Lioyd, G. O.; Atwood, J. L.; Barbour, L. J. Chem. Commun. 2005, 1845. (e) Khatua, S.; Dasgupta,; Biradha ,S. K.; Bhattacharjee, M. *Eur. J. Inorg. Chem.* **2005**, 5005.
15. Ikegame, M.; Tajima, K.; Aida, T. *Angew, Chem. Int. Ed.* **2003,** *42*, 2154.
16. (a) Kitaura, R.; Kitagawa, S.; Kubota, Y.; Kobayashi, T. C.; Kindo, K.; Mita, Y.; Matsuo, A.; Kobayashi, M.; Chang, H. C.; Ozawa, T. C.; Suzuki, M.; Sakata, M.; Takata, M. *Science,* **2002**, *298*, 2358.

The complexes reported in previous chapters, have been synthesized with metal / ligand ratio 1:1 where ligands behave as tetradentate (*S*-his) or tridentate (*S*-met, *S*-tyr). In this chapter we have attempted to synthesize the complexes by changing metal / ligand ratio from 1:1 to 1:2. Our objective was to understand the effect of metal ligand / ligand ratio on the formation of complexes. In this chapter we have reported the synthesized and structurally characterized a trinuclear assembly of Cu(II) using L-valine derived ligand (tridentate) with metal: ligand ratio 1:2. The new assembly consists of three mononuclear units of Cu(II), accommodating both cation and anion of a binary salt in solid state.

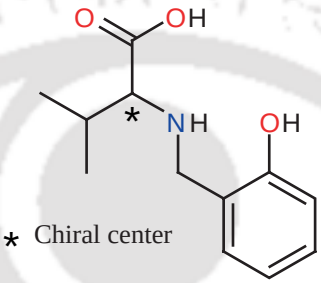

H_2*S*-Val **(1)**

Scheme 5.1. *Ligand used in this chapter*

5.1 Experimental Section

5.1.1 Solvents and Reagents

Details of solvent purification, analytical measurements have already been discussed in chapter 2. The starting materials L-valine was purchased from spectrochem and other than that is already discussed in chapter 2.

5.2. Syntheses

5.2.1 2-(2-Hydroxy-benzylamino)-3-methyl-butyric acid: [H_2*S*-Val] (1)

This ligand [H_2*S*-Val] (**1**) was synthesized following the procedure described in chapter 2 using the amino acid L-valine. Yield (78 %). IR (KBr, cm^{-1}) ν(COO) $_{(assym)}$ 1607, $\nu(COO)_{sym}$ 1370. $[\alpha]_D^{25^\circ}$ = -21° in MeOH, c = 1.00 (c = gm/100ml) , in presence of 2 equivalent LiOH.H_2O.^{1}H NMR Li_2*S*-Val (CD_3OD, 400 MHZ. ppm): 0.84 (d, 3H, J = 6.8, -C**H$_3$**CH_3), 0.87 (d, 3H, J = 6.8 -CH_3C**H$_3$**), 1.80 (m, 1H, -C**H**CH_3CH_3), 2.73 (d, 1H, J = 6.4 -C**H**NH), 3.55 (d, 1H, J = 13.6 -C**H**H-phenolate), 3.92 (d, 1H, J = 13.2 -

CH**H**-phenolate), 6.58-6.54 (m, 2H, -phenolate), 6.87 (d, 1H, J = 8.0 phenolate), 6.95 (t, 1H, J = 7.6 phenolate). ESI-Mass (-ve) for **1** at at 222 (calcd. 222.25).

5.2.2 $[K\{Cu(HS\text{-}Val)_2\}_3]ClO_4]\cdot(CH_3CN)_2$(1a)

A methanolic solution of $Cu(ClO_4)_2\cdot 6H_2O$ (0.167g, 0.450 mmol) was added dropwaise to a clear solution of H_2S-val (0.2 g, 0.883 mmol) and KOH (0.05g, 0.891 mmol) in 15 ml of methanol. The resulting bluish green color solution along with some undissolved white particle was stirred for 30 min. The solution was filtered through a medium porosity frit, after that the filtrate was reduced to dryness by rotary evaporation. The addition of acetonitrile to this bluish solid form a diamond shaped blue crystal instantly. Yield (60%). Anal. Calcd (%) for $K[Cu_3(C_{12}H_{16}NO_3)_6]ClO_4\cdot(CH_3CN)_2$: C, 52.31; H, 5.89; N 6.42. found: C, 51.92; H, 5.14; N, 6.12. IR (KBr, cm^{-1}): $\nu(COO)_{assym}$ 1609(broad), $\nu(COO)_{sym}$ 1373(s), $\nu(ClO_4)$ 1109(broad). UV-vis (λ, nm; ε, $M^{-1}\,cm^{-1}$): (MeOH) 380(sh), 580 (175). Δ_M (MeOH): 86.75 S $cm^{-2}\,mol^{-1}$.μ_{eff}(solid, 298 K) /Cu; 1.98 μ_B. EPR: MeOH, 77K, g_{II} = 2.23 $g_{\perp}$= 2.04, A_{II} = 182G.

5.2.3 X-ray data collection, structure solution and refinement

The data collection and structure refinement method are discussed in chapter 2. Selected crystallographic data are summarized in Table 5.A.

5.3 Results and Discussion

5.3.1 Synthesis and Selected Properties

Stirring H_2S-Val, KOH and $Cu(ClO_4)_2\bullet 6H_2O$ together in MeOH at 2:2:1 ratio, the solution turned blue color. Upon concentrating the solution followed by addition of acetonitrile instantly yielded the diamond shaped crystals in 60 % yield. Use of ligand: Base: metal ratio 2:4:1 produces the same complex. In IR spectra one broad peak at 1609 and a peak at 1373 cm^{-1} were identified as asymmetric and symmetric carboxylate stretches originated from the ligand respectively.[1] The complex also showed broad stretches at 1109 due to perchlorate anion. The elemental analysis supports the formulation of the complex as $K[Cu_3(HS\text{-}Val)_6]ClO_4\cdot(CH_3CN)_2$. Conductance of **1a** in MeOH falls in the range of 1:1 electrolyte indicating the dissociation of perchlorate in the H-bond capable solvent.[2] Solid state room temperature magnetic moments is 1.98 B.M./Cu which conforms well within expected range of Cu(II) complex.[3]

Table 5.A. Selected crystallographic data of complex **1a**

Empirical formula	$C_{72}\ O_{22}\ N_6\ H_{90}\ Cu_3\ K\ Cl$
Formula weight	1656.67
Wavelength (Å)	0.71073
Crystal system	Orthorhombic
Space group	$C222_1$
a, Å	19.3195(8)
b, Å	19.5670(9)
c, Å	26.2423(11)
α, deg	90.00
β, deg	90.00
γ, deg	90.00
Volume, $Å^3$	9920.2(7)
Z	4
ρ, Mg/m^3	1.109
μ, mm^{-1}	0.765
Reflections Collected	49737
Reflections indep	13236
Flack parameter	0.00
GOF	0.634
Final R indices [*I*>2sigma(*I*)]	R1 = 0.0545 wR2 = 0.1352
R indices (all data)	R1 = 0.1533 wR2 = 0.1546

5.3.2 Structure of $[K\{Cu(HS\text{-}Val)_2\}_3]ClO_4]\ (CH_3CN)_2$ (1a)

This complex crystallized in the orthorhombic space group of $C222_1$. The ORTEP[4] view of the complex $[K\{Cu(HS\text{-}Val)_2\}_3]ClO_4]$ **(1a)** has shown in Figure 5.2 (A). The selected bond distances and angles are in Table 5.B. Conformation of the six chiral centres on the ligand and six chiral centre generated due to amine coordination are *S* and *R* respectively.

The molecule **1a** consists of three units of bis Cu(II) complex encapsulating one hexa coordinated K^+ (Figure 5.1 B). In each of these units, the geometry of Cu(II) is distorted

octahedral, coordinated by two tridentate (H*S*-Val)$^{-1}$ ligand in facial mode (Figure 5.1 B). Carboxylates from the two ligands are cis to each other and provided coordination to K^+. On the other hand, both the secondary amine being cis to each other provided a docking site for perchlorate ion through H-bonding (Figure 5.1 C, N1b…O16a, 3.066Å). Two axial sites of the octahedral Cu(II) coordinated by protonated phenol group from two ligands.

Three such Cu(II) units provided six propeller shape coordination to K^+ with an average K-O bond length of 2.764 Å (Table 5.C) comparable to reported range 2.6 - 2.9 Å.[5] This shorter K-O bond might have forced the phenolic oxygen on one Cu(II) unit and carboxylate oxygen on another unit closer which helps to form the H-bond between them with average distance of 2.58 Å, are considered as strong H-bond compare to O...O range of 2.5 to 3.0 Å.[6] It is notable that in this structures six H-bond formed between non coordinated carboxylate oxygen (O3b) and phenolic oxygen (O1) from neighboring Cu(II) unit and strengthen the assembly (Table 5.C, Figure 5.1 C). The overall assembly is C_3 symmetric around K^+ and it has three sites for oxo anion binding (Figure 5.2 C). The K^+ encompassed completely on both sides by the six phenol rings from the ligands.

Table 5.B. Selected bond lengths (Å) and angles (°) of complex **1a**

Atoms	Bond distances	Atoms	Bond angles
Cu2-O2a	1.938(3)	N1a-Cu2-O2a	82.89(15)
Cu2-N1a	2.059(4)	O2a-Cu2-O2b	96.72(12)
Cu2-N1b	2.028(4)	O2b-Cu2-N1b	83.24(15)
Cu2-O2b	1.951(3)	N1b-Cu2-N1a	99.60(19)
Cu2-O1b	2.472	N1a-Cu2-O2b	167.5(2)
Cu2-O1a	2.506	O2a-Cu2-N1b	168.62(18)
Cu1-O2	1.950(3)	O2-Cu1-N1	82.87(15)
Cu1-N1	2.030(4)		
Cu1-O1		τ	0.02

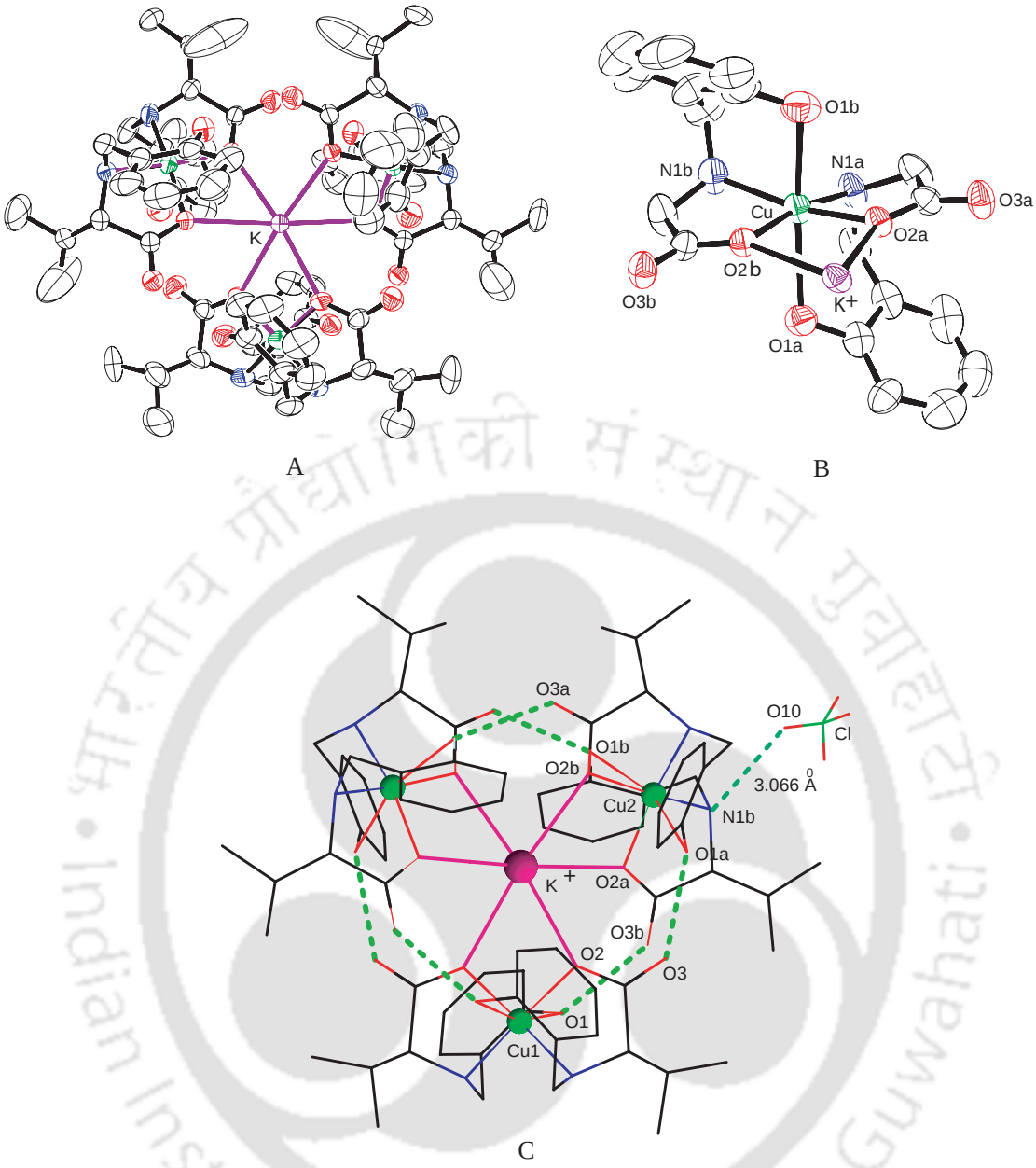

Figure 5.1. *(A) ORTEP figure of complex [K{Cu(HS-Val)$_2$}$_3$]ClO$_4$] **(1a)** (probability set to 30 % H and solvent atoms are removed for claraity. (B) ORTEP figure of one of the Cu(II) unit of complex **1a**. (C) Position of six H-bonds in the assembly*.

Table 5.C. Bond distance (Å) of (K-O)and (OH-O) H-bond

Atoms		**1a**	
K-O$_{carboxylate}$	2.764	2.755	2.775
OH…O	2.572	2.571	2.604

5.3.3 Absorption and EPR spectral study

In UV-visible spectrum the broad absorption maxima at ~580 nm with ε value 175 $dm^3\ mol^{-1}\ cm^{-1}$ is likely to be of ligand field origin (Figure 5.2 a). Several other distorted octahedral Cu(II) complexes showed similar spectral characteristics.[7] The solution EPR spectroscopic data for this complex at 77K is consistent with the distorted octahedral Cu(II) structures of the complexes (Figure 5.2 b).[8]

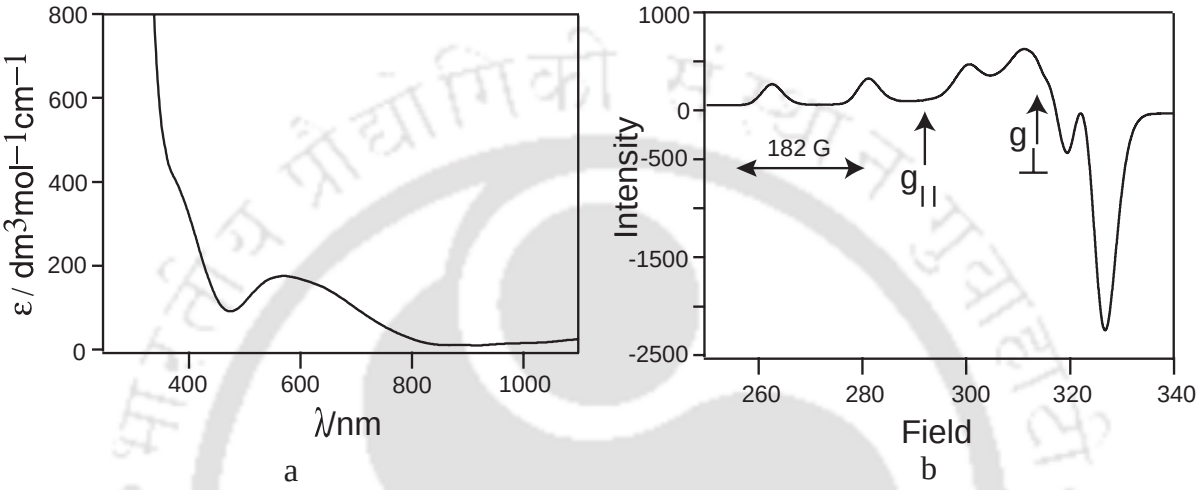

Figure 5.2. *UV-Visible (a) and EPR spectra (b) of complex **1a** in MeOH.*

Conclusion

We have characterized a trinuclear capsular assembly of Cu(II) capable of accommodating both cation and anion of a binary salt, like salt carrier using L-valine derived tridentate ligand in solid state. There has been considerable amount of work done on the assembly using the metal complexes with crown ether analogue,[9] as well as anion receptor.[10] A major difference between the reported assembly and our newly synthesized assembly is that the latter having the separate binding site of both cation and anion. This is very few in literature where assemblies having the separate binding site of both cation and anion.[11] The new assembly has also three C_2 symmetric chiral pockets on the surface for oxo anion binding through H-bonding. The assembly is further strengthened by six strong H-bond between phenolic and carboxylate oxygen.

One point to be noted here is the partial protonation of the ligand. Irrespective of ligand: base used 1:2 or 1:1 we end up isolating the complex where ligand is $(HS\text{-}Val)^{-1}$. Protonation of phenol unit of the ligand has also been observed in the case of Ni(II) bis complexes in the next chapter.

References

1. Nakamoto, K. Infrared and Raman Spectra of Inorganic Compounds, 5th ed.; Wiley-Interscience: New York, 1997; Part B.

2. Geary, W. J. *Coord. Chem. Rev*. **1971**, *7*, 81.

3. (a) Earnshaw, A. Introduction to Magnetochemistry; Academic Press: London, 1968. (b) Figgis, B. N.; Lewis, J. Prog. *Inorg. Chem*. **1964**, *6*, 37.

4. Johnson, C. K. *ORTEP, Report ORNL-3794*; Oak Ridge National Laboratory: Oak Ridge, TN, 1976.

5. (a) Saalfrank, R.; Maid, H.; Mooren, N.; Hampel, F. *Angew. Chem. Int. Ed***. 2002**, *41*. 304. (b) Gibney, B. R.; Wang, H.; Kampf, J. W.; V. L. Pecoraro. *Inorg. Chem*, **1996**, *35*, 6184. (c) Wang, X.; Vittal, J. J. *Inorg. Chem.* **2003**, *42*, 5135.

6. (a) Miyake, R.; Tashiro, S.; Shiro, M.; Tanaka, K.; Shionoya, M. *J.Am. Chem. Soc*. **2008**, *130*, 5646. (b) Desiraju, G. R. *Perspective in Supramolecular Chemistry*, Wiley, *Vol 7*.(c) Mckinlay, R. M.; Thallapally, P. K.; Cave, G. W. V.; Atwood, J. L. *Angew. Chem*, **2005**, *44*, 5733. (d) 4c. (f) Yang, C. T.; Moubaraki, B.; Murray, K. S.; Vittal, J. J. *Dalton Trans*, **2003**, 880.

7. (b) Ghattas, W.; Giorgi, M.; Gaudin, C.; Rockenbauer, A.; eglier, M. R.; Simaan, A. J. *Bioinorganic Chemistry and Applications*, **2007**. (c) Sun, Y.; Wang, Z.; Zhang, H.; Cao, Y.; Zhang, S.; Chen, Y.; Huang, C.; Yu, X. *Inorg. Chim. Acta*, **2007**, *360*, 2565.

8. Yokoi, H.; Addision, A. W. *Inorg. Chem.* **1997**, *16*, 1341.

9. (a) Mezei, G.; Zaleski, C. M.; Pecoraro, V. L. *Chem. Rev*. **2007**, *107*, 4933. (b) 4b. (c) Bowman-James, K. *Acc. Chem. Res*. **2005**, *38*, 671. (d) Saalfrank, R.; Maid, H.; Mooren, N.; Hampel, F. *Angew. Chem. Int. Ed***. 2002**, *41*. 304. (e) Nanda, P. K.; Aromi, G.; Ray, D. *Inorg. Chem*. **2006**, *45*, 3143. (f) 4c (g) Vittal, J. J.; Wang, X.; Ranford, J. D. *Inorg.com*. **2003**, *42*, 3390. (h) Mezei, G.; Kampf, J. W.; Pan, S.; Poeppelmeier, K. R.; Watkins, B.; Pecoraro, V. L. *Chem. Commun***., 2007**, 1148.

10. (a) Mizuno, T.; Wei, W. H.; Eller, L. R.; Sessler, J. *J. Am. Chem. Soc.* **2002**, *124*, 1134. (b) Chen, X. M.; Aubin, S. J.; Wu, Y. L.; Yang, Y. S.; Mak, T. W.; Hendrickson, D. *J. Am. Chem. Soc.* **1995**, *117*, 9600.

11. (a) Mahoney, J. M.; Stucker, K. A.; Jiang, H.; Carmichael, I.; Brinkmann, N. R.; Beatty, A. M.; Noll, B. C.; Smith, B. D. *J. Am. Chem. Soc*. **2005**, *127*, 2922. (b) Leharie, M. L.; Scopelliti, R.; Severin, K. *Chem. Commun.* **2002**, 2766.

In this chapter we have synthesized a set of octahedral Ni(II) complexes with L-tyrosine and L-tryptophan derived tridentate ligands along with phenanthroline as co-ligand with metal:chiral ligand: phenanthroline ratio of 1:2:1. In the previous chapters we have used Cu(II) which usually have four stronger coordination and one or two weaker axial binding site due to Jahn-Teller distortion. On the other hand, Ni(II) has six coordination site which can accommodate two tridentate ligand easily. Addition of phenanthroline, a strong bidentate ligand with cis site blocking capability, introduces an uncertainty on the type of complexes might form. The two possibilities are: (a) $[Ni(HL)_2]^{2-}$ (H_2L= tridentate amino acid derived ligand) similar to trinuclear Cu(II) complex reported in chapter 5 if phenanthroline is weaker ligand compared to L^{2-} or (b) [NiL(Phen)] if phenanthroline act as stronger ligand. Phenanthroline is a strong field ligand but amino acid derived ligands are tridentate chelating ligand thus [NiL(Phen)] is a likely situation. This would mean a five coordinated complex with one vacant site. Also, incorporation of phenanthroline in a chiral crystal likely led to chiral arrangement of phenanthroline in the lattice due to chiral nature of the complex. Chiral arrangements of photoactive molecules are important for the observation of non linier optical property (NLO).[1] However, as the results presented in this chapter will show that the complexes formed have general formula $[Ni(HL)_2(Phen)]$ where phenol donors from the amino acid derived ligands **1** and **2** remain protonated and does not coordinate.

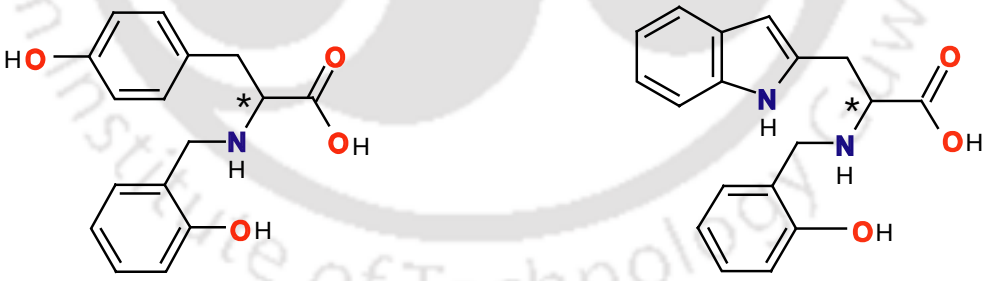

H_2*S*-tyr (**1**) H_2*S*-tryp (**2**)

Scheme 6.1. *Ligands used in this chapter*

6.1 Experimental Section

6.1.1 Solvents and Reagents

L-tryptophan and phenanthroline monohydrate (phen) were brought from Merck. Details of the solvent purification, analytical measurements and starting materials other than

those have already been discussed in chapter 2. The ligand H_2*S*-tyr (**1**) was synthesized as before.[2]

6.2 Syntheses

6.2.1 2-(2-Hydroxy-benzylamino)-3-(1H-indol-7-yl)-propionic acid [H_2*S*-trypt] (2)

This ligand H_2*S*-trypt (**2**) was synthesized following the procedure described in chapter **2** using the amino acid L-tryptophan. Yield (70 %). IR (KBr, cm^{-1}) $\nu(COO)_{(assym)}$ 1607, $\nu(COO)_{sym}$ 1370. $[\alpha]_D^{25^\circ}$ = -35° in MeOH, c = 1.00 (c = gm/100ml) , in presence of 2 equivalent LiOH.H_2O. ^{1}H NMR Li_2*S*-trypt (CD_3OD, 400 MHZ, ppm): 2.72 (dd, 1H, J = 10.4, 14.4 -C**H**H-indole), 2.99 (d, 1H, J = 11.6 -C**H**H-phenolate), 3.18 (dd, 1H, J = 4, 14.4-CH**H**-indole), 3.31 (dd, 1H, J = 4, 10.8 -C**H**CHH), 3.66 (d, 1H, J = 11.6 -C**H**H-phenolate), 6.15 (t, 1H, J= 8.8 -phenolate), 6.44 (d, J = 8 -phenolate), 6.53 (d, J = 8.8 -phenolate), 6.75 (t, J = 8 -phenolate), 6.86 (t, J = 8 –indole phenyl), 6.91 (s, indole), 6.94 (t, J = 8 –indole phenyl), 7.17 (d, J = 8 –indole phenyl), 7.56 (d, J = 8 –indole phenyl), . (All J values are in Hz.). ESI-Mass (-ve) for **1** at at 309 (calcd. 309.33).

6.2.2 [Ni(*S*-Htyr)$_2$(Phen)]·(DMF)$_2$] (1a) and [Ni(*S*-Htyr)$_2$(Phen)]·(DMF)·(H_2O)$_4$] (1b)

A methanolic solution of $Ni(NO_3)_2.6H_2O$ (0.076 g, 0.261 mmol) was added to a stirred 15 ml methanolic solution of [H_2*S*-tyr] (0.150 g, 0.522 mmol) and NaOH (0.020 g, 0.522 mmol), followed by addition of monohydrate phenanthroline (0.051 g, 0.260 mmol) in 5 ml of MeOH. The greenish precipitate came within 10 min. with constant stirring. After 20 min. stirring the reaction mixture was filtered with medium porosity frit. The residue was dried under vacuum and redissolved in dimethyl formamide for purified and recrystallization and kept in under the diffusion of diethyl ether, afforded light green needle shaped crystal with empirical formula [Ni(H*S*-tyr)$_2$.(Phen)] $(DMF)_2$ (**1a**). Yield 49 %. [Ni(*S*-Htyr)$_2$(Phen)].$(DMF)_2$: Anal. Calcd (%) for C 62.70, H 5.68, N 8.77; found C 61.39, H 4.58, N 7.16. IR (KBr, cm^{-1}) $\nu(COO)_{assym}$ 1651, $\nu(COO)_{sym}$ 1381, ν(phenolic,CO) 1250. Λ_M (DMF): 4.0 S cm^{-2} mol^{-1}. μ_{eff} (solid, 298K): 3.12 μ_B.

The light blue colored filtrate solution was evaporated to dryness followed by the addition of dimethyl formamide to this mixture and kept in an open atmosphere light blue crystals formed within 2 days with empirical formula [Ni(H*S*-tyr)$_2$(Phen)]·(DMF).(H_2O)$_4$ (**1b**). Yield 5 %. [Ni(*S*-Htyr)$_2$(Phen)].4H_2O.DMF: Anal. Calcd (%) for C 59.00, H 5.79,

N 7.32; found C 59.10, H 5.32, N 7.30. IR (KBr, cm^{-1}) $\nu(COO)_{assym}$ 1662, $\nu(COO)_{sym}$ 1384, ν(phenolic,CO) 1246.

6.2.3 [Ni(H*S*-trypt)$_2$(Phen)]·CH_3OH (2a)

This complex was synthesized by adding a methanolic solution of $Ni(NO_3)_2.6H_2O$ (0.070 g, 0.240 mmol) to a stirred methanolic solution of H_2*S*-trypt (0.150 g, 0.485 mmol) and NaOH (0.019 g, 0.475 mmol), followed by addition of monohydrate phenanthroline (0.047 g, 0.240 mmol) in 5 ml of MeOH. The greenish precipitate came with constant stirring within 30 min. After that the reaction mixture was filtered with medium porosity frit. The residue was dried under vacuum. It was purified as well as recrystallized from dimethyl formamide under the diffusion of diethyl ether, which formed block shaped light green crystal. Yield 58 %. [Ni(H*S*-trypt)$_2$(Phen)]·$CH_3OH·H_2O$. Anal. Calcd (%) for C 64.82, H 5.33, N 9.26; found C 63.57, H 5.09, N 9.12. IR (KBr cm^{-1}): $\nu(COO)_{assym}$ 1621(sh), 1601, $\nu(COO)_{sym}$ 1350, ν(phenolic CO) 1248. Λ_M (DMF): 2.5 S cm^{-2} mol^{-1}. μ_{eff} (solid, 298K): 2.95 μ_B.

6.2.4 X-ray Data Collection, Structure Solution and Refinement

The crystal structure of all the complexes was obtained by single crystal X-ray diffraction technique. Single crystal of [Ni(H*S*-tyr)$_2$(Phen)]·$(DMF)_2$ **(1a)** and [Ni(H*S*-trypt)$_2$(Phen)]·CH_3OH **(2a)** was obtained by slow diffusion of diethyl ether into the dimethyl formamide solution of the complex. The single crystal of [Ni(H*S*-tyr)$_2$(Phen)]·$4H_2O$·DMF(**1b)** was grown from dimethyl formamide solution. The selected crystallograpgic data of **1a**, **1b** and **2a** are given in Table 6.A. The data collection and structural refinement method were discussed in chapter 2. Perspective view of the complex was obtained by ORTEP.[3]

Table 6.A. Selected crystallographic data of complexes **1a**, **1b** and **2a**

Complexes	**1a**	**1b**	**2a**
Empirical formula	$C_{50}H_{54}NiN_6O_{10}$	$C_{47}H_{47}NiN_5O_{13}$	$C_{49}H_{46}NiN_6O_7$
Formula weight	957.68	948.59	889.61
Wavelength (Å)	0.71073	0.71073	0.71073
Crystal system	Orthorhombic	Triclinic	Orthorhombic
Space group	$P2_12_12_1$	P_1	$P2_12_12_1$

Complexes	**1a**	**1b**	**2a**
a, Å	10.2899(4)	9.9300(3)	14.67900(10)
b, Å	20.6229(8)	10.9185(4)	22.8003(2)
c, Å	22.9371(9)	12.0753(4)	13.12140(10)
α, deg	90.00	71.3940(10)	90.00
β, deg	90.00	88.3020(10)	90.00
γ, deg	90.00	68.7240(10)	90.00
Volume, $Å^3$	4867.4(3)	1150.71(7)	4391.54(6)
Z	4	1	4
ρ, Mg/m^3	1.307	1.369	1.345
μ, mm^{-1}	0.462	0.492	0.502
Reflections collected	51938	14505	57918
Reflections indep	11953	8582	10954
Flack parameter	0.004(13)	0.026(8)	-0.006(10)
GOF	0.816	1.336	0.953
Final R indices [*I*>2sigma(*I*)]	R1 = 0.0455 wR2 = 0.1146	R1 = 0.0407 wR2 = 0.0727	R1 = 0.0394 wR2 = 0.0764
R indices (all data)	R1 = 0.0938 wR2 = 0.1443	R1 = 0.0502 wR2 = 0.0748	R1 = 0.0755 wR2 = 0.0879

6.3 Results and Discussion

6.3.1 Synthesis and Selected Properties

The complexes $[Ni(HS\text{-}tyr)_2(Phen)]\cdot(DMF)_2$ (**1a**) and $[Ni(HS\text{-}tyr)_2(Phen)]\cdot4H_2O\cdot DMF$ (**1b**) were isolated from same reaction mixture using the ligand (H_2S-tyr): Ni(II): NaOH ratio of either 2:1:4 or 2:1:2 and subsequent addition of one equivalent another bidentate co-ligand phenanthroline (Scheme 6.2). Use of Ligand: Base ratio of 1:1 improves the yield but 1:2 ratio yields the identical compound. This shows that complexes with mono deprotonated form of the ligand is more stable and forms preferentially by acquiring H^+ from the solution presumably through hydrolysis of water. The complex **1a** was precipitated immediately as green solid which was purified and recrystallized from DMF under the diffusion of diethyl ether and **1b** from the filtrate of this reaction mixture by evaporating to drying the solvent followed by addition of DMF. The complex **1a** can also

converted to **1b** by dissolving **1a** in DMF within 3-4 days confirmed by checking the crystallographic a, b, c and α, β, γ parameter using single X-Ray diffraction technique.

The complex [Ni(H*S*-trypt)$_2$(Phen)]·CH$_3$OH (**2a**) was synthesized from the H$_2$*S*-tryp (**2**) ligand using the same reaction condition. But from this reaction we were able to isolate only one type of complex (Scheme 6.2).

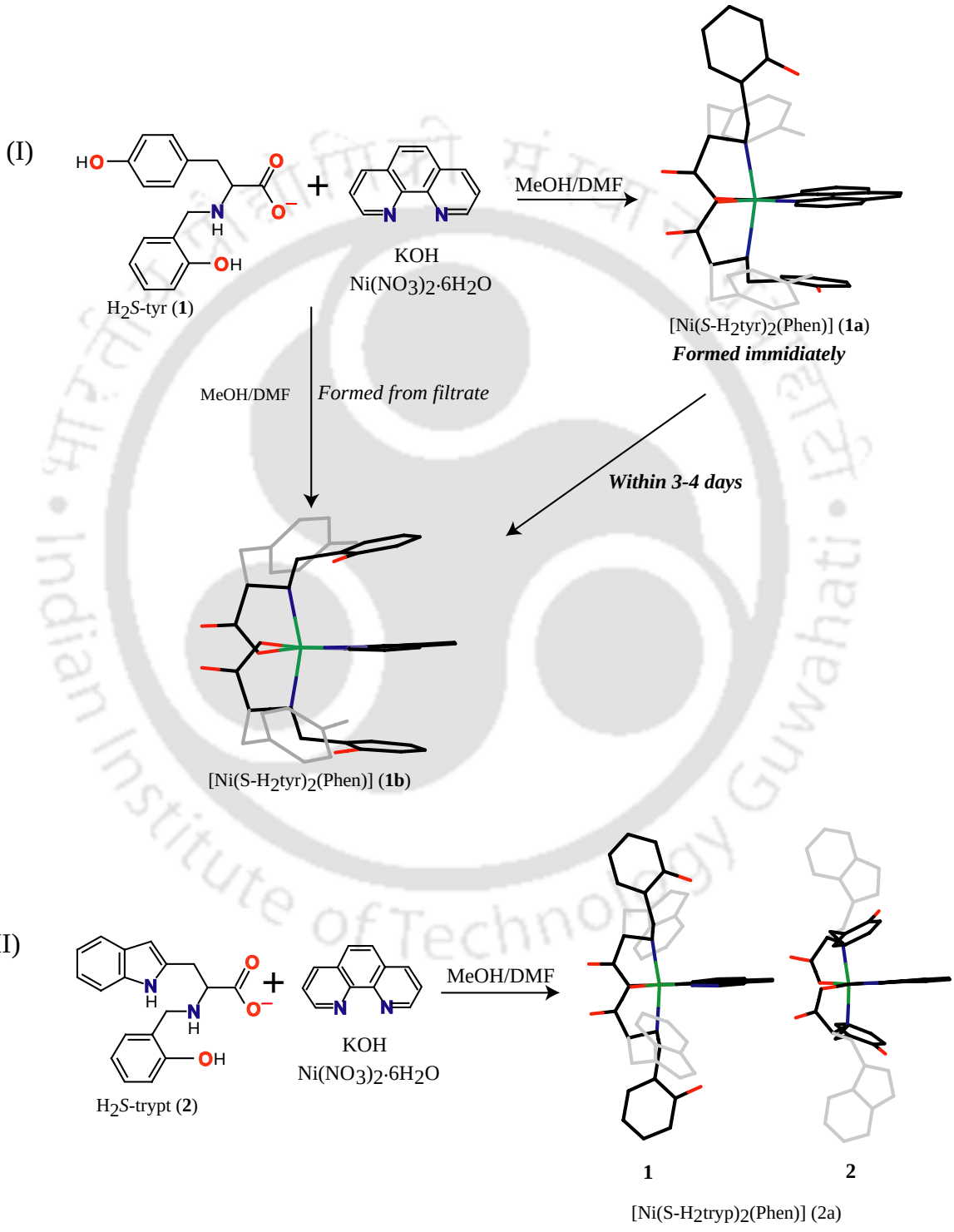

Scheme 6.2. *The schematic representation of the formation of complexes*

Comparing the IR spectra of **1a**, **1b** and **2a** with that of the Cu(II) complex (Chapter 5) coordinated by monodeprotonated ligand, the peaks at ~1615, 1660, and ~1380 for **1a** and **1b** and ~1600 and ~1350 for **2a** were identified as asymmetric and symmetric carboxylate stretches respectively.[4]

The elemental analyses of the complexes support the formulation of the complexes as $[Ni(S\text{-Htyr})_2(Phen)]\cdot(DMF)_2$, $[Ni(HS\text{-tyr})_2(Phen)]\cdot 4H_2O\cdot DMF$ and $[Ni(HS\text{-trypt})_2(Phen)]\cdot H_2O\cdot CH_3OH$ for **1a**, **1b** and **2a** respectively.

The room temperature magnetic moment for **1a**, and **2a** are 3.12 and 2.95 respectively which conforms well with expected range of 2.9 – 3.5 B.M. for octahedral Ni(II).[5] Poor yield of the **1b** made it difficult to scale up the reaction. Magnetic susceptibility on this complex has not been attempted. The molar conductance of **1a** and **2a** were found to be 4 and 2.5 S cm^2 mol^{-1} respectively in DMF, revealed the non-electrolyte nature of the complexes.[6] The complex **1b** is insoluble in common organic solvent so we could not do the solution study.

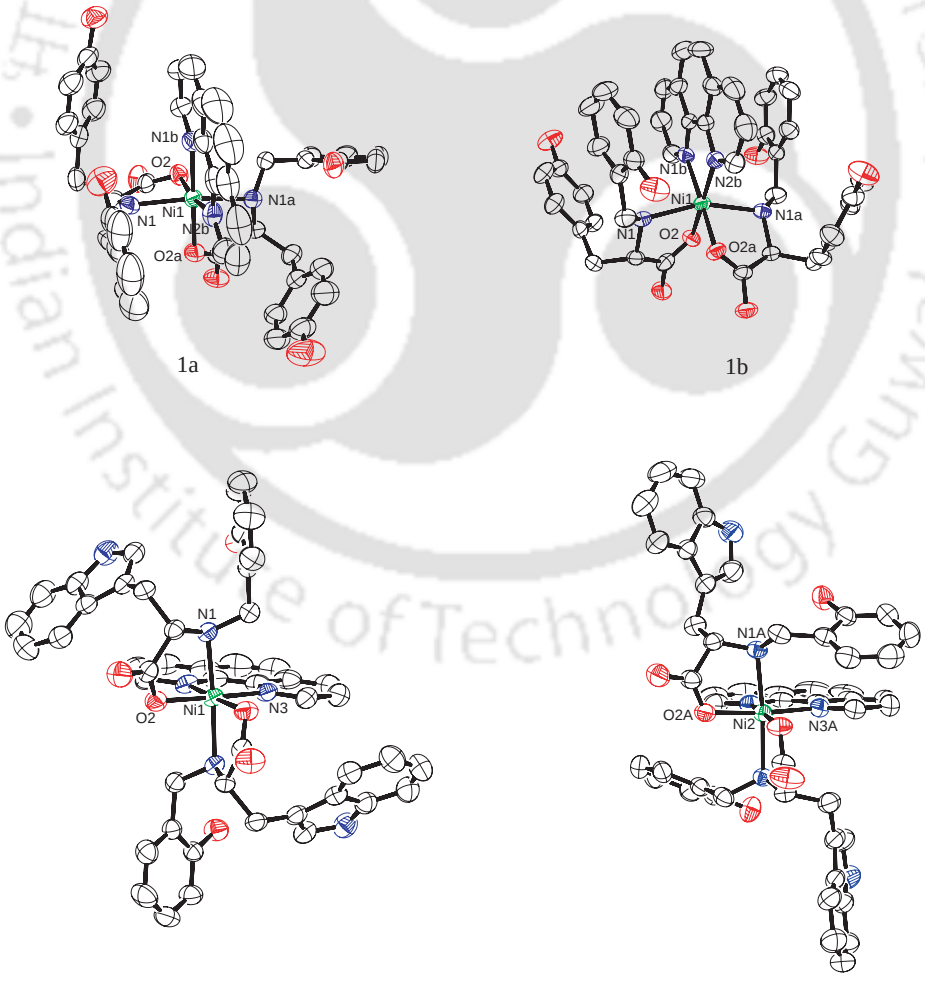

Figure 6.1. *ORTEP figure of complexes **1a**, **1b** and **2a**. probability set to 50%*

6.3.2 Crystal structure of [Ni(*S*-Htyr)$_2$(Phen)]·(DMF)$_2$ (1a)

The complex **1a** crystallized in the space group $P2_12_12_1$ in the orthorhombic crystal system. The ORTEP[3] figure, selected bond distances with angles are given in Figure 6.1 and Table 6.B respectively. The complex **1a** has distorted octahedral Ni(II) geometry with N_4O_2 donor set. The coordination environment of the Ni(II) is satisfied by two amine N and two carboxylate oxygen atom from the two ligands (*S*-H_2tyr) and the other two cis position is completed by N donor of bidentate phenanthroline ligand. Both the phenol arms remain non-coordinated. The in-plane bond distances Ni-O (carboxylate) and Ni-N (phen) are in agreement with those reported octahedral Ni(II) complexes (Table 6.B).[7] The axial bond distances Ni-N(amine) are also matched with those reported for octahedral Ni(II) complexes (Table 6.B).[8] Salicylaldehydic aromatic rings are oriented in two ways, one is parallel and another one is almost perpendicular to the coordinate phenanthroline group (Scheme 6.2). The two parallel phenyl rings are stabilized by intermolecular $\pi^{\cdots\cdots}\pi$ interactions with distance of 3.62 Å. The distance is within literature reported π-π interaction value.[9] Orientations of phenanthrolines in the lattice have been shown in Figure 6.2.

H-bond between non-coordinated carboxylate O atom and non-coordinated phenolate O atom of another unit at a distance of 2.630 Å (O3..O1A) and 2.644 Å (O4..O3A) respectively formed square like architecture in the lattice (Figure 6.2). The two solvent molecules (DMF) also formed H-bond but with different donor. One is H-bonded with tyrosine phenolic OH with a distance of 2.673 Å (O4..O5B) and another one is bonded with salicyaldehydic phenolic OH at a distance of 2.649 Å (O1..O6B). All the H-bonding distances are within literature limited.[10]

6.3.3 Crystal structure of [Ni(*S*-Htyr)$_2$(Phen)]·4H_2O·DMF (1b)

The complex **1b** was isolated by slow evaporation of dimethyl formamide and it was crystallized in the triclinic crystal system of space group P_1. The perspective view of the complex **1b** has shown in ORTEP[3] Figure 6.1 and selected bond distances and angles are given in Table 6.B. The similar coordination environment, N_4O_2 of distorted octahedral Ni (II) was observed which found in complex **1a** but the orientation of ligand backbone is quite different.

The major difference from the complex **1a** is in structural motif i.e. orientation of phenyl group as well as phenanthroline unit. Two phenyl groups from salicylaldehyde

part and phenanthroline unit are oriented in parallel fashion through π...π stacking interaction with distance of 3.730 and 3.868 Å respectively (Scheme 6.2).[9] The in-plane bond distances Ni-O (carboxylate), Ni-N (Phen) and the axial bond distances Ni-N (amine) are in well agreed with that of complex **1a** as well as reported complex (Table 6.B).[7,8]

In crystal lattice phenanthrolines are aligned in same direction (Figure 6.2). Like in complex **1a** it also formed square like frame through complementary H-bond between non-coordinated carboxylate and tyrosine phenol (Figure 6.2). The H-bonded water molecules are oriented in boat like fashion through H-bonding with phenolic OH (salicylaldehyde part and tyrosine part) of another unit. The H-bonding distance of water molecules along with phenolic OH are 2.728 Å, 2.985 Å, 2.628 Å for O8b..O6b, O6b..O1k and O4..O8b respectively (Figure 6.2).[10]

Table 6.B. Selected bond lengths (Å) and angles (°) of complexes **1a** and **1b**

Complexes	**1a**	**1b**
Ni-O2	2.037(2)	2.036(2)
Ni-O2A	2.024(2)	2.044(2)
Ni-N2B	2.087(3)	2.076(3)
Ni-N1B	2.108(3)	2.078(3)
Ni-N1	2.138(3)	2.123(3)
Ni-N1A	2.139(3)	2.131(3)
O2-Ni-O2A	91.00(10)	91.56(9)
O2A-Ni-N2B	98.58(11)	95.12(10)
N2b-Ni-N1B	78.75(11)	80.12(12)
N1B-Ni-O2	91.71(10)	93.43(11)
O2-Ni-N1A	87.12(9)	87.42(10)
N1A-Ni-N1B	100.08(10)	105.51(10)
O2A-Ni-N1	86.87(11)	84.80(10)
N1-Ni-N2B	103.58(11)	103.57(10)
N1-Ni-N1A	162.12(11)	158.74(10)
N1B-Ni-O2A	177.24(11)	173.84(12)
O2-Ni-N2B	169.77(11)	172.60(11)

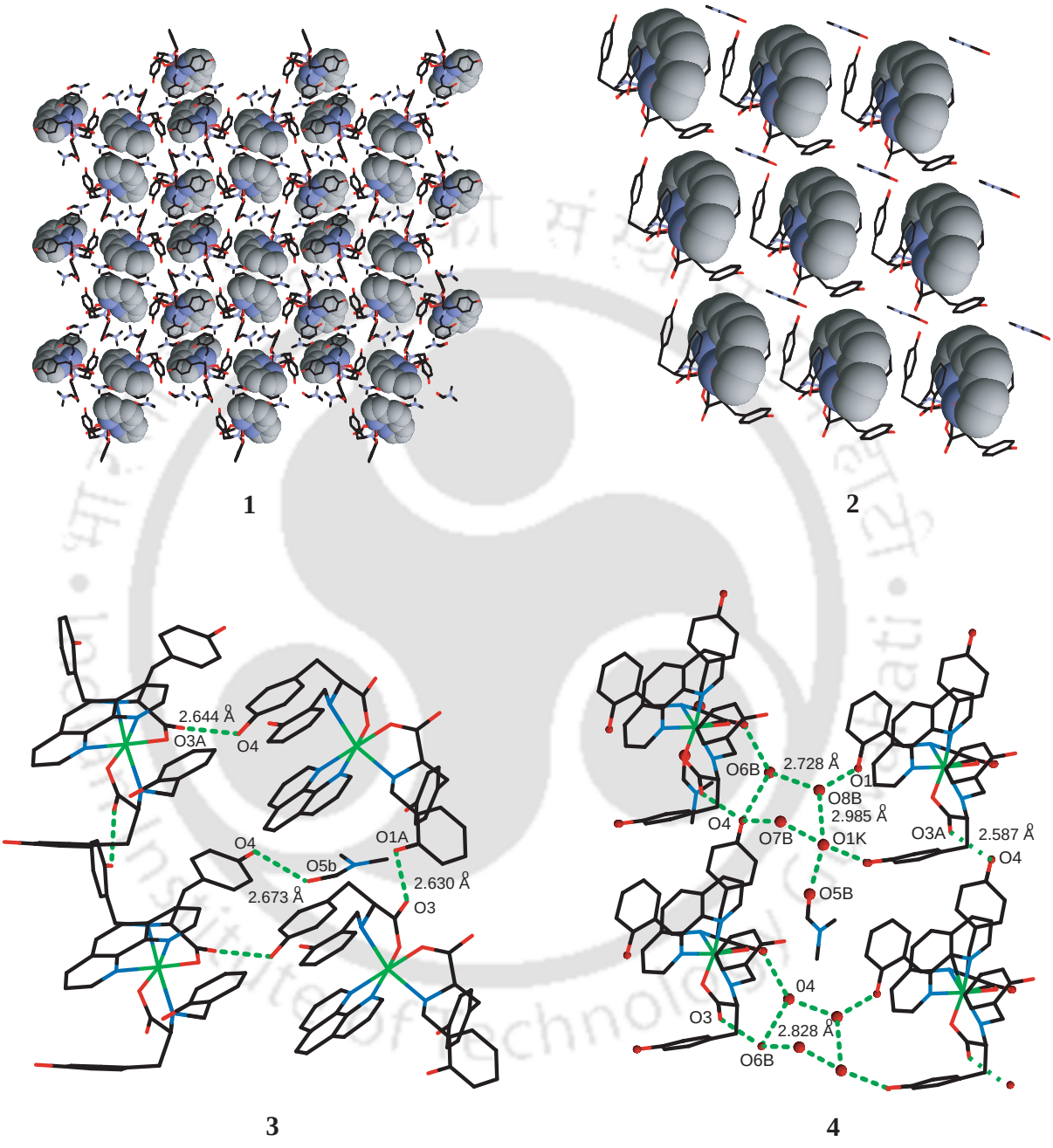

Figure 6.2. ***1*** *and* ***2*** *are the orientation of phenanthroline moiety in lattice of* ***1a*** *and* ***1b****.* ***3*** *and* ***4*** *are the H-bonded network of* ***1a*** *and* ***1b****.*

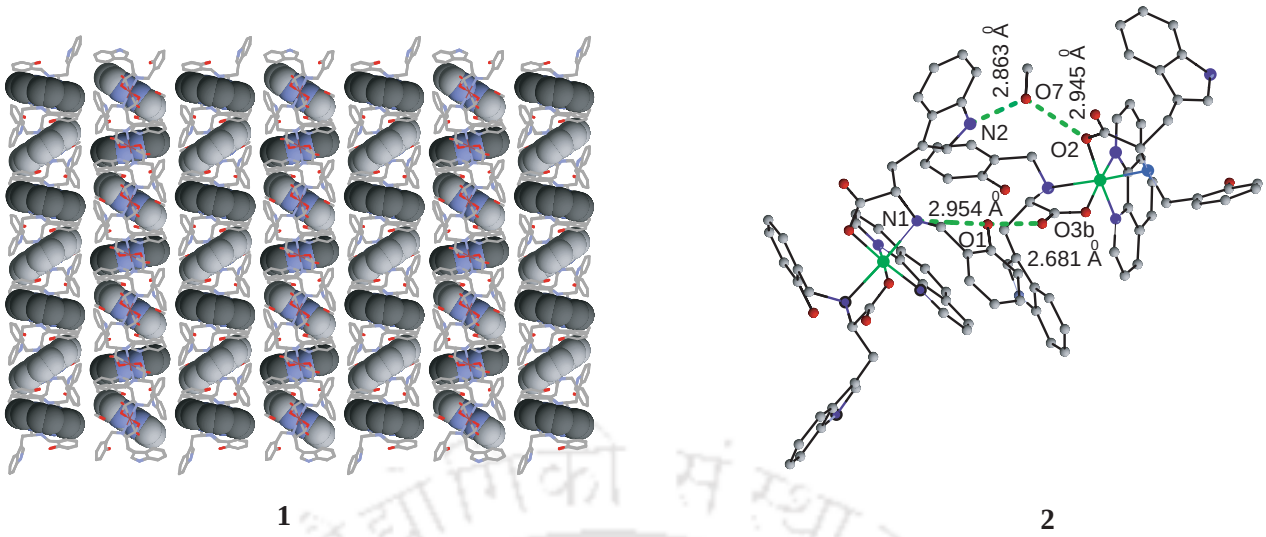

Figure 6.3. ***1*** *is Orientation of phenanthroline moiety and* ***2*** *is H-bonded network of compound* ***2a****.*

6.3.4 Crystal structure of [Ni(*S*-Htryp)$_2$(Phen)]·H$_2$O·CH$_3$OH (2a)

The crystallization of the complex **2a** from DMF and diethyl ether forming the crystals of single crystals of [Ni(*S*-Htryp)$_2$(Phen)]·CH$_3$OH. The complex was crystallized in the space group ***P*2$_1$2$_1$2** with two conformationally different monomeric units (**1** and **2**) in the unit cell (Scheme 6.2). The ORTEP[3] diagram and selected bond lengths along with angles are given in Figure 6.1 and Table 6.C respectively. The Ni(II) in both isomer is distorted octahedral geometry with N_4O_2 coordination environment like **1a** and **1b** and also matched the in-plane Ni-O(carboxylate), Ni-N(phen) and Ni-N(amine) bond distances (Table 6.C).

Unlike **1a** and **1b,** none of the phenyl and indol moiety is parallel to the coordinated phenanthroline ring in both isomers. In isomer **1** both the phenyl group is almost perpendicular to the coordinated phenanthroline group which was absent in isomer **2** in which indol moiety was perpendicular to the phenanthroline group (Figure 6.1). In crystal lattice phenanthrolines are also aligned in chiral cavity like **1a** and **1b** but the orientation is different (Figure 6.3). Due to H-bond donors and acceptors H-bonding network was observed in this lattice as well. Two monomeric units are held together by three centered H-bonding; (i) indole N-H of the ligand from one monomer H-bonded with solvent methanol O which again bonded with coordinated carboxylate O of another unit with distance of 2.863 Å (N2..O7) and 2.945 Å (O7..O2B) respectively. (ii) Non-coordinated carboxylate O from one monomer to another unit of uncoordinated phenolic OH and

secondary amine NH (Figure 6.3). The distance between non-coordinated carboxylate O to phenolic O and phenolic O to NH is 2.681 Å (O1..O3b) and 2.954 Å (O1...NH) respectively. The O..O and NH..O distances are within expected limits.[10,11]

Table 6.C. Selected bond distances and angles of complex **2a**

Atoms	**1**	**2**
Ni-$O_{carboxylate}$	2.0410 (15)	2.0236 (17)
Ni-N_{phen}	2.104 (2)	2.065 (2)
Ni-N_{amine}	2.1794 (18)	2.1498 (19)
$O_{carboxylate}$-Ni-$O_{carboxylate}$	86.30 (10)	91.89 (10)
$O_{carboxylate}$ -Ni-N_{phen}	97.82 (7)	93.97 (8)
N_{phen}-Ni-N_{phen}	78.39 (12)	80.12 (7)
$O_{carboxylate}$ -Ni-N_{amine}	80.69 (8)	81.11 (7)
N_{amine} -Ni-N_{phen}	93.13 (8)	98.55 (7)
$O_{carboxylate}$ -Ni-N_{amine}	91.60(8)	81.12 (7)
N_{amine} -Ni-N_{phen}	95.02 (7)	91.28 (8)
N_{amine} -Ni-N_{amine}	169.47 (11)	167.17 (11)
$O_{carboxylate}$ -Ni-N_{phen}	174.17 (8)	174.14 (8)

6.3.5 UV-Visible spectrum

The complexes **1a** and **2a** (Figure 6.4) exhibits two distinct absorption bands at ~570, ~ 580 nm and ~ 930, ~970 nm respectively (Table 6.D). Considering octahedral coordination around the Ni(II) ions, the two bands at ~570 nm and ~970 nm can be assigned to the spin allowed d-d transition A_{2g} to $^3T_{2g}$ and $^3A_{2g}$ to $^3T_{1g}$ transition respectively. These type of transition were observed in other distorted octahedral Ni (II) complexes.[12]

Table 6.D. UV-Visible data of complexes **1a** and **2a**

Complexes	λ_{max}, nm; ε, M^{-1}, cm^{-1}
1a	570 (17), 932 (13)
2a	582 (13), 970 (12)

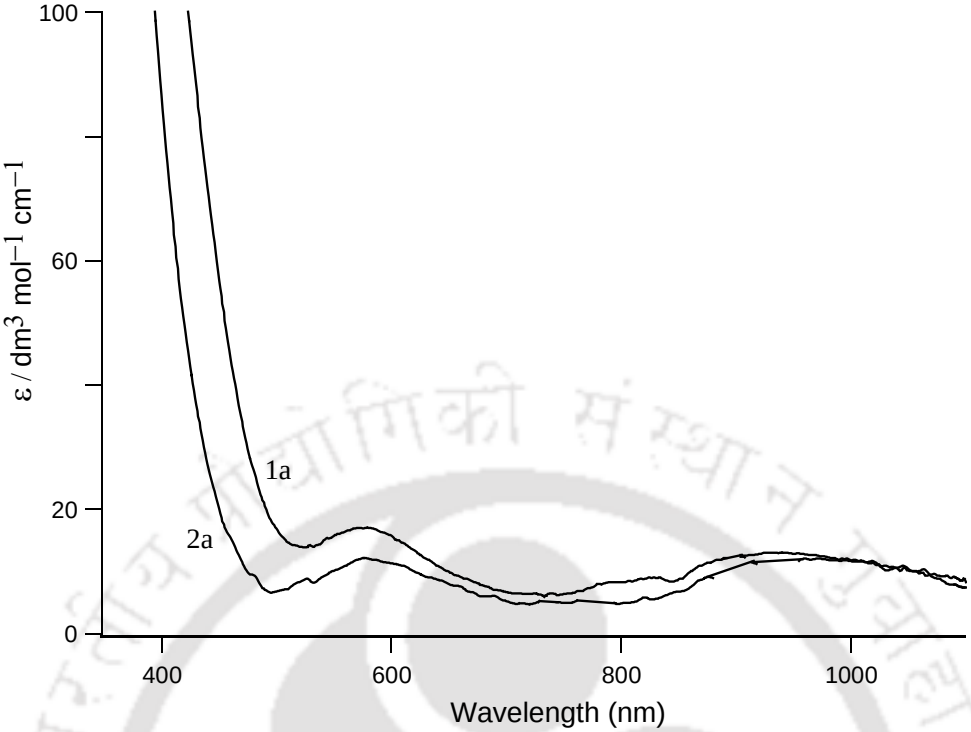

Figure 6.4. *UV-Visible spectra of complex **1a** and **2a***

Conclusion

Synthesis and structural characterization of the complexes showed: (a) octahedral Ni(II) complexes formed with two bidentate chiral ligands and phenanthroline where phenol groups of the chiral ligand were protonated form; (b) a set of structurally different isomers of Ni (II) complexes have been isolated from the same reaction due to the conformational change of the ligand; (c) phenanthrolines units were organized asymmetrically in the lattice. Non linear optical property of the Zn(II) coordinated phenanthrolines has been reported by others previously.[13]

Similar to what we have observed in the last chapter, the phenol unit in the bis-complexes gets protonated irrespective of amount of base used. Use of exactly ligand: base ratio of 1:1 does improve the yield but 1:2 ratio yields the identical complex. One difference though in this set of complexes is that the phenols remain non-coordinated whereas in the chapter 5 phenols (protonated) were coordinated.

References

1. (a) Verbiest, T.; Elshocht, S. V.; Kauranen, M.; Hellemans, L.; Snauwaert, J.; Nuckolls, C.; Katz, T. J.; Persoons, A. *Science*. **1998**, *282*, 913. (b) Dixit, V. K.; Vanishri, S.; Bhat, H. L.; Gomes, E. D.; Belsley, M.; Santinha, C.; Arunmozhi, G.; Venkataramanan, V.; Proena, F.; Criado, A. *J. Cryst. Growth*, **2003**, **253**, 460.
2. Yang, C. T.; Vetrichelvan, M.; Yang, X; Keith, B. M.; Murray, S.; Vittal, J. J. *J. Chem. Soc., Dalton Trans.* **2004**, 113.
3. Johnson, C. K. *ORTEP, Report ORNL-3794*; Oak Ridge National Laboratory: Oak Ridge, TN, 1976.
4. Nakamoto, K. Infrared and Raman Spectra of Inorganic Compounds, 5th ed.; WileInterscience: New York, 1997; Part B.
5. (a) Earnshaw, A. Introduction to Magnetochemistry; Academic Press: London, 1968. (b) Figgis, B. N.; Lewis, J. Prog. *Inorg. Chem*. **1964**, *6*, 37.
6. Geary, W. J. *Coord. Chem. Rev*. **1971**, *7*, 81.
7. (a) Butcher, R. J.; O'Connor, C. J.; Sinn, E. *Inorg. Chem.* **1982**, *21*, 616. (b) Zheng, Y. Q.; Lin, J. L.; Kang, Z. P.; Chen, B. Y. *J. Chem. Cryst.* **2002**, *32*, 399.
8. Koch, W. O.; Kaiser, J. T.; Krüge, H. J. *Chem. Commun*. **1997**, 2337.
9. (a) Yang, C. T.; Moubaraki, B.; K. Murray, S.; Vittal, J. J. *J. Chem. Soc., Dalton Trans*. **2003**, 880. (b) Li, X.; Y. Q.; Zheng, X. Jun.; Sun, H. L. *Inorg. Chem. Com.* **2008**, *11*, 779.
10. (a) Desiraju, G. R. *Perspective in Supramolecular Chemistry*, Wiley, *Vol 7*. (b) Miyake, R.; Tashiro, S.; Shiro, M.; Tanaka, K.; Shionoya, M. *J.Am. Chem. Soc.* **2008**, *130*, 5646. (c) Wang, X.; Vittal, J. J. *Inorg. Chem.* **2003**, *42*, 5135. (d) Yang, C. T.; Moubaraki, B.; Murray, K. S.; Vittal, J. J. *Dalton Trans*, **2003**, 880. (e) Mckinlay, R. M.; Thallapally, P. K.; Cave, G. W. V.; Atwood, J. L. *Angew. Chem*, **2005**, *44*, 5733.
11. Couchman, S. M.; Jeffery, J. C.; Ward, M. D. *Polyhedron*, **1999**, *18*, 2633.
12. Lever, A. B. *Inorganic Electronic Spectroscopy*, 2nd ed., Elsevier, 1984.
13. Das, S.; Jana, A.; Ramanathan, V. Chakraborty, T.; Ghosh, S.; Das, P. K. Bharadwaj, P. K. *J. Orgnomet. Chem.* **2006,** *691*, 2512.

We intend to attach chiral complexes / receptors onto the polymer support in future. Because of this reason we have explored synthesis of polymers with functional groups. We choose to synthesize aniline polymers because of having amine group at the terminal end. It is easier to make derivatives of amines. In this chapter we have taken a known polymerization reaction between aniline and formaldehyde, forming usually a resinous sticky polymer used in the adhesive industry.[1] The reaction involves electrophilic addition of protonated formaldehyde to the *ortho* and / or *para* position of aniline depending on the formaldehyde to aniline ratio.[1] Despite the presence of large number of functional amine group similar to chitosan,[2,3] the aniline formaldehyde condensate (AFC) has limited number of application presumably because of its resinous nature. In this chapter we have presented that addition of simple alcohols during synthesis and controlled temperature produces solid aniline formaldehyde condensate (AFC) instead of sticky resin with wide ranging morphology. Interestingly, addition of *t*-butanol leads to the formation of sub-micron (700 nm to 2 μm) sized spheroids. Nanometer to micrometer sized regular shaped polymer spheres with high surface area has been of interest because of their potential in biomedical applications.[4] The common method of polymer sphere preparation involves formation of polymers around a micelle or vesicle using surfactants.[4-7]

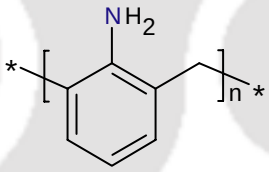

Scheme 7.1. *The polymer used in this chapter*

To test the usefulness of the polymers as well as to probe the accessibility of the amine functional groups by external reagents, we have also measured metal removal property of the polymers using Cr(VI) as a test case. Removal of Cr(VI), a pollutant in various industrial waste, has been studied by several groups using natural or synthetic adsorbant.[8-14] AFC was used for removal of Hg^{2+} from the aqueous solution.[15,16] Earlier, Chakraborty and Ray *et al*. demonstrated that AFC coated on silica gel effectively remove Cr(VI) from acidic solution[8] by acting as anion-exchanger in the acidic medium or Cu(II) in pH 6[9] similar to other amine rich natural adsorbent.[10–14] The resinous nature of AFC specially in acidic medium, oxidation of amines upon long term (months) storage and larger weight of support material put several hurdles for its effective use. The result

showing improved processibility, stability and Cr(VI) removal property of the present polymers over other synthetic [13-14] and natural polymers [10-12] has been presented in this chapter.

7.1 Experimental section

7.1.1 Solvents and Reagents

The solvents and reagents *t*-butanol, *iso*propanol, *n*-octanol and formaldehyde were brought from Merck. Aniline was distilled over KOH. Other than those stated above have already been discussed in previous chapter.

7.1.2 Measurements

SEM photographs were recorded using a Leo-1430 VP instrument with Energy Dispersive X-ray (EDAX) analysis attachment and the polymer samples were coated with gold vapor before measurements to reduce charging. Total chromium concentration of the aqueous solution before and after adsorption with polymers were measured using a Varian model 55B Atomic Absorption Spectrometer using air-acetylene flame at wavelength of 429 nm with slit width of 0.5 nm. Elemental analyses were done on Carlo Erba 1108. MALDI-TOF mass measurements were recorded on Micromass TOF Spec 2E instrument using a nitrogen 337 nm laser (4 nm pulses). At least 40-50 shots are summed up. The matrix used is 2,5-dihydroxy benzoic acid dissolved in methanol. The sample and the matrix spotted on MALDI target and allowed to dry before introducing into the mass spectrometer.

7.2 Syntheses

7.2.1 General Synthesis of the polymers

In a typical synthesis, alcoholic solution of aniline and conc. HCl was precooled to 0-5 ºC before mixing. Upon addition of a cold alcoholic solution of formaldehyde to the unstirred aniline solution, the solution turns turbid and slowly over few minutes thickened with white to pale yellow color. Over time the polymer solidifies and turned light yellow. If the reaction is performed at room temperature, the exothermic reaction resulted in a fragile and dark red polymer. The polymer formed in room temperature is not uniform in texture. The reported procedure for resinous AFC uses higher temperature and longer duration in the synthesis.[1] The solid polymers formed in shape of the reaction vessel were washed sequentially with 1M HCl, 1M NaOH and distilled water to remove unreacted

reagents and to form the polymers in the amine form. The light yellow polymers were dried in vacuum desiccator for 1-3 days (depending on alcohol used) over anhydrous calcium chloride to remove water and any traces of alcohols remain trapped in the polymer. A quantitative detail of one synthesis is given below.

7.2.2 Synthesis of Polymer in presence of *t*-butanol

Aniline (9 g, 0.096 mol) and *t*-butanol (3.5 ml) were dissolved in 2.25 ml of conc. HCl (0.025 mol). The solution was cooled to below 5º C with an ice bath. A solution of 37% w/V formaldehyde (7.5 ml, 0.094 mol) in 3.5 ml of pre-cooled *t*-butanol was added drop wise into the aniline-acid solution with vigorous stirring to obtain a uniform homogeneous solution. The temperature was maintained at 0-5 ºC for 25 min and then allowed to warm up to the room temperature. The solid polymer was cut into pieces and washed with 1M HCl solution followed by 1M NaOH solution and finally with distilled water and dried under vacuum desiccator.

Analysis of Polymers: *t*-butanol: C% 72.52, H% 6.37, N% 11.40; C:N mol ratio 7.5:1. *Iso*-propanol: C% 58.37, H% 7.07, N% 9.65; C:N mol ratio 7:1. Methanol: C% 58.03, H% 6.49, N% 9.06; C:N mol ratio 7.5:1. Glycerol: C% 70.16, H% 6.05, N% 10.15; C:N mol ratio 8:1.

7.3 Results and Discussion

7.3.1 Synthesis and characterization

The IR spectra of all the polymers show peaks at 3400 cm^{-1} (primary amine), sharp peaks at ~1650 and 1610 (amine bending), 1515 and at 808 cm^{-1}. The peaks are similar to the polymer prepared following the reported procedure without the use of alcohols.[8,9] The polymers are insoluble in common organic solvent including DMF and DMSO. Thus ^{1}H NMR could not be performed.

Elemental analysis (Carbon, Hydrogen and Nitrogen) data in terms of percentage on the polymers were varied widely (section 7.2.2) as it is difficult to control the amount of residual acid attached to amines and salts trapped within the solid. The Energy Dispersive X-ray (EDAX) analysis on the polymers during SEM measurements shows the presence of significant amount of chloride in the polymers. Thus washing the polymers with NaOH and water did not convert all the anilinium hydrochloride sites to free amine form or in other words, some anilinium sites remain inaccessible to acids and water. As the source

of C and N in the polymer is determined by the *o*-methylene aniline unit (C:N is 7:1) the of ratio of C:N determined from elemental analysis, lies between 7:1 to 8:1 are close considering the variation possible due to small amount of entrapped alcohols.

7.3.2 MALDI-TOF Mass spectral analysis

Matrix assisted laser desorption/ionization time of flight mass spectrometry (MALDI-TOF MS) is a soft ionization technique developed by Karas and Hillenkamp and has been found to be a valuable tool for the characterization of polymers.[17] The spectrum for polymer from *t*-butanol (Figure 7.1) shows at least four series of oligomers. The Δ_m calculated from MALDI-TOF Mass spectra (Figure 7.1) 105, equivalent to *o*-methylene aniline unit (C_7H_7N, calcd as 105.13). MALDI-TOF has been used to determine molecular weight distribution for polymer isolated from *para*-substituted phenol and formaldehyde.[18]

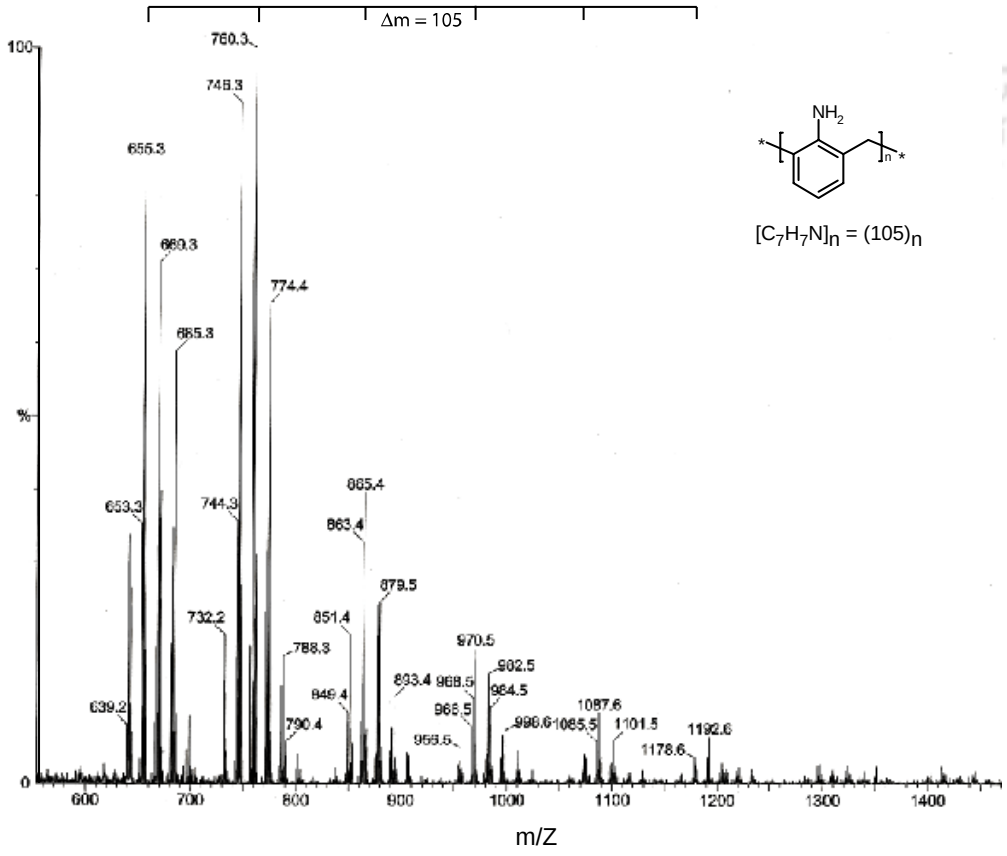

Figure 7.1. *The MALDI-TOF mass spectrum of the AFC polymer synthesized in presence of t-butanol.*

However, the presence of multiple positively charged centre (ammonium or amine+Na^+) and possibility of branching at the *para* position of the aniline moiety generate several structure with nearly same mass value and thus predicting structure of the oligomer series based only on mass spectrum with certainty is difficult. In Scheme 7.2 we have presented a set of probable series with calculated mass values which comes close to the mass values observed in the MALDI-Mass.

The structure I, II and IV are based on the products proposed in the formaldehyde phenol polymerization[19] Some of the structures presented in Scheme 7.2 can very well be branched at the *para* position as such branching only changes the value of *n* preserving the mass of the molecule nearly same. The polymer from isopropanol shows a similar spectrum. The identical Δ_m value for both the polymer confirmed that these are polymers with multiple units of *o*-methylene aniline as expected for AFC. Thus chemically the polymers are not very different.

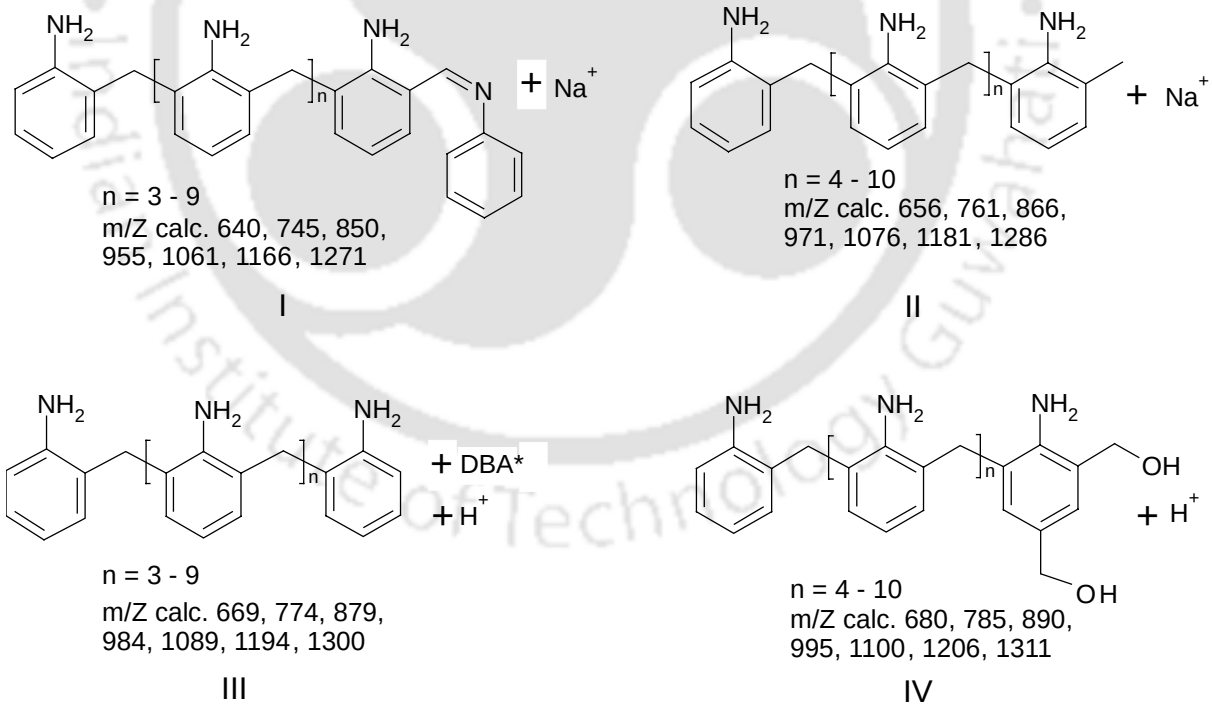

Scheme 7.2. *The series of oligomers with calculated mass values proposed on the basis of MALDI-TOF Mass spectrum. DBA is 2,5-dihydroxy benzoic acid used in the matrix preparation.*

7.3.3 Stability of the polymers

All the polymers were thermally stable up to 240 ºC with charring occurs above 240º. The polymer from *t*-butanol remains unchanged even at 250 ºC. The stability of the polymers in air varies and the polymer from methanol has a tendency to get darker in air with time due to aerobic oxidation of amines over 4-6 weeks. Rests of the polymers are air stable for over six months without any coloration due to aerobic amine oxidation. The lower initial reaction temperature and the presence of alcohols possibly allowed formation of few large molecular weight oligomer series where free amine groups remain protected because of the dense nature of the polymer. The well defined nature of the mass spectra (Figure 7.1) suggests the formation of fewer oligomeric series with narrow mass distribution. The multiple charge centres prevented precise molecular weight determination (Section 7.3.1).

7.3.4 Scanning Electron microscopy

The scanning electron microscope (SEM) images (Figure 7.2) revealed the formation of spheroids of polymers in presence of *t*-butanol but morphologically different solid polymer in case of other alcohols. The SEM photographs of different batches as well as from different parts of the polymer block prepared from *t*-butanol shows the spheroids size and distribution is almost uniform (almost uniformly 750 nm – 2 μm in size). In case of poly-alcohol such as glycerine the polymer formed as a semi transparent gel which once dried breaks in to flakes / layers consistent with its SEM image.

Although the exact reason for spherical formation in case of *t*-butanol is not known or observed in any other reports, theoretical studies on effect of salt addition to *t*-butanol/water mixture has been shown to form ring like distribution of hydrophobic *t*-butanol molecules with salts surrounding the *t*-butanol molecules which is unique for *t*-butanol.[20] Thus, *t*-butanol/ water mixture in presence of ionic aniline HCl might have arranged in a nano sized ring like distribution or droplets of t-BuOH acting as the core for polymerization on the surface of the ring, leading to the spheroid shape observed (Scheme 7.3). We expected that *n*-octanol with its ability to form micelle would give rise to spheroid polymer but phase separation between *n*-octanol and water due to the higher concentration of *n*-octanol and higher hydrophobicity of *n*-octanol prevented that. Both amount of solvent and temperature plays important role in determining the size of the spheroids. A tenfold increase in amount of water, keeping the temperature constant (<

0ºC), the spheroid size increases to 2-3 micron with wider distribution of size but the yield is poor.

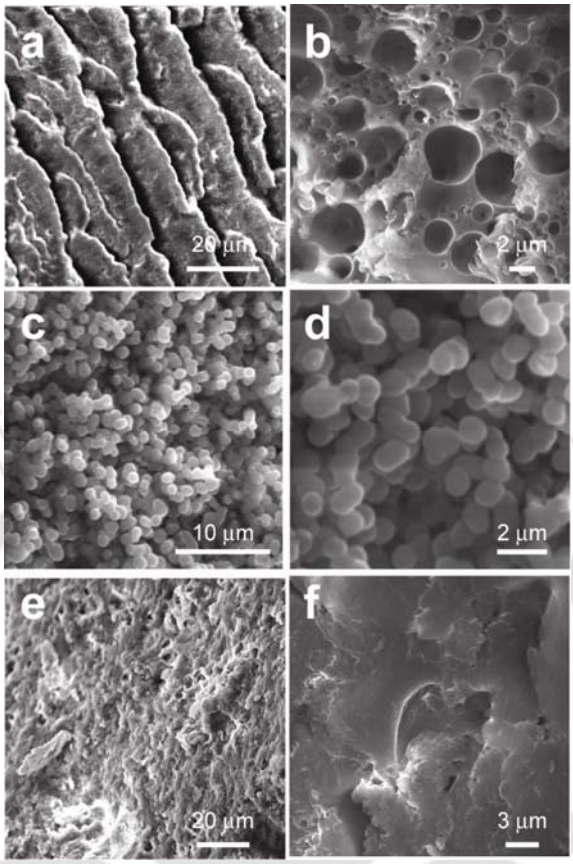

Figure 7.2. *(I) SEM images of the polymers formed in presence of (a) methanol, (b) isopropanol, (c,d) t-butanol, (e) n-octanol and (f) glycerine.*

This accompanies formation of large amount of soluble AFC which precipitates in alkaline medium. This observation indicate that at low temperature the polymer formation initiated around the *t*-butanol core (Scheme 7.3) which slowly grows in size and molecular weight over time forming spheroids until the space between spheroids diminished leading to solid formed out of partially fused spheroids (Figure7.2). Upon dilution some of the spheroids grow further until reagent concentration diminished. The dilution also causes formation of more seed which does not grow further leading to formation of smaller soluble form of AFC. On the other hand, in concentrated medium, several of the droplets of *t*-BuOH fuse together and large lump formation is observed along with spheroids (Figure 7.3 A). The rapid rate of reaction at room temperature causes partial evaporation of *t*-butanol and formation of significant amount of oxidized bright red irregular shaped polymer. If the temperature is maintained strictly at or below 0º C, spheroid shaped formation is also observed in iso-propanol (Figure 7.3 B). However, spheroid formed in isopropanol is much larger (~20 micron) and unlike

spheroids from *t*-BuOH (Figure 7.4) inside (Figure 7.3 B) is not empty. Overall, symmetrical shape of *t*-BuOH influences the formation of 700-2 micron spheroid and reproducibility possibly through a regular shaped solvent core (Scheme 7.3).

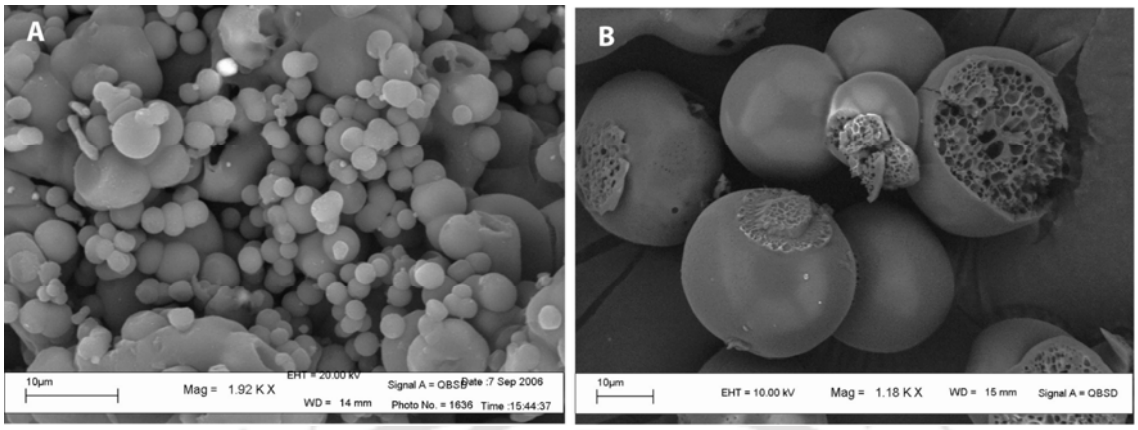

Figure 7.3. *SEM images of the t-BuOH-AFC polymer from concentrated medium (A) and i-PrOH-AFC from temperature controlled medium (B).*

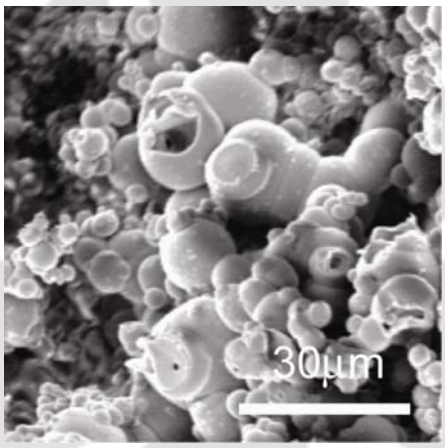

Figure 7.4. *SEM images of the AFC polymer after chromium binding.*

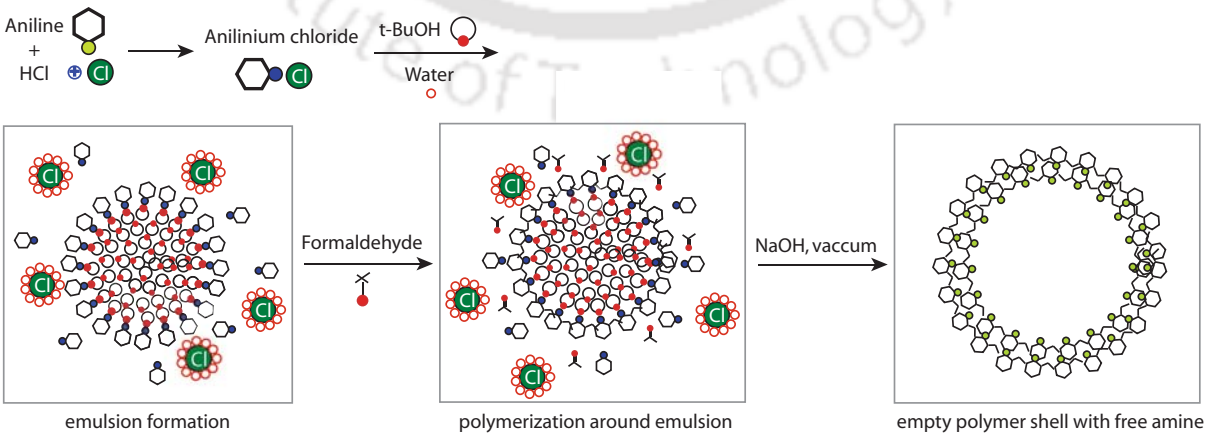

Scheme 7.3. *The proposed path of formation of polymer spheres in t-BuOH water mixture*

7.3.5 Chromium removal property

We chose to study the binding properties of these polymers with Cr(VI) because it will allow us (a) to probe the accessibility of the amine functional groups to aqueous reagents and (b) to check the probable application for these polymers. In acidic pH, AFC and other amine containing polymers or natural adsorbent has been used by us and other investigators to remove toxic Cr(VI) from aqueous solutions.[10-14] Usually at acidic pH, amines in the polymer exist as $–NH_3^+Cl^–$ which acting as anion exchanger absorbs $HCrO_4^–$. This has been confirmed by (a) presence of $\nu_{Cr=O}$ stretch at 932 cm^{-1} in the FT-IR spectrum of Cr(VI) treated polymer and (b) testing Cr(VI) treated polymer for presence of chromate with KI in presence of acid and subsequent iodine liberation.[21,22] The results of the Cr(VI) binding for the polymers is shown in Table 7.A.

Table 7.A. Binding properties of the grinded polymers for $HCrO^{-4}$ in different initial concentration at pH 3[a]

Initial conc.	100 mg/L		50 mg/L		9 mg/L	
Polymer Prepared from	Cr(VI) removal, %	q_e (mg/g)	Cr(VI) removal, %	q_e (mg/g)	Cr(VI) removal, %	q_e (mg/g)
Methanol	68	68	66	33	61	2.7
Isopropanol	39	39	50	25	70	3.1
t-butanol	13	13	28	14	50	2.2
n-Octanol	66	66	76	38	49	2.2
Glycerine	44	44	66	33	69	3.1

[a]*Quantity of polymer used: 1g/L for initial conc. of 100 mg/L and 50 mg/L, and 2 g/L for 9 mg/L. Each set was allowed to equilibrate for 3 h. Results are average of three sets.*

All the polymers, except spheroids from *t*-butanol show effective removal of Cr(VI) with high q_e (mg of Cr removed by 1 gm of polymer). In comparison, reported amine containing polymers have q_e values between 16 and 23.[23] The present polymers are effective even at a low concentration of 9 mg/L (9 ppm) and reduces Cr(VI) level by 70% (~3 mg/L) in case of polymer synthesized from isopropanol (Table 7.A).

The variation of q_e values for a particular initial concentration of Cr(VI) from polymer to polymer might be due to the differences in accessibility of the $–NH_3^+$ exchange sites. The removal is highest for polymers from MeOH and isopropanol. The polymer from *t*-

butanol shows considerably less removal of Cr(VI) compared to polymers synthesized from other alcohol. The EDAX spot analysis of Cr(VI) absorbed polymers from isopropanol shows presence of chromium on the surface but the spheroids from *t*-butanol indicate significantly less chromium on the surface. We think that in *t*-butanol, most of the amine sites are either in the inner surface of the spheroids or too much crowded to be accessible (Scheme 7.2). On the other hand, polymers from methanol, isopropanol or *n*-octanol due to their lack of seeding during formation yields exchange sites are more open for access to Cr(VI). The SEM photograph of the *t*-butanol sample after it was soaked in Cr(VI) solution for several hours followed by washing and vacuum drying (Figure 7.4) shows that some of the spheroids have been swollen to 2-3 μm size and burst open showing interiors as empty hollow sphere. Cr(VI) removal experiments were tested for both grinded and ungrinded form to check the effect of surface area (Table 7.B). Decreasing the surface area with large particle size (~100 mm^3 cubic blocks), the polymers remain effective in removing Cr(VI) (Table 7.B). Thus the polymers are porous enough to enable the solvent penetration through the matrix.

Table 7.B. Binding Properties of the Large Particles of Polymers (_ 100 mm3 Cubic Blocks) for $HCrO^{-4}$ in Different Initial Concentration at pH 3[a]

Initial conc.	100 mg/L		50mg/L	
Polymer prepared from	Cr(VI) removal, %	q_e, (mg/g)	Cr(VI) removal, %	q_e, (mg/g)
Methanol	40	40	52	26
Isopropanol	40	40	60	30
t-butanol	30	30	24	12
n-Octanol	27	27	22	11
Glycerine	31	31	44	22

[a] *Quantity of polymer used: 1 g/L. Polymers used are _ 3–5 mm square blocks. Each set was allowed to equilibrate for 3 h.*

Conclusion

Thus we are able to modify AFC polymerization reaction by controlling reaction temperature and addition of simple alcohols to produce stable solid polymers instead of sticky resin which increases the usefulness of AFC, a polymer with high amine content similar to chitosan. We have also characterized ~1 micron sized polymer spheres in bulk

quantity (multi gram) by adding *t*-butanol. All the polymers remove Cr(VI) from aqueous solution efficiently. Variation in metal removal capacity among the polymers also demonstrate that (a) the amine groups are accessible to outside reagent (b) the morphology plays a major role in the metal binding property (c) the template effect of *t*-butanol made the spheroids with free amine groups mostly in the inner surface. To the best of our knowledge, synthesis of sub-micron size polymer sphere using only alcohol template without using surfactants or micelles has not been reported before.

All the polymers except the spheroids are useful in removing Cr(VI), an industrial pollutant, from acidic aqueous solution. Compared to AFC coated on silica gel under the similar condition, removal efficiency showed 2.5 times increase in efficiency [ref at Cr(VI) conc. of 100 mg/L with 1 gm polymer /L, q_e value for AFC coated on silica gel 28.[8] All the polymers show significantly better removal of Cr(VI) compared to other known adsorbent in the similar concentration and pH range and it is effective even at very low concentration of ~ 10 ppm (70 % removal).[23]

References

1. Liu, G.; Freund, M. S. *Macromolecules,* **1997**, *30*, 5660.
2. Rinaudo, M. *Prog. Polym. Sci.* **2006**, *31*, 603.
3. Martino, A. D.; Sittinger, M.; Risbuda, M. V. *Biomaterials,* **2005**, *26*, 5983.
4. McKenna, B. J.; Birkedal, H.; Bartl, M. H.; Deming, T. J.; Stucky, G. D. *Angew. Chem. Int. ed. Eng.*, **2004**, *43*, 5652.
5. Hotz, J.; Meier, W. *Langmuir***, 1998**, *14*, 1031.
6. Okubo, M.; Katayama, Y.; Yamamoto, Y. *Colloid & Polymer Science*, **1991**, *269*, 217.
7. Motani, K.; Yamamoto, Y.; Harada, M.; Nakahara, A. *JP Pat.* 73-144511, 1975.
8. Kumar, P. A.; Ray, M.; Chakraborty S. *J. Hazardous Mat.*, **2007**, *143*, 24.
9. Kumar, G. P., Kumar, P. A., Chakraborty, S., Ray, M. *Separation and Purification Technology*, **2007**, *57*, 47.
10. Dakiky, M.; Khamis, M.; Manassra, A.; Mer'eb , M. *Adv. Env. Res.* **2002**, *6***,** 533.
11. Prakashama, R.S.; Sheno Merrie, J.; Sheel, R.; Saswathi, N.; Ramakrishna, S.V. *Environmental Pollution,* **1999**, *104*, 421.

12. Sankararamakrishnan, N.; Dixit, A.; Iyengar, L.; Sanghi, R. *Bioresource Technology* **2006**, *97* , 2377.

13. Bayramoglu, G.; Arıca, M. Y. *Separation and Purification Technology,* **2005**, *45*, 192.

14. Deng, S.; Bai, R. *Water Research,* **2004**, *38*, 2424.

15. Maity, T.; Samanta, B. C.; Dalai, S.; Banthia, A. K. *Pigment & Resin Technology*, **2006**, *35*, 12.

16. Ban, K.; Namba, Y.; Sekine, Y.; Matsuda, M. *US Pat.*, 4039446, 1977.

17. Hillenkamp, F.; Karas, M.; Beavis, R. C.; Chait, B. T. *Anal. Chem.*, **1991**, *63*, 1193A.

18. Mandal, H.; Hay, A. S. *Polymer*, **1997**, *38*, 6267.

19. Lenghaus, K.; Qiao, G. G.; Solomon, D. H. *Polymer*, **2001**, *42*, 3355.

20. Pascheka, D.; Geiger, A. *J. Chem. Phys*., **2006**, *124*, 154508.

21. Nakamoto, K. *Infrared and Raman Spectra of Inorganic and Coordination compounds, 5th ed.*; Part B, Willey-Interscience, Newyork, 1997, 273.

22. Svehla, G. *Vogel's Qualitative Inorganic Analysis, 7th ed.*; Wesley Longman (Singapur) Pte Ltd, Delhi, 1996, 124.

23. Cr(VI) removal q_e(mg/g) value 20.7 for acrilonitrile fibre at pH 2.4 with initial con. 50mg /L, ref. 14; 23 for crosslink polymer at pH 2 with initial con. 100mg /L, ref 13; 16 for Xanthated chitosan at pH 3 with initial con. 50mg /L, ref 12.

In the previous chapter we have looked into the polymer formation reaction between aniline and formaldehyde which essentially forms insoluble solid polymer. Anilines themselves form another kind of linear polymers namely polyanilines.[1] One of the advantage of polyanilines are that chain length of the polyanilines can be controlled to some extent.

Synthesis of low molecular weight polyanilines or oligoaniline and their Schiff base derivative are beneficial as these will be easier to characterize using usual molecular characterization techniques such as NMR and mass spectra. The chemistry can then be repeated with higher molecular weight polymers.

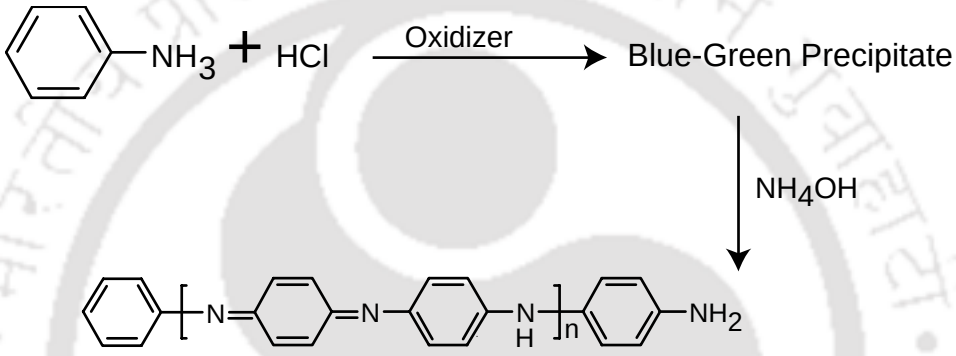

Scheme 8.1. *Formation of polyaniline*

In this chapter we have synthesized and characterized a set of oligoanilines derivative where Schiff base could be formed at the both end of the oligoaniline. We observed a reduction of the oligoaniline unit during Schiff base formation. One of the Schiff bases prepared initially for comparison purpose, serendipitously showed transformation to a highly fluorescent fluorescence active pyrido [1,2-a] quinoxalinylium derivative. A mechanism of the reaction based on the reactions with different metal ions and oxidizers has been proposed.

8.1 Experimental Section

8.1.1 Solvents and Reagents

Pyridine 2-carbaxaldehyde and $(NH_4)_2S_2O_8$ were purchased from Aldrich Chemical Co. and Merck respectively. *p*-phenylenediamine was purified using standard procedure.[2] The solvents and reagents other than those already stated in previous chapter.

8.1.2 Measurements

The electrochemical experiments were performed on CH 6XX electrochemical analyser by CH instruments, USA. The anhydrous N,N'-Dimethyl formamide (DMF) used for electrochemical measurements were purchased from Aldrich Chemical Co. All eletrochemical experiments performed using a CH Instruments electrochemical analyzer using glassy carbon working electrode and Ag^{+}/Ag as reference electrode. Electrochemical grade tetrabutylammonium perchlorate purchased from Fluka were used as supporting electrolyte and used at a concentration of 0.15 M while the concentration of oligoanilines were kept at 0.001 M. The setup was calibrated against Fc^{+}/Fc potential of +0.4V. The ΔEp of ferrocene couple using the setup was observed 100 mV in DMF.[3] All the potentials reported were measured at a scan rate of 50 mV/s.

8.2 Syntheses

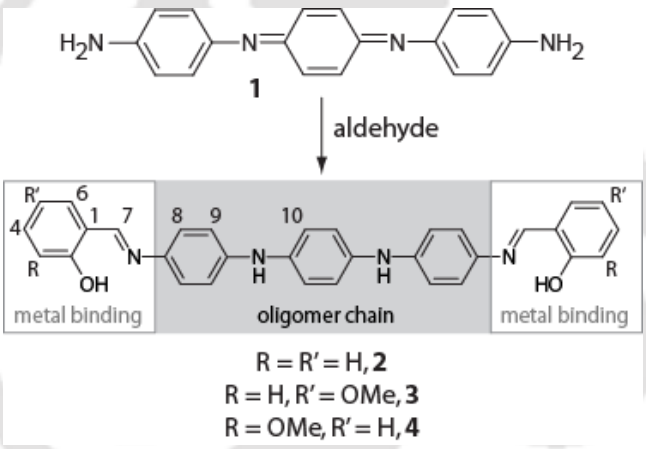

Scheme 8.2. *Schiff bases of oligoanilines with proton nmr labeling*

8.2.1 N,N′-Bis(4′-Aminophenyl)-1,4-Qunonenediimine (1). This has been synthesized modifying a reported procedure.[4] Aniline (3.6 g, 38.64 mmol) and 1,4 phenylenediamine (0.6 g, 5.52 mmol) were dissolved in 120 ml of 1M HCl (aq).The solution was cooled to below 5ºC with an icc bath. A solution of $(NH_4)_2S_2O_8$ (2.84 g, 14.76 mmol) in 30 ml of 1M HCl (aq) pre cooled to below 5ºC was poured into the monomer solution with vigorous stirring. The reaction was maintained at 0-5 ºC for 65 min. After that reaction mixture was allowed to come into the room tempture. The pH of the solution was adjusted to ~ 6 by using ammonia solution. The blue precipitate was then filtered through buchner funnel.To ensure the complete deprotonation, the product was then further washed with small amount of distilled water and 1M NH4OH and dried in desicator. Yield 45 %. Anal. Calcd for $C_{18}H_{16}N_4 \cdot H_2O$ C 70.56%, H

5.92%, N 18.28%; Found: C 71.35%, H 5.91%, N 17.92%. ESI-Mass (+ve) MeOH, MH^+ calc. 289, found 289. Isotopic abundance calc. for MH^+, 289 (100%), 290 (21%), 291(2) found 289 (100), 290 (78), 291 (19). UV-vis (λ, nm, ε, M^{-1} cm^{-1}): (DMF) 313 (21,500), 576 (11,400). IR (KBr, cm^{-1}) 3400br, 1598s, 1500s, 1287, 1165, 819s.

8.2.2 Schiff Base with Salicylaldehyde (2). Salicylaldehyde (0.085 g, 0.70 mmol) was added dropwaise to a methanolic solution of oligomer (0.100 g, 0.35 mmol). The resulting dark violet solution was heated in waterbath at 65ºC for 30 min. During heating, the color of the solution was changed from violet to purple resulting a precipitate which was filtered and washed with diethyl ether. The solid was dried in vaccum. Yield 42 %. Anal Calc. for $C_{32}H_{26}N_4O_2 \cdot H_2O$ C 74.40%, H 5.46%, N 10.85% found C 74.05%, H 5.38%, N 11.05%. ESI-Mass (+ve) MeOH, MH^+ calc. 499, found 499. Isotopic abundance calc., 499 (100%), 500 (37%), 501(7) found 499(100), 500 (14), 501(8). UV-vis (λ, nm, ε, M^{-1} cm^{-1}): (DMF) 410 (35,000), 576 (4,200). IR (KBr, cm^{-1}) 3400w, 1617s (imine), 1598sh, 1508s, 1406, 1309, 1287, 1189, 823s.

8.2.3 Schiff Base with *3*-OMe-Salicylaldehyde (3). This was synthesized follwing the procedure described for **2** using 2 hydroxy 3 methoxy benzaldehyde instead of salicylaldehyde. Yield 47 %. Anal Calc. for $C_{34}H_{30}N_4O_4$ C 73.10%, H 5.41%, N 10.03% found. C 71.69%, H 5.64%, N 11.41%. UV-vis (λ, nm; ε, M^{-1} cm^{-1}): (DMF) 413(31,000), 571(3,000). IR (KBr, cm^{-1}) 3340w, 1615s (imine), 1588sh, 1504s, 1300, 1252, 1200, 821s.

8.2.4 Schiff Base with *5*-OMe-Salicylaldehyde (4). This was synthesized follwing the procedure described for **2** using 2 hydroxy 5 methoxy benzaldehyde instead of salicylaldehyde. Yield 45 %. Anal Calc. for $C_{34}H_{30}N_4O_4$ C 73.10%, H 5.41%, N 10.03% found. C 72.15%, H 5.58%, N 11.20%. ESI-Mass (+ve) MeOH, MH^+ calc. 559, found 559. Isotopic abundance calc., 559 (100%), 560 (39%), 561(8) found 559(100), 560 (40), 561(8). UV-vis (λ, nm; ε, M^{-1} cm^{-1}): (DMF) 417(31,000), 573(2,600). IR (KBr, cm^{-1}) 3400br, 1616sh (imine), 1601s, 1495s, 1387, 1308, 1274, 1156, 821s.

8.2.5 N,N'-Bis-pyridine-2-ylmethylene-benzene-1,4-diamine (5)

2-pyridinecarboxaldehyde (99%, 900 μL, 9.43 mmol) was added drop wise to a stirred methanolic solution of *p*-phenylenediaamine (0.5 gm, 4.6 mmol). The solution was heated over a hot water bath for several minutes .The compound was precipitated as yellow solid. The yellow solid was filtered through Buchner funnel, washed with MeOH. The recrystallization was done in hot MeOH to give yellow crystals. All further analysis was done using these crystals. This structure was reported previously.[5] Yield 46%, m. pt 153 – 156°C. IR (KBr, cm^{-1}**):** ν(C=N) 1617(s) and ν(p-disubstituded benzene ring) 844.

8.2.6 2-Amino-pyrido[1,2-a]quinoxalin-11-ylium perchlorate ([6]ClO_4)

$Cu(ClO_4)_2 \cdot 6H_2O$ (0.097 g, 0.262 mmol) was added to a solution of **5** (0.150 g, 0.524 mmol) in 10 mL MeOH and stirred for 2h. The solution was filtered. The filtrate was evaporated to dryness and washed with diethylether. The solid obtained was recrystallized from MeOH to obtain [**6**]ClO_4 as dark orange crystals. Yield 65%. Anal. Calcd for $C_{12}H_{10}N_3ClO_4$: C, 48.80; H, 3.41; N 14.24. Found: C, 46.75; H, 3.41; N, 14.21. Λ_M (MeOH): 99 S cm^{-2} mol^{-1}. ESI-MS (M^+): Calcd 196.08747, Found 196.0870 UV/Vis (MeOH): λ_{max} [nm] (ε, M^{-1} cm^{-1}): 260 (55,400), 316 (10,800), 367 (8,900), 470 (25,300). IR (KBr, cm^{-1}): $\nu_{perchlorate}$ 1114, 1077, $\nu_{c=N}$ (bend) 1615, ν_{amine} 3297, 3185.

8.2.7 2-Amino-pyrido[1,2-a]quinoxalin-11-ylium thiocyanate ([6]SCN)

KSCN (0.016 g, 0.169 mmol) was added to a methanolic solution of [**6**]ClO_4 (0.050 g, 0.169 mmol). The solution was stirred for 20 min with undissolved $KClO_4$ particle which was filtered. The dark brown crystalline product obtained from slow evaporation of filtrate. Yield 30 mg. IR (KBr, cm^{-1}): ν_{SCN} 2062, 2031, $\nu_{c=N}$ (bend) 1620, ν_{amine} 3287, 3120.

8.2.8 Reactions of 5 with $(NH_4)_2Ce(NO_3)_6$ and $(NH_4)_2S_2O_8$. For each of these oxidizer, 100 mg of the **5** was dissolved in methanol : water (2:1) at room temperature followed by addition of 1eq. solid $(NH_4)_2Ce(NO_3)_6$ or $(NH_4)_2S_2O_8$ and stirring for 30 min. Reaction mixture was subjected to ESI-Mass and Fluorescence spectroscopic measurement to detect formation of [**6**]$^+$. Presence of unreacted starting material (m/e 287 in mass), spent

reagent and smaller amount of $[\mathbf{6}]^+$ formed (comparing mass spectrum of the same reaction performed in presence of Cu(II)) made it difficult to isolate any of the $[\mathbf{6}]^+$ salts.

8.2.9 Reactions of 5 with $HClO_4$. 100 mg of the **5** was dissolved in methanol : water (2:1) at room temperature followed by addition of 1eq. $HClO_4$ in water. Reaction was monitored using fluorescence spectroscopy for four days. Weak fluorescence was observed only after four days. Performing the same reaction anaerobically (N_2 atmosphere) does not show any fluorescence of $[\mathbf{6}]^+$. Anaerobic reaction shows the acid is not responsible for the formation of $[\mathbf{6}]^+$. Addition of 5 eqiv. acids immediately decolorizes the **5** solution probably due to the imine hydrolysis.

8.2.10 X-ray data collection structure solution and refinement

The single crystals of ([6]ClO_4) and ([6]SCN) are obtained by slow evaporation of methanol. Selected crystallographic data are summarized in Table 8.A. The data collection and structure refinement method are discussed in chapter 2.

Table 8.A. Selected crystallographic data

Compounds	([**6**]ClO_4)	([**6**]SCN)
Empirical formula	C_{12} H_{10} N_3 Cl O_4	C_{26} H_{20} N_8 S_2 O
Formula weight	295.05	524.64
Wavelength (Å)	0.71073	0.71073
Crystal system	Monoclinic	Triclinic
Space group	$P2_1/C$	P-1
a, Å	6.32910(10)	9.3055(9)
b, Å	12.9283(3)	11.6353(11)
c, Å	15.4054(4)	12.8604(13)
α, deg	90.00	106.728(6)
β, deg	100.0910(10)	90.896(7)
γ, deg	90.00	108.176(6)
Volume, $Å^3$	1241.04(5)	1258.4(2)
Z /ρ / μ	4 / 1.583/ 0.326	2 / 1.385/ 0.249
collected / indep reflns	12571 / 2939	13215 / 6383
GOF	0.871	1.057

Compounds	([**6**]ClO_4)	([**6**]SCN)
Final R indices	R1 = 0.0388	R1 = 0.0728
[*I*>2sigma(*I*)]	wR2 = 0.0801	WR2 = 0.1949
R indices (all data)	R1 = 0.0935	R1 = 0.1137
	wR2 = 0.1006	wR2 = 0.2211

8.3 Results and Discussion

8.3.1 Synthesis and characterization of oligoaniline Schiff bases

The Schiff bases **2** to **4** were prepared by warming oligotrianiline(**1**) and corresponding aldehyde in MeOH. The poor solubility of the products in MeOH facilitates the isolation. The formation of the Schiff base is indicated by the appearance of IR stretch of ν(C=N) at ~ 1616 cm^{-1}.[6] The characteristic blue color of oligotrianiline (λ_{max}, 576 nm) due to exciton absorption of quinoid ring[7] diminished and a new band appears between 413-435 nm (Figure 8.1) making the Schiff bases brown in color. Comparing the FT-IR of the oligoaniline and the Schiff bases, we found that the IR stretch at ~1580 cm^{-1} for quinoid ring ($\nu_{N=q=N}$) of oligoaniline decreased in intensity in **2**, **3** and **4** compared to benzenoid stretch (ν_{N-B-N}) at ~1500 cm^{-1}.[8]

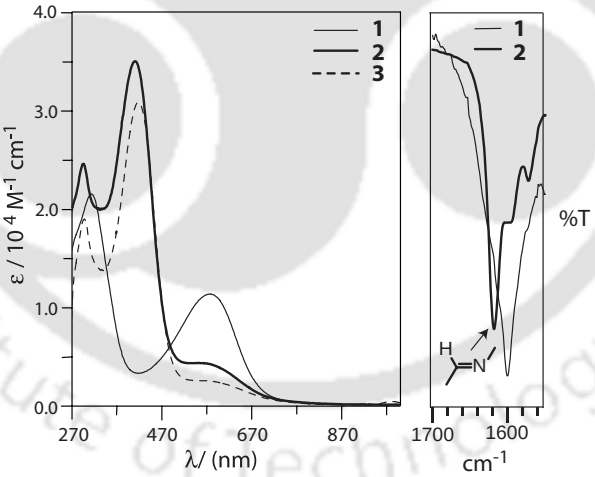

Figure 8.1. *Uv-Visible and partial FT-IR spectra*

These observations indicate the possible reduction of the oligoaniline part of the ligands (Figure 8.1). The ^1H NMR spectral assignments (Table 8.B) on the Schiff bases supports the reduction of the trianiline backbone. The singlet observed between 8.2-8.3 ppm has been assigned as the -NH- protons in **2, 3** and **4**. The ESI-Mass spectra confirmed the reduction as the two form differs by 2 mass units.

Overall the above analysis points out the formation of terminally functionalized oligoaniline in the reduced form and thus devoid of the conjugation. This is probably

the reason for the disappearance of the 576 nm absorption and weakening of the IR stretch at ~1580 cm^{-1} for quinoid ring ($\nu_{N=q=N}$). The reduction possibly occurred at the expense of some of the oligotrianiline starting material which is known to get oxidize easily.[4]

Table 8.B. The ^{1}H NMR data of **1- 4**

	-OH	H^7	-NH	H^8	H^9	H^{10}	OMe	H^3	H^4	H^5	H^6
2[a]	13.51s	8.89s	8.22s	7.33[b]d	7.02d	7.06s	-	6.92m[c]	7.33[b]	6.92[c]	7.55d
	2H	2H	2H	5H	4H	4H		4H			2H
				J 8.4	*J 8.4*						*J 7.6*
3[a]	13.69s	8.89s	8.22s	7.34d	7.02d	7.08s	3.80s	-	7.07d	6.86t	7.15d
	2H	2H	2H	4H	4H	4H	6H		2H	2H	2H
				J 8.4	*J 8.4*				*J 7.6*	*J 7.6*	*J 7.6*
4[a]	12.87s	8.87s	8.21s	7.32d	7.03d	7.09s	3.74s	6.85d	6.96d	-	7.17s
	2H	2H	2H	4H	4H	4H	6H	2H	2H		2H
				J 8.4	*J 8.4*			*J*	*J*		

[a] ^{1}H NMR data taken in DMSO. [b] H^8 and H^4 overlapped. [c] H^3 and H^5 overlapped.

8.3.2 Electrochemical Properties

In order to understand redox properties of the oligoanilines cyclic voltammetric experiments were performed. The selected electrochemical data are presented in Table 8.C and representative cyclic voltammograms in Figure 8.2.

Table 8.C. The selected electrochemical data of **1-4**

Compounds	E_{pa}, V	E_{pc}, V	ΔE_p, mV
1	0.154, 0.539	0.025, 0.364	129, 175
2	0.523	0.163	360
3	0.517	0.245	272
4	0.514	0.277	237

The starting oligotrianiline with terminal amine (N, N′-bis(4′-aminophenyl)-1,4-quinonediimine) shows two closely spaced quasi reversible oxidation at $E_{1/2}$ 0.09 (ΔE_p 129 mV) and 0.45 (ΔE_p 175 mV). Compared to this oligotrianiline without the terminal amine groups in acidic MeCN showed two reversible $1e^-$ reduction at 0.75 and 0.25 V due to the reduction of imines.[9] Thus presence of terminal amines made the oligotrianiline more susceptible to oxidation compared to trianiline without the terminal amine group. This supports our assumption that during Schiff base formation

the oxidation of the trianiline leads to the formation of the Schiff bases in the reduced form. The oxidations observed in starting oligotrianiline possibly occurs due to the oxidation of the terminal amine groups. Compared to the oligotrianiline starting material, Schiff base oligoanilines **2, 3** and **4** show irreversible oxidation with anodic peak potential (E_{pa}) ~0.5 V with reduction wave at ~0.2 V (Table 8.C). The current height measurement and comparison with trianiline suggest this is a $2e^-$ oxidation. This is most likely to be the oxidation of the oligoaniline backbone. The other possibility of Schiff base imine oxidation usually occurs at higher potential as has been observed for **5** and other related ligands.[5a] This results show that the ligands **2, 3** and **4** given their low oxidation potential, (~0.5 V, Table 8.C) should be easily oxidized chemically. The chemical oxidation of these ligands to confirm the location of the oxidation will be attempted in future.

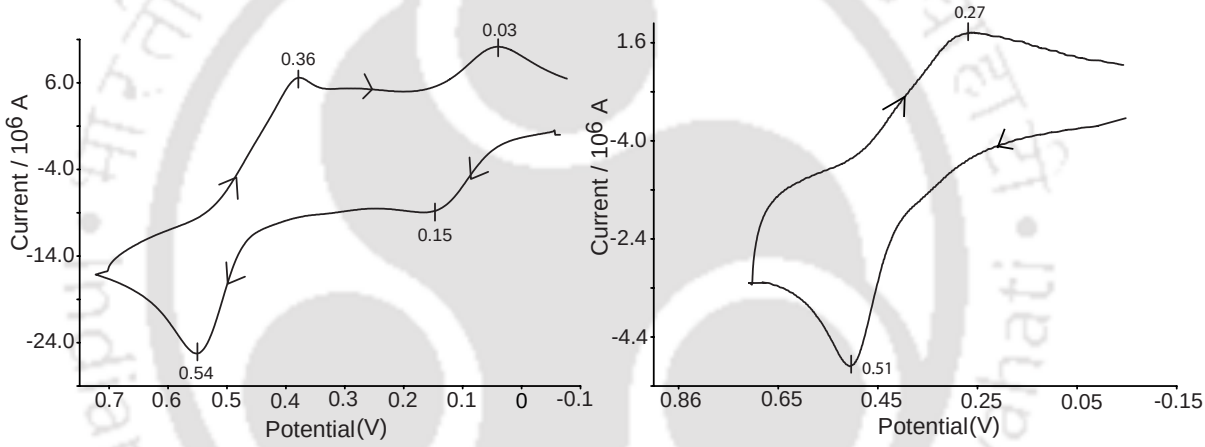

Figure 8.2. *Cyclic voltammograms of **1** and **2** in DMF at scan rate 50 mV sec^{-1}*

Overall, the electrochemical results showed that the oligoanilines, its terminal derivatives have distinctly different redox behavior. Terminal Schiff base formation stabilizes the reduced form of oligoaniline chain as observed by comparing potential of oligoaniline starting material with that of Schiff bases.

8.3.3 Synthesis of 2-Amino-pyrido[1,2-a]quinoxalin-11-ylium perchlorate ([6])$^+$

Quinoxalins are an important class of heterocyclic compounds, some of which are found to be useful as fluorophore, dye, and antibiotics.[10] There are different types of quinoxalin.[11] Among them, examples of pyrido[1,2-a]quinoxalin derivatives are rare and oxidized salt forms are unknown.[12] Syntheses of a few known closely related quinoxalins involve multiple steps.[12,13] In this section we are reporting the single step Cu(II) mediated synthesis of a previously unknown pyrido[1,2-a] quinoxalinylium derivative ([**6**]$^+$) and

also its structure (Scheme 8.3). The controlled reaction has been used to understand the role of metal ion in the reaction. The strong fluorescence observed, increases the versatility of application of the present compound.

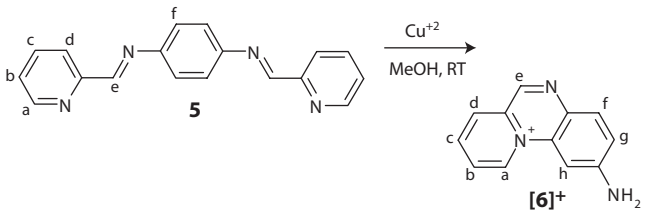

Scheme 8.3. *Formation of [6]+ from 5 with proton labeling*

Upon addition of $Cu(ClO_4)_2 \cdot 6H_2O$ to the methanolic solution of **5**, an orange solution with yellow fluorescence was formed within minutes. Filtration of the solution followed by slow evaporation yielded the compound [**6**]ClO_4 as orange crystals. Metathesis with KSCN in methanol yielded the crystals of [**6**]$SCN \cdot H_2O$.

8.3.4 Structure of pyrido[1,2-a] quinoxalinylium ion ([6]$^+$)

[**6**]ClO_4 and [**6**]$SCN \cdot H_2O$ crystallized in the space group $P2_1/c$ and P-1 respectively. The structures of [**6**]$^+$ is identical in both the crystal but the thermal parameters of several atoms in [**6**]ClO_4 are high. Thus the bond lengths of [**6**]SCN are used in the discussion. The ORTEP diagram and bond lengths of [**6**]$^+$ ions are shown in Figure 8.3 and Table 8.D respectively.

[**6**]$^+$ is essentially planar with a short C10-N1 distance of 1.357(3) Å, compared to usual C_{aro}-N_{amine} single bond distance of 1.43 Å.[14] This might be due to the electron withdrawing effect of positively charged pyridine which increased the C-N_{amine} bond order. Other C-C and C-N bond distances are well within the limits expected for aromatic rings.[14]

In [**6**]$SCN \cdot H_2O$, amine NH, water and N of SCN^- form two different types of H-bonded network resulting in two non-identical SCN^- in the crystal (Figure 8.4). The FT-IR of [**6**]SCN shows two stretches at 2062 and 2031 cm^{-1} for ν_{CN} of SCN^-.[6] In [**6**]ClO_4, perchlorate ion H-bonded with the free amine hydrogens (N…O , 3.1-3.2 Å), forms a 2D network (Figure 8.5). [**6**]ClO_4 shows strong absorption at ~1100 cm^{-1} due to perchlorate ion.[6] Both compounds show two ν_{NH} stretch between 3100 to 3300 cm^{-1}, characteristic of primary amine while that of ν_{imine} in the ring occurs at ~1620 cm^{-1}.[6]

Table 8.D. Bond length comparison between the structures.

Compounds	[**1**]ClO_4	[**1**]SCN	[**1**]SCN 2nd
Atoms	Distance (Å)	Distance (Å)	Distance (Å)
C1-C2	1.431 (3)	1.362 (4)	1.353 (5)
C2-C3	1.360 (3)	1.389 (5)	1.383 (6)
C3-C4	1.381 (3)	1.353 (4)	1.357 (6)
C4-C5	1.397 (3)	1.402 (4)	1.404 (5)
C5-C6	1.397 (3)	1.414 (4)	1.417 (5)
C6-N3	1.228 (3)	1.300 (4)	1.313 (5)
N3-C7	1.485 (3)	1.372 (3)	1.355 (4)
C7-C8	1.279 (3)	1.404 (4)	1.411 (5)
C8-C9	1.347 (3)	1.361 (4)	1.348 (5)
C9-C10	1.508 (2)	1.412 (4)	1.411 (5)
C10-C11	1.363 (3)	1.396 (3)	1.396 (4)
C11-C12	1.384 (2)	1.381 (3)	1.394 (4)
C12-C7	1.4119 (19)	1.420 (3)	1.417 (4)
C12-N2	1.424 (3)	1.424 (3)	1.414 (4)
N2-C1	1.342 (2)	1.369 (3)	1.375 (4)
N2-C5	1.409 (2)	1.377 (3)	1.373 (4)
C10-N1	1.276 (3)	1.357 (3)	1.350 (5)

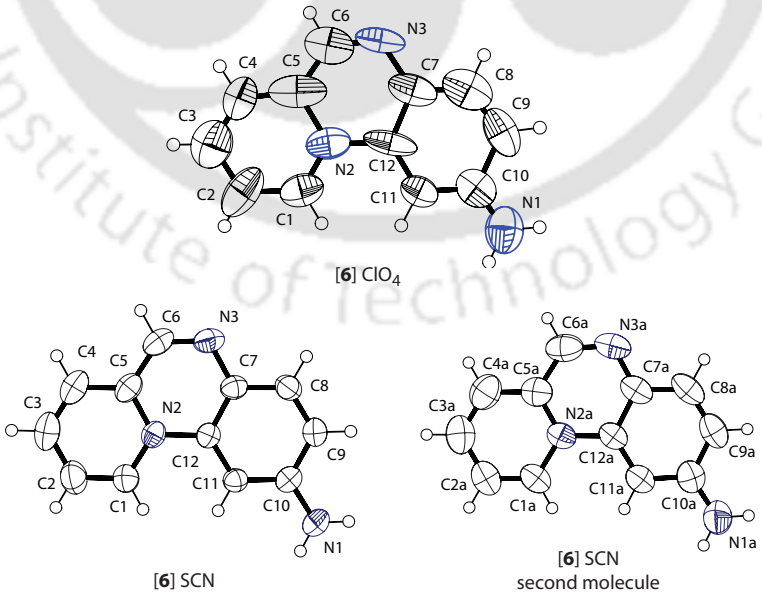

Figure 8.3. *ORTEP figure of [6]ClO_4 and [6]SCN. Thermal ellipsoid parameter set to 50 % probability*

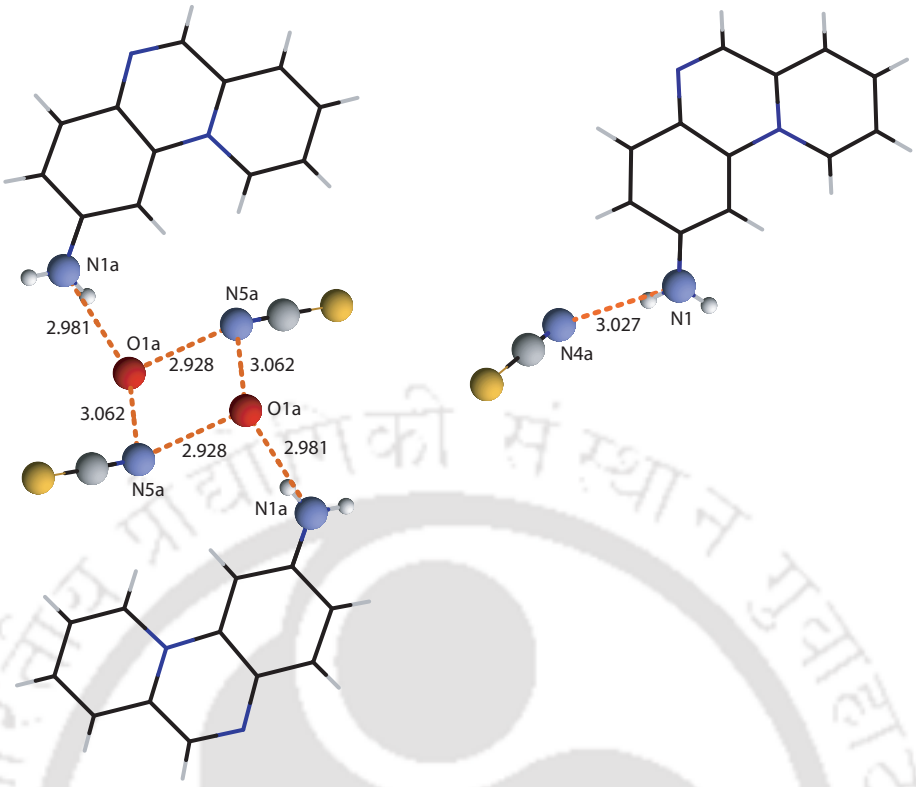

Figure 8.4. *The H-bonding Scheme present in the crystals of* ***[6]****SCN.*

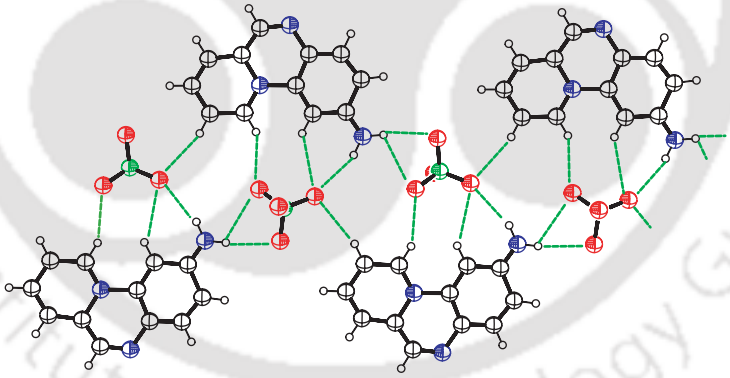

Figure 8.5. *The H-bonding Scheme present in the crystals of* ***[6]****ClO_4.*

8.3.5 Proton NMR of [6]ClO_4

In the ^{1}H NMR of [**6**]ClO_4 in CD_3OD, protons were identified from relative positions, coupling and integration (Table 8.E). Compared to **5**, both H^e and H^a in **[6]**$^+$ shifted considerably to downfield by 0.94 and 1.04 ppm respectively, presumably due to their proximity with quaternary nitrogen (Figure 8.6, labeling in Scheme 8.3). H^e and H^h were identified from the singlet nature and their proximity with the cationic pyridine and

electron rich amine respectively. Similarly doublets of H^a, H^f and H^g were identified from their proximity with pyridine ring, amine and imine respectively. The triplet at 8.25 ppm was identified as H^b as H^c being para to the cationic pyridine nitrogen expected to be more deshielded compared to the H^b which is in meta position. Thus multiplet at 8.6 ppm is due to both H^c and H^d.

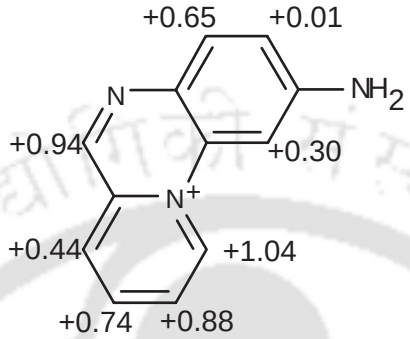

Figure 8.6. *^{1}H NMR shift compare to **5***

The protons in the pyridine ring are more shifted to downfield compared to the protons in the aniline ring. Thus pyridine ring is electron deficient compared to aniline ring which probably led to strong intra-molecular charge transfer (Section 8.3.6).

Table 8.E. ^{1}H NMR data for **5** and [**6**]ClO_4

H	a	b	c	d	e	f	g	h
L_1	8.73d,	7.39t,	7.84t,	8.22d,	8.24s,	7.38s,		
$CDCl_3$	2H	2H	2H	2H	2H	4H		
	J= 7.2	J= 7.6	J=7.6	J= 7.6				
[**1**]ClO_4	9.76d,	8.25m,	8.56m,	8.61m,	9.18s,	8.01d,	7.38dd,	7.66d,
CD_3OD	1H	1H	1H	1H	1H	1H	1H	1H
	J_{ab} 7, J_{bc} 7.5, J_{cd} 8, J_{fg} 9, J_{gh} 2.4, J_{ac} ~2, J_{bd} ~2, J_{ad} <1							
Shift	+1.03	+0.86	+0.72	+0.39	+0.94	+0.63	+0.00	+0.28

8.3.6 Electronic and fluorescence spectroscopic properties of [6]ClO_4

The solution of [**6**]ClO_4 in MeOH shows strong charge transfer bands. Upon excitation at 470 nm, the molecule fluoresce at 580 nm (Figure 8.7). The quantum yield was estimated using micromolar methanolic solution of quinine sulphate as reference at different absorbance and found to be 0.23 (Figure 8.8).[15] Reasonable quantum yield and emission in the useful 500-600 nm region for $[\mathbf{6}]^+$ is comparable with popular fluorescent dyes like acridine orange ($\lambda_{em.}$ 525 nm, Q. yield 0.20), fluorescein ($\lambda_{em.}$ 500-600 nm, Q.

yield 0.79) and quinine sulfate ($\lambda_{em.}$ 400-600 nm, Q. yield 0.54).[16] The fluorescence emission at 470 nm is due to the intra-molecular charge transfer between relatively electron rich amine ring and the electron deficient pyridinium ring.

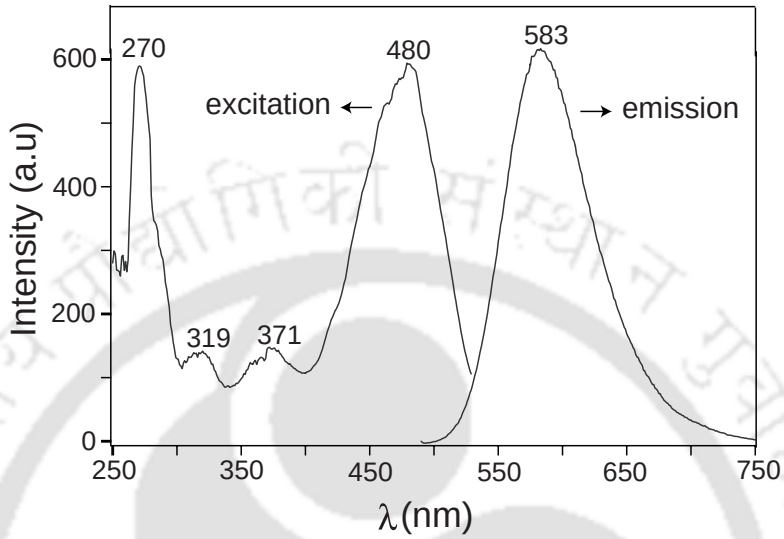

Figure 8.7. *Excitation and Emission spectrum of [**6**]ClO_4 in MeOH*

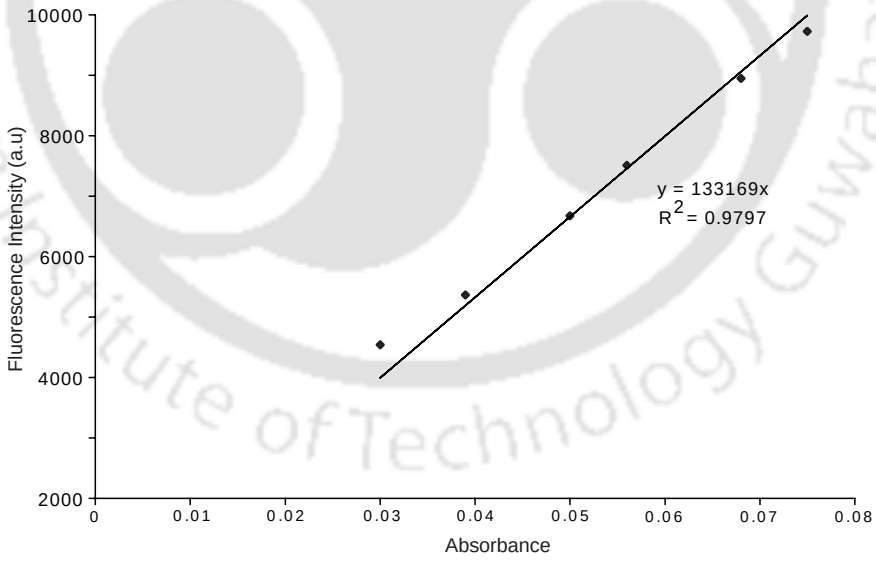

Figure 8.8. *The integrated Fluorescence Intensity vs. absorbance plot for [**6**]ClO_4 in MeOH used in quantum yield determination.*

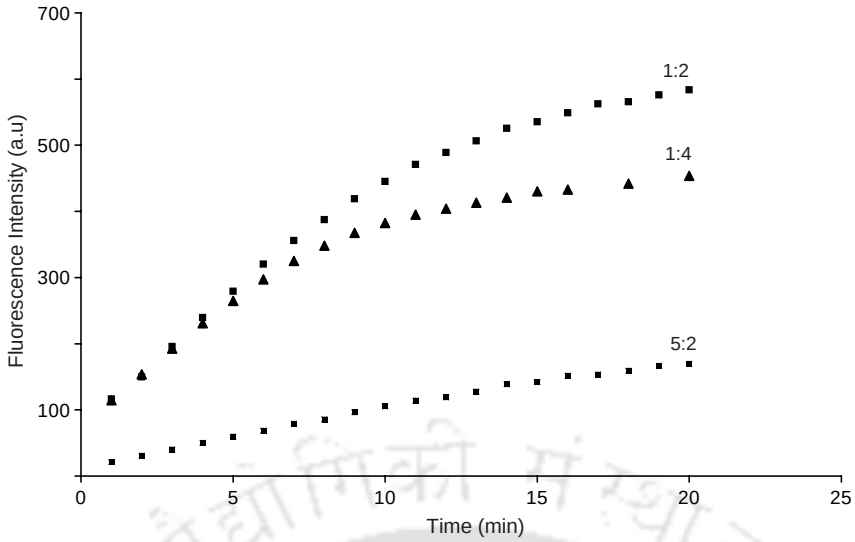

Figure 8.9. *The progress of the reaction with time monitored using fluorescence at different M:L ratio (1:2, 1:4 and 5:2). Concentration of L_1 ~10^{-5} M in MeOH*

8.3.7 Mechanism of the formation of $[6]^+$

Reaction of Cu^{II} and **5** most likely proceed through complexation (Scheme 8.4). EPR of the frozen solution at the beginning of the reaction shows strong signal at 77K for typical Cu(II) tetragonal complex with g_{II}, $g_{\perp}$ and A_{II} values of 2.37, 2.02 and 177 G respectively.[17] The formation of $[\mathbf{6}]^+$ monitored using fluorescence spectroscopy showed the completion of the reaction within 15 min (Figure 8.9). Amount of $[\mathbf{6}]^+$ produced, decreases with increasing metal ion concentration presumably because of formation of side product III (Scheme 8.4). Binuclear complexes of **5** with Ru^{II} and Zn^{II} similar to III are known which support the formation of side product III. [5, 18]

The reduction of Cu^{II} during reaction was indicated by the significant reduction of EPR signal intensity at the end of the reaction. Involvement of redox state of metal was also indicated by reaction in presence of redox inactive metal ion. Formation of $[\mathbf{6}]^+$ was not observed in presence of Zn^{+2} and Cd^{+2} even after prolonged stirring for two days. The **5** is known to stabilize lower oxidation state of metal (Ru^{III}/Ru^{II} potential for $[(bpy)_2Ru(\mathbf{5})Ru(bpy)_2]$ is 1.59 V vs. SCE).[5a,19] Thus reduction of metal ion with concomitant oxidation of ligand forming an intermediate II is conceivable (scheme 8.4). The reaction proceeded further with ring closure followed by hydrolysis of the imine bond (Scheme 8.4). If a cation radical indeed is the intermediate then proper oxidizer might be able to form $[\mathbf{6}]^+$.

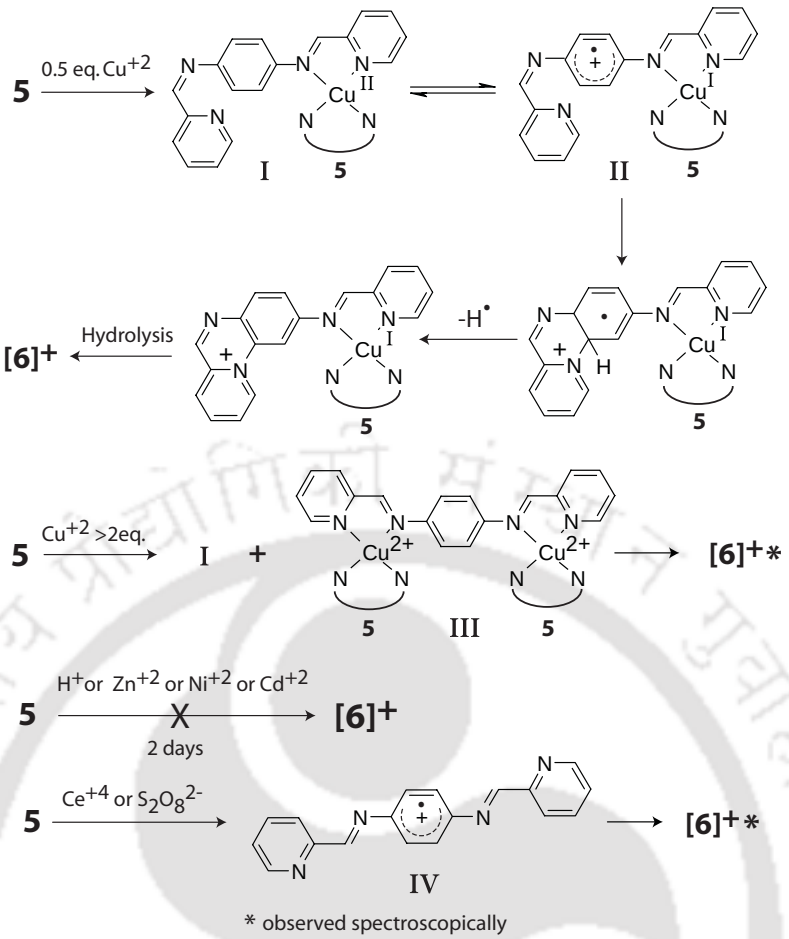

Scheme 8.4. *Proposed path of reaction*

To check this possibility, we have reacted **5** which gets oxidized[5a] at 1.79 V (vs SCE in MeCN) with strong oxidizers, Ce^{IV} and $S_2O_8^{-2}$ salts. ESI-Mass and fluorescence measurement of the resulting solutions formation of small quantity of $[\mathbf{6}]^+$ in comparison with reaction in presence of Cu(II). Formation of $[\mathbf{6}]^+$ supports the ligand oxidation as the key step for the formation of $[\mathbf{6}]^+$. The tendency of **5** to stabilize Cu(I)[19] possibly helps the formation of intermediate II. Thus the role of Cu(II) is to form the intermediate II (Scheme 8.4) and thereby facilitate the formation of $[\mathbf{6}]^+$ in larger quantity. The Cu(II) has been reported to stabilize radicals in several systems.[20] Our attempt to isolate product from these reaction mixture proved futile.

We have tried the reaction in presence of Mn^{II}, Ni^{II}, Fe^{II}, Fe^{III} and $[Fe(CN)_6]^{3-}$. In presence of Mn^{II} traces of **6** was formed only after two days. Product formation was not observed with Ni^{II}, Fe^{II} or $[Fe(CN)_6]^{3-}$. Formation of $[\mathbf{6}]^+$ was observed with Fe^{III} spectroscopically. However, formation of a purple coloured solution indicated a mixture of products. The fact that both Cu^{II} (0.16 V vs NHE in water) and Fe^{III} (Fe^{III}/Fe^{II} 0.77 V vs NHE in water) salts form $[\mathbf{6}]^+$ but $[Fe(CN)_6]^{3-}$ (0. 36 V) vs NHE in water)[21] does not,

indicates that metal ions which are capable of binding with the ligand and stabilizing radical intermediate upon reduction, have the potential to facilitate this reaction. While $[Fe(CN)_6]^{3-}$ has the redox potential between the Cu^{II} and Fe^{III}, its inability to bind to the ligand inhibits the reaction. On the other hand, oxidizers which are strong enough to oxidize the ligand directly can also form $[\mathbf{6}]^+$ but the unstability of the intermediate IV decreases the amount of the cyclized product. Our efforts are on to study the reaction with other metal ions.

Overall reaction stoichiometry of the reaction is likely to be as follows

$$\underset{(C_{18}H_{14}N_4)}{\mathbf{5}} + H_2O \rightarrow \underset{(C_{12}H_{10}N_3)}{[\mathbf{6}]^+} + \underset{(C_6H_5NO)}{\text{Pyridine-2-carboxaldehyde}} + \{H^+ + 2e^-\}$$

The ESI-mass spectrum of the reaction mixture from Cu^{II} mediated reaction at the end of reaction shows the presence of $\{C_6H_5NO\}^+$ and $\{Cu^I(C_6H_5NO)\}^+$ at 107.0 and 169.9 respectively, supporting the above reaction.

Cu(II) has earlier been used as a mediator in heterocyclic compound formation[22], but was never used as a mediator in any quinoxalin derivative. Recently, a fluorescent triazinium compound has been reported where pyridinium salt formation occurred via addition of acid followed by loss of H_2.[23] However, we have not observed the formation of $[\mathbf{6}]^+$ in presence of acid.

Conclusions

In this chapter we have synthesized a set of Schiff bases of an oligotrianiline (Section 8.3.1 and 8.3.2). Characterization of the Schiff bases (**2**-**4**) showed that simple functionalizations of the terminal amines are possible. However, the results also showed that redox properties of oligoaniline/polyanilines might interfere even with a simple aldehyde. Thus the idea of studying functionalization with oligoaniline instead of polyaniline is reasonably valid as direct Schiff base formation with polyaniline would be difficult to characterize.

In Section 8.3.3- 8.3.7, we have synthesized and characterized a new pyrido[1,2-a]quinoxalin-11-ium derivative from a Schiff base which was initially prepared to compare NMR and other spectral data of oligoaniline Schiff bases. The reaction proceeds through a primarily Cu(II) mediated pathway hitherto unobserved for similar reactions.

Strong fluorescence in the visible region and solubility of the compound in wide range of solvent increases the potential of the compound as a fluorescent dye.

From the above two results we conclude that before we proceed further synthesizing polymers of anilines (linear) and attempt to bind metal complexes to it, redox properties of oligoanilines/polyanilines and their functionalized product need more thorough investigation.

References

1. (a) MacDiarmid, A. G.; Chiang, J. C.; Richter, A. F.; Epstein, A. *J. Synth. Met.* **1987**, *17*, 285. (b) MacDiarmid, A. G.; Epstein, A. J. *Faraday Discuss. Chem. Soc*. **1989**, *88*, 317.
2. Furniss, B. S.; Hannaford, A. J.; Rogers, V.; Smith, P. W. G.; Tatchell, A. R. *Vogel's Textbook of Practical Organic Chemistry*, 4th ed, English Language Book Society/Longman, England, 1978, 661.
3. Ray, M.; Golombek, A. P.; Hendrich, M. P.; Yap, G. P. A.; Liable-Sands, L. M.; Rheingold, A. L.; Borovik, A. S. *Inorg. Chem.* **1999**, *38,* 3110.
4. Wei, Y.; Yang, C.; Ding, T. *Tet. Lett.*, **1996,** *37*, 731.
5. (a) Chakraborty, S.; Munchi, P.; Lahiri, G. K. *Polyhedron*, **1999,** *18*, 1437. (b) Chanda, N.; Mondal, B.; Puranik, V. G.; Lahiri, G. K. *Polyhedron,* **2002**, *21*, 2033.
6. Nakamoto, K. *Infrared and Raman Spectra of Inorganic and Coordination compounds*, 5th ed.; Part B, Willey- Interscience, New York, 1997, 273.
7. Yan, F.; Xue, G. *J. Mat. Chem.*, **1999**, *9*, 3035.
8. tarachiwin, L. ; Kiattibutr, P. ; Ruangchuay, L. ; Sirivat, A. ; Schwank, J. *J. Synth, Met*., **2002**, *129*, 303.
9. Shacklette, L. W.; Wolf, J. F.; Gould, S.; Baughman, R. H. *J. Chem. Phys.,* **1988**, *88,* 3955.
10. (a) Duffy, K. J.; Haltiwanger, R. C.; Freyer, A. J.; Li, F.; Luengo, J. I.; Cheng, Y. H. *J. Chem. Soc., Perkin Trans. 2*, **2002,** 181. (b) Gazit, A.; App, H.; McMahon, G.; Chen, J.; Levitzki, A.; Bohmer, F. D. *J. Med. Chem.,* **1996,** *39*, 2170. (c) Druey, J.; Riehen, B.; Hueni, A. U.S. Patent 2,748,117, 1956.
11. Brown, D. J.; Taylor, E. C.; Wipf, P. The Chemistry of Heterocyclic Compounds: Quinoxalines; Wiley: New York, 2004; Vol. 61, Supplement II.

12. A search in SciFinder scholar for pyrido[1,2-a]quinoxalinylium resulted in nine references, out of which only three have a core heterocycle similar to that of 1. (a) Margareta, U.; Druta, I.; Magda, P.; Zugravescu, I. *Chimie,* **1972,** *18*, 49. (b Warrener, N. R. *Chem. Ind*. **1966**, *9*, 381. (c) Eiden, F.; Peter, P. *Arch. Pharm.*, **1966**, *299*, 139.
13. (a) Fringuelli, F.; Pizzo, F.; Tortoioli, S.; Vaccaro, L. *J. Org. Chem*., **2004**, *69*, 7745. (b) Vierfond, J.; Mettey, Y.; Miocque, R. J. M. *J. Heterocycl. Chem*., **1979**, *16*, 753. Zhou, J.; Zhang, L.; Hu, Y.; Hu, H. *J. Chem. Res. S,* **1999**, 552.
14. Lide, D. R. *Handbook of Chemistry and Physics*, 76th ed.; CRC, Inc.: Boca Raton, FL, 1995.
15. Williams, A. T. R.; Winfield, S. A.; Miller, J. N. *Analyst,* **1983**, *108*, 1067.
16. (a) Soep, B.; Kellmann, A.; Martin, M.; Lindqvist, L. *Chem. Phys. Lett.,* **1972**, *13*, 241. (b) Umberger, J.; Lamer, V. *J. Am. Chem. Soc*. **1945**, 1099. (c) Moore, D.; Happe, J. *J. Phys. Chem.,* **1961**, *65*, 229.
17. Yokoi, H.; Addison, A. W. *J. Chem. Soc., Dalton Trans.,* **1977**, *16*, 1341.
18. (a) Yoshida, N.; Ichikawa, K.; Shiro, M. *J. Chem. Soc., Perkin Trans. 2*, **2000,** 17. (b) Cai, P.; Li, M.; Duan, C.; Lu, F.; Guo, D.; Meng, Q. *New J. Chem.*, **2005**, *29*, 1011.
19. The Cu^{II}/Cu^{I} potential for $Cu(bpy)_2PF6$, which has a coordination environment similar to that of I (Scheme 8.4), is 0.52 V vs SCE. The Ru^{III}/Ru^{II} potential of $[Ru(bpy)_3]^{2+}$ is 1.29 V. Kourkine, I. V.; Mirkin, C. A. *J. Am. Chem. Soc*. **2000,** *122*, 2659.
20. Min, K. S.; Weyhermu¨ller, T.; Bothe, E.; Wieghardt, K. *Inorg. Chem.,* **2004**, *43*, 2922.
21. Bard, J. A.; Faulkner, L. R. Electrochemical Methods Fundamentals and Applications, 2nd ed.; Wiley Eastern: New Delhi, India, 2006.
22. (a) Padhi, S. K.; Manivannan, V. *Inorg. Chem.,* **2006**, *45*, 7994. (b) Schneider, J. L.; Young, V. G., Jr.; Tolman, W. B. *Inorg. Chem.,* **2001**, *40*, 165.
23. Sinan, M.; Panda, M.; Ghosh, A.; Dhara, K.; Fanwick, P. E.; Chattopadhyay, D. J.; Goswami, S. *J. Am. Chem. Soc.* **2008**, *130*, 5185.

FINDINGS OF THE THESIS

The work in this thesis stems from earlier characterization of an capsule shaped octameric Cu(II) complex.[1] Literature published by us and others between that work and the present thesis showed a variety of structural motifs possible by this type of ligands.[2] We were particularly curious about the fact that using the same L-histidine derivative and Cu(II), complexes with two different nuclearity is being reported.[1,3] While the octanuclear complex itself was important considering its relevance to making cages with void space, the metal complexes of these chiral ligands have potential to generate crystals suitable for non linear optical materials. Apart from these the complexes of amino acids are relevant for bioinorganic chemistry as well.[4] Thus we thought it is worth exploring the coordination chemistry of this type of ligand.

As extensive H-bonded network formation has been observed and even a solvent can change the structural organization dramatically,[5] we have put emphasize on isolation and structural characterization of as many diverse species as possible. This is because we wanted to check the extent of the diversity to prepare the ground for rational design of materials. Between Chapter 2 to 6 we are reporting characterization of 13 new complexes varying the amino acid, ring substitution, external ligand, solvent, metal ligand ratio and eventually changing the metal ion itself. The major achievements of this thesis are summarized below.

Ligand preference for Cu(II). Cu(II), an intermediate soft acid, expected to prefer heterocyclic N donors which is intermediate soft base. Cu(II)'s preference for heterocyclic N donor over O donor is perhaps the most critical influence exerted in the type of complexes that has been formed. This was responsible for the conversion of bis-phenoxo bridged complexes to the octanuclear complex as well as other mononuclear complexes in the Chapter II.

Imidazole as in-plane ligand. Imidazole with its higher basicity is a strong ligand. What is however comes at a surprise is its ability to bind as in-plane ligand preferentially even if it means shifting the co-ligand to an otherwise uncomfortable axial position. All of the complexes reported in chapters 2-4 shows imidazole (individual or as a part of the ligand) as in-plane ligand only. These are also the only complexes where carboxylate part of

these ligands acts as axial ligand. Simple ball and stick molecular model shows considerable strain on this mode of ligation. Apart from our finding we have looked into the literature and found another complex[6] where 2,2'bipydyl ligand occupies one in-plane and one axial site of a Cu(II) complex in presence of imidazole as co-ligand instead of usual in-plane cis coordination.

Diassembly of the capsule. As a potential carrier of molecules it would be nice to have a way of dissembling the capsular cage to release the trapped molecules. The results described in Chapter 2 and 4 shows number of ways to disassemble the capsule by way of adding imidazole or substituted pyridines. Ironically use of kinetically labile Cu(II) provided us more ways to disassemble rather than to assemble (Chapter 3) or trapping molecules than needed.

Potential materials. The importance of crystals having channels with removable solvents or cages with void space have been highlighted by many[7] and have been discussed in Chapter 1. Number of complexes characterized in this thesis (Chapter 3 & 4) has void spaces or channels in the crystal lattice. While some of these crystals are fragile and thus may not survive the rigor of heating to empty the channels, few (**1a** and **1b** in Chapter 3, **2a** in Chapter 4 and **1a** in Chapter 5) however are strong enough worthy of the experiment. This is being continued in the laboratory.

H-bonding and conformation. Even though H-bonds are relatively weaker bond but nonetheless play many important roles in diverse areas of chemistry. We were particularly surprised to characterize **1b** in Chapter 3. Comparing it with **1a** the only difference in the mode of ligand coordination we are able to find is the rotation of histidine imidazole unit. Rotation along single bond is not unusual but what is unusual is that despite the minor energy difference between two rotamer, we were able to observe both in solid state. We think it is the stability gained by formation of large H-bonded network in **1b** (Chapter 3) which facilitated observation of two different rotamer in the solid state.

Substituted pyridines and H-bonding. Another observation we have made that in all the monomers in Chapter 4 have substituted pyridines as in-plane ligand. As such hydroxyl pyridines have pKa (4.80) values closure to pyridines (5.25) rather than to imidazole (6.92). Thus expected formation of either cages or **3a** (Chapter 2) like coordination. Curiously, these complexes (Chapter 4) have extensive H-bonded network. So is it the reason behind formation of monomers? We are unable to pinpoint the reason at this point.

Water in crystal. Understanding properties of water cluster is important[8] and observation of H-bonded water cluster in the crystals attracted both attention[9] as well as criticism[10]. We have observed myriad examples of networked water molecules in the form of chain cluster throughout this thesis because of the ligands ability to form H-bonds through almost all of their non-carbon hetero atoms. H-bonding has been the boon as well as bane during the isolation and characterization of these complexes. Numerous possible H-bonding made it difficult to isolate a single characterizable entity. For example, we were lucky to crystallize **1a** and **1b** separately in Chapter 6 differing only in number of solvent molecules. The complex **2a** in the same chapter had two different conformer (Scheme 6.2) within the same crystal. Number of solvent molecules in the crystal, desolvation and resolvation with water further complicated getting reasonable analysis in number of cases (p 38, p 58).

Chirality. It is expected that chirality of the ligand will play an important role in many of the complexes especially wherever multiple ligands are involved because of symmetry reasons. We have explored this aspect in Section 3.3.5 and results show that formation of the cage need all the ligands in same chirality due to symmetrical nature of the assembly.

Polymers. The last two chapters deal with an entirely different chemistry which may seem unconnected. As we have discussed in the first chapter that in order to use some of these molecules synthesized in the first few chapters for chiral separation, we need suitable polymer support to facilitate efficient separation. The soluble complexes may not be able to separate enantiomers effectively by interacting through H-bonded (weak) interaction. Thus during this thesis work we have initiated experimentation on polymers which we think we might be able to functionalize easily through terminal amine bond. The results are diverse and few interesting reactions has been observed (see Chapter 7-8 conclusions).

Overall, in this thesis work we have structurally characterized a diverse set of complexes through systematic modification of the ligand and reaction conditions. These and the one's already reported, forms a diverse structural library which along with the identification of some of the structural and chemical factors lays the foundation for future efforts on the rational synthesis of materials using amino acid based ligands which turned out to be a very versatile ligand set.

References.

[1] Alam, M. A.; Nethaji, M.; Ray, M. *Angew. Chem. Int. Ed.* **2003,** *42*, 1940.
[2] Ganguly, R.; Sreenivasulu, B.; Vittal, J. J. *Coord. Chem. Rev.*, **2008**, *252*, 1027.
[3] Yang, C. T.; Vetrichelvan, M.; Yang, X; Keith, B. M.; Murray, S.; Vittal, J. J. *J. Chem. Soc., Dalton Trans.* **2004**, 113.
[4] Sarkar, B. *Chem. Rev.* **1999**, *99*, 2535.
[5] Muthu, S.; Vittal, J. J. *Crystal Growth & Design*, **2004**, *4*, 1181.
[6] Morehouse, S. M.; Suliman, H.; Haff, J.; Nguyen, D. *Inorg. Chim. Acta* **2000**, *297*, 411.
[7] Kitagawa, S.; Kitaura, R.; Noro, S. *Angew. Chem. Int. ED.* **2004**, *43*, 2334.
[8] Keutsch, F. N.; Saykally, R. J. Proc. Natl. Acad. Sci. 2001, 98, 10533.
[9] Water cluster in crystal either review or article in very good journal
[10] Criticism Angew Chem

List of Publications

1. "Rationalizing the Effects of Amino Acid Side Chain, Pyridine, and Imidazole on the Assembly and Reversible Disassembly of a Octanuclear Cu(II) Complex", M. A. Alam, **R. R. Koner**, A. Das, M. Nethaji, M. Ray, *Crystal Growth & design*, **2007**, *7*, 1818.

2. "Synthesis of Morphologically Different, Metal Absorbing Aniline-Formaldehyde Polymers Including Micron-Sized Sphere Using Simple Alcohols as Morphology Modifier", **R. R. Koner**, P. A. Kumar, S. Chakraborty, M. Ray, *J. Appl. Poly. Sc.* **2008,** *110***,** 1158.

3. "Copper (II) mediated synthesis of a new fluorescent pyrido [1,2-a]quinoxalin-11-ium derivative", **R. R. Koner**, M. Ray, *Inorg. Chem.* **2008**, *47*, 9122.

Manuscript to be submitted

4. "Water assisted histidine coordination mode switching transforms capsule to networked crystal with 1D channels", **R. R. Koner**, M. Ray.

5. "Self-assembly of L-leucine derived ligand, Ni(II) or Cu(II) and alkali metal ion into trinuclear assembly held together by six short H-bonds" , M. Dubey, **R. R. Koner**, M. Ray.

Atomic coordinates for the complex **[Cu(S-met)(imidazole)]**

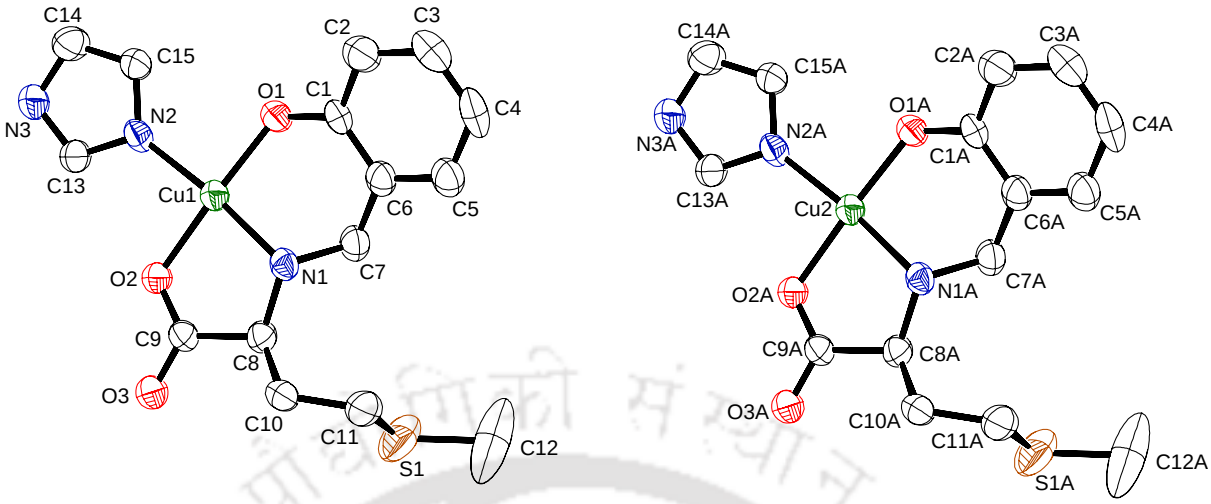

Atoms	x	y	z	U(eq)
Cu(1)	7189(1)	3651(1)	9626(1)	38(1)
Cu(2)	1242(1)	3878(1)	6618(1)	39(1)
O(1A)	1175(5)	3408(2)	8066(3)	44(1)
C(6A)	1736(8)	4228(3)	9565(5)	37(1)
C(1A)	1827(7)	3602(3)	9219(5)	40(1)
C(5A)	2375(8)	4402(3)	10780(5)	48(1)
C(2A)	2652(9)	3189(3)	10113(6)	51(2)
C(4A)	3107(8)	3990(3)	11692(5)	58(2)
C(7A)	901(7)	4690(2)	8624(5)	40(1)
N(1A)	1856(6)	4667(2)	7535(4)	38(1)
C(8A)	1351(8)	5194(2)	6683(5)	42(1)
C(9A)	778(8)	4972(3)	5365(5)	45(1)
O(2A)	902(5)	4405(2)	5173(3)	49(1)
O(3A)	173(7)	5362(2)	4577(4)	69(1)
C(10A)	3016(9)	5663(3)	6767(5)	58(2)
C(11A)	3522(9)	5963(3)	8058(6)	62(2)
N(2A)	914(6)	3136(2)	5611(4)	39(1)
C(15A)	852(8)	2542(3)	5980(6)	53(2)
N(3A)	287(7)	2547(2)	3994(5)	53(1)

C(13A)	539(8)	3109(3)	4417(6)	48(1)
C(14A)	463(10)	2172(3)	4993(6)	55(2)
N(1)	7378(5)	2892(2)	8668(4)	35(1)
N(2)	7481(6)	4379(2)	10655(4)	40(1)
O(1)	6119(5)	4129(2)	8194(3)	43(1)
O(2)	8138(5)	3129(2)	11053(3)	43(1)
O(3)	9216(6)	2199(2)	11577(3)	58(1)
C(1)	6094(6)	3939(3)	7036(4)	34(1)
C(6)	5841(7)	3319(3)	6699(5)	41(1)
C(7)	5647(7)	2858(3)	7650(5)	43(1)
C(13)	8256(8)	4393(3)	11843(5)	46(1)
C(15)	7238(8)	4982(3)	10294(5)	46(1)
N(3)	8514(7)	4974(2)	12237(4)	50(1)
C(14)	7888(9)	5350(3)	11260(6)	53(2)
C(9)	8421(7)	2577(2)	10814(5)	39(1)
C(8)	7695(8)	2357(2)	9489(5)	41(1)
C(10)	8994(8)	1863(2)	9081(5)	48(1)
C(11)	8180(9)	1548(2)	7869(5)	54(1)
S(1)	6033(3)	1125(1)	7965(2)	80(1)
C(5)	5798(8)	3148(3)	5499(5)	49(2)
C(4)	6016(8)	3584(3)	4609(5)	56(2)
C(3)	6289(8)	4177(3)	4932(6)	54(2)
C(2)	6350(8)	4362(3)	6156(6)	51(2)
C(3A)	3234(9)	3368(3)	11344(6)	59(2)
C(12)	5310(16)	874(5)	6424(8)	144(5)
S(1A)	5714(7)	6425(2)	8258(3)	175(2)
C(12A)	5320(20)	6825(5)	7343(16)	192(8)

Atomic coordinates for the complex **[Cu (*rac*-met)·(pyridine)$_2$] (2b)**

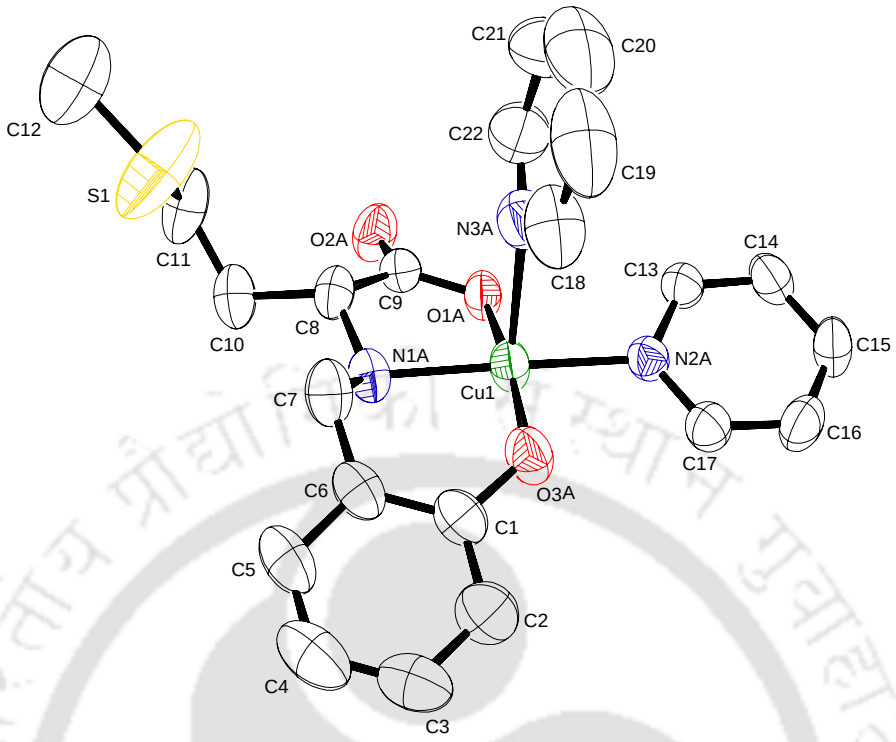

Atoms	x	y	z	U(eq)
Cu(1)	5396(1)	2318(1)	3507(1)	49(1)
S(1A)	4282(4)	-916(2)	1292(1)	147(1)
O(2A)	6644(4)	-1966(3)	4554(3)	65(1)
O(1A)	6561(3)	242(3)	4310(2)	48(1)
O(3A)	4013(3)	4313(3)	2870(2)	61(1)
N(2A)	6981(4)	2875(3)	4055(2)	43(1)
N(3A)	7023(5)	2182(5)	1990(3)	67(1)
C(8)	4783(5)	71(4)	3216(3)	49(1)
C(9)	6095(5)	-648(4)	4102(3)	45(1)
C(6)	1828(5)	3945(5)	2272(3)	57(1)
C(5)	183(6)	4487(6)	2018(4)	75(2)
C(15)	9189(6)	3567(5)	4830(4)	61(1)
C(16)	7613(6)	4513(5)	4603(4)	64(1)

N(1A)	3849(4)	1560(4)	3183(3)	50(1)
C(17)	6550(5)	4135(4)	4206(3)	54(1)
C(18)	6799(8)	3418(7)	1212(4)	89(2)
C(11)	4516(7)	-1888(5)	2670(4)	84(2)
C(14)	9637(5)	2276(5)	4671(3)	55(1)
C(13)	8537(5)	1957(4)	4292(3)	49(1)
C(21)	9345(9)	1068(11)	1163(7)	127(3)
C(2)	1391(6)	6097(5)	2673(4)	71(1)
C(3)	-231(6)	6604(7)	2414(4)	83(2)
C(22)	8273(8)	1031(8)	1957(5)	89(2)
C(7)	2898(6)	2545(5)	2178(4)	65(1)
C(10)	3813(6)	-851(5)	3260(4)	65(1)
C(4)	-826(7)	5798(8)	2079(5)	94(2)
C(1)	2455(5)	4761(5)	2626(3)	54(1)
C(12)	4649(11)	-2246(10)	766(7)	163(4)
C(20)	9080(13)	2373(15)	362(7)	151(5)
C(19)	7811(12)	3529(11)	400(6)	129(3)

Atomic coordinates for the complex **[Cu (*S*-tyr)·(pyridine)$_2$] (3a)**

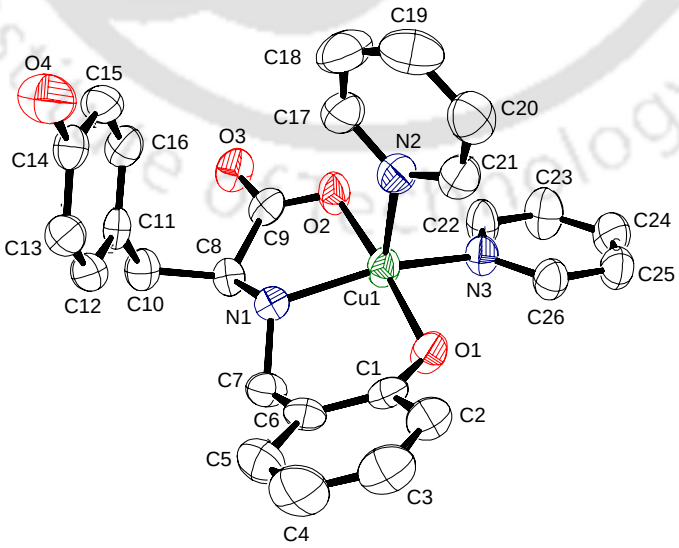

Atoms	x	y	z	U(eq)
Cu(1)	5935(1)	593(1)	1390(1)	42(1)
O(1)	5120(2)	1929(2)	1831(1)	45(1)
C(1)	3818(3)	1780(3)	2028(1)	36(1)
C(6)	3322(3)	527(3)	2215(1)	38(1)
C(5)	1970(3)	446(4)	2429(1)	61(1)
C(3)	1564(3)	2812(4)	2287(1)	60(1)
C(4)	1096(4)	1572(4)	2468(1)	71(1)
C(2)	2895(3)	2908(3)	2062(1)	47(1)
C(7)	4289(3)	-699(3)	2190(1)	45(1)
N(1)	4751(2)	-961(2)	1669(1)	32(1)
C(8)	5560(3)	-2271(2)	1594(1)	35(1)
C(9)	6553(3)	-2116(3)	1141(1)	40(1)
O(3)	7103(2)	-3138(2)	948(1)	51(1)
O(2)	6800(2)	-886(2)	997(1)	50(1)
C(13)	703(3)	-2799(3)	1219(1)	43(1)
C(14)	747(3)	-2843(3)	705(1)	40(1)
C(11)	3241(3)	-3341(2)	1266(1)	37(1)
C(12)	1937(3)	-3051(3)	1489(1)	45(1)
C(15)	2048(3)	-3106(3)	470(1)	49(1)
C(16)	3273(3)	-3348(3)	749(1)	45(1)
O(4)	-428(3)	-2610(3)	407(1)	66(1)
C(10)	4585(3)	-3536(3)	1581(1)	45(1)
N(3)	7734(2)	1750(2)	1305(1)	42(1)
C(26)	7699(3)	3107(3)	1390(1)	47(1)
C(22)	8977(3)	1241(3)	1145(1)	56(1)
N(2)	4525(2)	1270(2)	734(1)	45(1)
C(17)	4040(3)	392(3)	392(1)	55(1)

C(21)	4085(3)	2565(3)	687(1)	50(1)
C(20)	3195(4)	3014(3)	312(1)	62(1)
C(25)	8861(3)	3955(3)	1307(1)	52(1)
C(24)	10128(3)	3410(3)	1144(1)	58(1)
C(23)	10198(3)	2014(3)	1067(1)	64(1)
C(18)	3120(4)	738(4)	13(1)	72(1)
C(19)	2701(4)	2089(4)	-30(1)	72(1)

Atomic coordinates for the complex **[Cu_8(*S*-5omehis)$_8$(Pyridine)$_8$] (1a)**

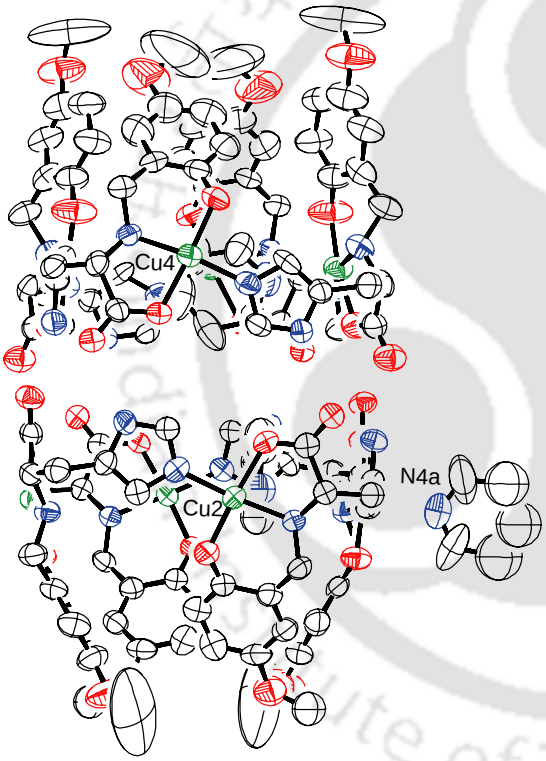

1a

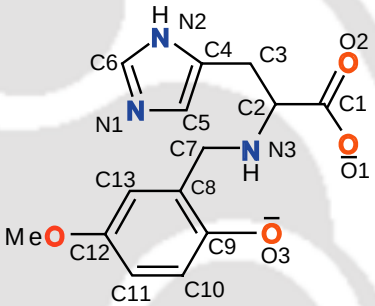

I

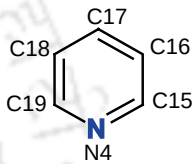

II

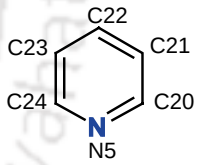

III

Numbering scheme of ligand for complex 1a and II and III are a pyridine outside the cavity and inside the cavity respectively

Atoms	x	y	z	U(eq)
C(14A)	5800(30)	6380(30)	3570(20)	980(130)
C(18A)	3560(20)	9270(20)	5328(13)	330(30)
C(17A)	3400(20)	8810(30)	5437(18)	460(40)
C(16A)	3594(16)	8450(20)	5296(12)	254(19)
Cu(1)	4398(1)	9041(1)	4094(1)	62(1)
Cu(4)	8287(1)	6938(1)	1574(1)	63(1)
Cu(3)	3772(1)	11867(1)	3470(1)	75(1)
Cu(2)	6700(1)	9082(1)	2909(1)	65(1)
O(1D)	8473(3)	6251(2)	1326(2)	66(2)
O(2D)	8751(3)	5922(3)	730(2)	70(2)
O(3D)	8181(3)	7619(3)	1804(2)	81(2)
O(4)	5260(6)	4153(5)	3257(5)	187(6)
C(2D)	8839(3)	6831(4)	819(2)	60(2)
C(9D)	8563(4)	7972(4)	1782(3)	66(2)
C(1D)	8675(3)	6286(3)	970(3)	54(2)
C(12D)	9339(7)	8756(5)	1774(5)	118(5)
C(11D)	9035(6)	8689(5)	2110(5)	109(4)
C(7D)	8783(5)	7744(4)	1059(3)	82(3)
C(10D)	8646(5)	8276(4)	2123(4)	91(3)
C(8D)	8874(4)	8064(4)	1442(3)	73(3)
C(13D)	9276(6)	8457(5)	1442(4)	110(4)
C(3D)	5636(4)	11806(4)	4426(3)	68(2)
C(4D)	5162(3)	11666(3)	4183(3)	58(2)
C(5D)	4810(4)	11941(4)	3953(3)	67(2)
C(6D)	4552(4)	11162(4)	3883(3)	69(3)
C(6C)	2870(4)	11124(4)	2142(3)	64(2)
C(5C)	2704(4)	11871(4)	2376(3)	64(2)
C(4C)	2501(4)	11530(4)	2644(3)	58(2)

N(3D)	8859(3)	7182(3)	1169(2)	63(2)
N(1C)	2934(3)	11614(3)	2054(2)	65(2)
N(1D)	4426(3)	11628(3)	3773(3)	71(2)
N(2D)	4989(3)	11163(3)	4135(2)	68(2)
N(4D)	7525(3)	6999(4)	1146(3)	81(2)
N(4C)	4024(4)	11712(5)	2784(3)	90(3)
O(1C)	3446(3)	11168(3)	3511(2)	73(2)
O(2C)	2658(3)	10767(3)	3511(2)	85(2)
N(3C)	3015(3)	12096(3)	3342(2)	71(2)
C(8C)	3196(5)	13018(5)	3441(3)	85(3)
C(12C)	3209(7)	13907(6)	3279(4)	110(4)
C(9C)	3761(5)	12983(4)	3416(3)	83(3)
C(11C)	3767(8)	13904(5)	3259(4)	113(5)
C(13C)	2932(6)	13504(5)	3354(4)	96(4)
C(10C)	4056(5)	13421(5)	3316(4)	106(4)
C(7C)	2863(4)	12578(4)	3554(4)	87(3)
O(3C)	4026(3)	12558(3)	3503(4)	121(3)
C(1C)	2950(5)	11159(4)	3481(3)	71(3)
O(8)	2951(5)	14370(4)	3189(4)	142(4)
C(18C)	4440(5)	11981(8)	2179(4)	109(5)
C(17C)	4502(6)	11487(10)	2032(5)	138(7)
C(19C)	4213(5)	12072(6)	2553(4)	103(4)
C(15C)	4075(5)	11216(6)	2657(3)	94(4)
C(16C)	4314(6)	11088(7)	2281(5)	126(5)
C(16D)	6842(6)	6592(7)	768(5)	131(5)
C(18D)	6757(5)	7476(7)	929(4)	113(5)
C(15D)	7297(5)	6587(6)	972(5)	108(4)
C(17D)	6544(7)	7066(7)	750(5)	129(5)
N(2C)	2611(3)	11057(3)	2493(2)	61(2)
O(3A)	4271(3)	8336(2)	3948(2)	75(2)

O(1A)	4622(3)	9768(2)	4204(2)	72(2)
O(2A)	5250(3)	10251(2)	4500(2)	68(2)
O(10)	5732(5)	6740(4)	3821(5)	164(5)
O(3B)	6474(3)	8420(3)	3100(2)	88(2)
O(14)	5949(3)	6742(3)	2135(3)	102(2)
N(3A)	5162(3)	8891(3)	4263(2)	59(2)
N(1B)	3719(3)	9273(3)	3821(2)	64(2)
N(2B)	3094(3)	9770(3)	3559(2)	62(2)
N(1A)	6468(3)	9408(3)	3437(2)	68(2)
N(2A)	6284(3)	9958(3)	3919(2)	63(2)
N(3B)	6995(3)	8808(3)	2384(2)	56(2)
O(1B)	6963(3)	9741(2)	2687(2)	63(2)
O(2B)	7570(3)	10058(3)	2251(2)	76(2)
C(10A)	4568(5)	7545(5)	3648(3)	81(3)
C(12A)	5363(5)	7140(4)	3847(4)	86(3)
C(13A)	5486(4)	7551(4)	4103(4)	84(3)
C(8A)	5110(4)	7964(3)	4161(3)	68(2)
C(9A)	4629(4)	7973(4)	3915(3)	63(2)
C(7A)	5244(4)	8383(3)	4451(3)	70(3)
C(11A)	4921(5)	7144(4)	3619(3)	81(3)
C(1A)	5057(4)	9823(3)	4402(2)	55(2)
C(2A)	5353(4)	9339(3)	4526(2)	58(2)
C(5B)	2949(3)	9270(3)	3467(3)	57(2)
C(6B)	3344(4)	8974(4)	3630(3)	61(2)
C(4B)	3555(4)	9752(4)	3760(3)	65(2)
C(3A)	5965(4)	9391(4)	4506(3)	65(2)
C(4A)	6178(3)	9481(3)	4084(3)	58(2)
C(6A)	6461(4)	9893(4)	3538(3)	67(2)
C(5A)	6293(4)	9139(4)	3785(3)	68(2)
C(12B)	6085(5)	7184(4)	2356(3)	77(3)

C(7B)	7141(4)	8247(3)	2386(3)	62(2)
C(11B)	5787(5)	7300(5)	2698(4)	101(4)
C(8B)	6667(4)	7922(3)	2490(3)	65(2)
C(9B)	6344(4)	8036(4)	2852(3)	70(2)
C(1B)	7315(3)	9707(4)	2399(3)	57(2)
C(13B)	6530(4)	7502(4)	2249(3)	66(2)
N(4A)	3998(5)	8923(6)	4770(3)	117(4)
C(10B)	5919(6)	7734(4)	2943(4)	96(4)
C(19A)	3853(9)	9303(11)	4985(7)	192(10)
C(15A)	3896(9)	8485(10)	4911(7)	189(10)
C(19D)	7239(4)	7428(5)	1120(3)	83(3)
C(2B)	7444(4)	9148(3)	2253(3)	59(2)
C(14C)	3199(12)	14835(7)	3204(12)	320(20)
C(2C)	2636(4)	11651(4)	3408(3)	68(2)
C(14B)	6314(6)	6529(5)	1870(4)	113(4)
C(14D)	5300(20)	4461(12)	2954(17)	570(60)
C(21A)	4966(6)	9005(7)	3092(4)	103(4)
C(22A)	5059(6)	9507(6)	3169(4)	103(4)
C(24A)	4210(5)	9671(6)	2833(4)	98(4)
C(23A)	4681(5)	9843(6)	3037(4)	110(4)
N(5E)	4130(4)	9184(5)	2763(4)	110(4)
C(20A)	4478(7)	8840(6)	2904(4)	118(5)
C(3B)	7536(4)	9126(4)	1782(3)	61(2)
C(3C)	2218(4)	11605(4)	3049(3)	67(2)

Atomic coordinates for the complex **[Cu_2(S-5OMehis)$_2$]·3H_2O (1b)**

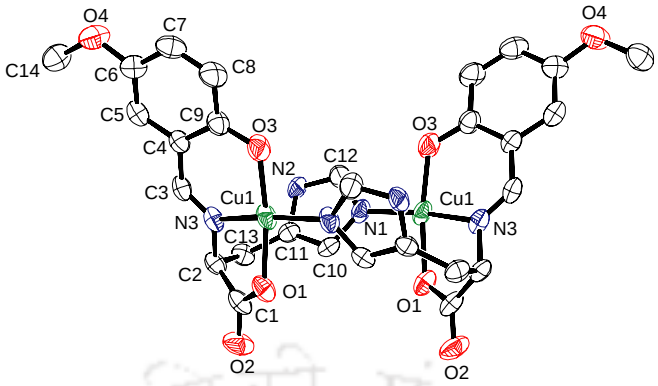

Atoms	x	y	z	U(eq)
Cu(1)	-1011(1)	4257(1)	8887(1)	40(1)
O(1)	-2752(2)	4205(2)	8873(2)	46(1)
O(2)	-4227(3)	3335(2)	9122(2)	66(1)
O(3)	648(3)	4228(2)	8746(2)	53(1)
O(4)	3305(3)	1628(2)	7487(2)	60(1)
N(1)	-1029(3)	5495(2)	9092(2)	41(1)
N(2)	-1150(3)	3021(2)	8862(2)	39(1)
C(4)	771(3)	2726(2)	8369(2)	36(1)
C(11)	-1603(3)	6743(2)	9585(2)	34(1)
C(12)	-188(4)	6063(2)	9009(3)	48(1)
C(3)	-389(4)	2497(2)	8624(2)	41(1)
C(1)	-3173(4)	3470(2)	9036(2)	45(1)
C(9)	1239(3)	3566(2)	8458(2)	42(1)
C(10)	-1927(3)	5921(2)	9444(2)	36(1)
C(5)	1455(4)	2067(2)	8040(2)	42(1)
C(13)	-2182(4)	7459(3)	10003(3)	41(1)
C(8)	2399(4)	3690(3)	8239(3)	51(1)
C(7)	3058(4)	3031(3)	7922(3)	51(1)
C(2)	-2290(3)	2739(2)	9161(2)	39(1)

C(6)	2587(4)	2229(3)	7816(2)	43(1)
C(14)	2820(4)	780(3)	7390(3)	57(1)
N(3)	-485(3)	6818(2)	9306(2)	42(1)
O(5)	13(4)	75(3)	8292(4)	110(2)
O(6)	1968(6)	5000	0	148(4)
O(8)	9141(9)	9357(5)	290(7)	242(5)

Atomic coordinates for the complex **[Cu_8(*R*-his)$_8$(Pyridine)$_{10}$] (3a)**

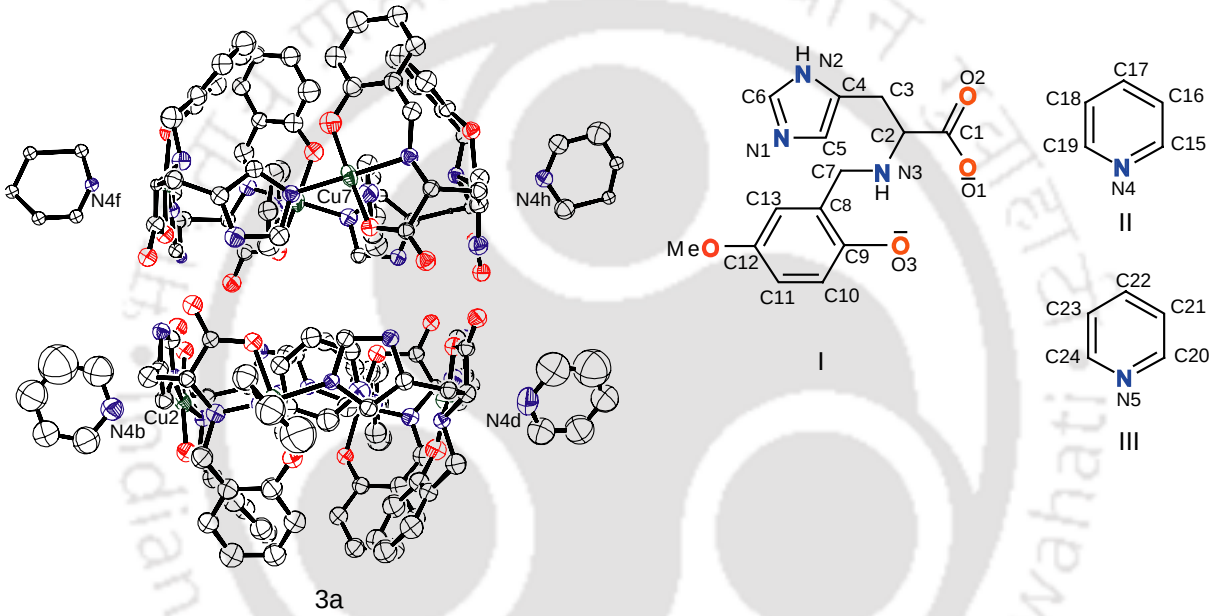

Numbering scheme of ligand for complex 3a and II and III are pyridine outside the cavity and inside the cavity respectively

Atoms	x	y	z	U(eq)
N(4H)	-3084	4096	-1903	50
C(18H)	-3430	3571	-1655	50
C(17H)	-4273	3270	-1955	50
C(15H)	-4366	3815	-3015	50
C(16H)	-4753	3148	-2737	50

C(14H)	-3258	4330	-2513	50
N(50)	8643	7761	1934	50
C(59H)	8811	7402	2555	50
C(58H)	9588	7564	3292	50
C(56H)	10061	8195	3143	50
C(57H)	10014	8500	2569	50
C(70H)	9328	8400	2032	50
N(6W)	8633	8538	10303	60
C(29W)	9122	8829	9887	50
C(31W)	8707	9096	9223	60
C(33W)	7804	9071	8975	60
C(35W)	7315	8780	9390	50
C(30W)	7730	8513	10054	60
C(70C)	7301	6085	6612	237
C(44D)	6366	5781	6267	203
N(4B)	5845	6242	5885	216
C(39C)	6259	7007	5847	308
C(79E)	7194	7311	6192	383
C(32C)	7715	6850	6575	206
N(4D)	-2259	830	644	145
C(14D)	-2553	1140	-16	264
C(15D)	-3445	848	-527	462
C(16D)	-4043	246	-378	280
C(17D)	-3749	-64	282	195
C(18D)	-2857	228	793	208
C(5E)	4586	8723	2798	90
N(1E)	4944	8092	2830	82
C(6E)	4823	7676	3404	91
N(2E)	4390	8050	3726	96
C(4E)	4243	8697	3352	89

C(4H)	-1217	6428	656	83
C(5H)	-472	7030	657	74
N(1H)	274	7099	1342	73
C(6H)	-9	6540	1763	98
N(2H)	-931	6126	1339	105
C(4G)	-263	3130	-1663	54
C(5G)	-618	3765	-1837	86
N(1G)	-935	3909	-1296	80
C(6G)	-776	3364	-787	59
N(2G)	-360	2882	-1014	44
N(2F)	3687	4870	140	96
C(6F)	3949	4447	747	73
N(1F)	4870	4823	1212	79
C(4F)	5177	5479	892	68
C(5F)	4445	5508	230	47
C(4B)	2178	6447	5092	78
C(5B)	1462	5776	5020	77
N(1B)	742	5713	4320	61
C(6B)	1013	6345	3959	77
N(2B)	1900	6799	4437	70
C(4A)	5783	4626	4023	85
C(5A)	5318	4558	4494	96
N(1A)	4874	5139	4378	105
C(6A)	5064	5567	3834	90
N(2A)	5625	5250	3614	77
N(4G)	1606	4903	-303	98
C(18G)	1390	5576	-522	152
C(17G)	937	5896	-199	124
C(16G)	701	5542	344	108
C(15G)	917	4870	563	143

C(14G)	1369	4550	239	128
C(18E)	2686	7287	1009	118
N(4E)	2445	7226	1607	106
C(14E)	2640	6667	2068	105
C(15E)	3077	6169	1931	134
C(16E)	3318	6231	1333	110
C(17E)	3123	6790	872	105
C(124)	1548	4100	3993	133
N(6)	2176	4793	4018	123
C(60)	2023	5184	3401	94
C(59)	1244	4882	2760	108
C(63)	616	4190	2735	91
C(62)	769	3798	3352	90
C(69)	3074	3858	2845	92
C(74)	2481	3785	2109	98
C(65)	1683	3177	1822	112
N(5)	1478	2640	2272	100
C(67)	2071	2713	3008	116
C(68)	2869	3322	3295	110
C(10H)	-86	6150	-2249	135
C(9H)	-745	5924	-1971	90
C(8H)	-983	6480	-1665	103
C(13H)	-563	7261	-1638	119
C(12H)	95	7487	-1916	157
C(11H)	334	6931	-2221	149
C(9G)	2456	5497	-1789	110
C(8G)	1845	4964	-2403	84
C(13G)	1420	5218	-3072	98
C(12G)	1606	6005	-3127	96
C(11G)	2217	6539	-2513	118

C(10G)	2642	6284	-1844	155
C(9F)	4803	8425	824	76
C(8F)	5105	7996	442	81
C(13F)	4728	7895	-327	134
C(12F)	4050	8222	-713	151
C(11F)	3749	8651	-330	129
C(10F)	4126	8753	439	128
C(9E)	1623	8887	630	99
C(8E)	2297	9497	1141	87
C(13E)	2803	10093	905	97
C(12E)	2634	10080	159	108
C(11E)	1961	9471	-351	126
C(10E)	1455	8874	-115	110
C(8B)	3484	4428	6090	86
C(13B)	2957	4039	6444	136
C(12B)	2621	3236	6315	139
C(11B)	2812	2823	5833	127
C(10B)	3339	3211	5478	139
C(9B)	3675	4014	5607	107
C(9C)	-274	3633	4787	115
C(10C)	301	3318	5335	117
C(11C)	23	2538	5405	126
C(12C)	-830	2073	4928	147
C(13C)	-1404	2388	4381	107
C(8C)	-1126	3169	4310	105
C(8D)	156	849	2685	96
C(13D)	833	632	3239	119
C(12D)	1080	892	3976	137
C(11D)	651	1370	4159	132
C(10D)	-26	1587	3605	123

C(9D)	-273	1327	2868	108
C(8A)	4738	1979	4391	108
C(13A)	4913	1983	5137	106
C(12A)	4304	1476	5358	134
C(11A)	3520	965	4832	114
C(10A)	3344	961	4085	100
C(9A)	3953	1468	3865	88
C(2B)	3831	6474	5609	83
C(1B)	3994	6832	4943	73
C(5C)	-1843	2665	1933	87
C(3D)	675	674	660	78
C(2D)	-157	973	725	64
C(4D)	1591	1257	1025	66
C(1A)	5382	3629	2652	78
C(2A)	5768	3454	3354	71
C(3A)	6323	4149	3940	86
C(3E)	3823	9236	3521	75
C(2E)	2768	8893	3068	70
C(1E)	2280	8141	3292	66
C(2H)	-2213	5511	-519	36
C(7H)	-1730	6239	-1397	125
C(2G)	1254	3110	-1599	69
C(3G)	158	2737	-2034	80
C(3F)	6062	6037	1230	9
C(2F)	6153	6693	1738	73
C(7F)	5801	7694	848	81
C(3H)	-2128	6151	-33	88
C(4C)	-2120	3288	1721	77
C(5D)	2174	1332	1687	71
C(7A)	5406	2496	4174	127

C(3B)	3038	6789	5679	73
C(18C)	-1688	5941	4050	86
C(6D)	2744	2164	1140	77
C(14C)	-864	5655	5055	120
C(1D)	-283	1606	268	76
C(6C)	-1500	3132	1017	92
C(1F)	6028	6466	2414	76
C(18F)	7162	9195	2587	107
C(7D)	-55	552	1951	88
C(14F)	7398	8357	3411	115
C(7E)	2454	9544	1893	86
C(3C)	-2667	3619	2079	109
C(18A)	5105	1924	1676	164
C(14A)	5260	1173	2597	156
C(7G)	1671	4134	-2359	124
C(7B)	3827	5295	6194	108
C(1H)	-2114	4835	-204	83
C(17C)	-1991	6376	4386	141
C(7C)	-1775	3484	3790	114
C(2C)	-2069	4251	2708	68
C(15A)	5714	677	2426	226
Cu(5)	1449	7896	1755	93
Cu(6)	5425	7767	2153	84
Cu(8)	-1435	4746	-1220	98
Cu(3)	-377	4885	3899	91
Cu(1)	4096	2281	2644	90
Cu(4)	-807	1789	1436	93
Cu(2)	4232	5357	4939	108
Cu(7)	2548	4476	-714	99
N(3G)	1573	3947	-1647	93

N(3F)	5536	7168	1338	73
N(3E)	2524	8863	2295	75
N(3H)	-1487	5757	-809	92
N(3D)	34	1166	1469	74
N(1C)	-1388	2603	1465	94
N(3B)	3572	5639	5495	67
N(3A)	5050	2940	3557	95
N(1D)	2962	1935	1749	76
N(4F)	6935	8538	2798	84
N(2C)	-1971	3570	1149	80
N(2D)	1940	1787	624	85
N(4A)	5038	1723	2282	119
N(3C)	-1409	3985	3317	86
N(4C)	-1192	5526	4356	87
O(1B)	4125	6335	4519	90
O(3B)	4186	4401	5278	118
O(3C)	4	4393	4769	95
O(1D)	-547	2119	572	91
O(3A)	3785	1443	3135	83
O(1A)	4475	3217	2184	93
O(1H)	-1642	4400	-325	82
O(3H)	-1199	5224	-2004	103
O(1E)	1728	7650	2721	74
O(3E)	1117	8288	873	120
O(1F)	5624	6845	2666	79
O(3F)	5142	8560	1529	85
O(1G)	2211	3486	-371	94
O(3G)	2894	5364	-1134	112
O(2G)	1384	2254	-735	106
O(2C)	-1954	5151	1887	93

O(2A)	5757	4170	2377	82
O(2E)	2546	8114	3952	92
O(2B)	4035	7484	4830	89
O(2D)	-261	1663	-327	107
O(2F)	6322	5971	2732	94
O(1C)	-753	5301	2953	82
O(3D)	-893	1466	2302	107
O(2H)	-2421	4598	298	89
C(1C)	-1602	4937	2489	67
C(17F)	8007	9768	2922	159
C(1G)	1604	2928	-902	80
C(17A)	5666	1555	1409	222
C(16A)	5818	962	1802	187
C(15C)	-993	6209	5519	287
C(16C)	-1689	6476	5143	189
O(9W)	5582	8733	6837	50
C(16F)	8439	9549	3479	50
C(15F)	8397	8933	3740	50
O(203)	3825	2642	9400	50
O(207)	6000	6323	8006	50

Atomic coordinates for the complex **Cu(*S*-his)(3-Hydpyridine)]·3H$_2$O (1a)**

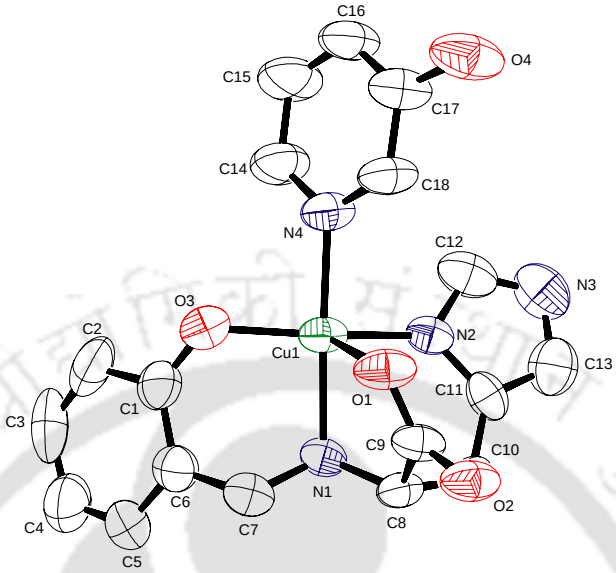

Atoms	x	y	z	U(eq)
Cu(1)	3758(1)	1956(1)	7948(1)	54(1)
O(3)	2058(4)	1500(6)	8089(4)	76(2)
C(6)	1995(5)	2160(10)	10098(6)	60(2)
C(1)	1641(6)	1272(9)	9124(8)	69(2)
C(3)	386(8)	-37(13)	10388(11)	104(3)
C(4)	777(8)	805(13)	11321(9)	99(3)
C(5)	1552(6)	1882(13)	11177(6)	77(2)
C(7)	2866(6)	3409(7)	9936(6)	57(2)
N(1)	4019(5)	2853(6)	9547(5)	47(2)
C(9)	4665(6)	4917(8)	8393(5)	50(2)
N(2)	5557(5)	1612(5)	8004(4)	51(2)
C(12)	6157(9)	789(9)	7283(7)	74(2)
C(11)	6479(6)	2397(7)	8651(6)	55(2)

N(3)	7372(8)	1011(9)	7432(7)	90(2)
C(13)	7567(7)	2005(14)	8291(7)	83(2)
O(2)	5114(5)	6160(5)	8409(3)	60(1)
C(2)	791(7)	135(11)	9313(10)	92(3)
O(1)	4048(4)	4353(5)	7531(4)	62(1)
O(6)	8961(10)	9690(20)	5966(10)	252(7)
O(7)	215(9)	2190(30)	6419(10)	351(12)
O(5)	7775(18)	820(20)	3835(17)	411(14)
C(8)	4940(6)	4037(7)	9522(5)	48(2)
C(10)	6225(6)	3419(8)	9593(6)	60(2)
N(4)	3497(6)	1322(7)	6255(5)	62(2)
C(18)	4019(6)	2065(11)	5437(5)	66(2)
C(16)	3382(8)	372(9)	3951(7)	77(2)
C(14)	2916(8)	86(10)	5943(7)	87(3)
C(15)	2856(9)	-381(11)	4782(8)	101(3)
O(4)	4534(6)	2483(5)	3540(4)	90(2)
C(17)	3963(7)	1648(8)	4277(6)	68(2)

Atomic coordinates for the complex **[Cu(*S*-5Omehis)(3-Hydpyridine)]·3H_2O (2a)**

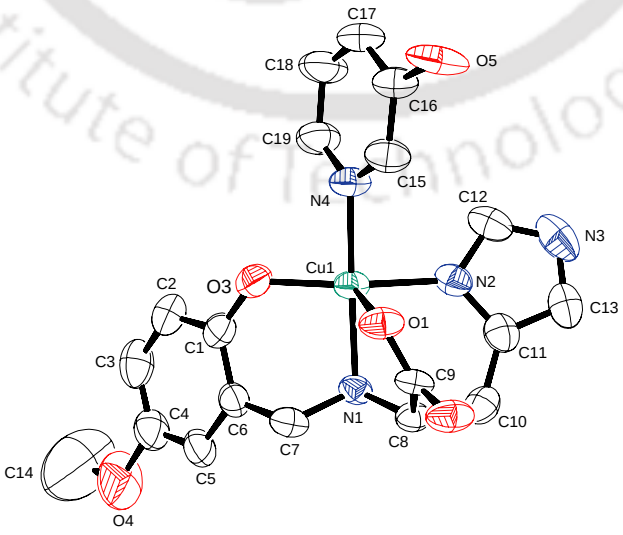

Atoms	x	y	z	U(eq)
Cu(1)	1254(1)	10143(1)	2014(1)	42(1)
N(2)	-611(4)	9851(5)	1969(4)	47(1)
C(11)	-1530(6)	10630(7)	1298(5)	51(2)
C(10)	-1267(6)	11610(7)	348(5)	52(2)
C(12)	-2644(6)	10298(10)	1680(6)	67(2)
C(13)	-1207(7)	9070(8)	2716(6)	61(2)
N(3)	-2430(6)	9334(8)	2559(6)	78(2)
O(3)	2945(4)	9643(4)	1848(3)	56(1)
N(1)	962(4)	11105(5)	396(4)	38(1)
C(15)	1082(5)	10227(9)	4541(4)	54(1)
C(8)	38(5)	12235(6)	454(5)	39(1)
C(9)	302(5)	13098(6)	1613(4)	40(1)
O(1)	983(4)	12537(4)	2465(3)	49(1)
O(2)	-187(4)	14317(5)	1615(3)	55(1)
C(16)	1129(6)	9767(6)	5702(5)	53(2)
N(4)	1533(5)	9447(6)	3698(4)	51(1)
C(17)	1676(7)	8452(8)	5998(6)	69(2)
C(18)	2142(8)	7677(10)	5132(7)	88(3)
C(19)	2067(7)	8196(8)	3991(6)	64(2)
O(5)	633(5)	10652(5)	6471(4)	76(2)
C(7)	2126(6)	11691(6)	60(5)	49(2)
C(6)	3027(5)	10490(6)	-131(5)	46(2)
C(5)	3488(5)	10356(10)	-1214(5)	59(2)
C(1)	3398(5)	9533(7)	795(5)	51(2)
O(4)	4773(6)	9278(9)	-2521(5)	120(2)
O(7)	7807(9)	8729(12)	5364(8)	177(4)
O(8)	4992(7)	4412(11)	6451(6)	151(3)

O(6)	5640(15)	6640(20)	4333(9)	329(11)
C(2)	4273(6)	8485(8)	593(6)	64(2)
C(4)	4328(7)	9320(10)	-1402(6)	67(2)
C(3)	4723(7)	8365(9)	-503(7)	74(2)
C(14)	5500(18)	8150(30)	-2811(14)	322(17)

Atomic coordinates for the complex **[Cu(*S*-5Omehis)(2-Mepyridine)]·3H$_2$O (2b)**

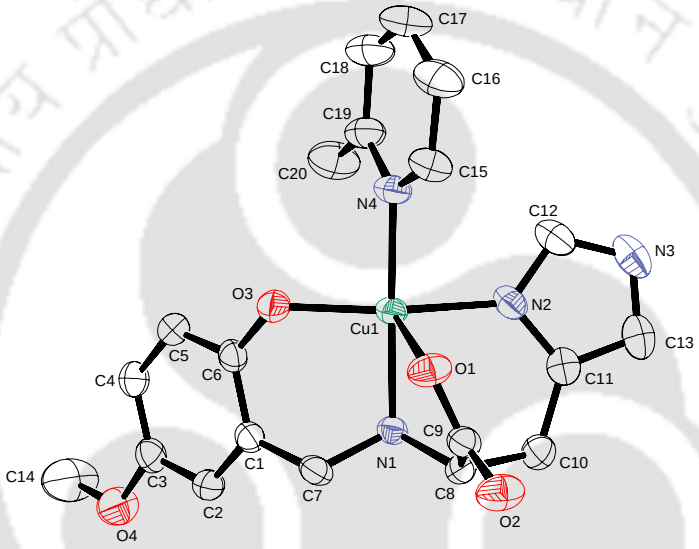

Atoms	x	y	z	U(eq)
Cu(1)	8824(1)	8338(1)	7957(1)	27(1)
C(1)	7022(2)	8838(2)	10108(2)	29(1)
C(6)	6597(2)	7917(2)	9152(2)	30(1)
C(4)	5242(2)	6738(3)	10449(2)	39(1)
C(3)	5669(2)	7664(3)	11366(2)	38(1)
C(2)	6567(2)	8699(2)	11198(2)	33(1)
C(5)	5706(2)	6872(3)	9346(2)	36(1)
C(15)	8803(2)	8271(4)	5408(2)	42(1)
C(19)	8148(3)	6061(3)	6082(2)	40(1)

C(17)	8253(4)	6425(4)	4001(3)	64(1)
C(16)	8675(3)	7806(3)	4237(2)	53(1)
C(18)	7997(3)	5551(4)	4923(3)	59(1)
C(7)	7975(2)	9978(2)	9919(2)	31(1)
N(1)	9146(2)	9321(2)	9584(2)	26(1)
O(3)	7033(2)	8068(2)	8094(1)	36(1)
C(13)	12788(3)	8557(3)	8204(2)	45(1)
O(4)	5291(2)	7622(2)	12495(2)	56(1)
C(8)	10086(2)	10474(2)	9489(2)	27(1)
C(9)	9743(2)	11351(2)	8332(2)	29(1)
C(11)	11666(2)	8843(3)	8608(2)	34(1)
C(12)	11314(3)	7328(3)	7148(2)	43(1)
C(10)	11416(2)	9839(3)	9595(2)	37(1)
N(2)	10724(2)	8051(2)	7934(2)	35(1)
N(3)	12548(2)	7610(3)	7288(2)	48(1)
O(1)	9079(2)	10710(2)	7481(1)	36(1)
O(2)	10130(2)	12615(2)	8321(2)	42(1)
C(20)	7938(4)	5112(3)	7100(3)	58(1)
C(14)	4506(5)	6513(5)	12778(4)	90(1)
N(4)	8528(2)	7434(2)	6314(2)	34(1)
O(6)	7770(3)	1652(3)	5283(2)	65(1)
O(5)	5100(2)	7579(3)	6307(2)	53(1)
O(7)	5564(3)	9689(4)	4425(3)	74(1)

Atomic coordinates for the complex **[Cu(*S*-3Omehis)(3-Hydpyridine)]·4H2O (3a)**

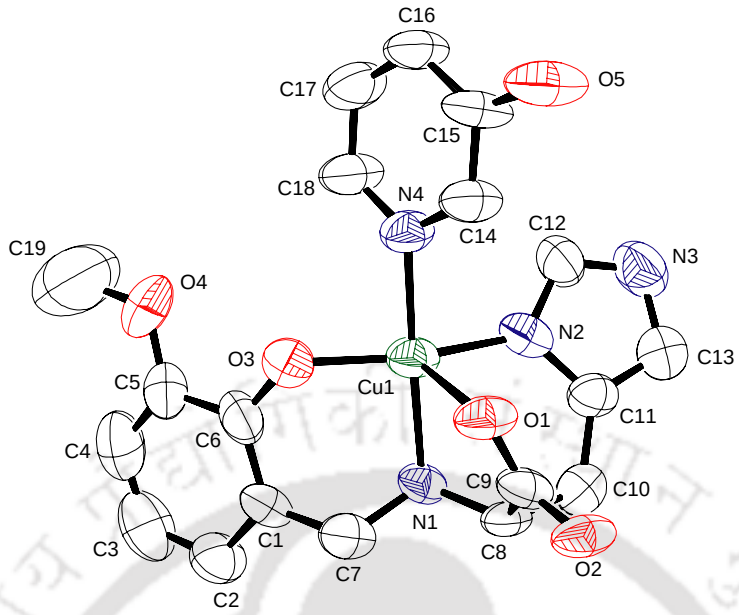

Atoms	x	y	z	U(eq)
Cu(1)	1737(1)	6402(1)	8903(1)	57(1)
N(4)	3353(6)	5747(8)	8679(6)	58(2)
N(2)	2143(6)	6060(7)	10499(6)	53(2)
O(3)	1205(5)	5995(6)	7407(5)	72(2)
C(9)	1509(7)	9359(11)	9670(8)	57(2)
C(8)	441(7)	8470(9)	9922(8)	50(2)
O(1)	2236(5)	8790(6)	9140(5)	62(2)
O(2)	1603(5)	10617(7)	10067(6)	64(2)
C(11)	1729(7)	6873(9)	11312(9)	60(3)
C(2)	-2052(7)	6278(15)	6912(8)	74(3)
C(3)	-2320(11)	5169(16)	6206(10)	98(4)
C(1)	-861(7)	6593(12)	7311(7)	60(2)
N(3)	3161(8)	5497(10)	12101(8)	85(3)
C(13)	2370(9)	6527(16)	12286(8)	79(3)
C(12)	2985(9)	5261(11)	11032(9)	71(3)
C(14)	4312(7)	6499(13)	9128(7)	69(2)

C(15)	5469(7)	6060(9)	9087(9)	63(3)
C(16)	5621(9)	4777(12)	8601(9)	76(3)
C(17)	4639(9)	4014(12)	8141(10)	90(4)
C(18)	3528(8)	4500(12)	8198(9)	76(3)
O(5)	6358(6)	6929(6)	9561(8)	95(3)
N(1)	165(5)	7296(7)	9122(5)	52(2)
C(7)	-488(8)	7815(10)	8080(8)	66(3)
C(10)	709(8)	7895(9)	11077(8)	59(3)
C(5)	-290(10)	4574(13)	6277(8)	76(3)
C(4)	-1483(12)	4301(14)	5886(9)	91(4)
C(6)	58(9)	5725(11)	7022(7)	67(3)
O(4)	664(8)	3808(10)	6040(7)	124(3)
C(19)	380(20)	2690(30)	5320(20)	247(13)
O(7)	5082(12)	4320(20)	3518(11)	222(7)
O(6)	3050(30)	410(30)	7470(20)	361(16)
O(8)	5457(19)	1930(40)	4730(20)	375(16)
O(9)	7290(15)	1400(40)	4070(17)	371(17)

Atomic coordinates for the complex **[K{Cu(HS-Val)$_2$}$_3$]ClO$_4$] (1a)**

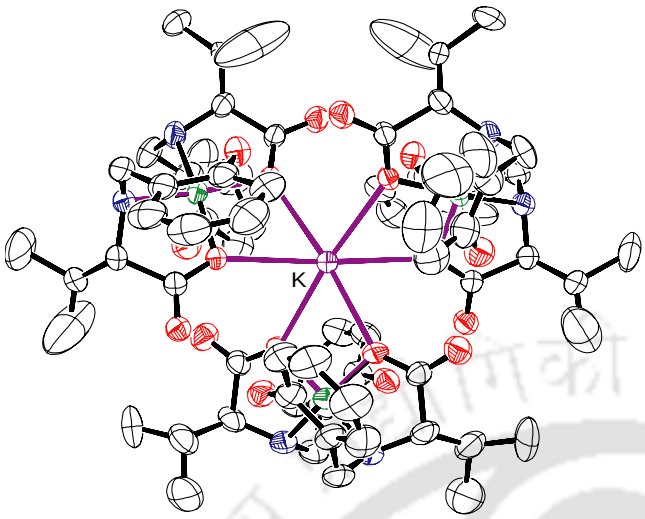

A

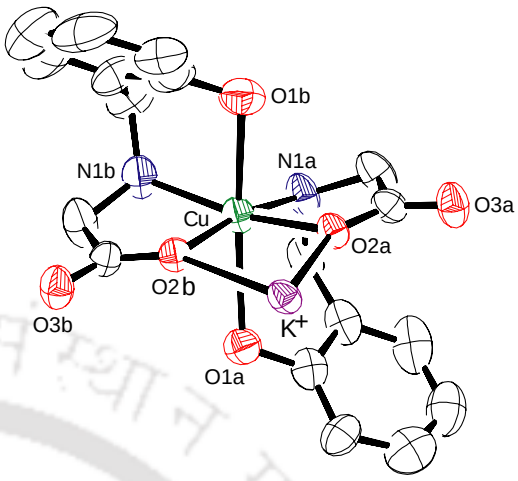

B

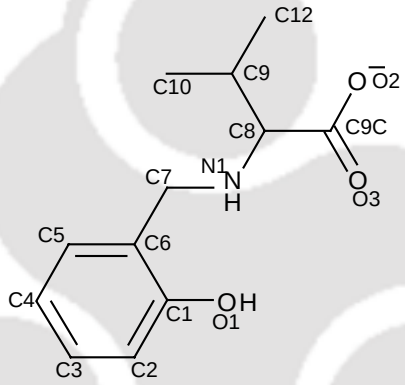

C

(A) molecular structure of 1a, B one of the Cu(II) unit of 1a and C the numbering scheme of ligand

Atoms	x	y	z	U(eq)
Cu(1)	9136(1)	10000	10000	67(1)
Cu(2)	6309(1)	9208(1)	8951(1)	66(1)
K(1)	7249(1)	10000	10000	63(1)
Cl(4)	5000	8068(1)	7500	81(1)
C(2B)	6234(4)	7870(3)	10317(3)	91(2)
C(6B)	6229(3)	7576(3)	9392(3)	86(2)
C(3B)	6592(5)	7280(6)	10406(4)	129(3)
C(4B)	6759(4)	6821(4)	10040(5)	126(3)
C(5B)	6585(3)	6987(4)	9535(5)	120(3)

C(7B)	6008(3)	7740(3)	8873(3)	86(2)
C(9B)	7535(3)	8514(3)	9061(2)	68(1)
C(8B)	7187(3)	8119(4)	8623(2)	90(2)
C(10B)	7513(4)	8330(7)	8058(3)	162(5)
C(11B)	7091(8)	7930(19)	7652(7)	440(30)
C(12B)	8168(11)	8296(17)	8003(5)	400(20)
O(2B)	7196(1)	8992(2)	9268(1)	60(1)
O(3B)	8124(2)	8346(2)	9180(2)	85(1)
N(1B)	6435(2)	8279(3)	8621(2)	82(1)
O(3A)	5258(2)	10733(2)	9553(1)	83(1)
O(2A)	6094(1)	9994(2)	9371(1)	61(1)
C(2A)	7087(5)	11242(5)	8445(3)	118(2)
C(9A)	5505(3)	10268(2)	9303(2)	63(1)
C(8A)	5070(3)	10001(4)	8849(2)	100(2)
C(1B)	6071(3)	8009(3)	9801(3)	82(2)
O(1B)	5755(2)	8602(2)	9670(1)	79(1)
N(1A)	5500(2)	9573(3)	8518(2)	90(2)
O(10)	4857(10)	8243(9)	7057(5)	354(10)
O(1A)	7062(2)	10001(3)	8446(2)	101(1)
C(1A)	6762(4)	10643(4)	8354(2)	101(2)
O(2)	8465(1)	9913(2)	10551(1)	65(1)
C(9C)	8716(3)	9908(3)	11000(2)	75(1)
C(8)	9514(2)	9974(3)	11038(2)	86(2)
C(9)	9740(4)	10697(5)	11232(3)	117(3)
N(1)	9819(2)	9759(2)	10559(2)	81(1)
C(7)	10033(3)	9032(3)	10547(3)	88(2)
C(2)	8397(3)	7956(3)	10431(3)	93(2)
C(1)	8930(3)	8424(3)	10318(2)	80(2)
C(3)	8401(4)	7616(4)	10864(3)	115(2)
C(6)	9452(3)	8536(3)	10674(2)	79(2)

C(5)	9429(4)	8187(4)	11139(3)	112(2)
C(4)	8889(5)	7701(4)	11223(4)	121(3)
O(3)	8370(2)	9894(3)	11392(1)	98(1)
C(10)	10469(5)	10892(5)	11113(6)	171(4)
C(11)	9609(7)	10757(9)	11777(5)	224(7)
C(7A)	5740(4)	9916(5)	8056(2)	106(2)
C(6A)	6089(4)	10617(5)	8158(2)	113(2)
C(4A)	6064(9)	11765(12)	8109(6)	193(6)
C(5A)	5802(8)	11184(9)	8039(4)	159(4)
O(1)	8974(2)	8768(2)	9865(2)	83(1)
C(10A)	4393(4)	9532(10)	9049(4)	259(12)
O(21)	4459(13)	7868(14)	7515(7)	530(30)
C(11A)	3938(4)	9544(11)	8546(7)	330(14)
C(3A)	6707(9)	11847(5)	8306(4)	160(4)
N(100)	1043(8)	9053(8)	1710(4)	228(6)
C(61Z)	1194(13)	9050(8)	2089(7)	279(12)
C(64)	996(15)	8943(8)	2689(5)	284(12)
N(101)	1258(5)	10000	0	200(7)
C(65)	1817(8)	9952(8)	319(6)	189(5)
C(67)	2302(9)	9902(11)	700(17)	450(20)
C(12A)	4258(11)	9592(13)	9355(11)	357(18)

Atomic coordinates for the complex **[Ni(*S*-Htyr)$_2$(Phen)]·(DMF)$_2$] (1a)**

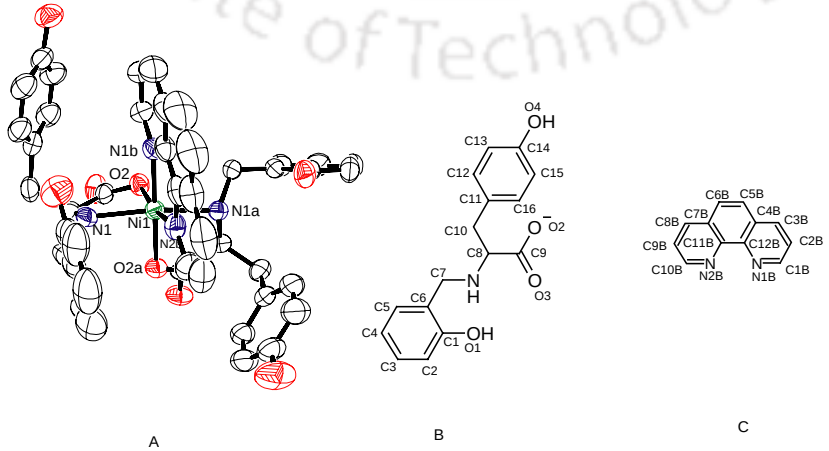

A B C

A molecular structure of 1a , B numbering scheme of ligand and C numbering scheme of phenanthroline

Atoms	x	y	z	U(eq)
Ni(1)	4268(1)	-39(1)	1131(1)	39(1)
N(1B)	4695(2)	-72(2)	233(1)	50(1)
N(2B)	5765(3)	640(1)	1072(1)	51(1)
C(12B)	5656(3)	337(2)	71(2)	53(1)
C(7B)	7238(4)	1155(2)	378(2)	72(1)
C(4B)	6081(4)	402(2)	-517(2)	76(1)
C(3B)	5458(5)	13(3)	-927(2)	91(2)
C(6B)	7637(5)	1204(3)	-216(3)	99(2)
C(1B)	4135(4)	-423(2)	-180(2)	62(1)
C(2B)	4484(5)	-391(3)	-766(2)	83(1)
C(5B)	7102(6)	848(3)	-636(3)	105(2)
C(11B)	6233(3)	718(2)	521(2)	54(1)
C(9B)	7317(5)	1430(2)	1393(3)	87(2)
C(8B)	7754(5)	1509(2)	835(3)	92(2)
C(10B)	6308(4)	980(2)	1492(2)	67(1)
O(2A)	3908(2)	33(1)	1996(1)	51(1)
O(3A)	3626(3)	-620(1)	2751(1)	62(1)
C(6A)	6625(3)	-1850(2)	1248(1)	45(1)
C(2A)	8809(4)	-2228(2)	1430(2)	65(1)
C(5A)	6174(4)	-2444(2)	1443(2)	58(1)
C(3A)	8332(5)	-2809(2)	1620(2)	78(1)
C(4A)	7000(5)	-2924(2)	1633(2)	71(1)
C(1A)	7967(3)	-1747(2)	1242(2)	49(1)
C(9A)	4140(3)	-469(2)	2276(1)	46(1)
C(8A)	5176(3)	-943(2)	2042(1)	46(1)
C(10A)	6308(4)	-999(2)	2482(2)	57(1)
C(11A)	7026(3)	-382(2)	2588(2)	56(1)
C(13A)	8809(4)	357(3)	2417(2)	87(1)

C(15A)	7115(4)	687(2)	3044(2)	70(1)
C(16A)	6522(3)	91(2)	2955(2)	62(1)
C(12A)	8203(4)	-232(2)	2324(2)	77(1)
C(14A)	8275(4)	818(2)	2771(2)	72(1)
N(1A)	5593(2)	-757(1)	1446(1)	39(1)
C(7A)	5724(3)	-1321(1)	1050(1)	45(1)
O(1A)	8375(2)	-1155(1)	1055(1)	62(1)
O(2)	2937(2)	-765(1)	1052(1)	48(1)
O(3)	886(2)	-1010(1)	1224(1)	67(1)
C(9)	1766(3)	-608(2)	1128(2)	47(1)
C(8)	1411(3)	109(2)	1115(2)	50(1)
N(1)	2551(3)	527(1)	1001(1)	47(1)
O(4A)	8910(4)	1398(2)	2830(2)	111(1)
C(10)	247(3)	238(2)	701(2)	62(1)
C(14)	1254(4)	-254(2)	-1063(2)	59(1)
C(13)	1294(4)	381(2)	-881(2)	66(1)
C(16)	467(4)	-562(2)	-130(2)	67(1)
C(11)	546(3)	67(2)	78(2)	58(1)
C(15)	819(5)	-719(2)	-686(2)	68(1)
O(1)	3268(4)	1532(2)	191(2)	87(1)
C(6)	3385(4)	1666(2)	1208(2)	71(1)
C(1)	3785(4)	1854(2)	655(2)	72(1)
C(7)	2365(4)	1161(2)	1309(2)	68(1)
C(12)	950(4)	535(2)	-313(2)	65(1)
C(5)	3884(5)	2008(2)	1680(3)	97(2)
C(4)	4754(7)	2508(3)	1614(4)	124(3)
C(3)	5158(6)	2666(3)	1067(5)	122(2)
C(2)	4695(5)	2345(2)	577(3)	99(2)
O(4)	1641(3)	-441(1)	-1612(1)	75(1)
N(3B)	2373(5)	7376(2)	584(2)	92(1)

C(14B)	2277(11)	7817(3)	103(3)	172(4)
C(13B)	2319(13)	6705(3)	463(3)	219(7)
C(15B)	2432(4)	7576(2)	1127(2)	73(1)
O(5B)	2517(4)	7234(2)	1551(2)	111(1)
N(4B)	507(4)	8144(2)	3213(2)	95(1)
C(17B)	-583(7)	7711(3)	3192(3)	145(3)
C(16B)	973(9)	8407(4)	2655(3)	182(4)
C(18B)	1052(6)	8286(3)	3704(4)	113(2)
O(6B)	775(5)	8055(2)	4185(2)	124(2)

Atomic coordinates for the complex [**Ni(*S*-Htyr)$_2$(Phen)]·(DMF)·(H$_2$O)$_4$] (1b)**

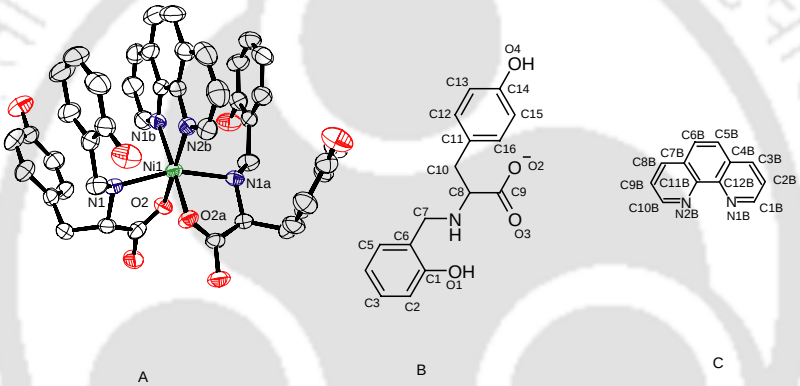

A molecular structure of 1b , B numbering scheme of ligand and C numbering scheme of phenanthroline

Atoms	x	y	z	U(eq
Ni(1)	1981(1)	-676(1)	9019(1)	33(1)
C(12)	1230(4)	1640(3)	11730(3)	42(1)
C(13)	659(4)	3048(3)	11136(3)	50(1)
C(17)	283(4)	1028(3)	12271(3)	49(1)
C(14)	-803(4)	3821(3)	11049(3)	56(1)
C(15)	-1721(4)	3204(3)	11571(3)	48(1)
C(16)	-1160(4)	1792(4)	12203(3)	54(1)
C(1)	2670(4)	3019(3)	6819(3)	45(1)
C(5)	813(4)	3655(3)	8041(3)	55(1)
C(2)	1787(4)	4092(4)	5878(3)	56(1)

C(3)	438(5)	4935(4)	6017(4)	64(1)
C(4)	-61(4)	4730(4)	7092(4)	68(1)
C(6)	2185(4)	2778(3)	7934(3)	40(1)
C(11)	2849(3)	813(3)	11723(3)	45(1)
O(1)	4031(3)	2187(3)	6711(3)	61(1)
O(4)	-3184(3)	3925(2)	11507(2)	69(1)
O(2)	2028(2)	-1664(2)	10768(2)	40(1)
O(3)	3228(3)	-2126(2)	12483(2)	54(1)
C(10)	2751(4)	-1380(3)	11417(3)	41(1)
C(9)	3145(3)	-70(3)	10910(3)	36(1)
C(1B)	2589(4)	186(3)	6425(3)	45(1)
C(12B)	253(4)	1191(3)	6835(3)	39(1)
C(4B)	-228(4)	1961(3)	5642(3)	48(1)
C(3B)	818(5)	1772(4)	4846(3)	62(1)
C(2B)	2218(5)	864(4)	5223(3)	60(1)
C(6B)	-2685(5)	2945(4)	6163(4)	67(1)
C(5B)	-1751(5)	2843(4)	5346(4)	66(1)
C(8B)	-3153(4)	2133(4)	8267(4)	63(1)
C(7B)	-2223(4)	2141(3)	7372(4)	48(1)
C(10B)	-1161(4)	455(4)	9626(3)	50(1)
C(9B)	-2645(4)	1314(4)	9376(4)	62(1)
C(11B)	-762(4)	1252(3)	7697(3)	40(1)
N(1B)	-248(3)	415(3)	8825(3)	38(1)
N(2B)	1661(3)	339(3)	7215(2)	34(1)
C(1A)	-1635(4)	-1992(3)	8494(3)	44(1)
C(5A)	-151(4)	-1701(3)	6927(3)	48(1)
C(4A)	-1369(4)	-912(4)	6141(3)	55(1)
C(3A)	-2694(4)	-639(4)	6534(3)	53(1)
C(2A)	-2849(4)	-1154(3)	7695(3)	54(1)
C(6A)	-258(3)	-2244(3)	8123(3)	36(1)

O(1A)	-1757(2)	-2578(3)	9657(2)	59(1)
C(14A)	4848(4)	-2838(3)	5207(3)	43(1)
C(11A)	4617(3)	-4154(3)	7562(3)	37(1)
C(12A)	3648(4)	-3984(3)	6665(3)	44(1)
C(13A)	3745(4)	-3339(3)	5517(3)	49(1)
C(15A)	5843(4)	-3023(3)	6072(3)	50(1)
C(16A)	5721(3)	-3672(3)	7236(3)	45(1)
C(8A)	3686(3)	-3630(3)	9408(3)	33(1)
C(10A)	4413(3)	-4754(3)	8836(3)	42(1)
C(9A)	4669(3)	-2863(3)	9499(3)	35(1)
O(2A)	4190(2)	-1563(2)	9079(2)	40(1)
O(3A)	5944(2)	-3578(2)	10006(2)	49(1)
O(4A)	5000(3)	-2148(3)	4075(2)	64(1)
N(1A)	2263(3)	-2597(3)	8767(2)	33(1)
C(7A)	1074(4)	-3134(4)	9016(3)	45(1)
O(8B)	4586(3)	2568(3)	4417(3)	101(1)
O(6B)	4837(6)	4996(4)	3069(4)	187(2)
N(4V)	9477(7)	6692(5)	2784(4)	112(2)
C(13B)	10774(8)	5609(7)	2522(5)	136(2)
C(14B)	8105(7)	6579(9)	2800(6)	190(4)
C(15B)	9752(8)	7663(6)	3013(5)	117(2)
O(5B)	8832(6)	8620(5)	3282(5)	181(2)
O(7B)	4857(7)	2579(8)	1558(7)	313(4)
N(1)	2397(3)	735(3)	9698(2)	35(1)
C(7)	3154(4)	1623(3)	8988(3)	42(1)
O(1K)	5951(4)	175(3)	3537(3)	114(1)

Atomic coordinates for the complex **[Ni(HS-trypt)$_2$(Phen)]·CH$_3$OH (2a)**

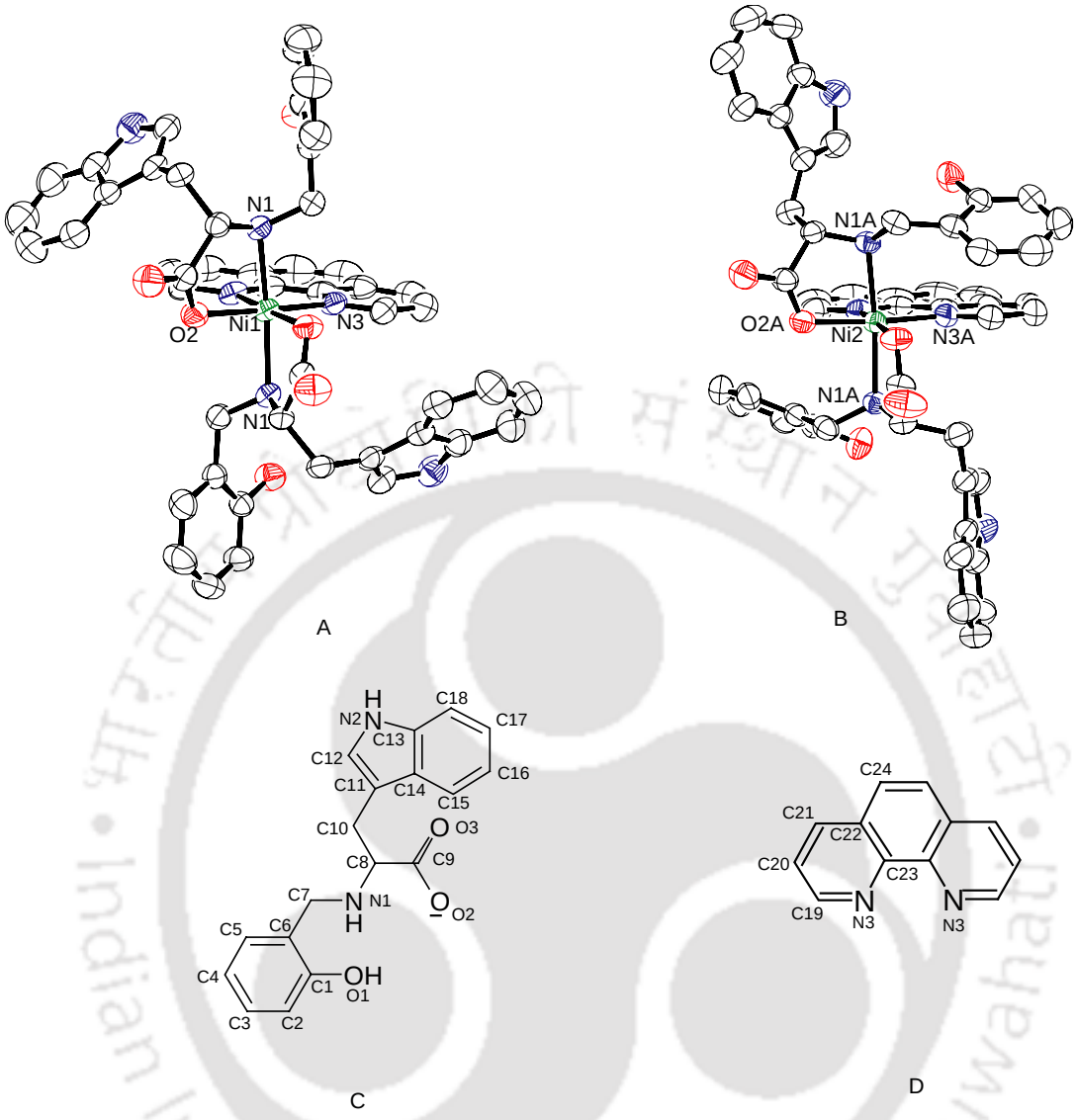

A and B molecular structures of two isomer in the unit cell .
C and D numbering scheme of the ligand and phenanthroline

Atoms	x	y	z	U(eq)
Ni(1)	5000	5000	928(1)	39(1)
Ni(2)	5000	0	4598(1)	38(1)
C(4)	7817(2)	1440(1)	4964(2)	44(1)
C(3)	8624(2)	1733(1)	4728(2)	54(1)
C(1)	7235(2)	1679(1)	3327(2)	56(1)
C(2)	8726(2)	1988(1)	3783(2)	67(1)
C(5)	7114(2)	1401(1)	4258(2)	42(1)

C(6)	8027(2)	1965(1)	3089(2)	70(1)
O(2)	5083(1)	4390(1)	2063(1)	51(1)
O(3)	4270(1)	3862(1)	3138(1)	73(1)
C(14)	2307(2)	6370(1)	-413(3)	62(1)
C(7)	4346(2)	4162(1)	2350(2)	48(1)
C(10)	2878(2)	5811(1)	1013(2)	47(1)
C(15)	2484(2)	5835(1)	43(2)	49(1)
C(8)	3506(2)	4232(1)	1675(2)	44(1)
C(12)	2930(2)	6867(1)	1034(3)	74(1)
C(9)	2968(2)	5236(1)	1574(2)	49(1)
C(11)	3104(2)	6335(1)	1494(2)	58(1)
C(13)	2531(2)	6881(1)	79(3)	72(1)
N(1)	3560(1)	4786(1)	1081(2)	41(1)
C(17)	983(2)	3356(1)	314(2)	57(1)
C(18)	1693(2)	3378(1)	1034(2)	50(1)
C(16)	3399(2)	3691(1)	989(2)	57(1)
C(20)	677(2)	2951(1)	2246(3)	78(1)
C(22)	132(2)	3124(1)	548(3)	71(1)
C(19)	1524(2)	3179(1)	2017(2)	63(1)
C(21)	0(3)	2923(1)	1515(3)	81(1)
N(3B)	5485(1)	-493(1)	5802(2)	45(1)
C(26)	5531(2)	-517(2)	7650(2)	62(1)
C(27)	5264(2)	-265(1)	6719(2)	49(1)
C(25)	6071(2)	-1019(2)	7591(3)	74(1)
C(23)	5999(2)	-972(1)	5774(2)	57(1)
C(24)	6312(2)	-1244(2)	6669(3)	73(1)
C(31)	8062(2)	-930(1)	4374(2)	47(1)
N(2B)	8861(2)	-589(1)	5717(2)	62(1)
C(29)	8555(2)	-119(1)	5173(2)	54(1)
C(28)	8058(2)	-295(1)	4345(2)	46(1)

N(1B)	6300(1)	421(1)	4415(2)	39(1)
C(33)	6690(2)	212(1)	3441(2)	40(1)
C(32)	6250(2)	1072(1)	4503(2)	46(1)
C(34)	7728(1)	95(1)	3498(2)	45(1)
O(1B)	7695(1)	1179(1)	5887(1)	57(1)
O(2B)	4463(1)	536(1)	3526(1)	48(1)
O(3B)	3577(1)	517(1)	2172(1)	61(1)
C(35)	3820(2)	320(1)	3014(2)	43(1)
O(1)	2285(1)	5306(1)	-408(1)	61(1)
C(39)	8576(2)	-1095(1)	5245(2)	55(1)
C(38)	8742(2)	-1675(2)	5491(3)	74(1)
C(37)	8379(3)	-2090(2)	4871(3)	89(1)
C(40)	7707(2)	-1366(1)	3754(2)	61(1)
C(41)	7869(2)	-1945(1)	4002(3)	80(1)
N(3)	4819(1)	5571(1)	-315(2)	47(1)
C(45)	4906(2)	5305(1)	-1229(2)	51(1)
C(42)	4623(2)	6141(1)	-306(3)	64(1)
C(44)	4827(2)	5609(2)	-2163(2)	70(1)
C(43)	4521(2)	6468(2)	-1207(3)	84(1)
C(48)	2207(2)	3728(1)	-441(3)	67(1)
N(2)	1316(2)	3577(1)	-579(2)	71(1)
C(49)	2471(2)	3616(1)	525(2)	53(1)
C(50)	4625(2)	6200(2)	-2116(3)	88(1)
C(51)	5252(2)	-243(2)	8578(2)	83(1)
C(52)	4928(3)	5289(2)	-3091(2)	91(1)
O(7)	4987(2)	1507(1)	2169(2)	97(1)
C(53)	4617(4)	2012(3)	2574(6)	122(2)